Application of Generalized Sturmian Basis Functions to Molecular Systems

Carlos Mario Granados Castro

École Doctorale SESAMES

Discipline : Physique
Spécialité doctorale : Physique Moléculaire

Thèse de Doctorat

Application of Generalized Sturmian Basis Functions to Molecular Systems

présentée et soutenue publiquement le 18 Février 2016 par

Carlos Mario GRANADOS–CASTRO

pour obtenir le grade de docteur délivré par

Université de Lorraine
et
Universidad Nacional del Sur

Directeur de thèse : **Lorenzo Ugo ANCARANI**
Co-directeurs de thèse : **Xavier ASSFELD** et **Gustavo GASANEO**

Membres du jury

M. Alain DUBOIS	Professeur, Université Pierre et Marie Curie (France)	Président
M. Osman ATABEK	Directeur de Recherche, CNRS, Université Paris Sud (France)	Rapporteur
M. Thierry STOECKLIN	Directeur de Recherche, CNRS, Université de Bordeaux (France)	Rapporteur
M. Sebastián OTRANTO	Professeur Adjoint, Universidad Nacional del Sur (Argentine)	Examinateur
M. Gustavo GASANEO	Professeur Associé, Universidad Nacional del Sur (Argentine)	Examinateur
M. Xavier ASSFELD	Professeur, Université de Lorraine (France)	Examinateur
M. Lorenzo Ugo ANCARANI	Professeur, Université de Lorraine (France)	Examinateur

Équipe TMS, Laboratoire SRSMC, UMR 7565
ICPM, Université de Lorraine, 57078 Metz



École Doctorale SESAMES

Discipline : Physics
Speciality : Molecular Physics

PhD Thesis

Application of Generalized Sturmian Basis Functions to Molecular Systems

presented and defended February 18 2016 by

Carlos Mario GRANADOS–CASTRO

to obtain the doctor degree at the

Université de Lorraine
and
Universidad Nacional del Sur

Director : **Lorenzo Ugo ANCARANI**
Co-directors : **Xavier ASSFELD** and **Gustavo GASANEO**

Jury members

M. Alain DUBOIS	Professeur, Université Pierre et Marie Curie (France)	President
M. Osman ATABEK	Directeur de Recherche, CNRS, Université Paris Sud (France)	Referee
M. Thierry STOECKLIN	Directeur de Recherche, CNRS, Université de Bordeaux (France)	Referee
M. Sebastián OTRANTO	Professeur Adjoint, Universidad Nacional del Sur (Argentine)	Examiner
M. Gustavo GASANEO	Professeur Associé, Universidad Nacional del Sur (Argentine)	Examiner
M. Xavier ASSFELD	Professeur, Université de Lorraine (France)	Examiner
M. Lorenzo Ugo ANCARANI	Professeur, Université de Lorraine (France)	Examiner

Équipe TMS, Laboratoire SRSMC, UMR 7565
ICPM, Université de Lorraine, 57078 Metz

To Daniel Castro, who always inspires my life

Acknowledgements

I am extremely grateful to my advisor Prof. Ugo Ancarani, for all his help, endless support, enthusiasm, knowledge, friendship and discussions during coffee breaks. I would also like to thank to Dr. Gustavo Gasaneo and Dr. Darío Mitnik, for their support and supervision, comments and inputs during all the phases of this thesis.

I would like to thank to Prof. Claude Dal Cappello, Prof. Bedros Joulakian, Dr. Arnaud Leclerc and Dr. Alessandro Genoni for their valuable comments, helpful suggestions and stimulating discussions. Thanks also to M. Philippe Senot, and all the Équipe TMS staff, for all their help.

Thanks also to all the people that I met both at Université de Lorraine and Univerdidad Nacional del Sur, with whom I had stimulating discussions, in particular Dr. Marcelo Ambrosio, Dr. Ana Laura Frapiccini, Jessica del Punta, Bruno Pascucci, Sol Otero, Dr. Carolina Zubieta, Ana Rossi, Walter Reimers, Daniel Zamo, Diana Franco, Cristina Calle, Dr. Bassem Hmouda, Dr. Rayan el Mir and Osman Alwan.

I express my gratitude to all other people, who have contributed directly or indirectly to this work, to my education and to my training.

Thanks also to my friends, in particular to Juliana Serna, Daniel Morales, Nicolás Salazar, Carolina González, Lorena Sánchez and Nadia Kujar, who always supported me.

Finally, and not less important, I express my gratitude to my family for their love and support, in particular to my mom, María V. Castro, her husband Javier Canal, my father Rubén Granados, my sister, my grandmother and my girlfriend.

Preface

This thesis is submitted for the degree of Doctor in Physics at the Université de Lorraine, Metz (France), and at the Universidad Nacional del Sur, Bahía Blanca (Argentina), under an agreement of "cotutelle internationale". The research described herein was conducted by Professor Lorenzo Ugo ANCARANI in Metz, Professor Xavier ASSFELD in Nancy, and by Dr. Gustavo GASANEO, in Bahía Blanca, between February 2013 and February 2016.

This work is to the best of my knowledge original, except where acknowledgements and references are made to previous works.

Prefacio

Esta tesis es presentada con el objetivo de obtener el título de Doctor en Física, otorgado por la Université de Lorraine, en Metz (Francia), y por la Universidad Nacional del Sur, en Bahía Blanca (Argentina), bajo un convenio de cotutela internacional. La investigación que acá se describe fue dirigida por Profesor Lorenzo Ugo ANCARANI en Metz, Dr. Xavier ASSFELD en Nancy y por el Dr. Gustavo GASANEO, en Bahía Blanca, entre Febrero de 2013 y Febrero de 2016.

Este trabajo de investigación es completamente original, excepto por los reconocimientos y referencias hechas a trabajos previos.

Carlos Mario GRANADOS–CASTRO
Metz, France
Bahía Blanca, Argentina
December 2015

Abstract

In this PhD thesis we implement a Sturmian approach, based on generalized Sturmian functions (GSFs), to study the ionization of molecules by collision with photons or electrons. Since the target Hamiltonian is highly non-central, describing molecular ionization is far from easy. Besides, as the spatial orientation of the molecule in most experimental measurements is not resolved, an important issue to take into account is its random orientation. In the literature, many theoretical methods have been proposed to deal with molecules, but many of them are adapted to study mainly bound states. An accurate description of the unbound (continuum) states of molecules remains a challenge. Here we propose to tackle these problems using GSFs, which are characterized to have, by construction, the correct asymptotic behavior of the studied system. This property allows one to perform ionization calculations more efficiently.

We start and validate our Sturmian approach implementation by studying photoionization (PI) of H, He and Ne atoms. Different model potentials were used in order to describe the interaction of the ejected electron with the parental ion. We calculated the corresponding PI cross sections in both length and velocity gauges. For H atom, the comparison with the analytical formula shows that a rapid convergence can be achieved using a moderate number of GSFs. For He and Ne we have also an excellent agreement with other theoretical calculations and with experimental data. For molecular targets, we considered two different strategies to deal with their random orientation: one makes use of a molecular model potential (non-central), while the other uses an angular averaged version of the same potential (central). We study PI for CH_4, NH_3, and H_2O, from the outer and inner valence orbitals, and for SiH_4 and H_2S from the outer orbitals. The calculated PI cross sections and also the asymmetry parameters (obtained from the corresponding angular distributions) are compared with available theoretical and experimental data. For most cases, we observed an overall fairly good agreement with reference values, grasping the main features of the ionization process.

In a second part of the thesis, we apply the Sturmian approach to study ionization of molecules by electron collisions. In the so-called $(e, 2e)$ processes, fully differential cross sections are investigated within both the first- or the second-Born approximations. Again, we show how to include in the description the random orientation of the molecule. We start with H atom, as a test system: the comparison of the calculated triple differential cross sections (TDCSs) with analytical results illustrates, similarly to the PI case, the efficiency of our GSF method. It is then applied to ionization of CH_4, H_2O and NH_3, and comparisons are made with the few theoretical and experimental data available in the literature. For most cases, our TDCSs can reproduce such data, particularly for H_2O and for slow ejected electrons in CH_4.

Résumé

Dans cette thèse nous implémentons une approche Sturmmienne, qui se sert de fonctions Sturmiennes généralisées (GSFs, en anglais), pour étudier l'ionisation de molécules par collisions de photons ou d'électrons. Comme l'Hamiltonian de la cible est non central, la description de l'ionisation des molécules n'est pas simple. En plus, puisque l'orientation spatiale de la molécule n'est généralement pas déterminée lors des expériences, une question importante à considérer est l'orientation aléatoire de la cible. Dans la littérature, des nombreuses méthodes théoriques ont été proposées pour traiter les molécules ; néanmoins, la plupart sont adaptées pour étudier, principalement, des états liés. Une description précise des états non-liés (continuum) des molécules reste un défi. Ici, nous proposons d'attaquer le problème avec les GSFs qui ont, par construction, un comportement asymptotique approprié au système étudié. Cette propriété permet de faire des calculs d'ionisation de façon plus efficace.

Dans une première partie, nous validons l'implémentation de notre approche Sturmienne par l'étude de la photo-ionisation (PI) d'atomes. Différents potentiels effectifs sont utilisés pour décrire l'interaction de l'électron éjecté avec la cible ionisée. Les sections efficaces de PI sont calculées dans les jauges de longueur et de vitesse. Pour l'atome d'hydrogène la comparaison avec la formule analytique, indique qu'une convergence très rapide est obtenue avec un nombre modéré de GSFs. Pour He et Ne, nos résultats montrent, également, un très bon accord avec d'autres résultats théoriques et expérimentaux. Dans le cas des molécules, nous avons abordé l'orientation aléatoire avec deux stratégies : une utilise un potentiel moléculaire modèle (non-central), et l'autre un potentiel moyenné (central). Nous étudions la PI de CH_4, NH_3 et H_2O à partir des orbitales de valence extérieure et intérieure, et aussi de SiH_4 et H_2S à partir des orbitales extérieures. Les sections efficaces de PI et les paramètres d'asymétrie (obtenus à partir des distributions angulaires) sont comparés avec ceux publiés dans la littérature. Nos résultats sont globalement satisfaisants et reproduisent les caractéristiques principales de ce processus d'ionisation.

Dans une deuxième partie de la thèse, nous utilisons l'approche Sturmienne pour étudier l'ionisation de molécules par impact d'électrons. Pour le processus $(e, 2e)$, les sections efficaces triplement différentielles (TDCSs) sont examinées dans la première et deuxième approximation de Born, également en traitant de deux façons l'orientation aléatoire des molécules. Nous avons testé la méthode en comparent nos TDCSs pour l'atome d'hydrogène, montrant aussi son efficacité. Enfin, nous l'avons apliqué à l'ionisation de CH_4, H_2O et NH_3, et nous avons comparé les résultats avec des données expérimentales et théoriques disponibles dans la littérature. Dans la plupart des cas, nos TDCSs sont en accord satisfaisant avec ces données, en particulier pour H_2O et pour des électrons lents dans le cas de CH_4.

Resumen

En esta tesis implementamos el método Sturmiano, que está basado en el uso de funciones Sturmianas generalizadas (GSFs, por sus siglas en inglés), para estudiar ionización de moléculas por impacto de fotones y electrones. Como el Hamiltoniano que describe el blanco es altamente no-central, no es sencillo describir la ionización de moléculas. Además, como en la mayoría de experimentos no se puede determinar la orientación de la molécula, se debe considerar una orientación aleatoria del blanco. Varios métodos han sido propuestos para estudiar moléculas, pero la mayoría han sido optimizados para tratar sólo estados ligados. Queda como un problema a resolver una descripción precisa de los estados no ligados (del continuo). Proponemos entonces tratar estos problemas usando GSFs, que se caracterizan por tener, por construcción, el comportamiento asintótico correcto del sistema estudiado. Esta propiedad nos permite realizar cálculos más eficientemente.

Nuestra implementación del método Sturmiano comienza con el estudio de la fotoionización (PI) de H, He y Ne. Diferentes potenciales modelo son usados para describir la interacción del electrón eyectado con el ión remanente. Calculamos las secciones eficaces de PI en los gauges de longitud y velocidad. Para H, comparamos nuestros resultados con la fórmula analítica. Los errores relativos muestran una rápida convergencia, usando siempre un número moderado de GSFs. Para He y Ne nuestros resultados también muestran una excelente concordancia con otros resultados teóricos y experimentales. Para el caso de moléculas, indicamos las diferentes estrategias usadas para incorporar su orientación aleatoria, donde se usa un potencial molecular modelo (no central), y también un potencial promediado (central). Estudiamos PI para CH_4, NH_3 y H_2O, desde los orbitales de valencia externos e internos, y para SiH_4 y H_2S desde los externos. Las secciones eficaces de PI y los parámetros de asimetría (para las distribuciones angulares correspondientes) calculados, son comparados con datos teóricos y experimentales disponibles en la literatura. Para casi todos los casos, nuestros resultados logran mostrar las características principales de la ionización.

En la segunda parte de esta tesis, exploramos la implementación del método Sturmiano, para estudiar ionización por colisión de electrones. En la denominado $(e, 2e)$, investigamos las secciones eficaces diferenciales, usando la primera y segunda aproximación de Born. También se indica cómo incluir la orientación aleatoria de la molécula. Comenzamos con el H, como un sistema de prueba, y comparamos las secciones eficaces triple diferenciales (TDCSs) con resultados analíticos. Similar al caso de PI, los errores relativos muestran una rápida convergencia, usando un número razonable de GSFs. Luego estudiamos la ionización de CH_4, H_2O y NH_3, y comparamos con los pocos datos teóricos y experimentales disponibles en la literatura. En la mayoría de casos, nuestras TDCSs logran reproducis dichos valores, en particular para H_2O y para electrones lentos eyectados en CH_4.

Contents

List of Figures

List of Tables

List of Acronyms

1CW Coulomb wave 77

AAP angular averaged potential 83

ADCS angular differential cross section 46

AO atomic orbital 20

BBK Brauner–Brigs–Klar 78

BC boundary condition 151

BO Born–Oppenheimer 44

CBF complex basis function 147

CI configuration-interaction 145

CKM complex Kohn method 78

CN Crank–Nicolson 152

CS complex scaling 147

DFT density functional theory 19

DIM depurated inversion method 32

DWBA distorted-wave Born approach 77

ECS exterior complex scaling 30

FC frozen core 44

GIPM ground state inversion potential method 59

GSF generalized Sturmian function 22

HF Hartree–Fock . . . 33

HS Herman–Skillman . . . 31

ISM iterative-Schwinger method . . . 68

KS DFT Kohn–Sham DFT . . . 146

KVM Kohn variational method . . . 150

L length gauge . . . 46

LAM linear algebraic method . . . 147

LCAO linear combination of atomic orbitals . . . 146

LDKM logarithmic derivative Kohn method . . . 150

LSE Lippmann–Schwinger equation . . . 79

MCF method of continued fractions . . . 152

MCTDHF multiconfiguration time-dependent Hartree-Fock . . . 146

MMP molecular model potential . . . 83

MSM multiple-scattering method . . . 147

MO molecular orbital . . . 20

OCE one-center expansion . . . 22

PAR parametric . . . 31

PI photoionization . . . 20

PWA plane-wave approximation . . . 148

QDT quantum defect theory . . . 148

RMM *R*-matrix method . . . 78

RPA random-phase approximation . . . 69

SAE single active electron . . . 22

SCF self-consistent field . . . 96

SEA static exchange approximation . . . 37

Chapter 0

French Translations
Traductions au Français

0.1. Chapitre 1 - Introduction

0.1.1. Motivations et Généralités

L'étude des processus collisionnels a toujours joué un rôle central en mécanique quantique : elle permet d'examiner la structure électronique de la cible et la nature des interactions entre le projectile et la cible. Les processus collisionnels entre atomes et molécules, et photons ou électrons ont été étudiés depuis longtemps, à la fois expérimentalement et théoriquement. Toutefois, d'un point de vue théorique, il reste de nombreux défis originaux, comme la description du spectre complet de la cible. Au cours des années, différentes méthodes ont été proposées afin d'évaluer avec un degré élevé de précision les états liés (particulièrement l'état fondamental) des atomes et molécules, comme la *théorie de la fonctionnelle de la densité* (DFT) ou les calculs variationnels, par exemple avec des fonctions Gaussiennes. Des difficultés surgissent lorsque l'on étudie les états non-liés (continuum), décrits par des fonctions d'onde oscillant à l'infini ; un grand nombre de méthodes adaptées aux états liés ne le sont pas pour ceux du continuum. Il est bien connu que la représentation de

ces fonctions d'onde sur une base peut être très coûteux en termes de ressources computationnelles. La description des états initial et final et l'interaction entre eux sont les ingrédients clés pour l'étude de l'ionisation des systèmes atomiques et moléculaires.

L'ionisation simple, par collision de photons (*photo-ionisation* (PI)) ou d'électrons (désignée par $(e, 2e)$), joue un rôle important au-delà de la physique atomique et moléculaire, puisqu'elle intervient dans une grande variété d'applications, de l'astrophysique à la physique des plasmas, en passant par la physique de l'environnement et la physique médicale. Par ailleurs, la plupart des outils théoriques peuvent être adaptés pour étudier les interactions en physique de la matière condensée et du solide. Il est donc nécessaire de disposer d'outils efficaces pour décrire avec assez de précision le phénomène d'ionisation, particulièrement dans le cas des interactions de longue portée (comme le potentiel de Coulomb).

Sur la figure 0.1 nous avons schématisé le processus de simple PI pour un atome ou une molécule ; dans ce cas, en plus de la cible ionisée, il y a un seul électron dans la voie de sortie : l'électron éjecté. De la même façon, nous avons illustré sur la figure 0.2 le processus $(e, 2e)$, dans lequel il y a deux électrons dans la voie de sortie : l'électron diffusé et l'électron éjecté. Ces deux électrons (s'il y a un diffusé) interagissent avec l'ion parent. La figure 0.3 représente le spectre de l'atome d'hydrogène et une transition d'un état lié vers le continuum. Comme mentionné ci-dessus, les deux ingrédients essentiels sont les états initial et final. Pour le premier, on impose aux fonctions d'onde correspondantes un comportement asymptotique de type décroissance exponentielle, c'est-à-dire qu'ils possèdent une extension spatiale finie. Pour les états du continuum, les fonctions d'onde ont aussi un comportement asymptotique bien défini, en terme d'ondes sortantes ou entrantes et, contrairement au cas lié, ils ont une extension infinie. Pour un problème d'ionisation, une des tâches les plus difficiles (tout du moins une les plus critiques) pour une méthode théorique est sa capacité à imposer aux fonctions d'onde de telles conditions asymptotiques. Parmi la variété de méthodes qui ont été développées au cours des années, seulement certaines peuvent satisfaire ce point délicat.

Bien que de tels processus d'ionisation aient été étudiés de manière approfondie pour les systèmes atomiques, ce n'est pas le cas pour les systèmes moléculaires. Le Hamiltonien correspondant est multicentrique et fortement non-central, rendant le problème plus difficile à résoudre par rapport au cas atomique. En effet, l'absence de symétrie sphérique couple les moments cinétiques des différentes *orbitales atomiques* (AOs) qui forment les *orbitales moléculaires* (MOs) ; par conséquent la convergence des méthodes traditionnelles est considérablement plus difficile à obtenir. De plus il y a des effets à plusieurs corps qui peuvent être importants dans les processus

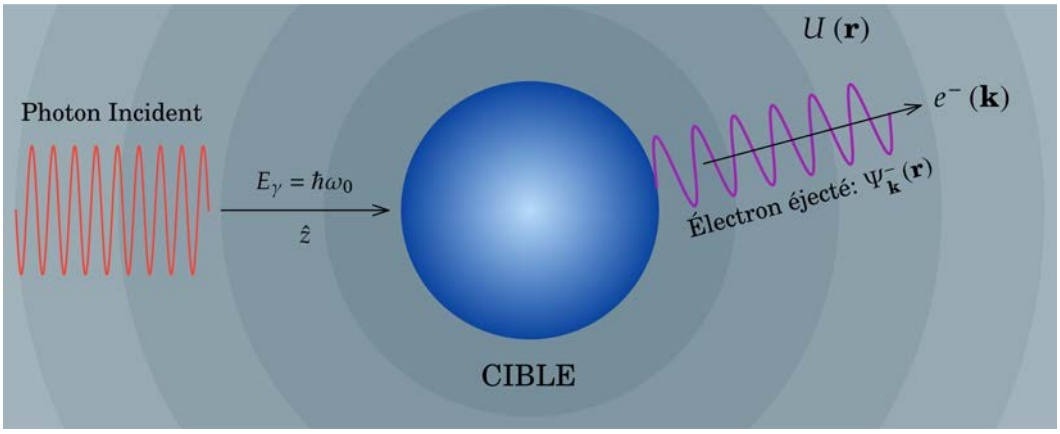

FIGURE 0.1 – Schéma d'un processus de PI pour une cible atomique ou moléculaire, représentée en bleu. L'électron éjecté dans la voie finale (violet et flèche à droite) est sous l'influence du potentiel $U(\mathbf{r})$ de la cible ionisée restante.

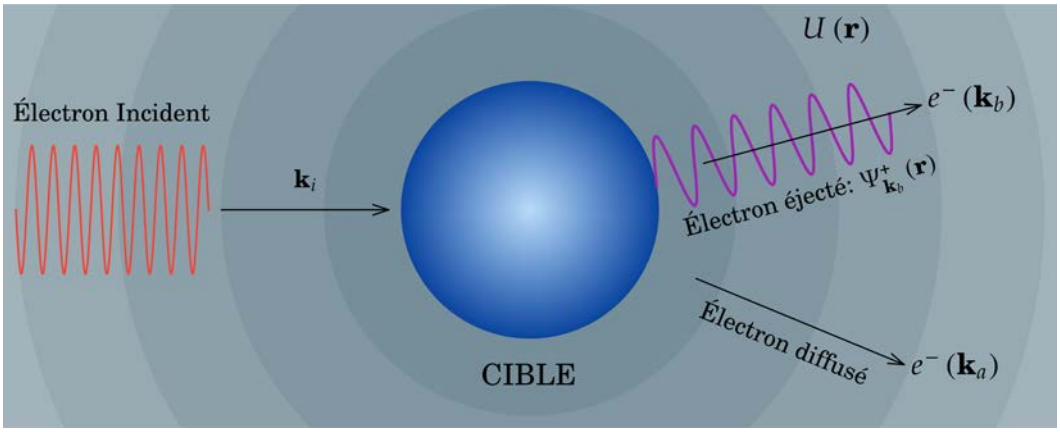

FIGURE 0.2 – Schéma d'un processus d'ionisation par impact électronique ($\mathbf{k}_i$), représenté en bleu. En plus de l'électron éjecté ($\mathbf{k}_b$), il y a un électron diffusé ($\mathbf{k}_a$) ; leurs rôles peuvent être interchangés. Les deux électrons sont sous l'influence du potentiel $U(\mathbf{r})$ de la cible ionisée.

d'ionisation, comme la relaxation de toutes les MOs, suite à la création d'un trou (électron ionisé), ou le changement des énergies de corrélation de la paire restante en raison de cette relaxation. En plus de cela, un problème qui n'est pas présent dans l'étude de l'ionisation atomique est l'orientation de la cible moléculaire. Dans la plupart des expériences, la molécule est orientée de façon aléatoire et ceci doit être pris en considération dans une description théorique. Pour traiter une partie de ces problèmes associés à la nature moléculaire de la cible, diverse méthodes ont été proposées avec des applications allant de la plus petite molécule, H_2, jusqu'à par exemple les bases de l'ADN. Le succès de chacune de ces méthodes dépend de la molécule étudiée et de la gamme d'énergie impliquée, de la validité des

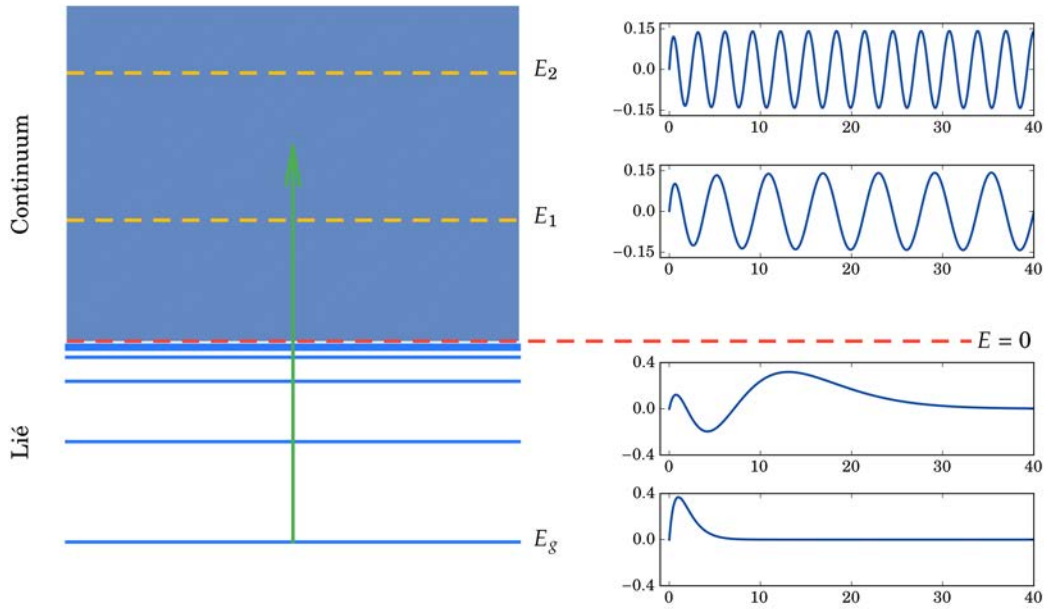

Figure 0.3 – Schéma des états liés et non-liés de l'hydrogène atomique ; une transition lié-continuum est représentée par une flèche verticale (verte). Dans la partie gauche, on représente les niveaux liés et du continuum d'énergie. Les fonctions d'onde de deux états liés et de deux états du continuum sont tracées à droite.

approximations, et de possibles problèmes de convergence ou de limitations liées aux implémentations numériques.

Dans cette thèse, nous nous sommes intéressés à une approche Sturmienne pour l'étude des processus d'ionisation simple par impact photonique ou électronique. Cette approche est basée sur une méthode spectrale avec des fonctions de type Sturmiennes, pour lesquelles différentes implémentations ont été proposées dans la littérature. Les fonctions Coulomb-Sturmiennes ont été utilisées, par exemple, pour l'étude du spectre d'atomes [18–23] et de molécules [23–26], pour des problèmes Coulombiens à trois corps [27], et différents processus d'ionisation atomique, comme la PI [28–30] ou l'ionisation par impact d'électrons, de protons ou d'ions [31–35]. Les *fonctions Sturmiennes généralisées* (GSFs) ont été introduites [1, 2] et appliquées à l'étude du spectre atomique [3, 4] et de l'ionisation simple et double de l'atome d'hélium par impact de photons [5], d'électrons [6] ou de protons [7]. Néanmoins l'implémentation de ce type de fonctions Sturmiennes pour étudier l'ionisation des cibles moléculaires reste relativement inexplorée. Une des vertus de l'approche basée sur les GSFs est que le comportement asymptotique correct pour la fonction d'onde diffusée est déjà incorporé, par construction, dans la base même. L'objectif de cette thèse est d'étendre, d'implémenter et d'appliquer l'approche Sturmienne pour étudier l'ionisation simple des cibles moléculaires (plus particulièrement la PI

et les processus $(e, 2e)$). Afin de simplifier les calculs numériques correspondants, différentes approximations seront faites, en particulier l'approximation à un *seul électron actif* (SAE). De plus, le *développement sur un centre* (OCE) sera utilisée pour les molécules. Pour cette raison, un nombre limité de systèmes atomiques et moléculaires polyatomiques a été sélectionné pour tester l'approche Sturmienne, à savoir : H, He, Ne, CH_4, NH_3 et H_2O, et dans une moindre mesure, SiH_4 et H_2S.

0.1.2. Plan

La thèse est divisée en cinq chapitres, introduction et conclusion comprises. Huit annexes détaillent des aspects plus techniques ou du matériel supplémentaires. Le chapitre 2 est dédié aux différentes généralités et définitions utilisées tout au long de cette thèse, des GSFs et pour la description des cibles atomiques et moléculaires. Les GSFs sont présentées dans la section 2.1. La section 2.2 fournit la description des cibles atomiques et moléculaires (les énergies des états fondamentaux et les fonctions d'onde), ainsi que les potentiels modèles utilisés pour représenter l'interaction entre l'électron et la cible.

Dans le chapitre 3, nous illustrons l'implémentation de l'approche Sturmienne pour l'étude de la PI d'atomes et de molécules. Tout d'abord, dans la section 3.2 nous décrivons brièvement certains des défis expérimentaux relatifs à l'orientation spatiale de la cible ; ensuite, la description théorique de la PI est décrite dans la section 3.3, où l'approximation dipolaire est définie, ainsi que les sections efficaces de PI ; puis, la section 3.4 décrit l'approche Sturmienne et la méthode pour calculer les sections efficaces. Enfin, dans la section 3.5 nous montrons les sections efficaces de PI obtenues pour les atomes H, He et Ne, et dans la section 3.6 nous présentons nos résultats concernant la PI des orbitales de valence pour les molécules CH_4, H_2O, NH_3, SiH_4 et H_2S.

Dans le chapitre 4, nous illustrons l'implémentation de l'approche Sturmienne pour l'étude du processus $(e, 2e)$ sur des molécules. Tout d'abord, la section 4.2 rappelle les défis liés aux mesures expérimentales ; ensuite, dans la section 4.3 nous introduisons une description théorique basée sur la série de Born. L'approche Sturmienne est détaillée dans la section 4.4. Les sections efficaces triplement différentielles pour l'hydrogène, et l'analyse de la convergence correspondante sont présentées dans la section 4.5. Finalement, les résultats dans l'approximation de Born au premier ordre pour CH_4, H_2O et NH_3 sont analysés dans la section 4.6.

Les conclusions finales et quelques perspectives sont présentées dans le chapitre 5.

Dans l'annexe A on décrit l'opérateur de rotation. L'annexe B contient diverses intégrales analytiques utilisées dans ce manuscrit. Dans l'annexe C nous présentons

la transformée de Fourier des potentiels d'interaction. L'annexe D est consacrée à la description de l'approximation de Born et des fonctions de Green, tandis que l'annexe E contient tous les détails pour le calcul des intégrales dans l'approximation de Born au deuxième ordre. L'annexe F décrit la méthode de collocation de Levin que l'on a utilisée pour calcul d'intégrands très oscillants. Finalement, dans l'annexe G nous proposons un revue de diverses méthodes théoriques utilisées pour l'étude de la PI des molécules, et dans l'annexe H nous fournissons une liste (assez exhaustive) des molécules étudiées théoriquement dans la littérature.

Sauf mention contraire, les unités atomiques ($\hbar = e = m_e = 1$) sont utilisées tout au long du manuscrit.

0.2. Chapitre 2 - Fonctions Sturmiennes généralisées et Description des Molécules

Dans ce chapitre, nous introduisons les outils qui sont communs à toutes les autres parties de cette thèse : les *fonctions Sturmiennes généralisées* (GSFs) et la description des cibles atomiques et moléculaires, c'est-à-dire leurs fonctions d'onde et les potentiels effectifs. Ils constituent les ingrédients utilisés pour étudier l'ionisation d'atomes et de molécules par collision de photons (chapitre 3) ou d'électrons (chapitre 4).

La section 2.1 est dédiée à la présentation du formalisme des fonctions Sturmiennes généralisées (GSFs). Tout d'abord, dans la partie 2.1.1, nous commençons par une brève introduction historique des bases Sturmiennes et leurs principales utilisations : l'étude de la diffusion et la description des états liés. Deuxièmement, dans la partie 2.1.2, nous donnons la définition des GSFs et leurs propriétés les plus importants. Ces fonctions, comme le nom le fait entendre, sont solutions d'un problème de Sturm–Liouville, et par conséquent, ils forment une base complète. Afin d'obtenir les GSFs, on définit un potentiel auxiliaire (de long portée), et un potentiel générateur (de courte portée). Même s'il y a beaucoup des similarités entre l'équation Sturmienne et l'équation du Schrödinger, une des principales différences est le rôle attribué à l'énergie. Pour l'équation des fonctions Sturmiennes l'énergie n'est plus considérée comme une valeur propre mais un paramètre fixé ; les valeurs propres des GSFs apparaissent comme des charges généralisées associées au potentiel générateur.

Une des caractéristiques les plus importantes des GSFs est leur comportement asymptotique : d'un part toutes ces fonctions ont le même comportement et, d'autre part, il est tel qu'il satisfait les conditions aux limites du problème physique que l'on souhaite résoudre. Pour la diffusion dans un potentiel de Coulomb, ce comportement

est constitué d'ondes sortantes ou entrantes, avec une énergie préfixée. Par ailleurs, toutes les fonctions de la base sont régulières à l'origine. La relation d'orthogonalité ainsi que la relation de fermeture possèdent une fonction poids qui n'est rien d'autre que le potentiel générateur. Dans la partie 2.1.3, nous fournissons certains aspects numériques et quelques exemples, où l'on explique la construction des GSFs en choisissent le comportement asymptotique désiré pour une énergie pré-sélectionnée.

Dans la section 2.2, nous donnons la description des cibles atomiques et moléculaires : la partie 2.2.1 fournit la définition des potentiels effectifs dans l'approximation à un *seul électron actif* (SAE) : le potentiel Herman–Skillman, un potentiel que l'on appelle paramétrique et celui obtenu par la "depurated inversion method". Nous avons utilisé ces potentiels pour étudier, en particulier, la PI des atomes d'hélium et de néon. Les fonctions d'onde de l'état initial sont obtenues à partir de la diagonalisation de ces potentiels, et leurs énergies des états fondamentaux sont en bon accord avec les énergies d'ionisation expérimentales.

Ensuite, dans la partie 2.2.2, nous décrivons les fonctions d'onde pour les cibles moléculaires, fournies par Moccia, en termes de *orbitales de type Slater* (STOs) et des harmoniques sphériques réelles. Comme dans notre formalisme on utilise les fonctions harmoniques complexes, nous avons transformées les fonctions originales (et les coefficients de développement) à leur forme complexe. Tous les paramètres nécessaires pour construire les fonctions d'onde pour les MOs que l'on utilise dans cette thèse (et aussi les géométries d'équilibre) de CH_4, NH_3, H_2O, SiH_4 et H_2S, sont explicitement donnés dans les tableaux 2.4 à 2.13.

Enfin, dans la partie 2.2.3, on trouve la définition des potentiels moléculaires effectifs, également dans l'approximation SAE, à savoir, le potentiel modèle moléculaire (non-central) et le potentiel moyenné angulairement (central). Le potentiel modèle est le terme directe d'un potentiel dans l'*approximation d'échange statique* (SEA). L'utilisation du potentiel non-central permet de tenir compte de l'orientation spatiale des cibles moléculaires. En revanche, avec le potentiel central, l'orientation aléatoire est incorporée avant le calcul. Puisque les deux potentiels sont décrits en fonction des MOs, publiées par Moccia, elles mêmes exprimés en termes de STOs, il est possible d'établir une expression analytique pour ces potentiels, donnée par l'équation (2.31). Avec une telle expression, on peut calculer les éléments de matrice dans une projection sur harmoniques sphériques (voir équation (2.32)) et, également, on peut avoir une formule analytique pour la transformée de Fourier du potentiel modèle (voir équations (2.35) et (C.11)).

0.3. Chapitre 3 - Photo-ionisation

Dans ce chapitre nous étudions la PI d'atomes et de molécules. Tout d'abord, dans la section 3.1 nous introduisons le processus de PI et ses applications, de l'astrophysique et la physique planétaire à la physique atmosphérique, en passant par la physique des plasmas, la biophysique et la physique médicale. Deuxièmement, dans la section 3.2, nous expliquons brièvement comment dans les mesures expérimentales de PI, l'orientation spatiale des cibles est ignorée. Ce problème est important dans l'étude de l'ionisation moléculaire en général : il faut tenir compte de l'orientation aléatoire des cibles. Ensuite, dans la section 3.3, nous donnons la description théorique de la PI dans l'approximation dipolaire, c'est-à-dire, le formalisme standard de PI ; les sections efficaces de PI et les distributions angulaires sont également définies.

Dans la section 3.4, nous montrons comment l'approche Sturmienne peut être utilisée pour étudier la PI. On commence par l'utilisation de la théorie de la perturbation dépendante du temps pour résoudre l'*équation de Schrödinger dépendante du temps* (TDSE). La fonction d'onde de diffusion est écrite comme une combinaison linéaire des états initial et final de la cible. Comme perturbation on utilise l'opérateur dipolaire, dans les jauges de *longueur* (L) ou de *vitesse* (V). Après avoir effectué une transformée de Fourier, on obtient une *équation de Schrödinger indépendante du temps* (TISE), et seulement le premier ordre est conservé ; on a donc une équation différentielle non homogène, dont la solution avec une comportement asymptotique sortant permet d'étudier la simple PI. Pour résoudre cette équation, on utilise les approximations du *cœur gelé* (FC), d'un *seul électron actif* (SAE) et *approximation d'échange statique* (SEA). La fonction d'onde de l'état final est séparée en ses parties radiale et angulaire ; sa partie radiale est développée sur un ensemble fini (de taille modérée) de GSFs. Chaque fonction de l'ensemble des GSFs a le comportement asymptotique correcte pour l'énergie finale sélectionnée. Signalons que, grâce à la définition des GSFs (voir équation (2.1)), il n'y a pas besoin de calculer leurs dérivée seconde, car elle s'exprime directement en fonction des potentiels auxiliaire et générateur. L'équation différentielle est ainsi transformée en une équation linéaire. En projectant sur un élément de base, on obtient finalement une équation matricielle ; les matrices sont données par les équations (3.23). Une fois l'équation résolue, on a les coefficients de développement et donc la fonction d'onde de l'état final. L'étape suivante consiste à calculer l'amplitude d'ionisation, qui est une élément de matrice de l'opérateur dipolaire entre les états final et initial. Comme les GSFs ont par construction le comportement asymptotique correcte, il n'est pas nécessaire de calculer ce type d'intégral. Le résultat est obtenu directement par la somme des coefficients du développement, et aucune autre intégrale doit être calculé. Cela résulte du choix adéquat de la base,

et rend le calcul numérique très efficace.

Un aspect important dans l'étude de l'ionisation des molécules est l'orientation de la cible quand un électron est éjecté. Puisque cette orientation n'est pas mesurée dans la plupart des techniques expérimentales, il faut considérer que la cible a une orientation aléatoire. Dans la partie 3.4.2 nous avons indiqué comment cela est inclus dans nos calculs. Nous adoptons deux stratégies : la première appelée schéma post-moyenné, consiste à calculer les amplitudes d'ionisation pour toutes les orientations possibles, et une moyenne angulaire est faite à la fin ; ce schéma utilise le potentiel modèle non-central. L'autre, appelée schéma pré-moyenné, utilise le potentiel modèle central, défini comme la moyenne angulaire du potentiel non-central ; dans ce cas, l'orientation aléatoire est incluse par le potentiel même. Nous avons comparé les résultats pour les deux stratégies de calcul.

Dans la section 3.5, nous présentons nos résultats pour la PI d'atomes ; dans la partie 3.5.1 nous avons étudié la convergence des GSFs pour calculer les sections efficaces de PI de l'atome d'hydrogène ; on a comparé les sections efficaces analytiques avec nos résultats, dans les jauges L et V. Les erreurs relatives montrent une convergence très rapide en fonction du nombre de GSFs ; les erreurs sont toujours petites, même pour des états du continuum de haute énergie. Dans les parties 3.5.2 à 3.5.4 nous montrons les résultats pour H, He et Ne ; ces sections efficaces ont été calculés aussi dans les jauges L et V. Toutes les résultats sont comparés avec d'autres sections efficaces théoriques et expérimentales.

Finalement, dans la section 3.6, nous avons étudié la PI de cibles moléculaires, particulièrement pour l'ionisation des orbitales de valence internes et externes de CH_4, NH_3, H_2O, et depuis des orbitales externes de SiH_4 et H_2S. Nous avons comparé les schémas post- et pré-moyennés, c'est-à-dire l'effet de faire une moyenne angulaire (pour décrire l'orientation aléatoire des cibles) avant ou après des calculs. Les sections efficaces ont été calculé avec les deux procédures, également dans les jauges L et V. Tous nos résultats sont comparés avec ceux publiés dans la littérature.

L'implémentation de l'approche Sturmienne est différente d'autres méthodes théoriques. Nous ne résolvons pas la TISE comme un problème aux valeurs propres, c'est-à-dire, nous ne calculons pas le spectre du Hamiltonien. Au lieu de cela, nous résolvons l'équation radiale non homogène pour le processus d'ionisation, pour un état final spécifique, avec une énergie E bien définie, pour le quel les GSFs ont le comportement asymptotique correcte. Cela constitue une caractéristique importante de l'approche Sturmienne en comparaison avec d'autres méthodes ; dans la plupart des cas la représentation du processus d'ionisation est limitée par la capacité de la base choisie à décrire la structure des états liés ainsi que les oscillations du continuum. Autrement dit, la même base doit représenter des états d'énergies

différentes (positive et négative) avec des comportements asymptotiques différents ; si la base n'est pas suffisamment flexible, elle peut donner lieu à divers problèmes de convergence numériques.

L'utilisation des GSFs est une manière efficace pour étudier les processus d'ionisation, puisque un nombre modéré d'éléments de base (60 GSFs) est suffisant ; de plus, avec le même nombre d'éléments on peut étudier toute la gamme d'énergie pour les systèmes atomiques et moléculaires. Grâce à la comparaison de la section efficace de PI de l'hydrogène avec les résultats analytiques de référence, nous avons montré que la taille de la base augmente lentement aux hautes énergies ; en termes de convergence il n'y a donc pas de limite en énergie pour étudier le continuum d'un atome ou d'une molécule.

Nos résultats peuvent se résumer comme ceci : l'approche Sturmienne donne des sections efficaces de PI raisonnables, particulièrement pour la PI à partir des orbitales de valence extérieures. Quelques caractéristiques générales sont : **(i)** petite différence entre les schémas post- et pré-moyennés, ce dernier améliorant légèrement les sections efficaces ; **(ii)** les résultats dans le jauge L sont systématiquement plus grands sur toute le gamme d'énergie que ceux obtenus dans le jauge V, et généralement ne sont pas en accord avec d'autres données théoriques et expérimentales. Cette différence indique que l'on doit améliorer la description de l'état initial ; **(iii)** nos résultats dans le jauge V ont un accord global avec autres sections efficaces théoriques, particulièrement à partir de 15-20 eV au-dessus du seuil d'ionisation ; **(iv)** pour l'étude des systèmes moléculaires, l'accord entre les résultats théoriques et les donnés expérimentales n'est pas uniforme. Pour des énergies de moins que 15 eV au-dessus du seuil d'ionisation, l'accord est généralement faible.

0.4. Chapitre 4 - Ionisation par Impact Électronique

Ce chapitre est dévoué à l'étude de l'ionisation de molécules par impact électronique, particulièrement aux *sections efficaces triplement différentielles* (TDCSs) pour les processus $(e, 2e)$. Tout d'abord, dans la section 4.1, nous rappelons que la compréhension des processus de collisions ont toujours été très importantes en physique atomique et moléculaire. Ils permettent d'étudier la structure électronique de la cible, et ont beaucoup d'applications, comme dans les lasers à électrons, le milieu interstellaire, l'atmosphère et l'ionosphère des planètes, le traitement avec plasmas, les plasmas de fusion, la physique des rayonnements, la chimie ou les aurores et les éclairs.

Dans un processus $(e, 2e)$ typique, nous avons un électron incident (dans la voie initiale) avec une impulsion fixe $\mathbf{k}_i$; dans la voie de sortie on a un électron

diffusé, avec une impulsion $\mathbf{k}_a$ (et détecté dans un angle de diffusion fixé θ_a) et un électron éjecté, avec une impulsion $\mathbf{k}_b$. Les deux électrons dans la voie de sortie sont détectés en coïncidence. L'énergie et l'impulsion sont conservés. Dans cette thèse, nous nous sommes intéressé à des conditions cinématiques asymétriques, où l'impulsion de l'électron diffusé est beaucoup plus grande que l'impulsion de l'électron éjecté, c'est-à-dire, $k_a \gg k_b$. Dans ces conditions, on peut ignorer l'échange et utiliser, sans ambiguïté, les étiquettes des électrons dans la voie finale. Lors de l'analyse et l'interprétation des sections efficaces différentielles, il est utile de définir le transfert d'impulsion comme la différence entre l'impulsion de l'électron incident et l'impulsion de l'électron sortant plus rapide : $\mathbf{q} = \mathbf{k}_i - \mathbf{k}_a$.

Dans ce ce chapitre, l'idée est d'utiliser l'approche Sturmienne pour calculer des TDCSs et les comparer à celles mesurées dans des expériences récentes. Les TDCSs sont différentielles par rapport à l'énergie totale et par rapport aux directions de détection des deux électrons. Elles caractérisent la distribution angulaire et énergétique des deux électrons de la voie finale. Nous nous limitons dans ce travail à des géométries coplanaires, pour lesquelles l'électron incident et les deux électrons sortants sont dans le même plan. Les TDCSs sont généralement caractérisées par deux pics : le premier, appelé *pic binaire*, est orienté vers l'avant (environ vers $+\mathbf{q}$), et il indique la direction où on peut attendre l'électron éjecté dans le cas d'une collision binaire. Le deuxième pic, connu comme *pic de recul*, est orienté environ vers $-\mathbf{q}$ et donne une indication d'une réflexion de l'électron éjecté vers l'arrière, suite à l'interaction avec le noyau. Dans l'approximation de Born au premier ordre, les pics binaire et de recul sont, respectivement, orientés exactement selon $+\mathbf{q}$ et $-\mathbf{q}$. Pour les processus $(e, 2e)$ sur des molécules, les TDCSs obtenues peuvent présenter d'autres pics ; cela est liée à la structure de la cible qui est plus complexe.

Une difficulté qui apparaît est la description précise de l'interaction entre le projectile et la cible. Une première approche consiste à utiliser l'approximation de Born au premier ordre, mais c'est clair que pour certaines conditions cinématiques cette approche n'est pas suffisante, car la dynamique du processus d'ionisation est plus complexe qu'une simple collision. Il faut alors considérer d'autres termes de la série de Born, comme décrit dans l'annexe D. Dans la littérature on peut trouver quelques tentatives d'utiliser l'approximation de Born au deuxième ordre, mais ce type de calcul est difficile à implémenter du point de vue numérique.

Dans la section 4.2, nous présentons une petite discussion sur les mesures expérimentales du processus $(e, 2e)$. Normalement, seulement les impulsions des deux électrons dans la voie de sortie sont détectées. L'impulsion et l'orientation des fragments ionisés ne sont pas mesurées, et donc l'orientation spatiale de la molécule au moment de l'éjection d'un électron n'est pas connue. Seulement quelques techniques

expérimentales peuvent donner l'information sur l'orientation.

Ensuite, dans la section 4.3 on présente la description théorique des processus $(e, 2e)$. Comme nous avons considéré des collisions à relativement haute énergie incidente, les électrons incident et diffusé sont représentés par des ondes planes, selon le formalisme de l'approximation de Born dans lequel l'amplitude d'ionisation est développée dans une série perturbative appelée série de Born. Dans les parties 4.3.2 et 4.3.3 nous indiquons comment on peut calculer ces amplitudes au premier et deuxième ordre, respectivement.

Dans la section 4.4, nous présentons l'approche Sturmienne pour l'étude des processus $(e, 2e)$. Elle est similaire au cas de PI : la fonction d'onde pour l'électron éjecté est séparée en parties radiale et angulaire, et la fonction radiale est développée sur un ensemble fini de GSFs. Chaque fonction Sturmienne a un comportement asymptotique sortant qui correspond précisément à l'énergie de l'électron éjecté E_b. Comme pour la PI, la TISE originale est transformée en une équation matricielle. Par rapport à l'équation pour la PI, seul le terme de droite est différent : le premier ordre est donné par l'équation (4.29) et le deuxième ordre par l'équation (4.32). Pour tenir compte de l'orientation aléatoire de la cible, on a utilisé cette fois uniquement le schéma post-moyenné, de manière à avoir toutes les interférences entre les ondes partielles de la fonction d'onde finale. Pour décrire l'interaction entre l'électron éjecté et la molécule ionisée, on utilise trois potentiels différents : le potentiel de Coulomb, le potentiel modèle moyenné (central) et le potentiel moléculaire modèle (non central). Une fois l'équation matricielle résolue, on obtient les coefficients du développement et donc la fonction d'onde. Par le choix adéquat du comportement asymptotique des GSFs, les amplitudes d'ionisation (qui définissent la TDCS) sont extraites directement à partir des coefficients, sans besoin de calculer un élément de matrice.

Dans la section 4.5, nous avons testé notre approche Sturmienne. Nous commençons dans la partie 4.5.1, par une étude de convergence des nos TDCSs, en considérant l'ionisation de l'atome d'hydrogène. Nous avons comparé les résultats numériques avec une expression analytique dans l'approximation de Born au premier ordre. Les erreurs relatives, en fonction du nombre de GSFs, décroissent très rapidement, pour différentes conditions cinématiques ; nous obtenons un bon accord si l'on utilise plus de 30 GSFs. En second lieu, nous avons testé la convergence des TDCSs en fonction du nombre d'ondes partielles ; il est bien connu que la convergence dans ce type de développement est lente, et nous avons trouvé que l'on a un bon accord si $\ell_{\max} \geqslant 6$. Nous présentons nos TDCSs pour l'hydrogène dans la partie 4.5.2, et les comparons avec la formule analytique et des données expérimentales. Nous observons un bon accord pour des électrons éjectés lents, mais un mauvais accord pour des électrons

plus rapides. Cela témoigne de la limitation de la validité de l'approximation de Born au premier ordre.

Finalement, dans la section 4.6, nous présentons nos résultats pour l'ionisation de molécules par impact électronique. Nous avons calculé les TDCSs pour l'ionisation depuis les orbitales de valence internes et externes de CH_4, H_2O et NH_3, et elles sont comparées avec d'autres calculs théoriques et les quelques données expérimentales que l'on trouve dans la littérature (pas nombreuses). En plus, ces données sont en échelle relative, et on a donc pu faire seulement une comparaison qualitative entre les TDCSs théoriques et expérimentales. La qualité de nos résultats est variable selon la molécule, l'orbital moléculaire ionisé et les conditions cinématiques. Dans la plupart de cas nos pics binaires, pour le trois potentiels modèles, sont en bon accord avec d'autres résultats théoriques. La région de recul est la plus difficile à représenter, particulièrement pour des électrons à basse énergie. Généralement, il n'y a pas de bon accord entre nos calculs (ou d'autres proposés dans la littérature) et les données expérimentales. Il est clair qu'une meilleur description de l'état initial est nécessaire, mais aussi qu'il faudrait tenir compte des interactions de deuxième ordre dans l'approximation de Born.

Pour résumer nos résultats, nos calculs dans l'approximation de Born avec les GSFs et les différents potentiels modèles reproduisent, comme d'autres calculs théoriques, certaines caractéristiques des TDCSs expérimentales, mais pas toutes. Dans la plupart des cas, des différences importantes ont été observées pour le ratio entre les pics binaire et de recul. Concernant l'échelle absolue, des variations importantes ont été également observées ; seulement des données expérimentales absolues pourraient indiquer quel modèle est adéquat. On peut espérer avoir un meilleur accord entre les modèles théoriques et les données expérimentales si la description de l'état initial et les potentiels modèles sont améliorés, et si l'on utilise l'approximation de Born au deuxième ordre.

0.5. Chapitre 5 - Conclusions

Dans cette thèse nous avons implémenté une approche Sturmienne pour l'étude de l'ionisation simple de molécules par l'impact de photons ou d'électrons. Dans une approche à un *seul électron actif* (SAE), du *cœur gelé* (FC) et d'un *développement sur un centre* (OCE), on a étudié les processus de diffusion ; cela revient à chercher la solution d'un système d'équations non homogènes couplées angulairement, qui viennent d'une approximation perturbative au premier ordre. Si l'on décrit les cibles par un potentiel modèle central, le système est réduit à une seule équation différentielle non homogène. Les GSFs sont utilisées comme fonctions de base pour

décrire la fonction d'onde du continuum qui représente l'électron éjecté de la cible. Puisque nos GSFs ont, par construction, le comportement asymptotique correct, on peut calculer les fonctions d'onde de diffusion avec des conditions aux limites bien définies sans imposer des restrictions supplémentaires sur la base, comme généralement fait dans d'autres méthodes théoriques. Par leur propriété intrinsèque, les GSFs permettent une extraction directe des amplitudes d'ionisation, et ainsi le calcul aisé des sections efficaces. Ces sections obtenues pour diverses molécules polyatomiques sont comparées avec des données expérimentales et autres calculs théoriques, pour la PI (chapitre 3) et le processus $(e, 2e)$ (chapitre 4). Comme état initial moléculaire, nous avons utilisé les fonctions d'onde calculées par Moccia, et nous avons considéré différents potentiels modèles pour décrire l'interaction entre l'électron éjecté et l'ion parent. Comme observation générale, nous pouvons dire que nos résultats, comme bien d'autres méthodes théoriques, ne peuvent pas reproduire toutes les caractéristiques des sections efficaces que l'on observe expérimentalement. Les conclusions pour chaque processus d'ionisation sont résumées ci-après.

0.5.1. Photo-ionisation

Pour l'étude des processus de PI simple, nous commençons par valider l'approche Sturmienne pour des atomes, et en particulier avec l'atome d'hydrogène, pour lequel des résultats analytiques permettent de tester la convergence numérique et sa précision. La convergence de l'approche Sturmienne est bonne, et cela indépendamment de l'énergie de l'électron éjecté ; il n'y a pas de limitation en énergie pour étudier le continuum d'un système atomique ou moléculaire. Ceci est l'une des principales différences avec d'autres méthodes théoriques, comme celles basées sur les principes variationnels, pour lesquelles la validité de leur calculs peut être très limité par le nombre d'éléments de base considérés et leur capacité de représenter des états du continuum pour des énergies différentes. Nos sections efficaces de PI pour He et Ne sont très bonnes, particulièrement dans la jauge de *longueur* (L), en utilisant n'importe quel potentiel modèle raisonnable. Pour Ne, nous avons trouvé une désaccord de jauge important, qui est une indication de l'échec de la description de la cible et de l'utilisation de l'approximation à un SAE. Il est clair que les effets de cœur ne peuvent être négligés.

Après avoir validé la méthode avec les atomes, nous avons étudié la PI de molécules. Plusieurs difficultés apparaissent, par la nature multicentrique du Hamiltonien de la cible et l'orientation aléatoire de la molécule relative au référentiel du laboratoire. Concernant le Hamiltonien, afin de simplifier nos calculs, nous utilisons les approximations SAE et le OCE. Concernant l'orientation, nous adoptons deux approches : les schémas pré- et post-moyennés, avec des potentiels modèles molécu-

laires. Nous avons calculé les sections efficaces de PI pour les orbitales de valence externes et internes pour CH_4, NH_3, H_2O, SiH_4 et H_2S, molécules pour lesquelles on considère que le OCE est valide. Pour les jauges L ou V, et pour les orbitales de valence externes, nos sections efficaces dans les schémas pré- et post-moyennés sont similaires, particulièrement pour les hautes énergies incidentes. Proche du seuil d'ionisation, en revanche, nous observons des différences importantes entre les deux schémas, et cela pour les deux jauges. En général, la jauge V, dans le schéma post-moyenné, donne le meilleur accord entre les données expérimentales et nos résultats théoriques. La description de l'ionisation des orbitales de valence internes est plus délicate, parce que l'interaction avec les autres électrons liés est plus forte ; il n'est donc pas surprenant que nos résultats montrent un accord moins bon avec les données expérimentales, spécialement pour la jauge L. Mais là encore, nos résultats avec la jauge V sont acceptables, particulièrement pour des photo-électrons de haute énergie.

Nous avons aussi étudié les *sections efficaces différentielles angulaires* (ADCSs) pour les mêmes cibles, et avons présenté le paramètre d'asymétrie β correspondant. Pour les molécules plus "symétriques", à savoir le CH_4 et le NH_3, nous avons obtenu des bons résultats en comparaison avec les données expérimentales disponibles. Pour les autres cas, comme le H_2O et le H_2S, nos résultats ne sont pas bons. Nous avons aussi trouvé que le schéma post-moyenné donne la meilleure description du paramètre d'asymétrie, où les différentes moments cinétiques sont couplés. En effet, ce sont les interférences entre les ondes partielles de la fonction d'onde de diffusion qui engendrent les distributions angulaires.

L'étude de l'ionisation moléculaire n'est pas facile, comme il peut être apprécié avec toutes nos comparaisons ; signalons que l'accord entre diverses approches théoriques est assez réduit. Comme les GSFs ont, par construction, le comportement asymptotique correct, les améliorations doivent être effectués dans la description de la fonction d'onde de l'état initial ainsi que dans la description des interactions à plusieurs corps. Enfin, plus de données expérimentales seraient bien utiles pour vérifier les différentes approches théoriques sur tout le spectre d'énergie, particulièrement proche du seuil d'ionisation.

0.5.2. Collisions Électron-Molécule

Pour l'étude de l'ionisation simple de molécules par impact électronique, nous nous sommes concentrés sur les processus $(e, 2e)$ qui fournissent, par la TDCS, l'information la plus détaillée de l'ionisation. Nous avons, de nouveau, travaillé dans le cadre SAE, FC et OCE, et nous avons donné la formulation théorique dans l'approximation de Born au premier et deuxième ordre. Concernant le deuxième ordre,

on utilise la relation de clôture, et on propose une stratégie numérique. De façon similaire à l'étude de PI, nous avons d'abord validé notre approche Sturmienne avec l'atome d'hydrogène, pour lequel on a reproduit de manière très précise les TDCSs analytiques au premier ordre de l'approximation de Born, et cela pour diverses conditions cinématiques coplanaires. À partir de l'analyse des erreurs relatives, on a montré qu'on a besoin d'un nombre modéré de fonctions de base pour obtenir des résultats convergents.

Nous avons ensuite étudié le processus $(e, 2e)$ sur des molécules, particulièrement pour l'ionisation depuis les orbitales de valence externes de CH_4, H_2O et NH_3. Afin d'intégrer dans nos calculs l'orientation spatiale aléatoire des cibles, nous avons adopté une stratégie similaire au schéma post-moyenné de PI, c'est-à-dire en effectuant une rotation des fonctions d'onde de l'état initial et une moyenne angulaire —finale— des sections efficaces. Lors de l'analyse de nos résultats au premier ordre, nous avons obtenu un cadre très varié, selon les orbitales et conditions cinématiques considérées. Comme pour la PI, il faut souligner de nouveau que l'ensemble des données expérimentales n'est pas reproduit par les différents calculs théoriques disponibles dans la littérature. Les régions binaires sont généralement bien décrites, mais il y a des désaccords importants dans les régions de recul.

Pour H_2O, nos résultats concordent avec les données expérimentales, dans la région binaire comme dans la région de recul. Pour le CH_4 et le NH_3, nous avons reproduit les données expérimentales pour la région binaire, spécialement pour des électrons éjectés à basse énergie. Le décalage important du pic binaire par rapport à la direction du transfert d'impulsion indique, en revanche, la limite de la validité de l'approximation de Born au premier ordre. Contrairement au cas de H_2O, et particulièrement pour le NH_3, nous avons trouvé que il n'est pas facile de reproduire la région de recul, même si l'on utilise des potentiels qui décrivent avec précision l'interaction entre le projectile et la molécule. De plus, diverses caractéristiques des TDCSs observées expérimentalement, comme la grande largeur du pic binaire pour NH_3, ne peuvent pas être reproduits par nos résultats ou par le seul autre calcul disponible dans la littérature. Quelques possibles explications ont été proposées mais, au moment d'écrire cette thèse, aucune d'entre elles n'a encore été démontrée.

Pour terminer, rappelons que toutes les mesures disponibles pour l'ionisation de molécules par impact électronique sont sur une échelle relative. Par conséquent on ne peut faire que des comparaisons de forme entre les résultats théoriques et les données expérimentales. L'on aurait besoin de données absolues pour faire des comparaisons directes entre les différents calculs, et en particulier pour déterminer quel peut donner, au moins, la magnitude correcte du pic binaire des TDCSs.

0.5.3. Perspectives

Nous avons montré comment l'implémentation de l'approche Sturmienne permet d'étudier de façon efficace la simple ionisation de molécules par impact photonique ou électronique. Après avoir analysé l'ensemble de nos résultats il est clair que certains d'entre eux doivent être améliorés : pour la PI mentionnons la description des sections efficaces pour des électrons lents ; pour les processus $(e, 2e)$ la position du pic binaire des TDCSs, et le ratio entre les pics binaire et de recul. Une partie de la solution pourrait provenir de l'utilisation de fonctions d'onde plus précises pour l'état initial, particulièrement des fonctions à plusieurs corps, fournies par exemple par des méthodes de chimie quantique. En plus, cela devrait permettre d'étudier l'ionisation de molécules plus complexes, comme les bases de l'ADN ou des petites protéines. Pour le processus $(e, 2e)$, on peut espérer obtenir des résultats plus précis si on utilise l'approximation de Born au deuxième ordre. Dans cette thèse, nous avons proposé une stratégie numérique pour calculer les amplitudes d'ionisation correspondantes, mais on n'a pas encore obtenu des résultats numériquement acceptables ; notons qu'il bien connu que ce n'est pas facile d'obtenir une bonne convergence dans ce genre de calculs. En plus, afin d'accélérer la convergence de notre approche Sturmienne, il est souhaitable de faire une étude plus détaillée de la méthode de collocation de Levin, particulièrement avec la grille numérique utilisée dans cette thèse pour résoudre les équations différentielles.

Une autre amélioration de notre approche Sturmienne consiste à aller au delà de la SAE et de l'*approximation d'échange statique* (SEA). L'utilisation de potentiels qui décrivent plus précisément la corrélation électronique, et l'utilisation de fonctions d'onde à plusieurs corps permettent d'étudier une dynamique plus riche du noyau de la cible. Également, il serait intéressant d'étudier les effets de l'inclusion de la structure vibrationelle des noyaux. Elle pourrait expliquer les structures observées dans certaines sections efficaces d'ionisation. Au niveau du calcul numérique, soulignons que nous n'utilisons pas des MOs adaptées à la symétrie, notamment pour les états du continuum ; leur utilisation pourrait aider à améliorer nos temps de calcul.

On peut envisager l'adaptation de l'approche Sturmienne pour étudier l'ionisation multi-photonique. Dans cette thèse nous avons montré comment l'implémenter pour étudier des processus du premier ordre (simple PI, par exemple). L'extension au deuxième ordre ou à des ordres supérieurs est, en principe, relativement directe ; on utiliserait les GSFs pour chaque états intermédiaire ou final. Par ailleurs, la solution à l'équation non homogène permettrait d'étudier des processus dépendant du temps, comme l'interaction avec des impulsions laser courtes et le contrôle cohérent. En effet, l'approche Sturmienne est bien adaptée à ce type de problèmes : la base même a le comportement asymptotique correcte, et il est facile d'extraire tout dé-

phasage attribué à un potentiel non Coulombien. Citons, comme exemple, le calcul du "time-delay" d'Eisenbud–Wigner–Smith.

Une autre application directe de la méthode est l'ionisation double de molécules par impact électronique (aussi appelé processus $(e, 3e)$). Dans ce cas on a besoin de fonctions d'onde à deux électrons actifs (à trois corps). De manière similaire au cas de l'atome d'hélium, on peut utiliser une expansion sur deux ensembles de GSFs couplés angulairement, avec les énergies adéquates. Un autre option est d'utiliser les coordonnées hypersphériques, qui facilitent la construction des conditions aux limites du continuum double (front hypersphérique). L'application de l'approche Sturmienne à l'ionisation double de molécules par impact des électron (ou protons) est encore inexploitée.

Pour terminer, signalons que sur une ligne de recherche séparée, des GSFs moléculaires pour états liés sont actuellement à l'étude. Cela est l'objet d'une collaboration entre l'Université de Lorraine, l'Universidad Nacional del Sur et l'Universidad de Buenos Aires.

Chapter 1

Introduction

1.1. Motivations and Generalities

The study of collision processes has always played a central role in quantum mechanics: it allows one to probe the electronic structure of the target and the nature of the interactions between the projectile and the target. Collision processes of atoms and molecules by impact of photons or electrons have been studied for decades, both experimentally and theoretically. However, from a theoretical point of view, many of the original challenges still remain, in particular the description of the full spectrum of the target. Over the years, different methods have been proposed in order to calculate with a high degree of precision the bound states (in particular the ground state) of atoms and molecules, such as *density functional theory* (DFT) or variational calculations using, e.g., Gaussian functions. Difficulties arise when studying the corresponding continuum states, since they are represented by wavefunctions oscillating up to infinity, and many of such methods fail or are not good enough. It is well known that the representation of these continuum wavefunctions in terms of basis sets can be very expensive in terms of computational resources. The description of both initial and final states and the interaction between them are key ingredients to study ionization in atomic or molecular systems.

Single ionization processes, induced by collision of photons (*photoionization* (PI)) or by electrons (also known as $(e,2e)$), play an important role beyond atomic and molecular physics, since they have a wide variety of applications, from astrophysics and plasma physics to environmental and medical physics. Many of the theoretical tools developed can be adapted also to study different interactions in condensed matter and solid state physics. Then, it is necessary to have efficient tools that describe with enough precision all such ionization phenomena, in particular when long-range interactions (as the Coulomb potential) are involved.

In Fig. 1.1 we schematize the single PI process for either an atomic or a molecular target; in such case, besides, the ionized target, only one electron is present in the final channel: the ejected one. Similarly, in Fig 1.2 we illustrate $(e,2e)$ processes, where there are two electrons in the final channel: the scattered and the ejected ones. Both ejected and scattered (if any) electrons interact with the parental ion. In Fig. 1.3 the spectrum of an H atom and a bound-free transition are schematized. As mentioned above, two of the essential ingredients are the initial and final states. For the former ones, decaying exponential asymptotic conditions are imposed to the corresponding wavefunctions. It means that they have a finite spatial extent. For continuum states, the wavefunctions have also well defined asymptotic conditions, in general in terms of outgoing or incoming waves which, in contrast to the bound case, have an infinite extent. For ionization problems, one of the most difficult tasks (or at least one of the most critical) for a given theoretical method relies in its ability to impose such well defined boundary conditions to the scattering wavefunctions. Among the variety of methods developed over the years, not all of them can comply with this formal task.

Although such ionization processes have been studied theoretically in some depth for atomic systems, the same cannot be stated for molecular systems. The corresponding Hamiltonian is multicenter and then highly non-central, making the problem, in comparison to the atomic case, more difficult to deal with. Indeed, the absence of any spherical symmetry couples different angular momenta from different *atomic orbitals* (AOs) that form the corresponding *molecular orbitals* (MOs), and thus convergence of "traditional" methods is considerably more difficult to achieve. Additionally, there are various many-body effects that can be important in ionization processes, such as the relaxation of all MOs, due to the creation of a hole (ionized electron), or the change of the remaining pair correlation energies because of such relaxation. Besides, an issue which does not arise in the study of ionization of atoms is the orientation of the molecular target. In most experiments the molecule is randomly oriented and this must be taken into account within a theoretical approach. To deal with part of these difficulties associated with the molecular

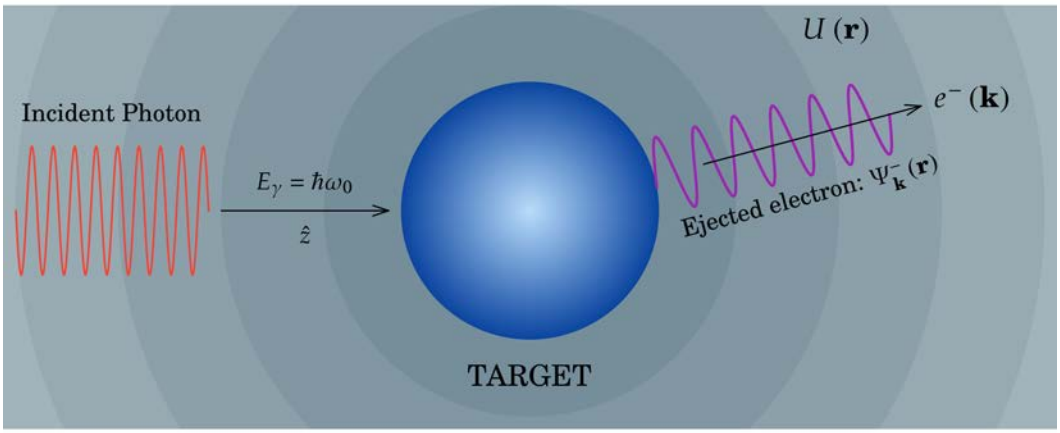

FIGURE 1.1 – Scheme of the PI process on an atomic or molecular target, represented in blue. The ejected electron in the final channel (purple and right-solid arrow) is under the influence of the potential $U(\mathbf{r})$ of the remaining ionized target.

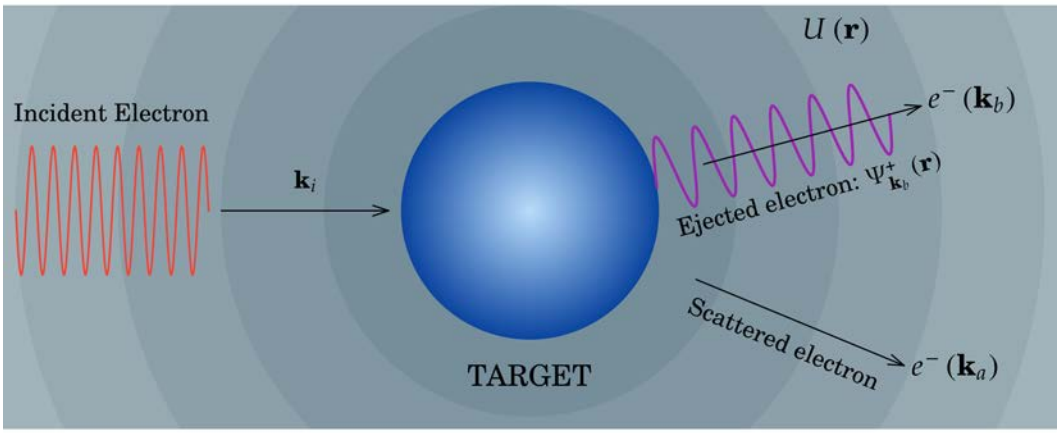

FIGURE 1.2 – Scheme of the electron impact ($\mathbf{k}_i$) ionization process on an atomic or molecular target, represented in blue. Additionally to the ejected electron ($\mathbf{k}_b$) we have a scattered electron ($\mathbf{k}_a$); their roles can be interchanged. Both are under the influence of the potential $U(\mathbf{r})$ of the ionized target.

nature of the target, several methods have been put forward, and applications range from the smallest molecule, H_2, up to, e.g., DNA bases. The success of each method depends on the studied molecule and the involved energy range, the validity of some approximations, and possibly on convergence issues or limitations related to the numerical implementation.

In this thesis we are interested in a Sturmian approach to study single ionization processes by photon or electron impact. It is based on a spectral method with Sturmian-type functions, for which different implementations have been proposed

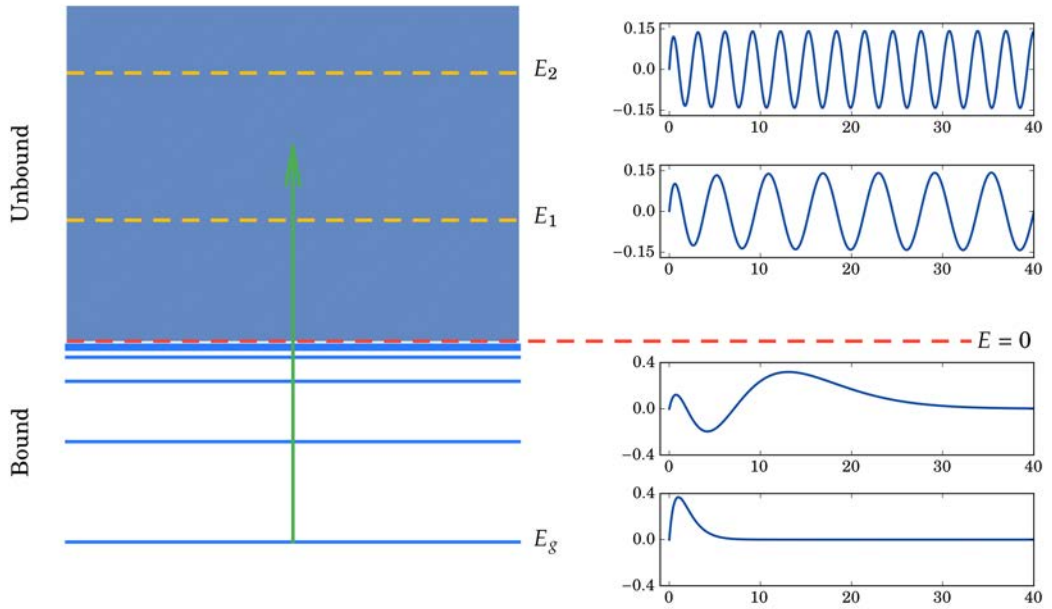

Figure 1.3 – Scheme of bound and unbound states of an H atom; a bound-free transition is represented by a vertical arrow (green). In the left panel we represent the bound and the continuum energy levels. In the right panel we plot the corresponding wavefunctions for two selected bound states and two continuum states.

in the literature. Coulomb–Sturmians functions have been used, for example, to study the spectra of atoms [18–23] and molecules [23–26], three-body Coulomb problems [27] and different ionization processes in atoms, as PI [28–30] or as by impact of electrons, protons or ions [31–35]. *Generalized Sturmian functions* (GSFs) have been introduced [1, 2] and applied to studies of atomic spectra [3, 4], and single and double ionization of atoms induced by photon [5], electron [6] or proton [7] impact. However, the implementation of any of these types of Sturmian functions to study ionization of molecular targets remains no man's land. One of the virtues of a GSF approach is that the correct asymptotic behavior of the scattering wavefunction is already incorporated, by construction, in the basis functions themselves. It is the purpose of this PhD thesis to extend, implement and apply such Sturmian approach to study single ionization (in particular PI and $(e, 2e)$) of molecular targets. In order to simplify the corresponding numerical calculations, different approximations will be made, in particular the *single active electron* (SAE) approximation. Also, for molecules, the *one-center expansion* (OCE) will be used. For that reason, a limited number of atomic and polyatomic molecular systems were chosen in order to test our Sturmian approach, namely: H, He, Ne, CH_4, NH_3 and H_2O, and to a lesser extent, SiH_4 and H_2S.

1.2. Outline

The thesis is divided into five chapters, including the introduction and the conclusions, and eight appendices with either technical aspects or supplementary material. Chapter 2 is devoted to different generalities and definitions used throughout this work: GSFs and the description of atomic and molecular targets. The GSFs are presented in Sec. 2.1, while Sec. 2.2 provides the description of the atomic and molecular targets (ground state energies and wavefunctions), together with the model potentials used to represent the electron-target interaction.

In Chap. 3 we illustrate the implementation of the Sturmian approach to study single PI in atoms and molecules. In Sec. 3.2 we briefly describe some of the experimental challenges related to the spatial orientation of the target; the theoretical description of PI is outlined in Sec. 3.3, defining the dipolar approximation and the corresponding PI cross sections; Sec. 3.4 describes the Sturmian approach and how to calculate such cross sections. Finally, in Sec. 3.5 we show some PI cross sections for atomic H, He and Ne, and in Sec. 3.6 we report our results for PI of CH_4, H_2O, NH_3, SiH_4 and H_2S, all from the corresponding valence orbitals.

In Chap. 4 we illustrate the implementation of the Sturmian approach to study $(e, 2e)$ in molecules. Similar to the previous chapter, in Sec. 4.2 we describe the challenges in experimental measurements; the theoretical description, using the Born series approximation, is given in Sec. 4.3. The Sturmian approach is explained in Sec. 4.4. Cross sections for the benchmark H atom, and the corresponding analysis of convergence, are presented in Sec. 4.5. Finally, results in the first Born approximation for CH_4, H_2O and NH_3 are given in Sec. 4.6.

The final conclusions and some perspectives are presented in Chap. 5.

In App. A the rotation operator is briefly described. In App. B we summarize different analytical integrals used in the thesis. The Fourier transform of the interaction potentials are given in App. C. The Born approximation and the Green's function are described in App. D, while details on how to calculate the integrals that appear when considering the second Born approximation are gathered in App. E. In App. F we describe Levin's collocation method, used to calculate numerically integrals with highly oscillating kernels. Finally, in App. G we present a survey of different theoretical methods that have been used to study PI on molecules, and in App. H we give a list of molecules studied theoretically in the literature.

Atomic units ($\hbar = e = m_e = 1$) are assumed throughout, unless stated otherwise.

Chapter 2

Generalized Sturmian Functions and Description of the Molecules

In this chapter we introduce the tools that are common to the remaining of this thesis: on one hand the GSFs and, on the other hand, the description of the molecular target, i.e., the initial state wavefunctions and the molecular model potentials. They are the ingredients used to study ionization of molecular targets either by photon (Chap. 3) or electron (Chap. 4) impact.

First, in Sec. 2.1.1, we start with a brief historical introduction of Sturmian functions; in Sec. 2.1.2 we define the generalized Sturmians used in this thesis, indicating their main properties, and providing some numerical aspects and an illustration in Sec. 2.1.3. In Sec. 2.2.1 we describe the model potentials used to treat atomic PI. Next, in Sec. 2.2.2, we introduce the bound wavefunctions calculated by Moccia (see Refs. [104–106]), used to describe the initial state of the molecule, in their equilibrium configuration (all needed parameters are tabulated); finally, in Sec. 2.2.3 we define the molecular model potential used to describe the interaction between the ejected electron and the ionized molecular target.

2.1. Generalized Sturmian Functions

2.1.1. Introduction

In the literature we can find different approaches to Sturmian functions, depending on the type of problem to be solved. There are essentially two lines, one associated to bound states and another to scattering problems. The first line, initiated by Shull and Löwdin [36], has been formalized by Goscinski [37] and impulsed later on by Aquilanti and coworkers [38, 39]. It is within this line that the generalized Sturmian functions were introduced by Avery and coworkers [40, 41] to deal with many electron atoms and chemical systems. On the scattering line, the work was initiated by Rawitscher [42, 43] and continued by Macek, Ovchinnikov and coworkers [44, 45]. The scattering functions proposed by Rawitscher have been extended (see Refs. [1, 2] and references therein) and used in scattering studies with the name GSFs to indicate that the basis functions are solving general atomic potentials.

Similarly to previous publications on scattering studies (see the recent review [1] and references therein), through all this work we name *Generalized Sturmian Functions* those defined below in Sec. 2.1.2; note that other authors use the same terminology to define a different class of Sturmian functions.

2.1.2. Definition and Properties

GSFs are solutions of a Sturm–Liouville problem, from which Rotenberg [46, 47] took the name. Noted in this work as $\mathcal{S}_n^{(\ell,E)}(r)$, they are regular at the origin and satisfy the two-body non-homogeneous Schrödinger equation

$$\left[-\frac{1}{2}\frac{\mathrm{d}^2}{\mathrm{d}r^2}+\frac{\ell\,(\ell+1)}{2r^2}+\mathcal{U}(r)-E\right]\mathcal{S}_n^{(\ell,E)}(r)=-\beta_n^{(\ell,E)}\mathcal{V}(r)\mathcal{S}_n^{(\ell,E)}(r), \tag{2.1}$$

where E is an externally fixed parameter and $\beta_n^{(\ell,E)}$ are the eigenvalues for a given angular momentum ℓ (called generalized charges), $\mathcal{V}(r)$ is the generating potential and $\mathcal{U}(r)$ the auxiliary potential. In general, we have that

$$\lim_{r\to\infty} r\,\mathcal{V}(r)=0, \tag{2.2a}$$

$$\lim_{r\to\infty} r\,\mathcal{U}(r)=Z, \tag{2.2b}$$

i.e., $\mathcal{V}(r)$ is a short-range potential, and it dictates the size of the inner region in which most of the dynamics is supposed to occur; on the other hand $\mathcal{U}(r)$ is a long range potential that determines the common asymptotic behavior of all GSFs, as can be easily understood by observing the asymptotic limit of Eq. (2.1)

$$\left[-\frac{1}{2}\frac{\mathrm{d}^2}{\mathrm{d}r^2}+\frac{\ell\,(\ell+1)}{2r^2}+\mathcal{U}(r)-E\right]\mathcal{S}_n^{(\ell,E)}(r)=0. \tag{2.3}$$

and will be illustrated in Fig. 2.1 below. In order to obtain a solution to the non-homogeneous Eq. (2.1), two boundary conditions must be imposed. As we are interested to study ionization problems, such conditions are

$$\lim_{r\to 0} \mathcal{S}_n^{(\ell,E)}(r) = 0, \tag{2.4a}$$

$$\lim_{r\to\infty} \mathcal{S}_n^{(\ell,E)}(r) \propto \exp\left[\pm \mathrm{i}\left(kr - \frac{Z}{k}\ln(2kr) - \ell\frac{\pi}{2} + \delta_\ell\right)\right], \tag{2.4b}$$

i.e., the regularity at the origin (2.4a) and a chosen asymptotic behavior (2.4b), where the sign "+" refers to outgoing and "−" to incoming boundary conditions; δ_ℓ is the Coulomb phase shift

$$\delta_\ell = \arg\left[\Gamma\left(\ell + 1 + \mathrm{i}\frac{Z}{k}\right)\right]. \tag{2.5}$$

Usually, the outgoing (incoming) GSF are notated $\mathcal{S}_n^{(+)}$ ($\mathcal{S}_n^{(-)}$) but we opted to keep the notation as simple as possible, i.e., without the "±" symbol. For each particular case of study the chosen behavior will be specified. The asymptotic behavior (2.4) means that, when the Coulomb potential is used as an auxiliary potential, all GSFs have the same asymptotic behavior as that of the complete Coulomb function.

Additionally, all the solutions form a complete basis set, with the potential-weighted closure and orthogonality relations [8, 9]

$$\sum_n \mathcal{S}_n^{(\ell,E)}(r')\mathcal{V}(r)\mathcal{S}_n^{(\ell,E)}(r) = \delta(r'-r), \tag{2.6a}$$

$$\int_0^\infty \mathrm{d}r\, \mathcal{S}_n^{(\ell,E)}(r)\mathcal{V}(r)\mathcal{S}_m^{(\ell,E)}(r) = \delta_{nm}, \tag{2.6b}$$

where that the integral (sum) is defined without taking the complex conjugate of the function $\mathcal{S}_{n'}^{(\ell,E)}(r)$. Since GSFs have this particular orthogonality relation, the overlap between two different functions

$$O_{nm} = \int_0^\infty \mathrm{d}r\, \mathcal{S}_n^{(\ell,E)}(r)\mathcal{S}_m^{(\ell,E)}(r), \tag{2.7}$$

converges for any energy [8].

In order to study scattering problems, the scattering wavefunction $\Psi_{\text{scatt}}(\mathbf{r})$ is usually separated in its radial and angular parts

$$\Psi_{\text{scatt}}(\mathbf{r}) = \sum_{\ell m} \frac{1}{r}\varphi_{\text{scatt}\,\ell}(r)Y_\ell^m(\hat{r}). \tag{2.8}$$

Whether the photon or electron impact ionization, $\Psi_{\text{scatt}}(\mathbf{r})$ solves a driven equation. The resulting driven radial equation takes the form (more details are given in Secs. 3.4 and 4.4)

$$\left[-\frac{1}{2}\frac{\mathrm{d}^2}{\mathrm{d}r^2} + \frac{\ell\,(\ell+1)}{2r^2} + V(r) - E\right]\varphi_{\text{scatt}\,\ell}(r) = f(r)\Phi_0(r), \tag{2.9}$$

where $V(r)$ is a two-body potential and $f(r)$ is a function that contains information about the possible transitions from the initial state $\Phi_0(r)$ (see, for instance, Eqs. (3.20) or (4.22)). To prove the convenience of using GSFs to study the scattering processes trough Eq. (2.9), we start by writing the solution to this driven equation in terms of the Green's function (see App. D)

$$\varphi_{\text{scatt}\,\ell}(r) = G_\ell f(r)\Psi_0(r), \tag{2.10}$$

where the Green's function satisfies the equation

$$\left[-\frac{1}{2}\frac{\mathrm{d}^2}{\mathrm{d}r^2} + \frac{\ell(\ell+1)}{2r^2} + V(r) - E\right] G_\ell(r, r'; E) = \delta(r - r'). \tag{2.11}$$

This function can be expanded in terms of GSFs as

$$G_\ell(r, r'; E) = \sum_n g_n^{(\ell)} \mathcal{S}_n^{(\ell,E)}(r)\mathcal{S}_n^{(\ell,E)}(r'). \tag{2.12}$$

Using Eq. (2.1) with the choice $\mathcal{U}(r) = V(r)$, Eq. (2.11) becomes

$$-\sum_n g_n^{(\ell)} \beta_n^{(\ell,E)} \mathcal{S}_n^{(\ell,E)}(r)\mathcal{V}(r)\mathcal{S}_n^{(\ell,E)}(r') = \delta(r - r'), \tag{2.13}$$

and comparing this to the closure relation (2.6a), one deduces that

$$g_n^{(\ell)} = -\frac{1}{\beta_n^{(\ell,E)}}, \tag{2.14}$$

i.e., the Green's function is diagonal in a GSF representation. Since the asymptotic region is associated with the range of the generating potential $\mathcal{V}(r)$, this also means that by definition the GSFs have the correct asymptotic behavior. Indeed, from Eq. (2.1), it is possible to obtain

$$G_\ell \mathcal{V}(r)\mathcal{S}_n^{(\ell,E)}(r) = -\frac{1}{\beta_n^{(\ell,E)}}\mathcal{S}_n^{(\ell,E)}(r), \tag{2.15}$$

i.e., GSFs are eigenfunctions of the operator $G_\ell\mathcal{V}(r)$, with eigenvalues $-1/\beta_n^{(\ell,E)}$.

More details on the GSFs used here are given in Refs. [1, 2, 9] and references therein.

2.1.3. Numerical Solutions and Some Examples

In order to generate numerically GSFs, Eq. (2.1) is solved first using a finite difference scheme of fourth order. The boundary condition (2.4a) is naturally fulfilled with the choice of scheme, but in order to satisfy the boundary condition (2.4b) the last element of the matrix representation of the linear operator of the differential

equation (2.1) is modified to acquire the correct value, assuming that the asymptotic behavior is already reached (see Ref. [2] for more details).

Now, the finite recurrence relation matrix obtained from Eq. (2.1), is a generalized eigenvalue problem, and it can be solved, in principle, using any numerical tool to solve linear algebra problems, as `LAPACK` [175]. However, this kind of approach brings many difficulties due to numerical instabilities, probably related to the short range character of the generating potential. For that reason, Mitnik *et al* [2] decided to implement a complex-orthogonal transformation, based on the works by Luk and Qiao [176], and using the implicit QR (factorization) method with the Wilkinson shift [177], replacing all unitary transformations by complex-orthogonal transformations. More details are given in Ref. [2].

In Fig. 2.1 we plot, separately, the real and imaginary parts of several GSFs, for a fixed energy $E = 0.5$ a.u. They were calculated using as auxiliary potential a Coulomb potential with charge $Z = -1$ and as generating potential a Yukawa potential, i.e.

$$\mathcal{U}(r) = -\frac{1}{r}, \tag{2.16a}$$

$$\mathcal{V}(r) = -\frac{e^{-\alpha_s r}}{r}, \tag{2.16b}$$

with $\alpha_s = 0.01$ and $\alpha_s = 0.07$. It is possible to appreciate that all functions reach exactly the same asymptotic behavior, in particular to the end of the box, where the match with the analytical outgoing asymptotic Coulomb wave, given in Eq. (2.4b), is perfect. The rate at which such functions reach the desired behavior is mediated by the decaying rate of the generating (short-range) potential, in this case by the value of α_s. This choice of potentials to generate the GSFs is used throughout the rest of the thesis, modifying only α_s, which we use as an energy-dependent parameter.

In conclusion, the use of GSFs allows one to simplify the description of continuum states and of ionization processes, since a significant part of the physical problem (the correct asymptotic behavior) is already solved by the basis itself. When solving the collision driven equation with the Sturmian approach (see Secs. 3.4 and 4.4) the basis need to concentrate on (i.e., to describe) the dynamics of the inner region; this is translated to a computationally efficient method, characterized by a rapid convergence (see, for instance Secs. 3.5.1 and 4.5.1). Another advantage of the use of GSFs is that their second derivative is already defined through their differential equation (2.1), and there is no need to calculate it explicitly; such derivative is given in terms of the generating and auxiliary potentials, and on the eigenvalues $\beta_n^{(\ell,E)}$. The method based on GSFs, called Sturmian approach, is able to deliver results with high accuracy and low computational cost. For scattering calculations there is not a rigorous way to perform efficiency comparisons; some estimations were given

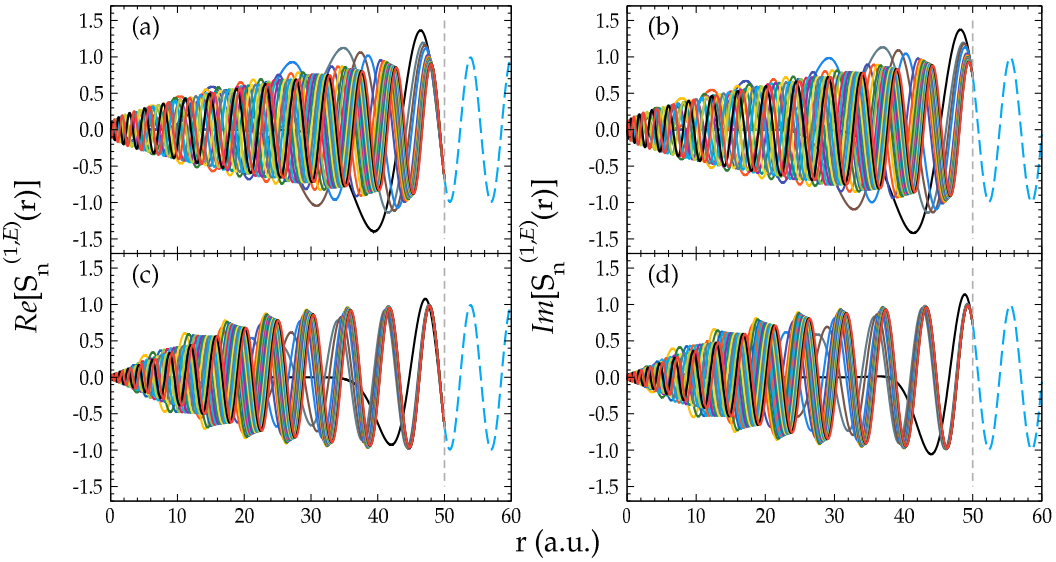

Figure 2.1 – 20 GSFs, with a fixed energy $E = 0.50$ a.u. and $\ell = 1$, obtained solving Eq. (2.1), in $r \in [0, 50]$, together with a Coulomb auxiliary potential with charge $Z = -1$, and a Yukawa potential as a generating potential with two different parameters α_s: **(a)** real and **(b)** imaginary part of the GSFs, using $\alpha_s = 0.01$, and **(c)** real and **(d)** imaginary parts using $\alpha_s = 0.07$. The exact Coulomb (analytic) regular function (blue, dash) is also shown. All functions are normalized so that they have a unit modulus at large distances.

in Refs. [5, 10] for three-body break-up problems. Comparisons between GSFs and state-of-the-art methods showed that our methodology improves the numerical efficiency by at least an order of magnitude. Recently, in a study of double PI of He by Randazzo *et al* [5], it was shown that the Sturmian approach could reproduce very precisely *exterior complex scaling* (ECS) differential cross sections with a substantial gain (more than 50%) in memory storage of the Hamiltonian matrix. The built in properties make GSF set very adequate and efficient to deal with scattering problems.

2.2. Description of Atomic and Molecular Targets

Since the idea is to use the GSFs together with the SAE approximation to study ionization of atoms and molecules, we need to implement model potentials that play the role of a scattering potential. In the next subsections we describe briefly such model potentials.

2.2.1. Atomic Model Potentials

For atoms, as explained in Refs. [12, 13], we use three different model potentials adapted to specific atomic systems, here He and Ne. For each potential, we calculate

by diagonalization the corresponding wavefunction of the valence orbitals, and the obtained energies are given in Tab. 2.1.

2.2.1.1. Herman–Skillman Potential

For He, we start with a modified *Herman–Skillman* (HS) potential [11, 48], given by

$$V_{\mathrm{HS}}(r) = \frac{Z_1}{r} + \left(Z_2 + \frac{Z_3}{r}\right) \mathrm{e}^{-\alpha r}, \tag{2.17}$$

with the parameters $Z_1 = Z_3 = -1$, $Z_2 = -2$ and $\alpha = 3.5499$. The one-electron energy obtained by diagonalization of (2.17) is given in Tab. 2.1, and is in good agreement with the experimental first ionization energy [95]. The effective charge $Z_{\mathrm{eff}}(r) = -rU(r)$ is shown in Fig. 2.2: for $r = 0$ its value is that of the nuclear charge $Z_N = 2$, and asymptotically it reaches the value 1, indicating a single ionized atom, He^+ in this case.

Table 2.1 – One-electron energies for valence electrons for different atoms. Each valence level is indicated. For He we use the HS (2.17) or the DIM (2.20) potentials, while for Ne we use the PAR (2.18) or the DIM potentials. All the energies are compared with experimental first-ionization energies I_0.

System	Model Pot.	level	Eigenvalue (a.u.)	I_0 (a.u.)
He	HS	$1s$	−0.903 717	0.903 569 [95]
	DIM		−0.903 679	
Ne	PAR	$2p$	−0.795 237	0.792 482 [96]
	DIM		−0.850 410	

2.2.1.2. Parametric Potential

For Ne, we use a slightly different model potential: the *parametric* (PAR) potential given by Rogers *et al* in Ref. [49]. In order to construct this potential, we start by defining the *parent configuration* as the electronic configuration of the remaining ion after the ionization process, and the resulting free electron is called *running electron*. The potential is defined as

$$V_{\mathrm{par}}(r) = -\frac{1}{r}\left[(Z_N - \nu) + \sum_{n=1}^{n_{\max}} N_n \, \mathrm{e}^{-\alpha_n r}\right], \tag{2.18}$$

where Z_N is the nuclear charge, $n_{\max}$ is the maximum value of n for the parent configuration, N_n is the number of electrons in the n-th shell, α_n is the screening parameter for electrons in shell n given in [49], and

$$\nu = \sum_{n=1}^{n_{\max}} N_n \tag{2.19}$$

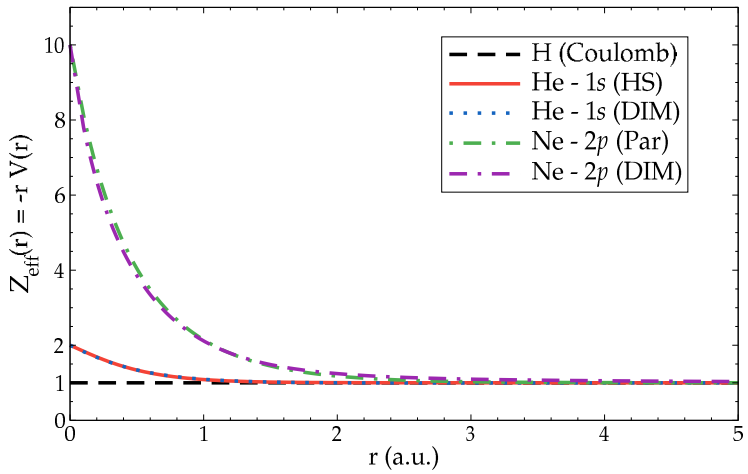

Figure 2.2 – Effective charges $Z(r) = -rV(r)$, associated with the different model potentials implemented in this work: the Coulomb potential (black, dashed); the HS potential (2.17) for He (red, solid); the PAR potential (2.18) for Ne (blue, dot-dashed) and the DIM potential for He (blue, dotted) and Ne (purple, dot-dash-dashed).

is the total number of electrons for the parent ion. Different coefficients for different parent configurations are given in Tab. 2.2. The effective charge associated with this potential, $Z_{\text{eff}}(r) = -rV_{\text{par}}(r)$, is shown in Fig. 2.2 for the Ne atom. Similarly to the case of HS potential, for $r = 0$ the effective charge is the same as the nuclear charge; as r grows $Z_{\text{eff}}(r)$ decreases due to the electronic screening and reaches the value of 1, that is to say the asymptotic charge that the running electron sees. The eigenenergies for valence electrons of Ne, obtained by diagonalization of (2.18), are given in Tab. 2.1.

Table 2.2 – Screening parameters for different atomic parent configurations, for the PAR potential (2.18). Taken from Ref. [49].

n	N_n	Parent configuration	α_1	α_2	α_3
1	1	$1s$	1.2929	−0.5110	0.2881
	2	$1s^2$	0.8855	0.2549	−0.0901
2	3	$2s$	0.2781	−0.0109	0.0275
	4	$2s^2$	0.2602	0.2755	−0.1445
	⋮	⋮	⋮	⋮	⋮
	9	$2s^2 2p^5$	0.3448	0.9838	−0.4094
	10	$2s^2 2p^6$	0.3386	1.1323	−0.4904

2.2.1.3. Depurated Inversion Method

Finally, for both He and Ne, another model potential we considered is that obtained with the *depurated inversion method* (DIM) [50], which includes the exchange

potentials for specific orbitals of noble gases by inverting the corresponding *Hartree–Fock* (HF) wavefunctions. The associated effective charge, $Z_{\text{eff}}(r) = -rV(r)$ can be written then as

$$Z_{\text{eff}}(r) = \sum_{j=1}^{n} \alpha_j \, \mathrm{e}^{-\beta_j r} + 1 \tag{2.20}$$

where the restriction $\sum_j \alpha_j = Z_N - 1$ guarantees that $Z_{\text{eff}} = Z_N$ at $r = 0$; also $Z_{\text{eff}} \to 1$ asymptotically, as desired. The parameters $\{\alpha_j, \beta_j\}$ for He and Ne are given in Tab. 2.3, the corresponding energies in Tab. 2.1, and the effective charge is shown in Fig. 2.2.

Table 2.3 – Parameters $\{\alpha_j, \beta_j\}$ for the DIM potential (2.20), for He and Ne atoms.

Atom	$n\ell$	α_j	β_j
He	$1s$	−0.317 45	5.043 72
		1.317 45	2.500 32

Atom	$n\ell$	α_j	β_j
Ne	$2p$	1.353 049	8.569 480
		0.335 881	0.464 942
		7.311 070	2.090 634

2.2.2. Molecular Orbitals

Consider an active electron placed in the MO i of the ground state of a molecular system, and denote $\phi_i(\mathbf{r})$ the corresponding wavefunction. In this work, we shall take the MOs given by Moccia in Refs. [104–106]; they are expressed as

$$\phi_i(\mathbf{r}) = \sum_{j=1}^{N_i} A_{ij} \mathcal{R}_j(r) S_{\ell_j}^{m_j}(\hat{r}), \tag{2.21}$$

where N_i is the number of basis elements and $S_{\ell_j}^{m_j}(\hat{r})$ are the real spherical harmonics [167]; the N radial wavefunctions are given in terms of *Slater-type orbitals* (STOs)

$$\mathcal{R}_j(r) = \alpha_j \, r^{n_j - 1} \, \mathrm{e}^{-\zeta_j r}, \tag{2.22}$$

where

$$\alpha_j = \left[\frac{\left(2\zeta_j\right)^{2n_j+1}}{\left(2n_j\right)!} \right]^{1/2}, \tag{2.23}$$

with tabulated integers n_j and exponents ζ_j. These MOs allow one to calculate analytically, in a partial-wave expansion, the different angular and radial integrals in which they appear in collision calculations (see Chaps. 3 and 4). For practical purposes, in some cases it is more convenient to change the real spherical harmonics into the

more familiar, complex, spherical harmonics, transforming the real coefficients A_{ij} into complex ones B_{ij}, then

$$\phi_i(\mathbf{r}) = \sum_{j=1}^{N_i} B_{ij} \mathcal{R}_j(r) Y_{\ell_j}^{m_j}(\hat{r}). \tag{2.24}$$

In ket notation we have

$$|i\rangle = \sum_{j=1}^{N_i} B_{ij} \left| j \ell_j m_j \right\rangle , \tag{2.25}$$

where

$$\left\langle \mathbf{r} \right| \left. j \ell_j m_j \right\rangle = \mathcal{R}_j(r) Y_{\ell_j}^{m_j}(\hat{r}). \tag{2.26}$$

2.2.2.1. CH_4

The ground state electronic structure of methane is $1a_1^2\, 2a_1^2\, 1t_2^6\, {}^1A_1$. In this work we will study ionization from the outer valence orbital $1t_2$ (that is triply degenerated) and from the inner valence $2a_1$. The equilibrium configuration of the molecule, and the corresponding energies, are given in Tab. 2.4; the STO parameters $\left(n_j, \ell_j, m_j, \zeta_j\right)$ and the expansion coefficients B_{ij} are given in Tab. 2.5, for each MO i. All these data were provided by Moccia in Ref. [104].

2.2.2.2. NH_3

The ground state electronic structure of ammonia is $1a_1^2\, 2a_1^2\, 1e^4\, 3a_1^2\, {}^1A_1$. In this work we will study ionization from the outer valence orbital $3a_1$, and from the inner valence $1e$ (that is doubly degenerated) and $2a_1$ orbitals. The equilibrium configuration of the molecule, and the corresponding energies, are given in Tab. 2.6. The basis parameters and the expansion coefficients B_{ij} are given in Tab. 2.7. All these data were provided by Moccia in Ref. [105].

2.2.2.3. H_2O

The ground state electronic structure of water is $1a_1^2\, 2a_1^2\, 1b_2^2\, 3a_1^2\, 1b_1^2\, {}^1A_1$. In this work we will study ionization from the outer valence orbital $1b_1$ and from the inner valence $3a_1$. The equilibrium configuration of the molecule, and the corresponding energies, are given in Tab. 2.8. The basis parameters and the expansion coefficients B_{ij} are given in Tab. 2.9. All these data were provided by Moccia in Ref. [106].

2.2.2.4. SiH_4

The ground state of silane is $1a_1^2\, 2a_1^2\, 1t_2^6\, 3a_1^2\, 2t_2^6$. In this work we will study PI only from the outer valence orbital $2t_2$ (triply degenerated) and from the inner valence

Table 2.4 – **Left:** Equilibrium position (R_n, θ_n, ϕ_n) of each H atom respect to the center of mass for CH_4. **Right:** Energies for the two valence orbitals of the molecule. All data from Ref. [104].

R_n	θ_n	ϕ_n
2.0800	54.73°	45.00°
2.0800	54.73°	225.00°
2.0800	125.27°	135.00°
2.0800	125.27°	315.00°

MO	E_0 (a.u.)
$2a_1$	−0.9204
$1t_2$	−0.5042

Table 2.5 – STO basis parameters and complex expansion coefficients B_{ij}, taken from Ref. [104], employed to calculate, using Eq. (2.24), $2a_1$ and $1t_2$ orbitals of CH_4.

$2a_1$					$1t_{2z}$				
n_j	ℓ_j	m_j	ζ_j	B_{ij}	n_j	ℓ_j	m_j	ζ_j	B_{ij}
1	0	0	9.5	0.008 770	4	2	±2	2.400	∓0.047 313
1	0	0	5.5	−0.212 48	4	2	±2	1.900	±0.231 750 i
2	0	0	1.5	0.982 04	2	1	0	1.373	1.2600
4	0	0	2.0	0.050 760	3	1	0	2.950	−0.057 620
4	0	0	3.0	−0.017 990	4	1	0	2.950	−0.267 38
7	3	±2	2.9	±0.100 790 i	7	3	0	2.900	−0.086 950

$1t_{2x}$					$1t_{2y}$
n_j	ℓ_j	m_j	ζ_j	B_{ij}	B_{ij}
4	2	±1	2.400	0.047 334 i	±0.047 334
4	2	±1	1.900	−0.231 820 i	∓0.231 820
2	1	±1	1.373	∓0.890 93	−0.890 930 i
3	1	±1	2.950	±0.040 729	0.040 729 i
4	1	±1	2.950	±0.189 08	0.189 080 i
7	3	±1	2.900	∓0.037 696	−0.037 696 i
7	3	±3	2.900	±0.048 614	−0.048 614 i

$3a_1$. The equilibrium configuration of the molecule, and the corresponding energies, are given in Tab. 2.10. The basis parameters and the expansion coefficients B_{ij} are given in Tab. 2.11. All these data were provided by Moccia in Ref. [104].

2.2.2.5. H_2S

Finally, the ground state electronic structure of hydrogen sulfide is $1a_1^2\,2a_1^2\,1b_2^2\,3a_1^2\,1b_1^2\,4a_1^2\,2b_2^2\,5a_1^2\,2b_1^2$. In this work we will study PI from the outer valence orbital $2b_1$ and from the inner valence $5a_1$. The equilibrium configuration of the molecule, and the corresponding energies, are given in Tab. 2.12. The basis parameters and the expansion coefficients B_{ij} are given in Tab. 2.13. All these data were provided by Moccia in Ref. [106].

Table 2.6 – **Left:** Equilibrium position (R_n, θ_n, ϕ_n) of each H atom respect to the center of mass for NH_3. **Right:** Energies for the three valence orbitals of the molecule. All data from Ref. [105].

R_n	θ_n	ϕ_n
1.9280	108.90°	90.00°
1.9280	108.90°	210.00°
1.9280	108.90°	330.00°

MO	E_0 (a.u.)
$2a_1$	−1.1224
$1e$	−0.5956
$3a_1$	−0.4146

Table 2.7 – STO basis parameters and complex expansion coefficients B_{ij} taken from [105], employed to calculate, using Eq. (2.24), the $2a_1$, $1e$ and $3a_1$ orbitals of NH_3.

				$2a_1$	$3a_1$
n_j	ℓ_j	m_j	ζ_j	B_{ij}	B_{ij}
1	0	0	11.00	0.011 570	0.006 050
1	0	0	6.400	−0.232 68	−0.064 610
2	0	0	1.75	0.751 14	0.243 13
2	0	0	1.28	0.125 76	−0.141 77
2	0	0	2.56	0.147 93	0.075 100
3	2	0	1.60	−0.078 300	−0.014 400
3	2	0	2.35	0.006 590	−0.006 990
2	1	0	1.34	−0.143 57	0.954 05
2	1	0	1.99	−0.018 260	−0.295 04
2	1	0	2.90	−0.009 380	0.401 88
4	3	0	2.00	0.049 920	−0.040 980
4	3	±3	2.00	0.056 660 i	−0.017 112 i

				$1e_x$	$1e_y$
n_j	ℓ_j	m_j	ζ_j	B_{ij}	B_{ij}
3	2	±1	1.60	±0.132 890	0.132 890 i
3	2	±1	2.35	∓0.026 234	−0.026 234 i
3	2	±2	1.60	∓0.162 130 i	−0.162 130
3	2	±2	2.35	±0.037 349 i	0.037 349
2	1	±1	1.34	∓0.709 26	−0.709 260 i
2	1	±1	1.99	±0.202 08	0.202 080 i
2	1	±1	2.90	∓0.220 40	−0.220 410 i
4	3	±1	2.00	±0.028 341	0.028 341 i
4	3	±2	2.00	±0.042 992 i	0.042 992

2.2.3. Molecular Model Potential

To study ionization of molecules, we shall use the SAE approximation [53] for the initial state wavefunction. We then need a molecular model potential that plays the role of a scattering potential. For an active electron in the MO i, the molecular

Table 2.8 – **Left:** Equilibrium position (R_n, θ_n, ϕ_n) of each H atom respect to the center of mass for H_2O. **Right:** Energies for the two valence orbitals of the molecule. All data from Ref. [106].

R_n	θ_n	ϕ_n
1.8140	53.27°	90.00°
1.8140	53.27°	270.00°

MO	E_0 (a.u.)
$3a_1$	−0.5561
$1b_1$	−0.4954

Table 2.9 – STO basis parameters and complex expansion coefficients B_{ij} given in Ref. [106], employed to calculate, using Eq. (2.24), the $3a_1$ and $1b_1$ orbitals of H_2O.

$3a_1$					$1b_1$				
n_j	ℓ_j	m_j	ζ_j	B_{ij}	n_j	ℓ_j	m_j	ζ_j	B_{ij}
1	0	0	12.60	−0.008 480	2	1	±1	1.51	∓0.509 69
1	0	0	7.45	0.082 410	2	1	±1	2.44	∓0.081 544
2	0	0	2.20	−0.307 52	2	1	±1	3.92	∓0.175 78
2	0	0	3.24	−0.041 320	3	2	±1	1.60	∓0.038 700
2	0	0	1.28	0.149 54	3	2	±1	2.40	∓0.002 849 6
2	1	0	1.51	0.799 79	4	3	±1	1.95	∓0.006 611 4
2	1	0	2.44	0.004 830	4	3	±3	1.95	±0.019 028
2	1	0	3.92	0.244 13					
3	2	0	1.60	0.059 350					
3	2	0	2.40	0.003 960					
3	2	±2	1.60	−0.065 711					
3	2	±2	2.40	0.012 063					
4	3	0	1.95	−0.019 290					
4	3	±2	1.95	−0.046 620					

model potential we shall use is the following [51, 52]

$$V_{i\,\mathrm{mol}}(\mathbf{r},\mathbf{R}) = -\sum_{n=1}^{M}\frac{Z_n}{|\mathbf{r}-\mathbf{R}_n|} + \sum_{j=1}^{N_{\mathrm{MO}}}\mathcal{N}_{ij}\int \mathrm{d}\mathbf{r}'\,\frac{\left|\phi_j(\mathbf{r}')\right|^2}{|\mathbf{r}-\mathbf{r}'|}, \tag{2.27}$$

where M is the number of nuclei in the molecule, Z_n is the charge of each nucleus, $\mathbf{R}_n$ is the position of each nucleus with respect to the molecule center of mass, N_{MO} is the number of MOs and $\mathcal{N}_{ij} = 2-\delta_{ij}$. This potential is the direct term within the *static exchange approximation* (SEA). For the sake of simplicity, the nuclei $\mathbf{R}_n$ dependence, collectively represented as $\mathbf{R}$, is omitted hereafter.

As we use the MO in a STOs expansion, the molecular model potential (2.27) can be calculated analytically. To do so, we first expand the electron-electron and the electron-nuclei interactions in partial waves through

$$\frac{1}{|\mathbf{r}-\mathbf{r}'|} = \sum_{\lambda=0}^{\infty}\sum_{\mu=-\lambda}^{\lambda}\frac{4\pi}{2\lambda+1}\frac{r_<^{\lambda}}{r_>^{\lambda+1}}Y_\lambda^{\mu}(\hat{r})Y_\lambda^{\mu*}(\hat{r}'), \tag{2.28}$$

Table 2.10 – **Left:** Equilibrium position (R_n, θ_n, ϕ_n) of each H atom respect to the center of mass for SiH_4. **Right:** Energies for the two valence orbitals of the molecule. All data from Ref. [104].

R_n	θ_n	ϕ_n
2.7870	54.73°	45.00°
2.7870	54.74°	225.00°
2.7870	125.27°	135.00°
2.7870	125.27°	315.00°

MO	E_0 (a.u.)
$3a_1$	−0.7119
$2t_2$	−0.4391

Table 2.11 – STO basis parameters and complex expansion coefficients B_{ij} taken from Ref. [104], employed to calculate, using Eq. (2.24), the $3a_1$ and $2t_2$ orbitals of SiH_4.

$3a_1$					$2t_{2z}$				
n_j	ℓ_j	m_j	ζ_j	B_{ij}	n_j	ℓ_j	m_j	ζ_j	B_{ij}
1	0	0	19.00	−0.008 680	3	2	±2	1.15	±0.328 890 i
1	0	0	12.60	0.072 770	4	2	±2	2.15	∓0.046 436 i
2	0	0	4.85	−0.216 470	2	1	0	4.85	−0.163 450
3	0	0	1.30	1.298 000	3	1	0	1.30	0.856 850
4	0	0	1.15	−0.364 630	4	1	0	1.20	0.061 340
4	3	±2	1.50	±0.131 440 i	4	3	0	1.50	−0.118 160

$2t_{2x}$					$2t_{2y}$
n_j	ℓ_j	m_j	ζ_j	B_{ij}	B_{ij}
3	2	±1	1.15	−0.328 980 i	∓0.328 980
4	2	±1	2.15	0.046 450 i	±0.046 450
2	1	±1	4.85	±0.115 570	0.115 570 i
3	1	±1	1.30	∓0.605 830	−0.605 830 i
4	1	±1	1.20	∓0.043 388	−0.043 381 i
4	3	±1	1.50	∓0.051 216	−0.051 216 i
4	3	±3	1.50	±0.066 065	−0.066 065 i

where $r_< \equiv \min(r, r')$ and $r_> \equiv \max(r, r')$. With such expansions, and the MO given by Eq. (2.24), the molecular model potential (2.27) can be rewritten as

$$
\begin{aligned}
V_i(\mathbf{r}) = \sum_{\lambda\mu} \frac{4\pi}{2\lambda+1} \Bigg[& -\sum_{n=1}^{M} Z_n \frac{\min(r, R_n)^\lambda}{\max(r, R_n)^{\lambda+1}} Y_\lambda^\mu(\hat{r}) Y_\lambda^{\mu *}\left(\hat{R}_n\right) \\
& + \sum_{j=1}^{N_{\mathrm{MO}}} \mathcal{N}_{ij} \sum_{k=1}^{n} \sum_{l=1}^{n} B_{jk}^* B_{jl} \int_0^\infty r'^2 \mathrm{d}r' \, \mathcal{R}_k(r') \frac{r_<{}^\lambda}{r_>{}^{\lambda+1}} \mathcal{R}_l(r') \\
& \times Y_\lambda^\mu(\hat{r}) \int \mathrm{d}\hat{r}' \, Y_{\ell_k}^{m_k *}(\hat{r}') Y_\lambda^{\mu *}(\hat{r}') Y_{\ell_l}^{m_l}(\hat{r}') \Bigg] .
\end{aligned}
\tag{2.29}
$$

The radial integral in the second term of this potential can be calculated analytically

Table 2.12 – **Left:** Equilibrium position (R_n, θ_n, ϕ_n) of each H atom respect to the center of mass for H_2S. **Right:** Energies for the two valence orbitals of the molecule. All data from Ref. [106].

R_n	θ_n	ϕ_n
2.5090	44.70°	90.00°
2.5090	44.70°	270.00°

MO	E_0 (a.u.)
$5a_1$	−0.4543
$2b_1$	−0.3506

Table 2.13 – STO basis parameters and complex expansion coefficients B_{ij} given in Ref. [106], employed to calculate, using Eq. (2.24), the $5a_1$ and $2b_1$ orbitals of H_2S.

$5a_1$					$2b_1$				
n_j	ℓ_j	m_j	ζ_j	B_{ij}	n_j	ℓ_j	m_j	ζ_j	B_{ij}
1	0	0	22.00	0.003 760	3	2	±1	1.40	∓0.028 914
1	0	0	14.00	−0.035 570	4	2	±1	1.40	∓0.016 737
2	0	0	5.80	0.103 340	2	1	±1	5.77	∓0.144 730
3	0	0	1.57	−0.776 260	3	1	±1	1.56	∓0.945 540
4	0	0	1.57	0.581 990	4	1	±1	1.56	±0.252 030
3	2	0	1.40	0.071 910	4	3	±1	1.25	∓0.016 850
4	2	0	1.40	0.043 630	4	3	±3	1.25	±0.023 306
3	2	±2	1.40	−0.047 291					
4	2	±2	1.40	−0.033 969					
2	1	0	5.77	−0.180 200					
3	1	0	1.56	1.126 200					
4	1	0	1.56	−0.193 360					
4	3	0	1.25	−0.003 820					
4	3	±2	1.25	−0.069 502					

using the explicit form of the STOs (2.22) (see App. B), and is given by

$$\begin{aligned}\frac{\vartheta_{ij}^{(\lambda)}(r)}{r} &= \int_0^\infty \mathrm{d}r'\, r'^2 \mathcal{R}_i(r') \frac{r_<^\lambda}{r_>^{\lambda+1}} \mathcal{R}_j(r') \\ &= \alpha_i \alpha_j \left[\frac{1}{r^{\lambda+1}} \zeta_{ij}^{-\beta_{ij\lambda}} \gamma\left(\beta_{ij\lambda}, \zeta_{ij} r\right) + r^\lambda \zeta_{ij}^{-\delta_{ij\lambda}} \Gamma\left(\delta_{ij\lambda}, \zeta_{ij} r\right) \right], \end{aligned} \tag{2.30}$$

where $\zeta_{ij} = \zeta_i + \zeta_j$, $\beta_{ij\lambda} = n_i + n_j + \lambda + 1$, $\delta_{ij\lambda} = n_i + n_j - \lambda$; $\gamma(n, x)$ and $\Gamma(n, x)$ are the incomplete and the complement gamma functions [168] (see more details in App. B.3). The remaining angular integral in the second term of (2.29) can also be calculated analytically, and is given by Eq. (B.2) in terms of the Wigner 3-j symbols [167].

Collecting these results, the analytical form of the molecular model poten-

tial (2.27) reads

$$V_i(\mathbf{r}) = \sum_{\lambda\mu} \frac{4\pi}{2\lambda+1} \left[-\sum_{n=1}^{M} Z_n \frac{\min(r,R_n)^\lambda}{\max(r,R_n)^{\lambda+1}} Y_\lambda^\mu(\hat{r}) Y_\lambda^{\mu*}\left(\hat{R}_n\right) + \sum_{j=1}^{N_{\mathrm{MO}}} \mathcal{N}_{ij} \sum_{k,l=1}^{n} (-1)^{m_k+\mu} B_{jk}^* B_{jl} \frac{\vartheta_{kl}^{(\lambda)}(r)}{r} \Upsilon_{\ell_k\lambda\ell_l}^{-m_k,-\mu,m_l} Y_\lambda^\mu(\hat{r}) \right]. \tag{2.31}$$

In the different implementations of this potential, as to study PI or $(e,2e)$ processes, we need to calculate the matrix elements $V_{i\,\ell'\ell}^{\,m'm}(r) = \langle \ell' m' | V_i(\mathbf{r}) | \ell m \rangle$. Using the analytical formula given above, together with the angular integral (B.2), it is straightforward to calculate such matrix elements

$$V_{i\,\ell'\ell}^{\,m'm}(r) = (-1)^{m'} \sum_{\lambda\mu} \frac{4\pi}{2\lambda+1} \Upsilon_{\ell'\lambda\ell}^{-m',\mu,m} \left[-\sum_{n=1}^{M} Z_n \frac{\min(r,R_n)^\lambda}{\max(r,R_n)^{\lambda+1}} Y_\lambda^{\mu*}\left(\hat{R}_n\right) + \sum_{j,k,l} \mathcal{N}_{ij} (-1)^{m_k+\mu} B_{jk}^* B_{jl} \frac{\vartheta_{kl}^{(\lambda)}(r)}{r} \Upsilon_{\ell_k\lambda\ell_l}^{-m_k,-\mu,m_l} \right]. \tag{2.32}$$

In a typical ionization experiment the molecules are randomly oriented, and this must be taken into account. Although this is not the proper way to proceed, we may consider as starting point an angular average of the model potential (2.27), i.e., a central potential

$$U_{i\,\mathrm{mol}}(r) = \frac{1}{4\pi} \int_{4\pi} \mathrm{d}\hat{r}\, V_{i\,\mathrm{mol}}(\mathbf{r}). \tag{2.33}$$

Using Eq. (2.32), this angular averaged potential can also be calculated analytically, from only one matrix element, and reads $U_{i\,\mathrm{mol}}(r) = V_{i\,00}^{\,00}(r)$. Such an averaging procedure is illustrated through Fig. 2.3, where the effective charges $rV_{i\,\mathrm{mol}}(\mathbf{r})$ for several set of angles (θ,ϕ), and for $rU_{i\,\mathrm{mol}}(r)$, are compared in the case of H_2O. The effective charges go from -8 at $r=0$ and to -1 asymptotically. The local minimum is at $r \approx 1.8140$ a.u., i.e. at the equilibrium position of each H atom (see Tab. 2.8); its depth and sharpness depend on the orientation and whether the angular average has been performed or not.

As we use an independent particle approximation, some many-body aspects (i.e., correlation) are only included indirectly through the use of MO in Eq. (2.27) but not explicitly.

Finally, to study electron impact ionization (Chap. 4), we shall need the Fourier transform of the molecular model potential

$$\mathcal{V}_i(\mathbf{k}) = \int \mathrm{d}\mathbf{r}\, \mathrm{e}^{\mathrm{i}\,\mathbf{k}\cdot\mathbf{r}}\, V_i(\mathbf{r}). \tag{2.34}$$

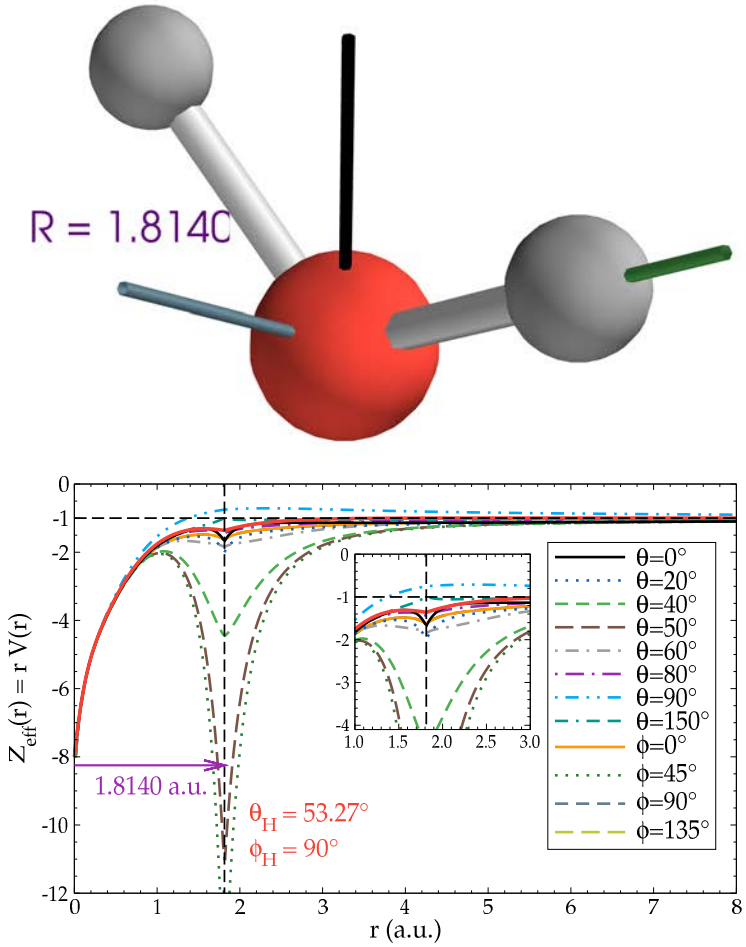

FIGURE 2.3 – **Upper panel:** Representation of the H_2O molecule at its equilibrium configuration given in Tab. 2.8; the mean equilibrium distance is indicated. **Bottom panel:** Molecular model (2.27) and angular averaged (2.33) (red, solid) potentials for H_2O, at indicated angles. The potentials in green, black and gray correspond to the variation along the lines on the figure of the upper panel.

Making use of the integrals given in App. C, in particular Bethe's integral (C.1) and Eq. (C.4), such transform, i.e., the potential in the momenta space, reads

$$\mathcal{V}_i(\mathbf{k}) = -\frac{4\pi}{k^2}\sum_{n=1}^{M} Z_n e^{i\,\mathbf{k}\cdot\mathbf{R}_n} + \Theta(\mathbf{k}), \tag{2.35}$$

where $\Theta(\mathbf{k})$ is given in Eq. (C.11).

The molecular model potential (2.27) can be improved in many aspects. One of them is the inclusion of exchange. Also, as we use an independent particle approximation, some many-body effects (i.e., correlation) are only included indirectly through the use of MO in the definition of the potential, but not explicitly.

Chapter 3

Photoionization

In this chapter we deal with the *photoionization* (PI) of atoms and molecules. After a short introduction (Sec. 3.1), in Sec. 3.2 we explain briefly most common experimental PI measurements, defining the quantities that can be measured and calculated; also the issue of the experimental determination of the molecular spatial orientation at the moment of the electron ejection is stated. In Sec. 3.3 we describe the theoretical apparatus used to study PI; in Sec. 3.4 we show how the Sturmian approach can be implemented to study PI, in particular to calculate PI cross sections. Our results for atomic systems are given in Sec. 3.5, where a particular attention is given to the convergence of the GSF basis; results for molecular systems are in Sec. 3.6, where two different approaches to deal with the random orientation of the molecule are explained. Finally, the discussion of our results are in Sec. 3.7.

3.1. Introduction

The quantum description of both bound and unbound orbitals is necessary to study collisions with atoms and molecules. The study of single PI provides an indirect tool to test our capacity to describe the target before and after the interaction correctly and thus correlation and many-body effects. PI plays an important

role beyond atomic and molecular physics, since it has a wide variety of applications, such as astrophysics [75, 76, 206], planetary [77–79], atmospheric [80, 81], plasma [82–84] or medical physics [85, 86]. Also PI helps to understand different processes in surfaces, such as structural changes upon surface adsorption, quantifying the relationship between shape resonances and the bond lengths [87–90]; or to characterize the relation between gas, chemisorbed and solid-state phases in surface reactions [91–94].

In order to calculate the transition amplitudes for single PI in atomic or molecular systems, many considerations must be taken into account. Usually the starting point is the treatment of the ionized electron as a one-electron function, the OCE. For molecules, the vibrational structure can be ignored in many cases, especially in high energy collisions, justifying the use of the *Born–Oppenheimer* (BO) approximation. Also, in order to simplify the calculations of the corresponding scattering wavefunctions, the *frozen core* (FC) approximation and the SEA are considered. In the literature it is possible to find many different theoretical approaches to study PI, that use (or not) the already mentioned approximations (see App. G for a comprehensive list of such methods). Our goal is to implement, with the help of a molecular model potential (described in Sec. 2.2.3), the generalized Sturmian approach, within a BO, FC, SEA and OCE framework. As explained in Sec. 2.1, one of the advantages of such a method is that it ensures that the continuum wavefunction has the correct asymptotic behavior. To assess the validity of our approach, we first study single PI in atoms, comparing the calculated cross sections with theoretical and experimental data found in the literature. After that we study PI for several small molecules, comparing also with available theoretical and experimental data.

In the study of the interaction of a radiation field (a photon) with a molecular target several processes may occur. Consider a photon of energy $E_\gamma = \hbar\omega$, such that $E_\gamma > I_0$, where I_0 is the ionization potential of the molecule. Once it strikes a polyatomic molecule RA in an initial vibrational state ν_0 (R is the polyatomic radical and A is an individual atom), the different outcomes may be

$$\hbar\omega + \mathrm{RA}(\nu_0) \rightarrow \begin{cases} \mathrm{RA}^+ + e^-(\ell) & \text{Photoionization,} \\ \mathrm{R}^* + \mathrm{A}^* & \text{Photodissociation,} \\ \mathrm{R}^* + \mathrm{A}^{+*} + e^-(\ell) & \text{Dissociative photoionization.} \end{cases} \tag{3.1}$$

If we have a dissociation process, the final products can be in an excited state. If we have an ejected electron, called photoelectron, it has a defined angular momentum ℓ. In this contribution, we will concentrate only on single PI which can be considered as a "half-scattering" processes, involving a bound-free transition.

3.2. Experimental Measurements

Interaction of radiation with matter is one of the fundamental tools to understand the physical world, but the use of feasible light-sources is always challenging. Historically, the use of synchrotron radiation (see, for instance, Refs. [54, 55]) was one of the main sources of UV light. Recently, different laser configurations allows one to access the continua of different atomic and molecular systems.

In single PI, as represented through the reaction (3.1), the process yields a photoelectron in the continuum and a residual ion (or several ions, in case of subsequent photofragmentation). The emission of such photoelectron can be characterized by five dynamical quantities [56]: the cross section σ, which is a measure of the probability that an absorbed photon will produce ionization [56, 169]; the angular distribution of the ejected electron, characterized by the asymmetry parameter β [169]; and three spin polarization parameters of the emitted photoelectron and the ion [57]. We will concentrate only in the first two quantities: PI cross sections and the asymmetry parameter β. Observables related with consequent processes as fluorescence or Auger decay are not considered.

To observe the products of a PI process, it is necessary the use of a detector sensitive to the selected product species and possibly to a specific polarization, and which can be oriented in space relative to the incoming photon beam of a given polarization. Then, the detector signal will depend on the properties of the incoming photon beam. The spatial orientations of the photon beam and the gas beam (target species) are described with two coordinate systems, one defined in the collision frame and the other in the detector frame, both fixed at the target (for more details, see, for example, Ref. [54]). In a typical PI experiment only the energy (and also the angular distribution) of the produced species is measured. In the case of molecules, the specific orientation of the target with respect to the photon beam (or the polarization of the radiation field) cannot be reconstructed from such measurements, and remains as one of the experimental unknowns. This is an important fact to keep in mind at the moment of studying theoretically ionization of systems that do not have spherical symmetry, as in the case of molecules.

Amongst all experimental methods developed in the past (see, for instance, Ref. [56]), we can mention here absorption measurements [58, 59], electron spectrometry [60, 61], charge analysis of ions [62, 63] and fluorescence spectrometry [64, 65]. Most of these are developed to deal with emitted photoelectrons and, again, without resolving the spatial orientation of the target. Only a few advanced experimental techniques can perform a full angle-resolved spectroscopy, such as the one based on ultrashort pump-probe laser pulses [66, 67, 192] and the full kinematic experiments as COLTRIMS (cold target recoil ion momentum spectroscopy) [68].

3.3. Theoretical Description

3.3.1. The Dipolar Approximation

As mentioned above, PI involves a bound-free transition for which one needs to know only the initial state Ψ_0 of the target, usually its ground state (energy E_0), and the final state of the ionized electron. The transition operator, that connects both initial and final states, is described semi-classically via the dipolar approximation; the dipolar operator in both *length gauge* (L) and *velocity gauge* (V) reads

$$\widehat{D}^{(\mathrm{L})} = -\hat{\boldsymbol{\varepsilon}} \cdot \mathbf{r}, \tag{3.2a}$$

$$\widehat{D}^{(\mathrm{V})} = -\hat{\boldsymbol{\varepsilon}} \cdot \mathbf{p}, \tag{3.2b}$$

where $\hat{\boldsymbol{\varepsilon}}$ gives the polarization of the field. In this work we consider linear polarization along the z direction. From the these definitions, it is clear that the dipolar operator in the L gauge puts —at larger distances— a larger weight than in the V gauge. Results obtained with any of the two gauges are exactly the same only if exact wavefunctions are used. In any other approximate case, the agreement between both gauges provides a quality test of the involved wavefunctions.

The major task is to calculate accurately the wavefunction Ψ of the photoelectron, that is an electron in a continuum state of the ionized atomic or molecular target, with an energy $E = k^2/2$ defined by the energy of the incident photon $E = E_\gamma - I_0$. Such continuum wavefunctions are more difficult to calculate than the low-lying bound-states as they oscillate up to infinity. They are solutions of the *time-dependent Schrödinger equation* (TDSE) or the *time-independent Schrödinger equation* (TISE), with well defined properties. They must be regular at the origin of the coordinate system, and the asymptotic boundary conditions are given by the superposition of an incoming-wave Coulomb function plus an incoming spherical wave, generated by the non-Coulomb part of the molecular potential [170]

$$\lim_{r\to\infty} \Psi^{(-)} \propto \mathrm{e}^{-\mathrm{i}\left(kz + \frac{Z}{k}\ln k(r-z)\right)} + f\left(\hat{k},\hat{r}\right)\frac{1}{r}\,\mathrm{e}^{-\mathrm{i}\left(kr - \frac{Z}{k}\ln(2kr)\right)}, \tag{3.3}$$

where $f\left(\hat{k},\hat{r}\right)$ is the transition amplitude and $Z = -1$ for an initial neutral target.

3.3.2. Photoionization Cross Sections

Two of the dynamical quantities that can be measured are the *angular differential cross section* (ADCS) and the PI cross section. The first is defined as [169]

$$\frac{\mathrm{d}^2\sigma}{\mathrm{d}E\,\mathrm{d}\Omega_k} = \frac{\overline{\sigma}}{4\pi}\left[1 + \beta(E)\,P_2(\cos\theta_k)\right], \tag{3.4}$$

where E is the energy of the ejected electron, θ_k is the photoelectron ejection angle with respect to the polarization vector of the incident field (photon), $P_2(\cos\theta)$ is a Legendre polynomial of degree 2, β is the angular distribution (or asymmetry) parameter and $\overline{\sigma}$ is the total PI cross section. The ADCS involves all the interferences between the partial waves of the ejected electron, which is strongly influenced by the motion of the other bound electrons [69]; it can therefore be used as a sensitive test of the description of the interaction electron-ionized target.

The PI cross section is defined as [169]

$$\frac{\mathrm{d}\sigma}{\mathrm{d}E} = \frac{\pi e^2}{m^2\hbar^2 c}\omega^{(\mathrm{g})}\left|\langle\Psi|\,\widehat{D}^{(\mathrm{g})}\,|\Psi_0\rangle\right|^2, \tag{3.5}$$

where c is the speed of light and $\omega^{(\mathrm{L})} = E - E_0$ or $\omega^{(\mathrm{V})} = (E-E_0)^{-1}$ are the difference between final and initial energies in either L or V gauges. As mentioned in Sec. 3.2, from this definition it is clear that cross sections are a measure of the probability than a photon absorbed by an electron in a state Ψ_0 will be ionized to a final state Ψ.

In the case of molecular targets, both the angular distribution (3.4) and the energy differential cross sections (3.5) depend also on the orientation of the molecules. As described in Sec. 3.2, generally one must consider a random orientation of the molecule when it interacts with the radiation field. In order to do that, and to define properly the pre- and post-averaged schemes, two different coordinates systems, whose origin coincide with the center of mass of the target, are considered [70]: the laboratory frame, $\mathbf{r}'$, defined by the polarization axis of the electric field, and a molecular-fixed frame, $\mathbf{r}$, defined by the axis of highest symmetry. Let β and α be the polar angles of this molecular axis with respect to the laboratory frame, and let the set of Euler angles $\hat{\mathfrak{R}} = (\alpha, \beta, \gamma)$ denote hereafter the molecular orientation. A rotation $\hat{\mathfrak{R}}$ will bring the molecular fixed frame into coincidence with the laboratory frame. The rotated dipolar operators in both L (3.2a) and V (3.2b) gauges, for a linearly polarized field (axis z), in the laboratory frame are

$$z' = \left(\frac{4\pi}{3}\right)^{1/2}(-r)\sum_{\mu=-1}^{+1} Y_1^{\mu}(\hat{r})\mathscr{D}^1_{0\mu}\left(\hat{\mathfrak{R}}\right), \tag{3.6a}$$

$$p'_z = -\,\mathrm{i}\sum_{\mu=-1}^{+1}\mathscr{D}^1_{0\mu}\left(\hat{\mathfrak{R}}\right)\nabla_\mu, \tag{3.6b}$$

where $\mathscr{D}^1_{0\mu}\left(\hat{R}\right)$ is the rotation matrix [167] (see App. A for more details), it rotates the operator to the molecular frame; ∇_μ gives the spherical tensor components of the gradient operator [167]. In order to calculate a cross section for a randomly oriented molecule, we must calculate first the orientation-dependent transition amplitudes

appearing in Eq. (3.5), and then perform an angular average over $\hat{\mathfrak{R}}$, defined as

$$\int \mathrm{d}\hat{\mathfrak{R}}\, f\left(\hat{\mathfrak{R}}; x\right) \equiv \frac{1}{8\pi^2} \int_0^{2\pi} \mathrm{d}\alpha \int_0^{\pi} \sin\beta\, \mathrm{d}\beta \int_0^{2\pi} \mathrm{d}\gamma\, f\left(\hat{\mathfrak{R}}; x\right), \tag{3.7}$$

of the square modulus of such transition amplitudes.

3.4. Sturmian Approach to Photoionization

As we are mainly interested in PI of molecules, hereafter we shall develop our Sturmian approach for the general case (where atomic targets are a sub-case) considering an arbitrary potential $U\left(\mathbf{r}; \hat{\mathfrak{R}}\right)$, such as the one given by Eq. (2.27). The Hamiltonian can be written as

$$\widehat{\mathcal{H}} = \widehat{\mathcal{H}}_0 + \widehat{W}(t), \tag{3.8}$$

where $\widehat{\mathcal{H}}_0 = \widehat{T} + U\left(\mathbf{r}; \hat{\mathfrak{R}}\right)$ is the field-free Hamiltonian of the target with $\hat{\mathfrak{R}} = (\alpha, \beta, \gamma)$ the set of Euler angles that specify the spatial orientation of the molecule; $\widehat{T}$ is the kinetic energy operator, and

$$\widehat{W}(t) = \begin{cases} -F^{(\mathrm{L})}(t)\, \hat{\boldsymbol{\varepsilon}} \cdot \mathbf{r} = F(t)\, \widehat{D}^{(\mathrm{L})}, & \text{length gauge} \\ -F^{(\mathrm{V})}(t)\, \hat{\boldsymbol{\varepsilon}} \cdot \mathbf{p} = F(t)\, \widehat{D}^{(\mathrm{V})}, & \text{velocity gauge} \end{cases} \tag{3.9}$$

where $F^{(\mathrm{g})}(t)$ is the electric field in the L gauge or the vector potential in the V gauge, $\hat{\boldsymbol{\varepsilon}}$ gives the polarization of the field and $\widehat{D}$ are the dipolar operators (3.2); $F(t)$ contains the time-dependent profile of the radiation field.

We begin with the TDSE for the total Hamiltonian (3.8)

$$\left(\mathrm{i}\frac{\partial}{\partial t} - \widehat{\mathcal{H}}\right) \Psi\left(\mathbf{r}, t; \hat{\mathfrak{R}}\right) = \left(\mathrm{i}\frac{\partial}{\partial t} - \widehat{\mathcal{H}}_0 - \widehat{W}(t)\right) \Psi\left(\mathbf{r}, t; \hat{\mathfrak{R}}\right) = 0, \tag{3.10}$$

and propose the general solution to be

$$\Psi\left(\mathbf{r}, t; \hat{\mathfrak{R}}\right) = \mathrm{e}^{-\mathrm{i}\,\omega_0 t} \left[\Phi^{(0)}\left(\mathbf{r}; \hat{\mathfrak{R}}\right) + \Psi_{\mathrm{scatt}}\left(\mathbf{r}, t; \hat{\mathfrak{R}}\right)\right], \tag{3.11}$$

where $\Phi^{(0)}\left(\mathbf{r}; \hat{\mathfrak{R}}\right)$ is the wavefunction of the initial ground state of the molecule, usually the active MO to ionize, with energy ω_0, and $\Psi_{\mathrm{scatt}}\left(\mathbf{r}, t; \hat{\mathfrak{R}}\right)$ is the wavefunction of the photoelectron, with energy $\omega = E$ (in atomic units). Replacing (3.11) in (3.10), we obtain

$$\left[\mathrm{i}\frac{\partial}{\partial t} - \omega_0 - \widehat{\mathcal{H}}_0 - \widehat{W}(t)\right] \Psi_{\mathrm{scatt}}\left(\mathbf{r}, t; \hat{\mathfrak{R}}\right) = \widehat{W}(t)\, \Phi^{(0)}\left(\mathbf{r}; \hat{\mathfrak{R}}\right). \tag{3.12}$$

Now, if we apply a Fourier transform to (3.12), we obtain the TISE

$$\begin{aligned} \left(\omega - \omega_0 - \widehat{\mathcal{H}}_0\right) \Psi_{\mathrm{scatt}}\left(\mathbf{r}, \omega; \hat{\mathfrak{R}}\right) - \frac{1}{\sqrt{2\pi}} \int_{-\infty}^{\infty} \mathrm{d}\omega'\, \widehat{\mathcal{W}}(\omega') \Psi_{\mathrm{scatt}}\left(\mathbf{r}, \omega - \omega'; \hat{\mathfrak{R}}\right) \\ = \widehat{\mathcal{W}}(\omega)\, \Phi^{(0)}\left(\mathbf{r}; \hat{\mathfrak{R}}\right), \end{aligned} \tag{3.13}$$

where $\widehat{\mathcal{W}}(\omega)$ is the Fourier transform of $\widehat{W}(t)$.

Eq. (3.13) contains the interaction with the field to all orders, and therefore $\Psi_{\text{scatt}}\left(\mathbf{r},\omega;\hat{\mathfrak{R}}\right)$ contains information over all possible processes. Considering the integral term of (3.13) as a perturbation, we can introduce a perturbation expansion for the scattering wavefunction [170]. Conserving only the first-order in that expansion, the scattering wavefunction is noted $\Psi^{(1)}\left(\mathbf{r},\omega;\hat{\mathfrak{R}}\right)$. This approximation allows one to study single PI, since only the transition operator $\widehat{\mathcal{W}}(\omega)$ for a single transition is kept. To first order, Eq. (3.13) results in the driven equation for the final state wavefunction

$$\left(\omega-\omega_0-\widehat{\mathcal{H}}_0\right)\Psi^{(1)}\left(\mathbf{r},\omega;\hat{\mathfrak{R}}\right)=\widehat{\mathcal{W}}(\omega)\,\Phi^{(0)}\left(\mathbf{r};\hat{\mathfrak{R}}\right). \tag{3.14}$$

This is the equation that we want to solve; the scattering wavefunction at first order, $\Psi^{(1)}\left(\mathbf{r},\omega;\hat{\mathfrak{R}}\right)$, will provide the PI information.

To solve Eq. (3.14), we separate first the scattering wavefunction in its radial and angular parts

$$\Psi^{(1)}\left(\mathbf{r},\omega;\hat{\mathfrak{R}}\right)=\frac{1}{r}\sum_{\ell m}\varphi_\ell\left(r,\omega;\hat{\mathfrak{R}}\right)Y_\ell^m(\hat{r}). \tag{3.15}$$

Usually, the radial wavefunction $\varphi_\ell\left(r,\omega;\hat{\mathfrak{R}}\right)$ is expanded in some radial basis set. Within our Sturmian approach it is expanded in a GSF set (see Section 2.1)

$$\varphi_\ell\left(r,\omega;\hat{\mathfrak{R}}\right)=\sum_j a_j^{(\ell,E)}\left(\omega;\hat{\mathfrak{R}}\right)\mathcal{S}_j^{(\ell,E)}(r). \tag{3.16}$$

Here the $\mathcal{S}_j^{(\ell,E)}(r)$ satisfy Eq. (2.1), with incoming boundary conditions

$$\lim_{r\to\infty}\mathcal{S}_n^{(\ell,E)}(r)\propto\exp\left[-\mathrm{i}\left(kr-\frac{Z}{k}\ln(2kr)-\ell\frac{\pi}{2}+\delta_\ell\right)\right], \tag{3.17}$$

where $\delta_\ell=\arg[\Gamma(\ell+1+\mathrm{i}\,Z/k)]$ is the Coulomb phase shift.

Performing an angular projection, Eq. (3.14) is converted into a set of angular-coupled differential equations

$$\sum_{\ell m}\left[\left(\omega-\omega_0+\frac{1}{2}\frac{\mathrm{d}^2}{\mathrm{d}r^2}-\frac{\ell\,(\ell+1)}{2r^2}\right)\delta_{\ell'\ell}\delta_{m'm}-U_{\ell'\ell}^{m'm}\left(r;\hat{\mathfrak{R}}\right)\right]\varphi_\ell\left(r,\omega;\hat{\mathfrak{R}}\right)=\varrho_{\ell'}^{m'}\left(r,\omega;\hat{\mathfrak{R}}\right), \tag{3.18}$$

where $U(\mathbf{r})$ is a noncentral potential, and the matrix elements are defined as

$$U_{\ell'\ell}^{m'm}\left(r;\hat{\mathfrak{R}}\right)=\langle\ell'm'|\,U\left(\mathbf{r};\hat{\mathfrak{R}}\right)|\ell m\rangle\,, \tag{3.19}$$

$$\varrho_{\ell'}^{m'}\left(r,\omega;\hat{\mathfrak{R}}\right)=r\left\langle\ell'm'\middle|\widehat{\mathcal{W}}(\omega)\middle|\Phi^{(0)}\right\rangle. \tag{3.20}$$

As mentioned in the Introduction, the use of a non-central potential to describe the molecular target couples directly the different angular momenta of the initial state.

Now, to solve the coupled system of Eqs. (3.18), we use the GSF expansion (3.16) and obtain

$$\sum_{\ell m}\sum_{j} a_j^{(\ell,E)}\left(\omega;\hat{\mathfrak{R}}\right)\left[\left(\omega-\omega_0+\frac{1}{2}\frac{\mathrm{d}^2}{\mathrm{d}r^2}-\frac{\ell\,(\ell+1)}{2r^2}\right)\delta_{\ell'\ell}\delta_{m'm}-U_{\ell'\ell}^{m'm}\left(r;\hat{\mathfrak{R}}\right)\right]\mathcal{S}_j^{(\ell,E)}(r) = \varrho_{\ell'}^{m'}\left(r,\omega;\hat{\mathfrak{R}}\right). \tag{3.21}$$

Using the definition of GSFs (2.1), the second derivative of the GSFs is replaced by terms which depend on the generating and auxiliary potentials, and on the generalized charges $\beta_j^{(\ell,E)}$. Then, if the continuum energy for which the GSFs have been calculated is E, the differential equation (3.21) is transformed into a linear system of equations

$$\sum_{\ell m}\sum_{j} a_j^{(\ell,E)}\left(\omega;\hat{\mathfrak{R}}\right)\left[\left(\omega-\omega_0-E+\mathcal{U}(r)+\beta_j^{(\ell,E)}\mathcal{V}(r)\right)\delta_{\ell'\ell}\delta_{m'm}-U_{\ell'\ell}^{m'm}\left(r;\hat{\mathfrak{R}}\right)\right]\mathcal{S}_j^{(\ell,E)}(r) = \varrho_{\ell'}^{m'}\left(r,\omega;\hat{\mathfrak{R}}\right), \tag{3.22}$$

for the unknown coefficients $a_j^{(\ell,E)}\left(\omega;\hat{\mathfrak{R}}\right)$. The final step consists in projecting (3.22) on $\mathcal{S}_i^{(\ell',E)}(r)$ (note that it is not the complex conjugate, see Eq. (2.6)). We define then the matrix elements

$$\mathcal{O}_{ij}^{(\ell'\ell,E)} = \int_0^\infty \mathrm{d}r\,\mathcal{S}_i^{(\ell',E)}(r)\,\mathcal{S}_j^{(\ell,E)}(r), \tag{3.23a}$$

$$\mathcal{U}_{ij}^{(\ell'\ell,E)} = \int_0^\infty \mathrm{d}r\,\mathcal{S}_i^{(\ell',E)}(r)\,\mathcal{U}(r)\,\mathcal{S}_j^{(\ell,E)}(r), \tag{3.23b}$$

$$\mathcal{V}_{ij}^{(\ell'\ell,E)} = \int_0^\infty \mathrm{d}r\,\mathcal{S}_i^{(\ell',E)}(r)\,\mathcal{V}(r)\,\mathcal{S}_j^{(\ell,E)}(r), \tag{3.23c}$$

$$\mathcal{P}_{ij}^{(\ell'\ell,E)\,m'm}_{\ell'\ell}\left(\hat{\mathfrak{R}}\right) = \int_0^\infty \mathrm{d}r\,\mathcal{S}_i^{(\ell',E)}(r)\,U_{\ell'\ell}^{m'm}\left(r;\hat{\mathfrak{R}}\right)\mathcal{S}_j^{(\ell,E)}(r), \tag{3.23d}$$

$$\mathfrak{h}_i^{(\ell',E)\,m'}_{\ell'}\left(\omega;\hat{\mathfrak{R}}\right) = \int_0^\infty \mathrm{d}r\,\mathcal{S}_i^{(\ell',E)}(r)\,\varrho_{\ell'}^{m'}\left(r,\omega;\hat{\mathfrak{R}}\right), \tag{3.23e}$$

which can be calculated as indicated in Refs. [1, 2]. We also note here that the element (3.23c) reduces to a Kronecker delta δ_{ij}, because of the orthogonality relation (2.6b) satisfied by GSFs. Here we kept it explicitly in order to avoid any numerical roundoff error, since it is calculated numerically on a finite grid. The linear system of equations (3.22) becomes

$$\sum_{\ell m}\sum_{j}\left\{\left[(\omega-\omega_0-E)\,\mathcal{O}_{ij}^{(\ell'\ell,E)}+\mathcal{U}_{ij}^{(\ell'\ell,E)}+\beta_j^{(\ell,E)}\mathcal{V}_{ij}^{(\ell'\ell,E)}\right]\delta_{\ell'\ell}\delta_{m'm}-\mathcal{P}_{ij}^{(\ell'\ell,E)\,m'm}_{\ell'\ell}\right\} \times a_j^{(\ell,E)}\left(\omega;\hat{\mathfrak{R}}\right) = \mathfrak{h}_i^{(\ell',E)\,m'}_{\ell'}\left(\omega;\hat{\mathfrak{R}}\right). \tag{3.24}$$

We solve numerically this linear system, using the subroutine ZGESV, of LAPACK [175], to obtain the expansion coefficients $a_j^{(\ell,E)}\left(\omega;\hat{\mathfrak{R}}\right)$.

For problems described with central potentials, as atoms, or when using the angular averaged molecular potential (2.33), there is no angular coupling, $U_{\ell'\ell}^{m'm}(r) = V(r)$ is diagonal and the dependence on the spatial orientation of the target is absent, by symmetry considerations. We then have a single driven radial equation

$$\left[\omega - \omega_0 + \frac{1}{2}\frac{\mathrm{d}^2}{\mathrm{d}r^2} - \frac{\ell\,(\ell+1)}{2r^2} - V(r)\right]\varphi_\ell(r,\omega) = \varrho_\ell^m(r,\omega). \tag{3.25}$$

After expanding the radial wavefunction in GSFs, this equation is transformed into

$$\sum_j a_j^{(\ell,E)}(\omega)\left[\omega - \omega_0 - E + \mathcal{U}(r) + \beta_j^{(\ell,E)}\mathcal{V}(r) - V(r)\right]\mathcal{S}_j^{(\ell,E)}(r) = \varrho_\ell^m(r,\omega). \tag{3.26}$$

Using the matrix elements defined by Eqs. (3.23), the linear system of equations reads

$$\sum_j \left[(\omega - \omega_0 - E)\,\mathcal{O}_{ij}^{(\ell,E)} + \mathcal{U}_{ij}^{(\ell,E)} + \beta_j^{(\ell,E)}\mathcal{V}_{ij}^{(\ell,E)} - \mathcal{P}_{ij}^{(\ell,E)}\right] a_j^{(\ell,E)}(\omega) = \mathfrak{K}_i^{(\ell,E)\,m}{}_\ell(\omega). \tag{3.27}$$

All GSFs of the basis set have the same and correct asymptotic behavior (in this case the behavior dictated by the Coulomb potential), expressed for PI as an incoming boundary condition (3.17) (see Section 2.1). This means that our basis functions possess, by construction, important physical information and need to expand essentially the inner region, whose size will be determined by the range of the driven term. This makes the basis set adequate and finally computationally efficient. Comparing the asymptotic behavior of the photoelectron wavefunction, given in Eq. (3.3), with the asymptotic property of the GSFs, we obtain the PI transition amplitude directly from the expansion coefficients of the scattering wavefunction in (3.16) [13, 14]

$$\begin{aligned} f\left(\omega,\hat{r};\hat{\mathfrak{R}}\right) &= -\sqrt{2\pi}\left\langle\Psi_{-\mathbf{k}}^{(-)}\middle|\,\widehat{W}(\omega)\,\middle|\Phi^{(0)}\right\rangle \\ &= \sum_{\ell m j} a_j^{(\ell,E)}\left(\omega;\hat{\mathfrak{R}}\right)\mathrm{e}^{-\mathrm{i}\left(\delta_\ell - \ell\frac{\pi}{2}\right)}\,Y_\ell^m(\hat{r}). \end{aligned} \tag{3.28}$$

With this result we can calculate easily the ADCS (3.4), as

$$\frac{\mathrm{d}^2\sigma\left(\hat{\mathfrak{R}}\right)}{\mathrm{d}E\,\mathrm{d}\hat{r}} = \frac{4\pi^2\,\omega(\mathrm{g})}{c}\,k\,\frac{1}{2\pi}\left|\frac{f\left(\omega,\hat{r};\hat{\mathfrak{R}}\right)}{\mathscr{F}(\omega)}\right|^2, \tag{3.29}$$

where $\omega^{(\mathrm{L})} = E - E_0$ or $\omega^{(\mathrm{V})} = (E - E_0)^{-1}$, according to the gauge choice, and $\mathscr{F}(\omega)$ is the Fourier transform of the radiation field profile $F(t)$. The PI cross section can

be obtained from this expression, after integrating over $\hat{r}$ [13], and reads

$$\frac{\mathrm{d}\sigma\left(\hat{\mathfrak{R}}\right)}{\mathrm{d}E} = \frac{4\pi^2\,\omega(\mathrm{g})}{c}\,k\,\frac{1}{2\pi}\sum_{\ell m}\left|\frac{\sum_j a_j^{(\ell,E)}\left(\omega;\hat{\mathfrak{R}}\right)}{\mathscr{F}(\omega)}\right|^2 . \tag{3.30}$$

In summary, with our Sturmian approach we can calculate easily the ADCS, through Eq. (3.29), and the PI cross section, through Eq. (3.30). Both expressions depend only on the expansion coefficients $a_j^{(\ell,E)}$, and no further integrals are needed, making the calculation of this observables very efficient.

3.4.1. Matrix Elements of the Dipolar Operator

Consider the initial state to be the MO ϕ_i, given by Eq. (2.24). Let us see how to calculate the radial functions $\varrho_{\ell'}^{m'}\left(r,\omega;\hat{\mathfrak{R}}\right)$ of the *right-hand side* (RHS) in the radial equations (3.18) or (3.25). We make use of the rotated dipolar operators (3.6), and then we only need to calculate the corresponding angular integrals.

For the L gauge, we have that

$$\varrho_{\ell'}^{m'}\left(r,\omega;\hat{\mathfrak{R}}\right) = -\mathscr{F}(\omega)r\left(\frac{4\pi}{3}\right)^{1/2}\sum_j B_{ij}\sum_{\mu=-1}^{+1}\mathscr{D}_{0\mu}^{1}\left(\hat{\mathfrak{R}}\right)\left\langle \ell' m'\right|(-r)\,Y_1^{\mu}(\hat{r})\mathcal{R}_j(r)\left|\ell_j m_j\right\rangle , \tag{3.31}$$

which, using (B.2), becomes

$$\varrho_{\ell'}^{m'}\left(r,\omega;\hat{\mathfrak{R}}\right) = -\mathscr{F}(\omega)\sum_j B_{ij}r^2\mathcal{R}_j(r)\sum_{\mu}\mathscr{D}_{0\mu}^{1}\left(\hat{\mathfrak{R}}\right)\Upsilon_{\ell' 1\ell_j}^{m'\mu m_j} . \tag{3.32}$$

Similarly for the V gauge, the radial RHS function is given by

$$\varrho_{\ell'}^{m'}\left(r,\omega;\hat{\mathfrak{R}}\right) = -\mathscr{F}(\omega)i\sum_j B_{ij}\sum_{\mu=-1}^{+1}\mathscr{D}_{0\mu}^{1}\left(\hat{\mathfrak{R}}\right)\left\langle \ell' m'\right|\nabla_{\mu}\mathcal{R}_j(r)\left|\ell_j m_j\right\rangle . \tag{3.33}$$

The angular matrix elements for the gradient operator are a little more complicated to calculate. Using the gradient formula (B.3), together with the derivative of the STOs (2.22), the RHS radial function in the V gauge becomes

$$\varrho_{\ell'}^{m'}\left(r,\omega;\hat{\mathfrak{R}}\right) = -i\mathscr{F}(\omega)\sum_j B_{ij}\Delta_{\ell'\ell_j}\left(n_j + b_{\ell'\ell_j} - 1 - \zeta_j r\right)\mathcal{R}_j(r)\sum_{\mu}\mathscr{D}_{0\mu}^{1}\left(\hat{\mathfrak{R}}\right)\Pi_{\ell' 1\ell_j}^{m'\mu m_j} , \tag{3.34}$$

where the coefficients $\Delta_{\ell'\ell_j}$ and $\Pi_{\ell' 1\ell_j}^{m'\mu m_j}$ are defined by Eqs. (B.4).

3.4.2. Considerations Over the Molecular Orientation

Before closing this section, we summarize here briefly our strategy to include the molecular orientation in our Sturmian approach. As indicated explicitly in

expressions (3.32) and (3.34) for the RHS, a specific orientation of the molecule, dictated by the Euler angles $\hat{\Re}$, is included in the RHSs. Calculations for individual spatial orientations must be performed. We used the molecular model potential (defined in Eq. (2.27), with the corresponding angular matrix elements $U_{\ell'\ell}^{m'm}\left(r;\hat{\Re}\right)$ given by Eq. (2.32)) in the radial Eq. (3.21), and solved the corresponding linear system (3.24), for a number of $\hat{\Re}$ sets. We found that using 24, 12 and 24 points for α, β and γ, respectively, were sufficient to span all possible orientations. After that, an angular average of the PI cross sections (3.30), over all possible orientations in a numerical quadrature, is performed as indicated by Eq. (3.7). We call this procedure the *post-averaged scheme*.

In the past other strategies were proposed, in order to avoid the high computational cost and numerical difficulties that such scheme implies. One of them is an angular average of the corresponding MOs (see Refs. [115]), but it was found that it works only for some special cases, such as H_2 or N_2. An alternative, proposed in Ref. [51], uses an angular averaged potential. Then the random orientation of the target is already included in the resulting central potential. We also apply and test such strategy here; the potential is defined by Eq. (2.33), and given explicitly through the angular matrix element (2.32). It is used in the radial equation (3.21), and consequently in the linear system of equations (3.27). After solving such linear system, the PI cross section (3.30) is obtained directly without need to perform any further average. This procedure is called here the *pre-averaged scheme*.

Both post- and pre-averaged schemes were employed in our calculations of PI cross sections for molecules, and the results are presented in Sec. 3.6.

3.5. Results for Atomic Systems

We start showing our results for atomic systems. We solve the linear system of equations (3.27) for a given model potential, in both L and V gauges. With the obtained expansion coefficients $a_j^{(\ell,E)}(\omega)$ we directly calculate the PI cross section via Eq. (3.30). Before we proceed to the results of our implementation of the Sturmian approach to study PI in atoms and molecules, we present first an analysis of the convergence as a function of the number of basis functions.

3.5.1. Convergence of the GSF Basis Set

In order to determine the optimal number of functions, we first calculate PI cross sections for a H atom from its ground state, for five different final photoelectron energies, E = 0.1, 0.5, 1.0, 1.5 and 2.0 a.u., in both L and V gauges. They are compared

with the analytical results of Harriman [97],

$$\frac{\mathrm{d}\sigma}{\mathrm{d}E} = \frac{2^5\pi^2}{3cE_\gamma^4}\frac{\exp\left[-\frac{4}{k}\arctan k\right]}{1-\exp\left(-\frac{2\pi}{k}\right)}, \tag{3.35}$$

where E_γ is the energy of the incident photon and $k^2 = 2E$, where E is the energy of the ejected photoelectron.

For all considered energies, we calculated the GSF basis set using a Yukawa potential with $\alpha = 0.03$ as a generating potential, and a Coulomb potential with charge -1 as auxiliary potential (see Sec. 2.1 for more details). We use between 5 and 80 basis functions, generated in a box of 50 a.u.; the relative errors are shown in Fig. 3.1. For all energies we can see that the convergence of our results is fast, and that only a moderate number of functions is needed to reproduce with sufficient accuracy the reference values. Clearly for photoelectrons with higher energies, more basis functions are needed, but the number remains moderate. The use of only 60 functions for any of our PI calculations, in either atomic or molecular systems, gives a more than sufficient precision in any studied region of the continuum.

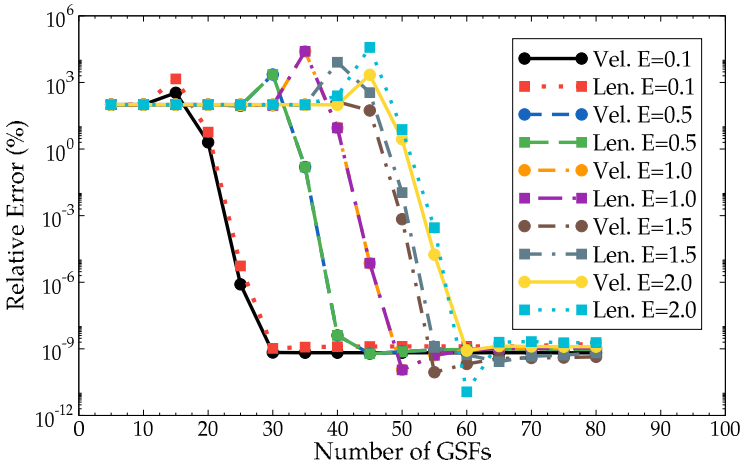

Figure 3.1 – Relative error with respect to the analytical result [97] of the H PI cross section as a function of the number of GSFs basis used in (3.30), for both L (squares) and V (circles) gauges. Five final energies E (a.u.) were considered: 0.1 (black, solid; red, dots), 0.5 (blue, dash; green, dash), 1.0 (orange, dot-dash; purple, dot-dash), 1.5 (brown, dot-dot-dash; gray, dot-dash) and 2.0 (yellow, solid; cyan, dots).

3.5.2. H Atom

We start by looking at the PI cross sections for several initial states (ground and excited, including non-s states) of the H atom, i.e., the simplest target, in order to check the validity of our Sturmian approach. Some of these results appear in

Ref. [13]. We use a pure Coulomb potential and the exact wavefunction for the corresponding initial states of the atom.

PI calculations were performed for photoelectron energies in the range [0.00, 3.00], in both L and V gauges. The final energy was chosen as the fixed energy E to generate the GSFs basis. For PI from the $1s$ state, we compare our calculated cross section with the analytical formula [97]. As can be seen in Fig. 3.2(a), the agreement between all three cross sections is perfect. In order to prove this, we calculated the relative errors, shown in Fig. 3.3, with respect to the analytical result [97]. For both gauges we obtain errors of about $10^{-9} \sim 10^{-10}$ % in the whole energy range, showing that our results with the selected parameters for the GSFs give very stable and numerically exact solutions to the TISE (3.25).

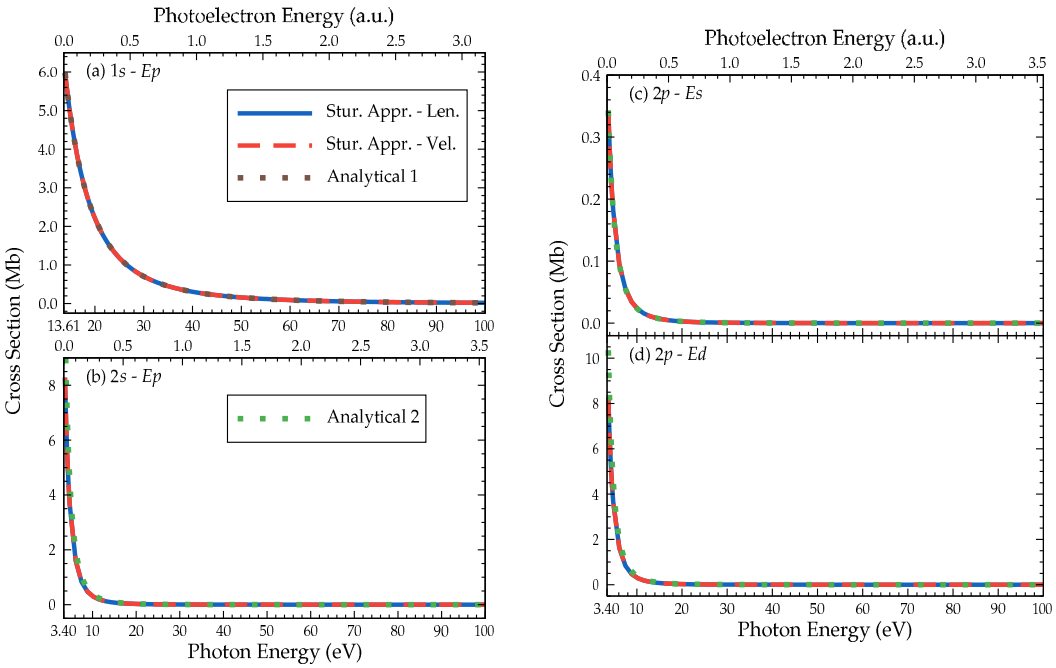

FIGURE 3.2 – PI of H atom, in Mbarns versus photon energy in eV and photoelectron energy in a.u., from different initial states. Our results in L (blue, solid) and V (red, dash) are compared with the exact analytical formula, either [97] (brown, dotted - Analytical 1), or [98] (green, dotted - Analytical 2). **(a)**: From the ground state $1s$. **(b)**: From the excited $2s$ state. **(c)**: For transitions $2p \rightarrow Es$. **(d)**: For transitions $2p \rightarrow Ed$.

Next we considered PI from different excited states, using also the corresponding exact initial state wavefunctions. For transitions from $2s$ state we plot, in Fig. 3.2(b), the PI cross section in L and V gauges, and we compare them with the analytical formula of Shafer and Bersohn [98]. Results in both gauges are identical, and they match perfectly with the analytical results, as evidenced in the relative errors given in Fig. 3.3. This time the error grows for higher energies, starting around 10^{-10} %

and finishing around 10^{-3} % for results in the V gauge and around 10^{-5} % for the L gauge. Even if the relative errors are higher than for the $1s$ case, we stress that the actual cross sections are particularly small for photoelectron energies over 0.7 a.u. (or photon energies over 20 eV). In that region, the absolute error is very small (and certainly smaller than any experimental error bars), so that our results are more than acceptable on the whole energy range.

Finally, we plot the PI cross section for transitions $2p \rightarrow Es$ in Fig. 3.2(c), and for $2p \rightarrow Ed$ in Fig. 3.2(d), for both L and V gauges. The comparison of our result with the analytical formula [98] indicates that calculations in the Sturmian approach are very accurate; the relative errors, plotted in Fig. 3.3, show the same behavior as for transitions from the $2s$ orbital.

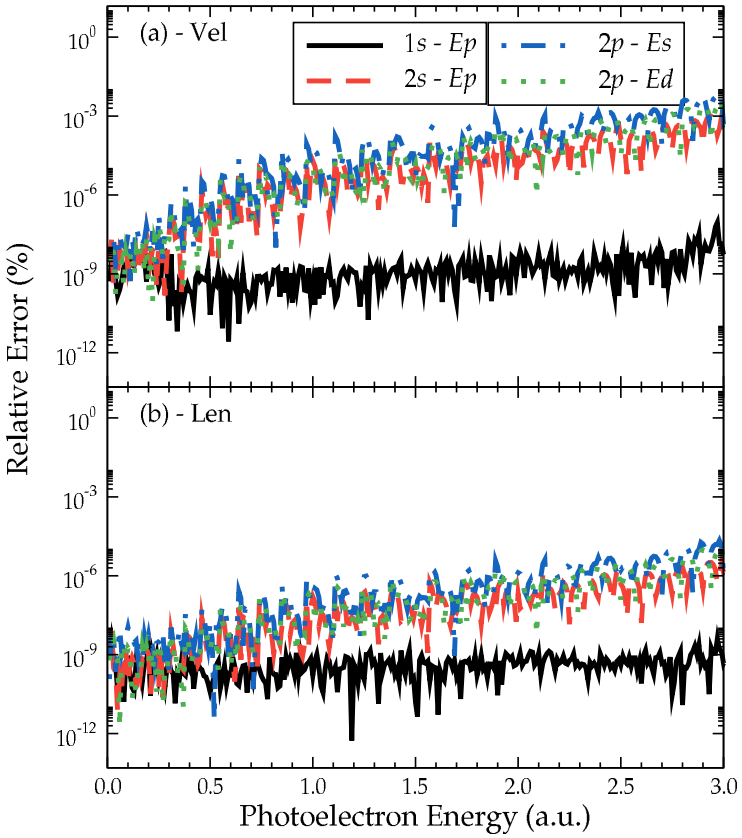

Figure 3.3 – Relative errors for the calculated PI cross sections for atomic H, shown in Figs. 3.2(a) (transitions $1s \rightarrow Ep$, black, solid), 3.2(b) ($2s \rightarrow Ep$, red, dash),3.2(c) ($2p \rightarrow Es$, blue, dot-dash) and 3.2(d) ($2p \rightarrow Ed$, green, dotted). The errors are calculated comparing with the analytical formulas given in [97] and [98]. **(a):** For the results in V gauge and **(b):** in L gauge.

The use of the Sturmian approach to study PI in H atom, gives us results that are numerically "exact", in the whole studied energy range, either from the ground or

first excited states of the target. We stress here that, for the four considered cases, we used the same basis functions for all final energies.

3.5.3. He Atom

For the case of He (results published in Refs. [12, 13]), we use the same GSFs as described in the previous section. As scattering potential we took both the HS (2.17) and the DIM (2.20) model potentials. The corresponding ground state energies (given in Tab. 2.1) and wavefunctions were obtained through diagonalization.

Our calculated PI cross sections for electron energies in [0.00, 3.00] a.u. in both L and V gauges, are given in Fig. 3.4. We compare them with the nonresonant cross section by Granados–Castro and Sanz–Vicario [99, 100], and with experimental data by Samson *et al* [101]. The differences between the used model potentials are small, and all have the same gauge-to-gauge behaviors. Our Sturmian results show an acceptable agreement for all the calculated energies, specially in L gauge. As demonstrated with the continuum states for H atom (see Fig. 3.3), GSFs allow one to calculate the exact wavefunctions, with the correct asymptotic behavior, for a given two-body potential. A perfect gauge agreement in transition amplitudes (and thus in cross sections), is obtained only for exact initial state wavefunctions. Any gauge discrepancy provides an indication of their quality. In our case, both the HS and DIM

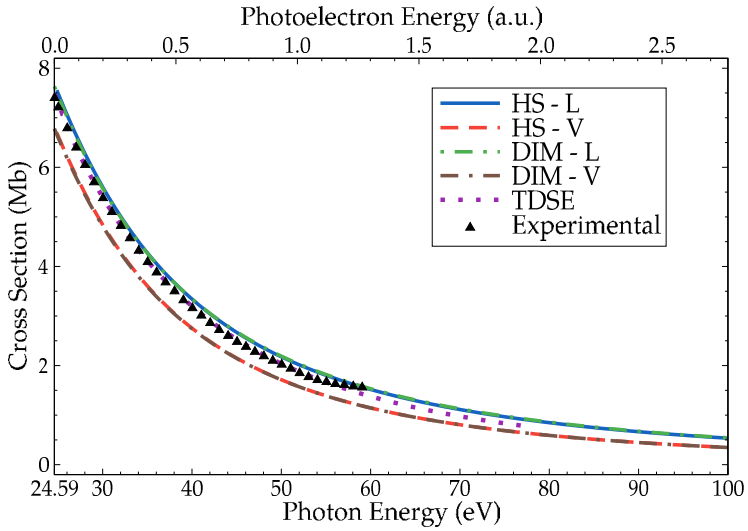

FIGURE 3.4 – PI of He atom, in Mbarns vs. photon energy in eV and photoelectron energy in a.u., for ionization from the ground state. Our results using the HS potential (2.17) for both L (blue, solid) and V (red, dash) gauges, and using the DIM potential (2.20) for L (green, dot-dashed) and V (brown, dot-dash-dashed) gauges. They are compared with the nonresonant cross section [99, 100] (purple, dotted), and with experimental data [101] (black, triangles).

model potential are sufficient to describe the PI cross sections, but the L-V magnitude discrepancy indicates that such model potentials do not yield a sufficiently precise description of the He target, in particular at short distances.

3.5.4. Ne Atom

Now we study PI of Ne atom (some of these results are published in Refs. [12, 13]). We use both the PAR potential (2.18) and the DIM potential (2.20) in order to calculate the wavefunction for a valence electron in $2p$ orbital. The corresponding PI cross sections, in both L and V gauges, obtained using the same GSFs as for H atom, are shown in Fig. 3.5. Our results are compared with the theoretical calculation by Farnoux and Lamoreux [102] (calculated in L gauge) and with experimental data by Samson and Stolte [103]. We see that our cross sections for each model potential, PAR and DIM, have the same gauge-to-gauge behavior, similar to our He results. In contrast, we see that while the L gauge results are in a reasonable agreement with theoretical and experimental data, the V gauge calculation is largely underestimating the cross section, independently of the used model potential. Again, the gauge agreement is sensitive to the quality of the initial state wavefunction. Since the L gauge gives us a better result, it indicates that such wavefunction has a good large distance behavior, but it is not so good in the inner region; this explains the poor results in V gauge. Our result in L gauge is as good as that of Farnoux and Lamoreux, obtained from HF calculations, also within that gauge.

3.6. Results for Molecular Systems

Let us now move to the application of the Sturmian approach for molecular systems. We name hereafter partial PI cross sections those corresponding to the ionization of a specific MO. We restricted ourselves to study only the outer and inner valence orbitals of several molecules, specified in Sec. 2.2.2. In order to calculate each PI cross section, we solve the angular-coupled linear system of equations (3.24) for the post-averaged scheme, or (3.27) for the pre-averaged scheme. Using the obtained expansion coefficients $a_j^{(\ell,E)}\left(\omega;\hat{\mathfrak{R}}\right)$ we calculated directly the PI cross sections, from Eq. (3.30), and the ADCSs from Eq. (3.29). For the latter, we derived the asymmetry parameters β, comparing our calculated distributions with the definition (3.4), at two points $\theta_k = 0$ and $\theta_k = \pi$. We also tried to compare with the so-called "magic angle" θ_m (for which $P_2(\theta_m) = 0$), but the most consistent results were obtained with the first choice.

Again, for all cases we used the same GSFs indicated in Sec. 3.5.2, i.e., for each final partial wave we used 60 functions, calculated in a box of 50 a.u., a generating

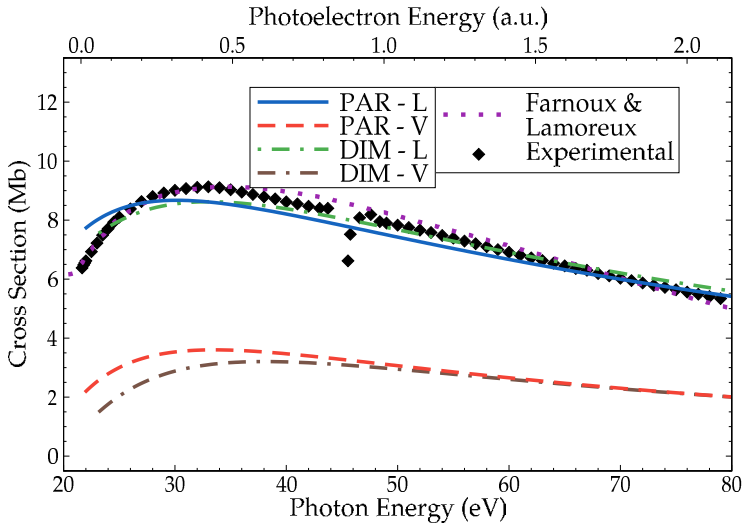

FIGURE 3.5 – PI cross section in Mbarns versus photoelectron energy in atomic units, for ionization of Ne atom from its $2p$ valence orbital. Our results using the PAR potential (2.18) for L (blue, solid) and V (red, dashed) gauges, and using the DIM potential (2.20) for L (green, dot-dashed) and V (brown, dot-dash-dashed) gauges, are compared with the theoretical calculations [102] (purple, dotted) and with experimental data [103] (black, diamonds).

potential taken to be a Yukawa potential with an energy dependent parameter α, and an auxiliary Coulomb potential with charge $Z = -1$. Most of calculations were performed at the `SIMPA` cluster at the Université de Lorraine. The particular used nodes are composed, individually, by four dual-core 2.66 GHz processors.

We first present our results comparing them with experimental data and some selected theoretical sets. Further general statements are collected in Sec. 3.7.

3.6.1. CH_4

First, we show our PI results for CH_4, in particular from the valence orbitals $2a_1$ and $1t_2$. Some of these results are published in Refs. [12, 14–16]. The calculated cross sections in both L and V gauges for the inner valence MO $2a_1$ ($E_0 = -25.0454$ eV) are shown in Fig. 3.6, and the asymmetry parameters β in Fig. 3.7; for the outer valence MO $1t_2$ ($E_0 = -13.7199$ eV), the PI cross section in Fig. 3.8 and β in Fig. 3.9. They are compared with *time-dependent DFT* (TD-DFT) calculations by Stener *et al* [221], *ground state inversion potential method* (GIPM) by Kilcoyne *et al* [284], and with *Stieltjes–Tchebycheff technique* (STT) by Cacelli *et al* [344]; the experimental data are taken from Backx and van der Wiel [107] and from Marr and Holmes [108]. For any of the studied MOs, for the pre-averaged scheme 63 s was the time needed to calculate each energy point of the PI cross sections. For the post-averaged scheme, it

was approximately 16.20 hours to calculate (unparallelized) each energy point, and considering all the spatial orientations.

For the inner valence orbital $2a_1$, the L gauge calculation shows no agreement with any other theoretical result. For higher energies, say beyond 40 eV, we have a good agreement between our V results and experimental and other theoretical data; our results are similar to those obtained with GIPM. We also observe that neither TD-DFT or GIPM results can reproduce the experimental data for energies below 40 eV, but the STT results show a good agreement. It is also possible to observe that calculations in pre- and post-averaged schemes do not coincide in the low energy regime, particularly for L gauge results.

We also calculated the ADCS, in both pre- and post-averaged schemes, and for both L and V gauges. The asymmetry parameter β, shown in Fig. 3.7, is compared only with TD-DFT calculations; we are not aware of any experimental data for this case. The values obtained using the pre-averaged scheme are always constant, and close to the TD-DFT results, while using the post-averaged our results underestimate those values in the whole energy range.

For outer valence orbital $1t_2$, results obtained in V gauge show a fair agreement with experimental data, at least for photon energies higher than 30 eV; near threshold the position of the experimental peak is rather well reproduced but not its magnitude. L gauge results are about a factor two too large. In contrast, TD-DFT and GIPM results can reproduce the experimental data, while calculations using STT reproduce them only over 30 eV. This time our calculations in both pre- and post-averaged schemes are fairly similar in the whole studied energy domain.

Concerning the asymmetry parameter β, presented in Fig. 3.9, we compare our results again with TD-DFT calculations, and with experimental data by Marr and Holmes [108]. The values obtained using the pre-averaged scheme are always constant, while using the post-averaged, they are of the same order of the experimental data in the small energy regime (below 30 eV). For higher values there are no available experimental values, and our results are lower than those reported using TD-DFT.

3.6.2. NH_3

Next we study PI for both $1e$ and $3a_1$ valence orbitals of NH_3. Some of these results are published in Refs. [14, 16]. For the inner valence MO $1e$ ($E_0 = -16.2071$ eV), the cross section is shown in Fig. 3.10, and the asymmetry parameter β in Fig. 3.11; for the outer valence MO $3a_1$ ($E_0 = -11.2819$ eV), the cross section in Fig. 3.12 and β in Fig. 3.13. Our results are compared with the TD-DFT results by Stener *et al* [221], GIPM by Kilcoyne *et al* [284] and with STT by Cacelli *et al* [345]; the experimental

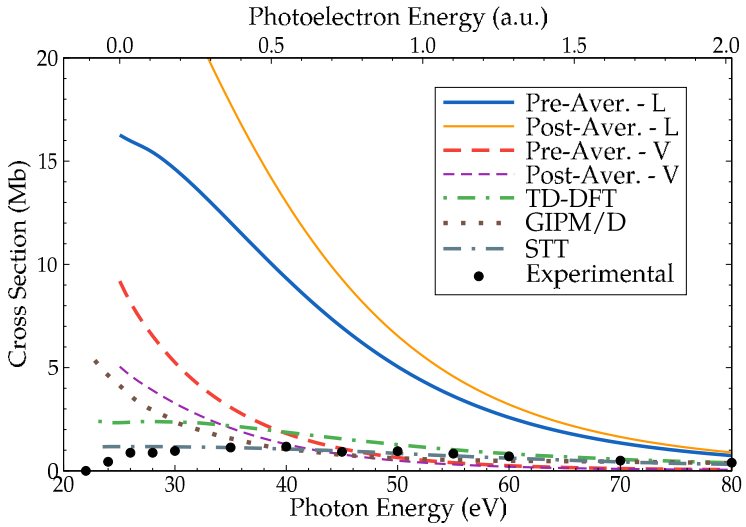

FIGURE 3.6 – Partial PI cross section in Mb versus photon energy in eV for CH_4 $\left(2a_1^{-1}\right)$. Our results in the pre-averaged scheme for L (blue, solid) and V (red, dash) gauges, and in the post-averaged scheme for L (orange, thin solid) and V (purple, thin dash) gauges, are compared with TD-DFT [221] (green, dash-dot); GIPM [284] (brown, dots); STT [344] (gray, dash-dash-dot) and with experimental data [107] (black dots).

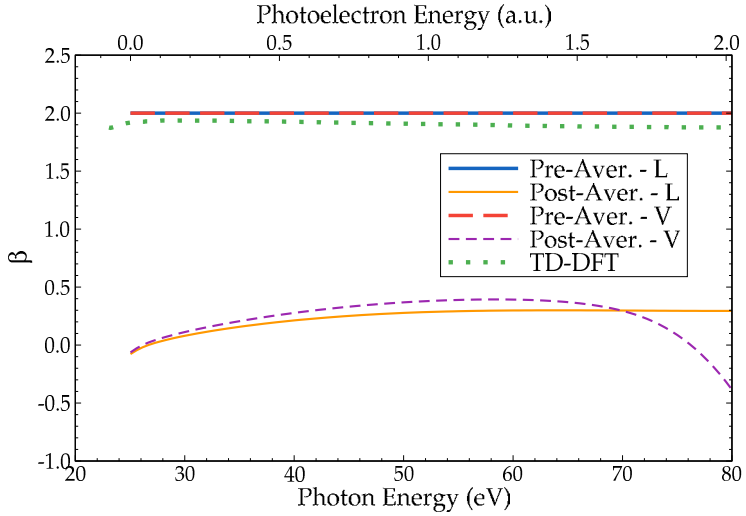

FIGURE 3.7 – Angular asymmetry parameter, for PI of CH_4 $\left(2a_1^{-1}\right)$. Our results correspond to the presented ones in Fig. 3.6, and they are compared with TD-DFT calculations [221].

data were reported by Brion *et al* [109]. Concerning the calculation times, for any of the MOs studied we needed 53 s to calculate an energy point in the pre-averaged scheme, and 16.20 hours for NH_3 $\left(3a_1^{-1}\right)$ and 13.80 hours for NH_3 $\left(1e^{-1}\right)$, in the post-averaged scheme.

For the orbital $1e$, our V gauge results show only a fair agreement with all reported data, in particular at high photon energies. Gauge discrepancy is again im-

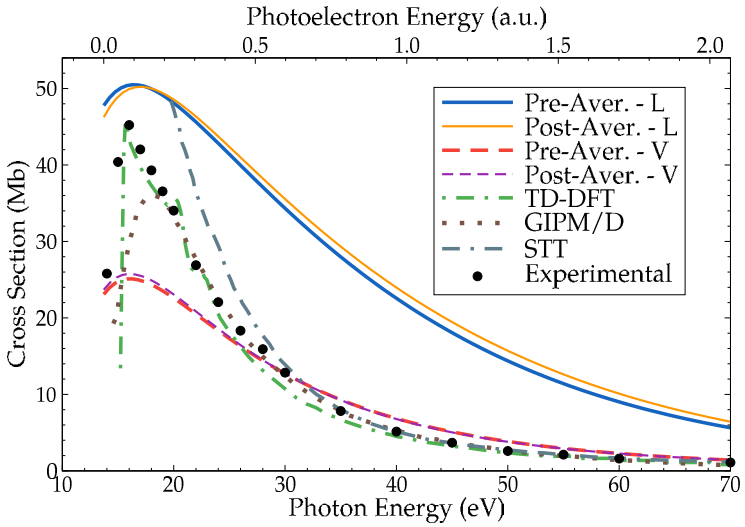

Figure 3.8 – Same as Fig. 3.6 for CH_4 $\left(1t_2^{-1}\right)$.

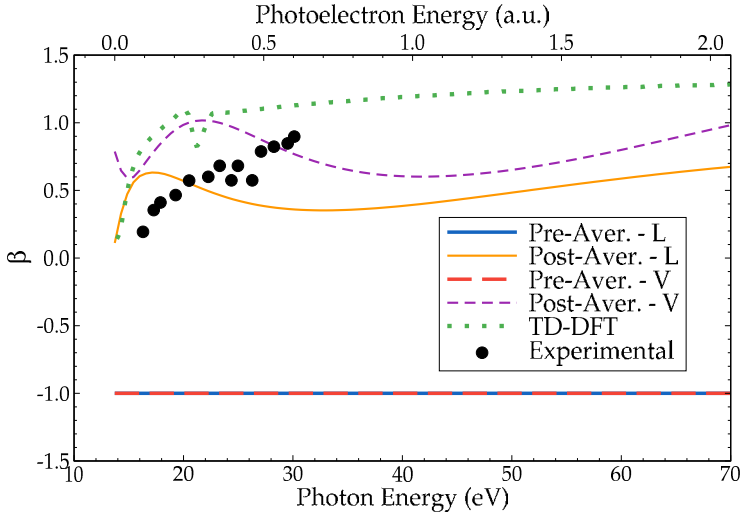

Figure 3.9 – Angular asymmetry parameter, for PI of CH_4 $\left(1t_2^{-1}\right)$. Our results correspond to the presented ones in Fig. 3.8, and they are compared with TD-DFT calculations [221] and with experimental data [108].

portant and, fortuitously, the L gauge results reproduce the experimental magnitude around 22 eV. Here we see an important disagreement between all the theoretical calculations and experimental data, particularly for the low energy regime. Concerning our results using the pre- and post-averaged schemes they are similar, with only small differences below 22 eV.

The β parameter for the orbital $1e$ is shown in Fig. 3.11. Our results are calculated for both L and V gauges, in both pre- and post-averaged schemes. We compare them with TD-DFT calculations and with experimental data by Banna *et al* [110]. Results for both L and V gauges in the pre-averaged scheme are constant, but cannot reproduce

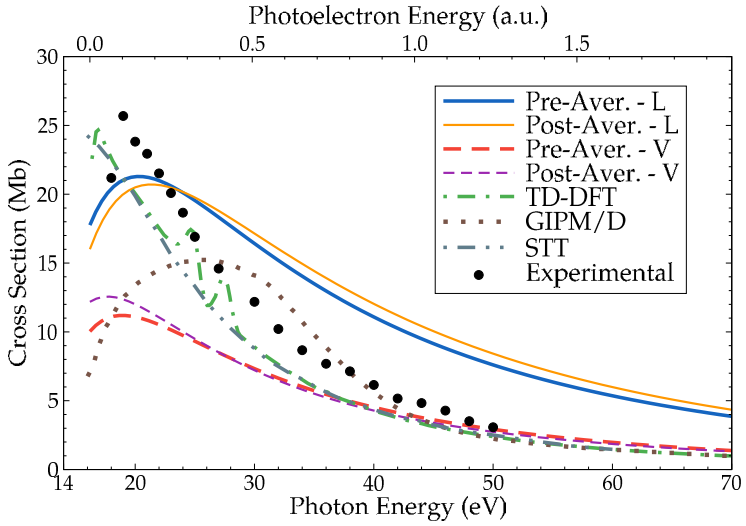

FIGURE 3.10 – Partial PI cross section in Mb versus photon energy in eV for NH_3 $\left(1e^{-1}\right)$. Our results in the pre-averaged scheme for L (blue, solid) and V (red, dash) gauges, and in the post-averaged scheme for L (orange, thin solid) and V (purple, thin dash) gauges, are compared with results for TD-DFT [221] (green, dash-dot); GIPM [284] (brown, dots); STT [345] (gray, dash-dot-dot) and with experimental data [109] (black dots).

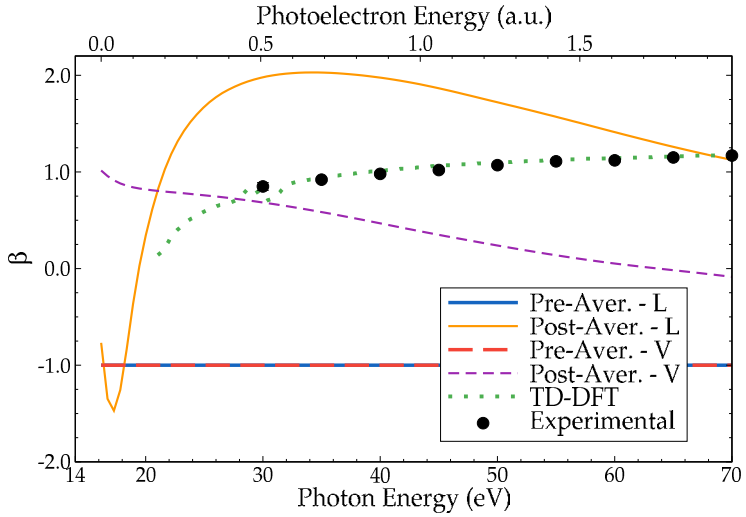

FIGURE 3.11 – Angular asymmetry parameter, for PI of NH_3 $\left(1e^{-1}\right)$. Our results correspond to the presented ones in Fig. 3.10, and they are compared with TD-DFT calculations [221] and with experimental data [110].

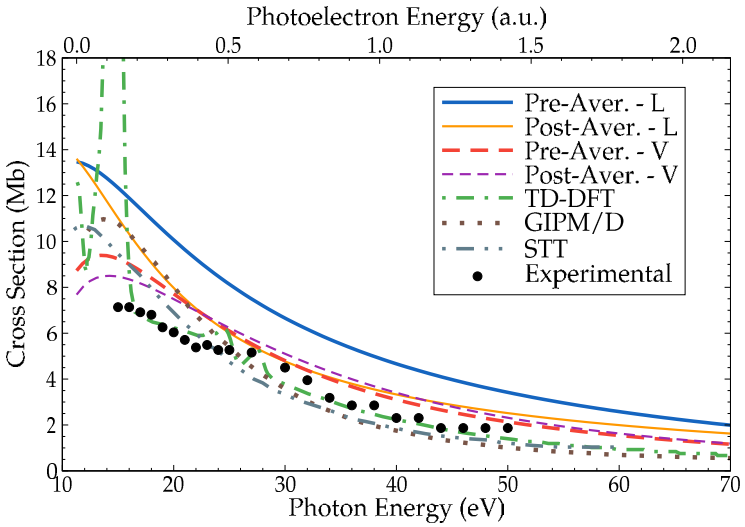

Figure 3.12 – Same as Fig. 3.10 for NH_3 $\left(3a_1^{-1}\right)$.

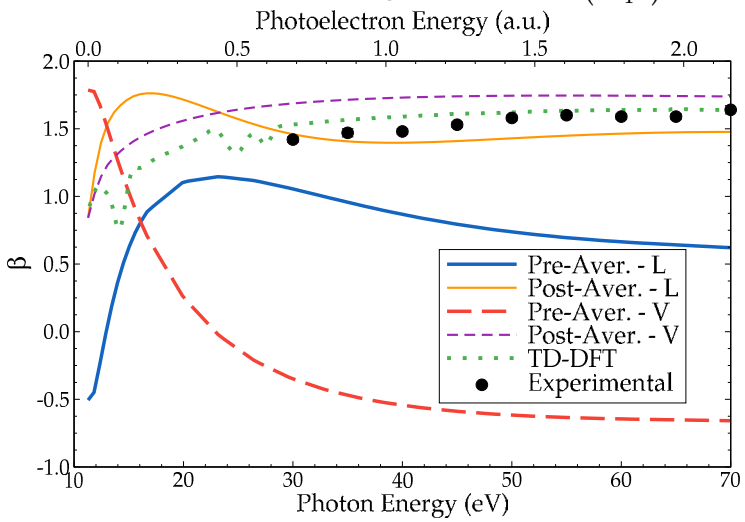

Figure 3.13 – Angular asymmetry parameter, for PI of NH_3 $\left(3a_1^{-1}\right)$. Our results correspond to the presented ones in Fig. 3.12, and they are compared with TD-DFT calculations [221] and with experimental data [110].

experimental data.

For the orbital $3a_1$, our results show a slightly better gauge agreement, the L gauge cross section presenting the same shape but with a larger magnitude. The results in V gauge are in acceptable agreement with the experimental data over the whole energy range. Ignoring the strange behavior of TD-DFT results around 15 eV, all theoretical calculations are in a fair agreement between them and with experimental data. Concerning our results using the pre- and post-averaged schemes, for V gauge they coincide over almost the whole energy range; below 20 eV results using the pre-averaged scheme are in a better agreement with other theoretical calculations.

Within the L gauge, results using both schemes are particularly different; the post-averaged calculation are in a very good agreement with theoretical and experimental data.

The β parameter for PI from $3a_1$ is shown in Fig. 3.13. This time results for the pre-averaged scheme are not constant (in contrast to PI from the inner valence orbital), but cannot reproduce experimental data. However, for the post-averaged scheme, our results follow closely experimental and TD-DFT calculations, particularly in the V gauge.

3.6.3. H_2O

Now, we study PI from the valence orbitals of H_2O, i.e., from $3a_1$ and $1b_1$. These results are published in Refs. [12, 14, 16]. For the inner valence orbital $3a_1$ ($E_0 = -15.1323$ eV), the calculated PI cross sections are shown in Fig. 3.14, and the asymmetry parameter β in Fig. 3.15; for the outer orbital $1b_1$ ($E_0 = -13.4805$ eV), the cross section in Fig. 3.16, and the parameter β in Fig. 3.17. They are compared with TD-DFT calculations by Stener *et al* [221], GIPM by Kilcoyne *et al* [284] and STT by Cacelli *et al* [345]; the experimental data were reported by Banna *et al* [111]. The calculation times of one energy point, for any of the MOs, was 63 s in the pre-averaged scheme and 16.20 hours in the post-averaged scheme.

For the MO $3a_1$, we observe a good agreement between our results in V gauge and other theoretical calculations, in particular for photon energies beyond 30 eV, where our results are close to those of the TD-DFT and very close to GIPM; on the other hand, the L gauge results considerably overestimate the cross sections for all calculated energies. Except for the strange behavior of TD-DFT results around 16-18 eV, all results are in a good agreement with experimental data. In general, the cross sections for inner valence orbitals are difficult to calculate accurately, due to the presence of different many-body effects, such as relaxation of the core. Concerning the use of pre- and post-averaged schemes, we see differences for the low energy domain, particularly for the L gauge, but results for both schemes practically coincide over 30 eV, for the V gauge.

We also calculated the β parameter. It is presented in Fig. 3.15, and compared only with the same TD-DFT calculations and with experimental data. Similar to the NH_3 case, for PI from the outer valence orbital, results for both L and V gauges in the pre-averaged scheme are not constant. The parameter for the former follows the global behavior of the experimental data. Conversely, for the post-averaged scheme we see that the behavior of the asymmetry parameter is of the same order than experimental data, in particular for energies below 30 eV, but any of the results in L or V gauges can follow the behavior of the reference values for higher energies.

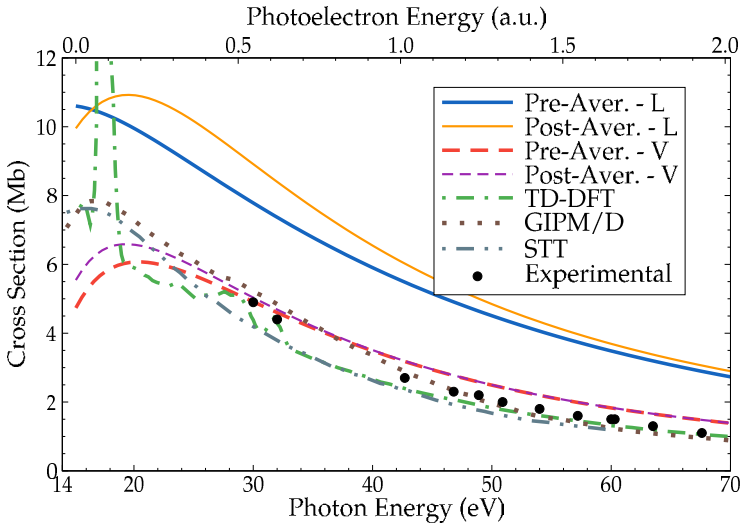

Figure 3.14 – Partial PI cross section in Mb versus photon energy in eV for $H_2O\left(3a_1^{-1}\right)$. Our results in the pre-averaged scheme for L (blue, solid) and V (red, dash) gauges, and in the post-averaged scheme for in L (orange, thin solid) and V (purple, thin dash) gauges are compared with results for TD-DFT [221] (green, dash-dot); GIPM [284] (brown, dots); STT [345] and with experimental data [111] (black dots).

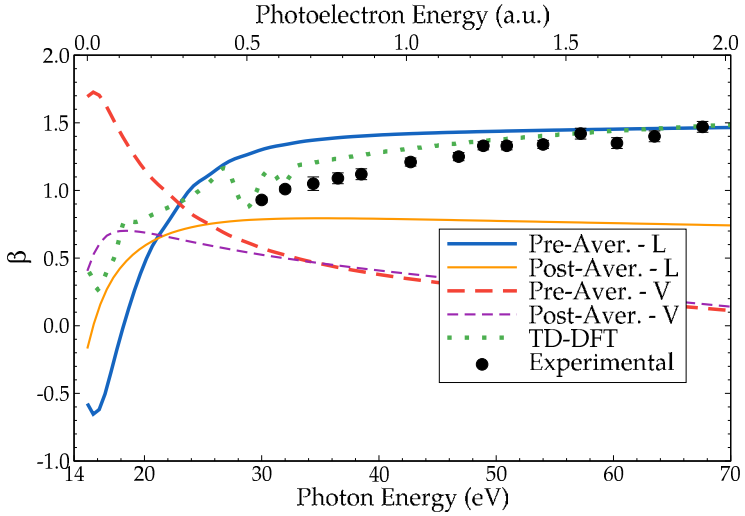

Figure 3.15 – Angular asymmetry parameter, for PI of $H_2O\left(3a_1^{-1}\right)$. Our results correspond to the presented ones in Fig. 3.14, and they are compared with TD-DFT calculations [221] and with experimental data [111].

For the MO $1b_1$, the gauge discrepancy is of the same order as for the $3a_1$ case. Our cross sections compare fairly with other theoretical results, ours being seemingly too low in the threshold region where unfortunately no experimental data are available. The peculiar behavior of TD-DFT calculations is also present in this case, and for small energies results of GIPM and STT are in a fair agreement. Calculations using both pre- and post-averaged schemes now are quite similar, except for V gauge below 30

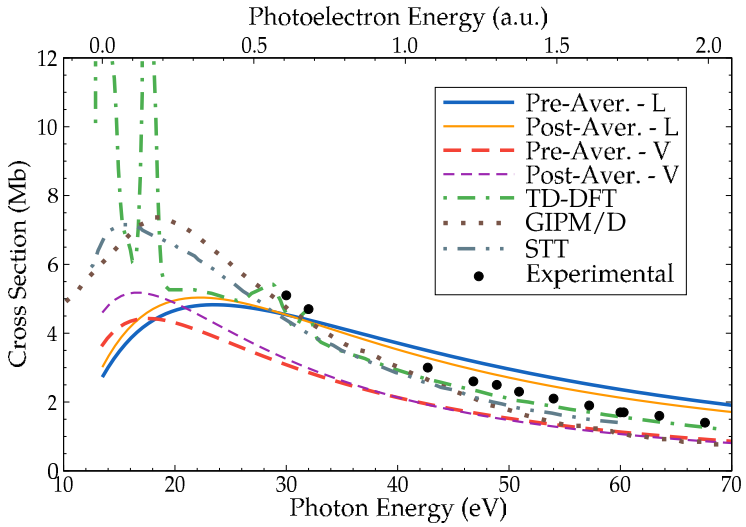

FIGURE 3.16 – Same as Fig. 3.14 for $H_2O\left(1b_1^{-1}\right)$.

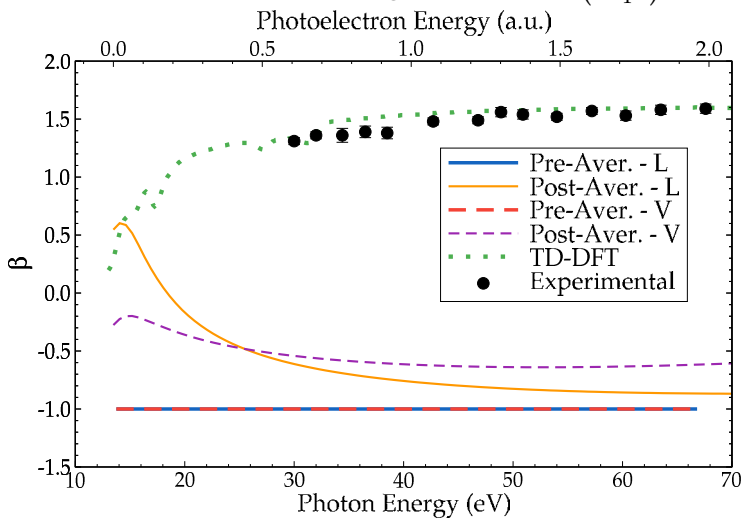

FIGURE 3.17 – Angular asymmetry parameter, for PI of $H_2O\left(1b_1^{-1}\right)$. Our results correspond to the presented ones in Fig. 3.16, and they are compared with TD-DFT calculations [221] and with experimental data [111].

eV. Together with the results for PI from $3a_1$, we can conclude that the use of the central potential (2.33) is good enough to study this molecule.

Our calculated β parameter for $1b_1$, is presented in Fig. 3.17, and compared only with the same TD-DFT calculations and experimental data. Similar to the CH_4 case, the results for both L and V gauges in the pre-averaged scheme are constant. However, in the post-averaged scheme we see that the behavior of the asymmetry parameter underestimates considerably the experimental data. This is a surprising result in view of the PI cross sections for this molecule and the fair β parameter behavior observed for CH_4 and NH_3 and $H_2O\left(3a_1^{-1}\right)$. However, water is the less

"symmetric" molecule studied here, and it is therefore reasonable to expect that the performance of the OCE will be poorer than for CH_4 or NH_3, at least as the angular distribution is concerned. A more detailed study, using multicenter wavefunctions is expected to give better results.

3.6.4. SiH_4

We now study PI on SiH_4, in particular from the valence orbital $2t_2$. These results are published in Ref. [16]. Our calculated cross sections for the outer valence orbital $2t_2$ are plotted in Fig. 3.18, and the asymmetry parameter β in Fig. 3.19. They are compared with TD-DFT calculations by Fronzoni *et al* [222], *iterative-Schwinger method* (ISM) calculations by Machado *et al* [381], and with experimental measurements by Cooper *et al* [112]. The calculation times for each energy point, similar to other molecules, was 63 s in the pre-averaged scheme and 16.20 hours in the post-averaged.

We see that our V gauge cross sections are in a good agreement with experimental data, while results in L gauge overestimate them, similar to the CH_4 $\left(1t_2^{-1}\right)$ observations. V gauge results within the pre-averaged scheme agree well with experimental data for photon energies larger than 20 eV, and for higher energies (say larger than 40 eV) such agreement is even better. TD-DFT and ISM calculations can reproduce experimental data, including the resonance position. As observed for other molecules, the use of either the pre- or post-averaged schemes give us similar results, but the gauge differences this time are more accentuated, a behavior that is observed only in CH_4. This particular large difference could be due to the description of the molecular symmetry, and to the presence of diffuse orbitals [112]. The latter make screening effects have a more active role than in other molecules with a central heavy atom, as water or ammonia. For the silane case, such effects are particularly pronounced, due to the presence of a third row element [222]. This means that the representation of such MOs must be treated more carefully. Additionally, it would be necessary to consider the role that the satellite states of the molecular ion could play [222]; however those excited states are not included within our FC approximation.

The asymmetry parameter β, shown in Fig. 3.19, is compared only with TD-DFT calculations; we are not aware of any experimental data for such parameter. It is possible to appreciate that the values obtained using the pre-averaged scheme are always constant, similar to their CH_4 counterpart. On the other hand, for the post-averaged calculations, the parameter obtained for V gauge is close to the TD-DFT results, for photon energies below 30 eV but not close to threshold; for the L gauge, our results underestimate these reference values in the whole energy range.

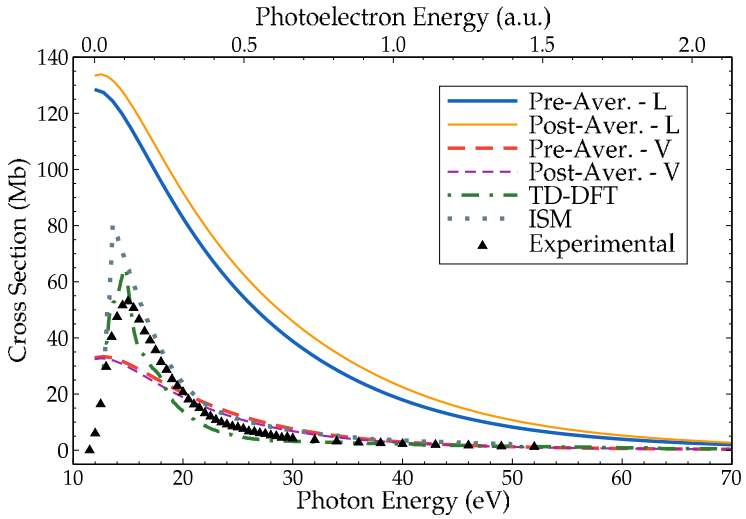

FIGURE 3.18 – Partial PI cross section in Mb versus photon energy in eV for SiH_4 $\left(2t_2^{-1}\right)$. Our results in the pre-averaged scheme for L (blue, solid) and V (red, dash), and for the post-averaged scheme for L (orange, thin solid) and V (purple, thin dash) gauges, are compared with TD-DFT [222] (green, dot-dash) and with ISM [381] (gray, dots) calculations. Experimental data (black, triangles) from Ref. [112].

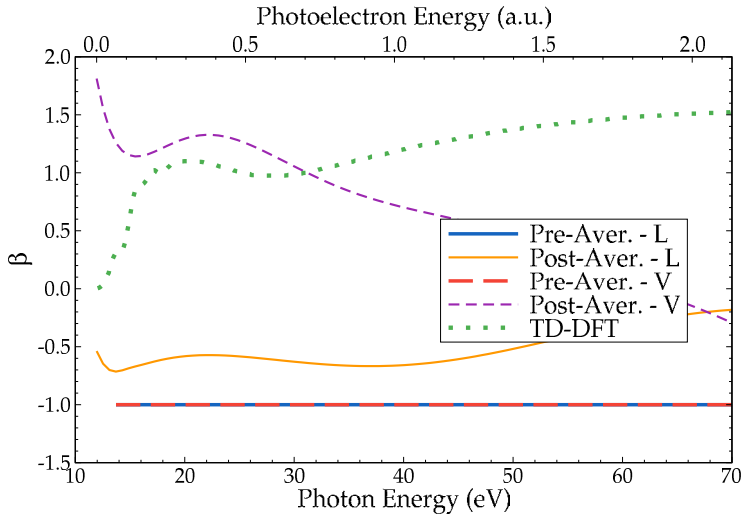

FIGURE 3.19 – Angular asymmetry parameter, for PI of SiH_4 $\left(2t_2^{-1}\right)$. Our results correspond to the presented ones in Fig. 3.18, and they are compared with TD-DFT calculations [222].

3.6.5. H_2S

We finish with PI from the $2b_1$ orbital of H_2S. The results shown here were published in Ref. [16]. Our results in V and L gauges are shown in Fig. 3.20, and the asymmetry parameter β in Fig. 3.21. They are compared with DFT calculations by Stener and Decleva [223], with *random-phase approximation* (RPA) calculations by

Cacelli *et al* [325], and with experimental data reported by Brion *et al* [113]. The calculation times was 69 s in the pre-averaged scheme, and 16.20 hours for the post-averaged scheme.

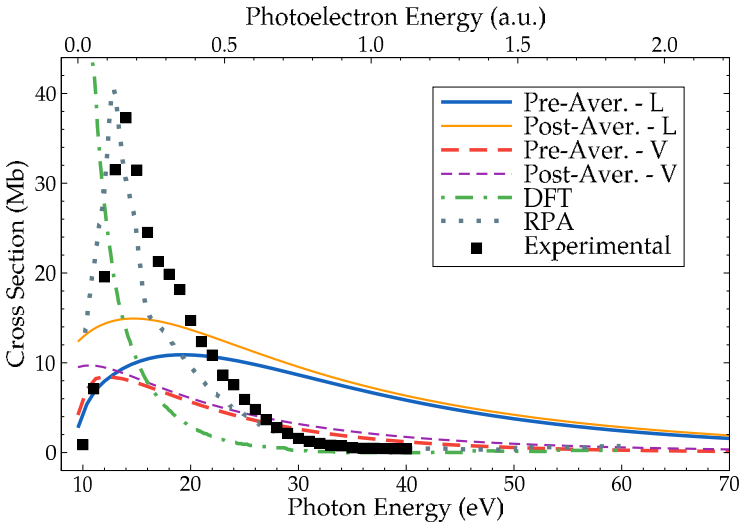

Figure 3.20 – Partial PI cross section in Mb versus photon energy in eV for $H_2S\left(2b_1^{-1}\right)$. Our results in the pre-averaged scheme for L (blue, solid) and V (red, dash) gauges, and in the post-averaged scheme for L (orange, solid) and V (purple, dash) gauges, are compared with theoretical DFT [223] (green, dot-dash) and RPA calculations [325] (gray, dots), and also with experimental data [113] (black, squares).

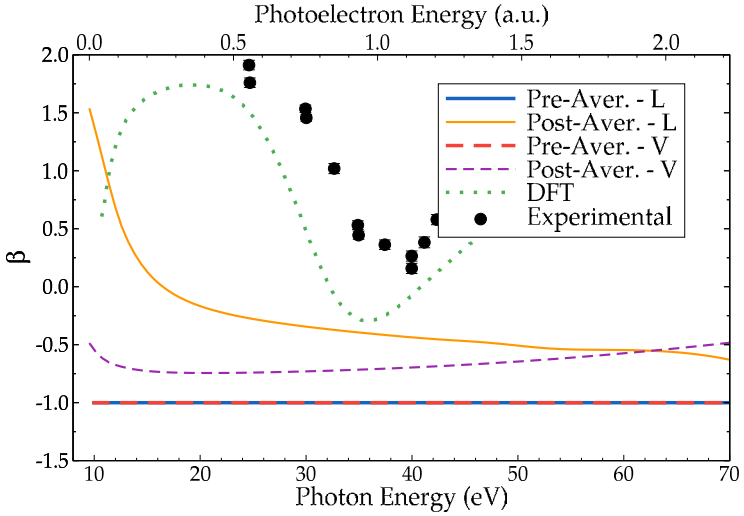

Figure 3.21 – Angular asymmetry parameter, for PI of $H_2S\left(2b_1^{-1}\right)$. Our results correspond to the presented ones in Fig. 3.20, and they are compared with DFT calculations [223] and with experimental data [114].

This time, and in contrast with the results for H_2O, we see that results in L gauge overestimate the experimental data at high energy; V gauge results cannot reproduce the resonance position at low photon energies, but can reproduce the cross section

for photon energies over 25 eV. DFT results fail to reproduce experimental data, except for energies over 30 eV. RPA calculations have an acceptable agreement, particularly over 30 eV. Also, when using the pre- and post-averaged schemes for L gauge we see a large difference between the results, for energies below 30 eV. Such a difference is smaller for the V gauge.

The asymmetry parameter β are plotted in Fig. 3.21, for both L and V gauges. They are compared with DFT results and with experimental data by Adam *et al* [114]. We have here a picture similar to the H_2O case: results in the pre-averaged scheme are constant, and fail completely to reproduce experimental data. The post-averaged results seriously underestimate theoretical and experimental data, and do not present any oscillations. This failure, together with the important gauge discrepancy observed for cross sections, clearly indicates that a much more precise description of the target is needed in this case.

3.7. Conclusions

The implemented Sturmian approach, differs substantially with other theoretical methods, we do not solve the TISE as an eigenvalue problem, i.e., we do not calculate the spectrum of the Hamiltonian. Instead, we solve, for a ionization process (here PI), the driven equation, in particular the radial equation (3.21) for a specific final (continuum) state, with a defined energy E, for which the GSFs have the correct asymptotic behavior. This is an important characteristic of the Sturmian approach in comparison with other methods, where in many cases the representation of the ionization process is limited by the ability of the chosen basis set to represent the oscillations of several bound and continuum states. In other words, the same basis set (with a huge number of elements in some cases) must represent states of different energies, i.e., with different asymptotic behaviors; if such basis is not flexible enough it may give rise to different numerical errors. This point is discussed, for example, in Ref. [99] for the case of B-polynomials and B-splines basis sets.

The use of GSFs is an efficient way to study ionization processes, the number of basis elements included in our calculations being always moderated (60 GSFs); moreover, with the same number of elements we can study with the same tool any energy region of the continuum of both atomic or molecular systems. From the comparison of PI cross sections with the H benchmark analytical result, we showed that the basis size increases slowly for higher energies, so that there is no virtual energy limit to study the continuum of an atom or a molecule, in terms of convergence.

Here is a summary of our observations after applying our Sturmian approach to

PI of atoms and molecules.

1. Our calculations of the PI cross sections for H atom (ground or excited) are excellent for both L and V gauges. Since we use the exact wavefunctions for the initial state, the gauge agreement is perfect and we can reproduce in a numerically "exact" way the analytical results.

2. Results for He atom are also good, at least when we compare with precise non-resonant PI cross sections. The gauge agreement is also fairly good, considering we are using approximated ground state wavefunctions obtained from different model potentials.

3. Results for Ne are of mixed quality. We are aware of the poor representation a SAE approximation yields for an atom with a full $2p$ level. However, L gauge results can reproduce the experimental data in the whole energy range, independently of the used model potential. On the other hand, V gauge results always underestimate the measurements; since this failure is independent of the chosen potentials, we attribute it to a spurious behavior of the wavefunction and its derivative at small and intermediate distances of the nucleus. A more complete description of the atom, i.e., the use of many-body wavefunctions, would be needed to achieve gauge invariance.

4. We tested different model potentials in order to study PI of atoms, particularly He and Ne. The differences between the results, using exactly the same set of GSFs, are small, indicating that such potentials give a similar representation of the ground state wavefunction. The fact that results are better in L gauge are better than in V gauge indicates that such ground state wavefunctions have a good asymptotic behavior, but need to be improved at small and intermediate distances.

5. For molecules, we explored the random orientation with two different schemes: pre- and post-averaged, i.e., using either an angular averaged molecular model potential or a non-central model potential (and performing at the end an angular average over all possible molecular orientations). Results for both are quite similar, in particular for high photoelectron energies. However, for low energies some differences appear, depending on the symmetry of the molecule: for CH_4 and SiH_4 results are almost identical, but for H_2O, NH_3 and H_2S there are some discrepancies. The latter are particularly important close to the ionization threshold, just where the ejected electron feels the strongest interaction with other bound electrons of the parental ion. Even if the description using the non-central potential (2.27) is more accurate than

using the angular averaged potential (2.33), the latter is easier to implement numerically and is computationally less expensive. Here we show that it can be sufficient in many situations.

6. For most molecular cases considered, we observed that gauge agreement is not particularly good, especially for inner valence orbitals. Also, generally, L gauge results overestimate experimental PI cross sections, while V gauge results are always of the same order as the reference data. It is clear that the description of the bound wavefunctions is not good enough at large distances, and a more sophisticated description of the target is needed to achieve gauge invariance.

7. For the ADCSs, actually the β parameter, we have a very mixed picture. The pre-averaged scheme works partially only for MOs with a strong atomic character, as the $3a_1$ MOs, but give wrong constant values for other cases. For the post-averaged scheme, our results are, in some cases, in fair agreement with experimental data, but cannot reproduce TD-DFT results. In particular, for PI from the outer valence orbitals of H_2O and H_2S, our results are not good enough, but for NH_3 they can reproduce experimental data. Such ADCSs are characterized by a high sensibility to the interferences of the partial waves that compose the scattering wavefunction, i.e., to the phase shifts that are due to the pure Coulomb (long-range) and to the short-range interactions. Our Sturmian approach provides all such phase shifts: the long-range is given by definition on the basis functions themselves, and the short-range are calculated via the angular coupled radial equation (3.21). The range of validity of different approximations made here, in particular those concerning many-body interactions, clearly manifest themselves more strongly in our results for ADCS than for PI cross sections.

8. As illustrated in Sec. 3 of Ref. [14], except for H_2, when studying PI in molecular systems, and comparing the cross sections, clearly there are major disagreements between theoretical methods; also, experimental data are generally not well reproduced (in particular near threshold). These conclusions are also true for results using our Sturmian approach.

As a summary, our Sturmian approach can give reasonable PI cross sections, in particular for PI from outer MOs. Some general features are: (i) little difference between the use of the pre- and post-averaged schemes, where the latter improves marginally the cross sections; (ii) the L gauge results are systematically much larger over the whole energy range than those obtained with the V gauge, and are generally

not in agreement with other data (experimental or theoretical). This discrepancy indicates that the initial state description needs to be improved; (iii) our V gauge results are in overall fair agreement with other theoretical cross sections, in particular for energies above, say, 15-20 eV over the ionization threshold; (iv) when studying molecular systems, the agreement between theoretical results (including ours) and experimental data is not uniform. For energies less than 15 eV above ionization threshold agreement is generally poor (see Ref. [14]).

Chapter 4

Ionization by Electron Collision

In this chapter we explore and apply the Sturmian approach adapted to study electron impact ionization of molecular targets. We shall focus on fully differential cross sections, i.e., the so called $(e, 2e)$ processes.

We provide, in Sec. 4.1, a brief introduction of the process and, in Sec. 4.2, some details of the experimental $(e, 2e)$ measurements; in Sec. 4.3 we give the necessary theoretical formulation of the problem, including a description of the first- and second-Born approximations, that constitutes the basis to our Sturmian approach, described in Sec. 4.4. In Sec. 4.5 we explore, in the case of an H atom, the convergence of such an approach, in particular with respect to the involved partial-wave expansions; finally in Sec. 4.6 we present our results, using the first-Born approximation for CH_4, H_2O and NH_3 molecules. Some general comments are summarized in Sec. 4.7.

4.1. Introduction

Studies in collisions of projectiles of different nature, such electrons or ions, with atoms and molecules have been important since the early days of atomic and molecular physics. Such studies allow one to study directly or indirectly the electronic

structure of the target, and have a huge variety of different applications, such in electron-lasers [146]; interstellar mediums, upper atmospheres and ionosphere of planets [116, 147–154]; processing of plasmas, fusion edge plasmas and plasmas diagnostics [116, 155, 156]; radiation physics and chemistry [116]; mass spectrometry [116]; gas discharges [116] and also auroras [157, 158] and lightnings [159]; or radiation damage within cells [160].

A typical $(e, 2e)$ processes is written as [117, 118]

$$e^-(\mathbf{k}_i) + \mathrm{XH}_n(E_0) \longrightarrow \mathrm{XH}_n{}^+ + e^-(\mathbf{k}_a) + e^-(\mathbf{k}_b) \tag{4.1}$$

where an incident electron with an initial momentum $\mathbf{k}_i$, that defines the laboratory frame, interacts with a neutral molecular target (here in an initial state with a defined energy E_0, usually its ground state). The scattered projectile has a final momentum $\mathbf{k}_a$, detected at the scattering angle θ_a, and the ejected electron has a momentum $\mathbf{k}_b$. Energy conservation indicates that $E = k_a^2/2 + k_b^2/2 = k_i^2/2 + E_0$. Also, momentum is conserved, i.e., $\mathbf{k}_i = \mathbf{k}_a + \mathbf{k}_b + \mathbf{k}_R$, where $\mathbf{k}_R$ is the recoil momentum of the ionized target. The momentum transfer is defined as the difference between the momenta of the incident $\mathbf{k}_i$ and fast outgoing $\mathbf{k}_a$ electrons, i.e., $\mathbf{q} = \mathbf{k}_i - \mathbf{k}_a$. We shall study only asymmetric kinematic conditions in which the momentum of the incident (scattered) electron is much larger than the momentum of the ejected one, i.e., $k_a \gg k_b$. Under these conditions one may neglect any exchange term and, then, use unambiguously the final electron labels defined above. In this work we describe only single ionization; other possible outcomes as scattering, multiple ionization, dissociative ionization or rotational or vibrational excitation are ignored.

In order to study single ionization, different quantities can be calculated or measured: the total cross sections or the single-, double- and *triple-differential cross sections* (TDCSs) (see Refs. [116–118]). They all depend not only of the ionization mechanism itself, but also on the structure of the target and the resulting ion. The TDCS provides the most complete description of the ionization event, since it determines the energy and momentum of all particles involved in the collision: this is the quantity we shall analyze throughout the chapter.

For most atomic cases, the TDCS is characterized by the presence of two peaks [117]: the first, called *binary peak*, is oriented in the forward direction (roughly towards $+\mathbf{q}$), and indicates the direction in which the ejected electron is expected in the case of a binary (classical) collision; the second one, called *recoil peak*, is oriented roughly towards $-\mathbf{q}$, i.e., is an indication that, after the binary collision event, the ejected electron suffers a backward reflection in the potential well of the parental ion. Within the first-Born approximation the binary and recoil peaks are found exactly in the $+\mathbf{q}$ and $-\mathbf{q}$ directions, respectively. These characteristics are typical for $(e, 2e)$ processes in atomic targets; for the molecular case the situation is not necessarily as simple,

since the structure of the target is much more complex and the TDCS may present a more involved picture.

As mentioned in Chap. 1, the description of elastic and inelastic collisions with molecules is far from easy because the target Hamiltonian is highly non-central and has a multicenter nature [14]. For ionization processes, different methods have been developed [14, 116, 119, 120], but many challenges still remains, in particular the accurate description of the molecular continuum and issues related to the spatial random orientation of the target.

Another difficulty arises with the description of the projectile-target interaction. As a first approach one may use the Born approximation, based in the first-order term of the Born series (see App. D). From theoretical-experimental comparisons, however, it is clear that, for some kinematic conditions, the use of such approximation is not sufficient, and that the involved mechanisms are more complex than a simple collision. This indicates that higher terms of the Born series are necessary. Some attempts have been made in the past, in particular with the second-Born approximation. We mention, for the atomic case, the first calculations of Woolings and McDowell [121], Tweed [122] and Byron *et al* [162]. More recently, we have some calculations by Marchalant *et al* [123], Reid *et al* [124], Kheifets [125], Dal Cappello *et al* [126], and references therein. Also, we can find by, for example, the study of Ajana *et al* [127] on laser-assisted $(e, 2e)$ on H atoms. For the molecular case, we can cite the works by Houamer *et al* [128], Dal Cappello *et al* [129, 130] and Sahlaoui and Bouamoud [131]. These type of calculations are quite difficult to perform, and they can be heavily limited by the approximations used, as the SAE or the FC.

In the literature it is possible to find several studies on electron momentum spectroscopy for molecules [132], but these focus only on the large momentum transfer regime. For intermediate and low transfer regimes, electron-molecule ionization has not been studied as deeply as its atomic counterpart, and just a few small molecules, such as H_2 or N_2, have been studied extensively. For $(e, 2e)$ processes, several theoretical approaches, adapted to deal with the complexity of the problem, started to appear in the last few years. Their development has been motivated by recent experimental data for different polyatomic molecules. However, the detailed description and understanding of $(e, 2e)$ processes on molecules is still very limited. Without giving an exhaustive survey, among the methods presented in the literature, we can mention the first-Born approximation *Coulomb wave* (1CW) model [133], where the wavefunction of the ejected electron is described by a Coulomb wave, and the wavefunctions for the incident and ejected electrons are described by plane waves; similarly, the *distorted-wave Born approach* (DWBA) [115, 134, 135], uses a distorted

wave to describe the ejected electron; the *Brauner–Brigs–Klar* (BBK) model [136], describes the final state wavefunction by three Coulomb waves, and has been applied in Refs. [164, 165]. We can find also the *R-matrix method* (RMM), summarized in App. G.9 (see also Ref. [120] for electron-molecule collisions), or the *complex Kohn method* (CKM), briefly described in App. G.12.2 (see also Refs. [362, 363]).

In this chapter we explore the implementation of our Sturmian approach to study $(e, 2e)$ on molecular targets. We explore some of the issues addressed above, using GSFs in order to achieve a good description of the molecular continuum and incorporating explicitly the orientation of the target.

4.2. Experimental Measurements

In a $(e, 2e)$ process we have in the final channel two electrons in the continuum and a residual ion. The momenta of the incident and scattered projectiles, $\mathbf{k}_i$ and $\mathbf{k}_a$ respectively, define the so-called collision plane. When all particles lie on such plane one talks of measurements in *coplanar geometry* [118].

As mentioned above, the most complete description of the process is given by the TDCS that, by definition, measures the probability that an electron, with a defined energy, will be ejected in a given direction, for given energy and direction of the scattered electron [116, 117]. The other observables contain less information of the ionization process. A double-differential cross section is obtained by integrating the TDCS over the solid angle of one of the unobserved electrons. A single-differential cross section is obtained integrating over the solid angles of all unobserved electrons, and represents the energy distribution of the outgoing electrons. The total cross section is obtained after integrating over such energy, and provides a measure of the ionization event for a given incident energy.

To observe the products of an $(e, 2e)$ process, in most experiments, and in particular as explained in Refs. [116, 118, 137, 138] (most of the experimental data used in this chapter were obtained as described there), a beam of electrons collides with a gas jet. A coplanar geometry is used to observe the electrons in the collision plane. The ejected (or "slow") electron is analyzed in a multi-angle detector, and the momenta of both scattered and ejected electrons are observed in coincidence. However, the relative orientation of the molecule respect to the incident beam is not observed. Then, similar to the situation described for PI (see Sec. 3.2), the orientation of the molecule is unknown and this must be taken into account in any theoretical description, including ours. Only few experiments can resolve the spatial orientation of the molecule during the ionization process as, for example, using reaction microscopes [71, 72], triple-coincidence techniques [73], or COLTRIMS [74].

As a last comment, most of TDCSs measurements are made on a relative scale [118]. This means that only shape comparisons can be made between theoretical calculations and experimental data.

4.3. Theoretical Description

Within the SAE approximation, in the initial (final) channel we have two electrons: the incident one and the active molecular electron (or, respectively, the scattered and ejected electrons). With that in mind, we set $\mathbf{r}_a$ as the coordinates of the incident (scattered) electron, and $\mathbf{r}_b$ as the coordinates of the active (ejected) electron.

The wavefunction $\Phi(\mathbf{r}_b)$ of the ejected electron have well defined boundary conditions. At the origin of the coordinate system it must be regular, and asymptotically it has the form of an incident plane wave plus outgoing waves

$$\lim_{r_b\to\infty} \Phi(\mathbf{r}_b) \propto \mathrm{e}^{\mathrm{i}\,\mathbf{k}_b\cdot\mathbf{r}_b} + f\left(\mathbf{k}_i, \mathbf{k}_a, \mathbf{k}_b, \hat{r}_b; \hat{\mathfrak{R}}\right) \frac{1}{r_b}\, \mathrm{e}^{\mathrm{i}\,k_b r_b + \ln(2k_b r_b)}, \tag{4.2}$$

where $f\left(\mathbf{k}_i, \mathbf{k}_a, \mathbf{k}_b, \hat{r}_b; \hat{\mathfrak{R}}\right)$ is the transition amplitude, defined explicitly as

$$f\left(\mathbf{k}_i, \mathbf{k}_a, \mathbf{k}_b, \hat{r}_b; \hat{\mathfrak{R}}\right) = \left\langle \Psi_f \middle| \widehat{T} \middle| \Psi_i \right\rangle, \tag{4.3}$$

where $\widehat{T}$ is the transition operator that couples the initial (Ψ_i) to the final (Ψ_f) states. From the definition of this operator one can define different approximations to the problem. One possibility is to use the *Lippmann–Schwinger equation* (LSE) (see App. D), whose solutions are —though— not easy to obtain. Alternatively, the Born series, defined in App. D.1, can be used to approximate the solution. In this chapter we will use the two first terms of such series.

As mentioned earlier, we will consider only asymmetric kinematic conditions, for which the collision process can be treated perturbatively, similarly to the PI case (see Sec. 3.4). Also, in order to incorporate the spatial orientation of the molecule with respect to the laboratory frame, it is specified by the Euler angles $\hat{\mathfrak{R}} = (\alpha, \beta, \gamma)$ (they give the required rotation to orient the molecule into coincidence with the laboratory frame [70], defined by the direction of the incident electrons). Then, keeping only the first perturbative order, the corresponding initial and final wavefunctions can be written as

$$\Psi^{(0)}\left(\mathbf{r}_a, \mathbf{r}_b; \hat{\mathfrak{R}}\right) = \frac{1}{(2\pi)^{3/2}} \left\langle \mathbf{r}_a, \mathbf{r}_b \middle| \mathbf{k}_i, \Phi^{(0)}\left(\hat{\mathfrak{R}}\right) \right\rangle = \frac{1}{(2\pi)^{3/2}} \mathrm{e}^{\mathrm{i}\,\mathbf{k}_i\cdot\mathbf{r}_a} \Phi^{(0)}\left(\mathbf{r}_b; \hat{\mathfrak{R}}\right), \tag{4.4a}$$

$$\Psi^{(1)}\left(\mathbf{r}_a, \mathbf{r}_b; \hat{\mathfrak{R}}\right) = \frac{1}{(2\pi)^{3/2}} \left\langle \mathbf{r}_a, \mathbf{r}_b \middle| \mathbf{k}_a, \Phi^{(1)}\left(\hat{\mathfrak{R}}\right) \right\rangle = \frac{1}{(2\pi)^{3/2}} \mathrm{e}^{\mathrm{i}\,\mathbf{k}_a\cdot\mathbf{r}_a} \Phi^{(1)}\left(\mathbf{r}_b; \hat{\mathfrak{R}}\right), \tag{4.4b}$$

where $\Phi^{(0)}\left(\mathbf{r}_b; \hat{\mathfrak{R}}\right)$ is the initial state wavefunction of the active electron (usually the ground state), and $\Phi^{(1)}\left(\mathbf{r}_b; \hat{\mathfrak{R}}\right)$ is its final state wavefunction of the ejected electron.

4.3.1. Triple-Differential Cross Sections

The observable that describes $(e, 2e)$ is the TDCS which is defined as [117, 171]

$$\frac{\mathrm{d}^3\sigma}{\mathrm{d}\hat{r}_a\,\mathrm{d}\hat{r}_b\,\mathrm{d}E} = (2\pi)^4\,\frac{k_a k_b}{k_i}\left|f\left(\mathbf{k}_i, \mathbf{k}_a, \mathbf{k}_b, \hat{r}_b; \hat{\Re}\right)\right|^2, \tag{4.5}$$

and it is actually a five-fold differential cross section.

In order to take into account the spatial random orientation of the target, the following angular average is performed

$$\frac{\overline{\mathrm{d}^3\sigma}}{\mathrm{d}\hat{r}_a\,\mathrm{d}\hat{r}_b\,\mathrm{d}E} = (2\pi)^4\,\frac{k_a k_b}{k_i}\frac{1}{8\pi^2}\int_0^{2\pi}\mathrm{d}\alpha\int_0^{\pi}\sin\beta\,\mathrm{d}\beta\int_0^{2\pi}\mathrm{d}\gamma\left|f\left(\mathbf{k}_i, \mathbf{k}_a, \mathbf{k}_b, \hat{r}_b; \hat{\Re}\right)\right|^2. \tag{4.6}$$

4.3.2. The Born Approximation

Taking only the first term of the Born series (D.11), the T matrix is given then by

$$T_{fi} \approx T_{fi}^{(1)} = \left\langle \Psi^{(1)}\right| V \left|\Psi^{(0)}\right\rangle, \tag{4.7}$$

and the amplitude can be defined as

$$\begin{aligned} f \approx f_{\mathrm{B1}} &= -(2\pi)^2\left\langle \Psi^{(1)}\right| V \left|\Psi^{(0)}\right\rangle \\ &= -(2\pi)^2\,\frac{1}{(2\pi)^3}\left\langle \mathbf{k}_a, \Phi^{(1)}\right| V \left|\mathbf{k}_i, \Phi^{(0)}\right\rangle \\ &= -\frac{1}{2\pi}\left\langle \Phi^{(1)}\right|\widehat{\mathcal{T}}\left(\mathbf{r}_b; \mathbf{q}\right)\left|\Phi^{(0)}\right\rangle, \end{aligned} \tag{4.8}$$

where

$$\begin{aligned} \widehat{\mathcal{T}}\left(\mathbf{r}_b; \mathbf{q}\right) &= \left\langle \mathbf{k}_a\right| V\left(\mathbf{r}_a, \mathbf{r}_b\right)\left|\mathbf{k}_i\right\rangle \\ &= \int \mathrm{d}\mathbf{r}_a\,\mathrm{e}^{\mathrm{i}\,\mathbf{q}\cdot\mathbf{r}_a}\,V\left(\mathbf{r}_a, \mathbf{r}_b\right) \end{aligned} \tag{4.9}$$

is the Fourier transform of the potential, where $\mathbf{q} = \mathbf{k}_i - \mathbf{k}_a$ is the momentum transfer. It is clear that in the first Born approximation the transition amplitude depends explicitly on $\mathbf{q}$. The structure of the corresponding TDCS is rotationally symmetric around $\mathbf{q}$.

From the transition amplitude (4.8), we can interpret the first-Born approximation as the description of a single collision, that ionizes directly the active electron in the target.

4.3.3. The Second Born Approximation

From Eq. (D.11), at second-order, the transition amplitude is given by

$$\begin{aligned} T_{fi}^{(2)} &= \left\langle \Psi^{(1)} \right| V \widehat{G}^0(E_i) V \left| \Psi^{(0)} \right\rangle \\ &= \frac{1}{(2\pi)^3} \left\langle \mathbf{k}_a, \Phi^{(1)} \right| V \widehat{G}^0(E_i) V \left| \mathbf{k}_i, \Phi^{(0)} \right\rangle . \end{aligned} \tag{4.10}$$

The second order amplitude is

$$f_{\mathrm{B2}} \propto \left\langle \mathbf{k}_a, \Phi^{(1)} \right| V(\mathbf{r}_a, \mathbf{r}_b) \widehat{G}^0(E) V(\mathbf{r}_a, \mathbf{r}_b) \left| \mathbf{k}_i, \Phi^{(0)} \right\rangle , \tag{4.11}$$

where $\widehat{G}^0(E) = \left(E - \widehat{\mathcal{H}}_0\right)^{-1}$ is the Green function (D.3). The latter can be written as an expansion in terms of all the eigenstates (bound and unbound) of the total Hamiltonian of the system. Let the spectrum of target Hamiltonian $\widehat{\mathcal{H}}_0$ be given by

$$\widehat{\mathcal{H}}_0 \left| m \right\rangle = E_m \left| m \right\rangle . \tag{4.12}$$

Using, additionally, a wave-packet to represent any possible final state for the scattered electron (a free wave), the Green's function is given by

$$\widehat{G}^0(E) = \sum\!\!\!\!\!\!\int_m \int \frac{\mathrm{d}\mathbf{k}'}{k'^2 - k_m^2} \left| m \right\rangle\!\left\langle m \right| , \tag{4.13}$$

where $k_m^2 = 2E_m$, and the sum is over all bound states and the integral over all continuum states. Then, the transition amplitude can be written as [129, 130, 139]

$$\begin{aligned} f_{\mathrm{B2}} &= \frac{1}{8\pi^4} \sum\!\!\!\!\!\!\int_m \int \frac{\mathrm{d}\mathbf{k}'}{k'^2 - k_m^2} \left\langle \mathbf{k}_a, \Phi^{(1)} \right| V(\mathbf{r}_a, \mathbf{r}_b) \left| \mathbf{k}', m \right\rangle \left\langle \mathbf{k}', m \right| V(\mathbf{r}_a, \mathbf{r}_b) \left| \mathbf{k}_i, \Phi^{(0)} \right\rangle \\ &= \frac{1}{8\pi^4} \sum\!\!\!\!\!\!\int_m \int \frac{\mathrm{d}\mathbf{k}'}{k'^2 - k_m^2} \left\langle \Phi^{(1)} \right| \widehat{\mathcal{T}}(\mathbf{r}_b; \mathbf{k}' - \mathbf{k}_a) \left| m \right\rangle \left\langle m \right| \widehat{\mathcal{T}}(\mathbf{r}_b; \mathbf{k}_i - \mathbf{k}') \left| \Phi^{(0)} \right\rangle . \end{aligned} \tag{4.14}$$

From this transition amplitude, the second-Born approximation can be interpreted as the description of a "binary" ionization process, where the first collision takes the active electron of the target from its initial state to an intermediate one $|m\rangle$ (bound or unbound). Later, a second collision takes such active electron from its intermediate state $|m\rangle$ to the final state $\left|\Phi^{(1)}\right\rangle$.

Putting together the first and second Born amplitudes (Eqs. (4.8) and (4.14)) the transition amplitude is given by

$$f \approx f_{\mathrm{B1}} + f_{\mathrm{B2}}. \tag{4.15}$$

4.4. Sturmian Approach to (e, 2e)

The implementation of the Sturmian approach to study $(e,2e)$ processes is similar to that used to study PI (see Sec. 3.4) for which the first-order perturbation theory is used. We thus give here only the main features. Many of the involved analytic calculations are summarized in Apps. C and E.

The corresponding first-order driven equation reads

$$\left(E - \widehat{\mathcal{H}}_0\right) \Psi^{(1)}\left(\mathbf{r}_a, \mathbf{r}_b; \hat{\mathfrak{R}}\right) = \widehat{T}(\mathbf{r}_a, \mathbf{r}_b) \Psi^{(0)}\left(\mathbf{r}_a, \mathbf{r}_b; \hat{\mathfrak{R}}\right), \tag{4.16}$$

where $\Psi^{(0)}\left(\mathbf{r}_a, \mathbf{r}_b; \hat{\mathfrak{R}}\right)$, defined in Eq. (4.4a), is the wavefunction of the initial channel (projectile plus ground state of the molecule), $\Psi^{(1)}\left(\mathbf{r}_a, \mathbf{r}_b; \hat{\mathfrak{R}}\right)$, defined in Eq. (4.4b), is the scattering wavefunction at first order, with total energy E and $\widehat{T}(\mathbf{r}_a, \mathbf{r}_b)$ is the transition operator, that at first order is given by the interaction potential (see Secs. 4.4.1, 4.4.2 and App. D.1 for more details)

$$\widehat{T}(\mathbf{r}_a, \mathbf{r}_b) = V(\mathbf{r}_a, \mathbf{r}_b). \tag{4.17}$$

In order to solve Eq. (4.16), we first project it onto the final wavefunction of the scattered projectile, represented by a plane wave (well suited for high-energy cases) with momentum $\mathbf{k}_a$. The sought after wavefunction of the ejected electron is expanded in its radial and angular parts

$$\Phi^{(1)}\left(\mathbf{r}_b; \hat{\mathfrak{R}}\right) = \sum_{\ell m} \varphi_\ell\left(r_b; \hat{\mathfrak{R}}\right) Y_\ell^m(\hat{r}_b), \tag{4.18}$$

and the radial part is expanded on a GSFs basis set (see Sec. 2.1)

$$\varphi_\ell\left(r_b; \hat{\mathfrak{R}}\right) = \frac{1}{r} \sum_j a_j^{(\ell,E)}\left(k_b; \hat{\mathfrak{R}}\right) \mathcal{S}_j^{(\ell,E)}(r_b). \tag{4.19}$$

The GSF $\mathcal{S}_j^{(\ell,E)}(r)$ satisfy Eq. (2.1), with $E = k^2/2 = k_b^2/2$, and with outgoing boundary conditions

$$\lim_{r\to\infty} \mathcal{S}_j^{(\ell,E)}(r) \propto \exp\left[\mathrm{i}\left(kr - \frac{Z}{k}\ln(2kr) - \ell\frac{\pi}{2} + \delta_\ell\right)\right], \tag{4.20}$$

where δ_ℓ is the Coulomb phase shift. Using these expansions, from the driven equation (4.16) one obtains the radial equation

$$\begin{aligned}\sum_{\ell m}\sum_j \left[\left(E + \frac{1}{2}\frac{\mathrm{d}^2}{\mathrm{d}r_b^2} - \frac{\ell(\ell+1)}{2r_b^2}\right)\delta_{\ell'\ell}\delta_{m'm} - U_{\ell'\ell}^{m'm}(r_b)\right] \mathcal{S}_j^{(\ell,E)}(r_b) \\ \times a_j^{(\ell,E)}\left(k_b; \hat{\mathfrak{R}}\right) = \varrho_{\ell'}^{m'}\left(r_b; \hat{\mathfrak{R}}\right),\end{aligned} \tag{4.21}$$

where

$$\varrho_\ell^m\left(r_b; \hat{\mathfrak{R}}\right) = r_b \left\langle \ell m \middle| \widehat{\mathcal{T}}(\mathbf{r}_b; \mathbf{q}) \middle| \Phi^{(0)}\left(\hat{\mathfrak{R}}\right)\right\rangle. \tag{4.22}$$

This driven term includes information of the spatial molecular orientation with respect to the incident momentum $\mathbf{k}_i$ (similar to its counterpart in PI). In order to determine it, we use a Coulomb potential with charge -1 in order to describe the projectile-target interaction, i.e.

$$\begin{aligned}\widehat{\mathcal{T}}(\mathbf{r}_b;\mathbf{q}) &= \int \mathrm{d}\mathbf{r}_a \, \mathrm{e}^{\mathrm{i}\,\mathbf{q}\cdot\mathbf{r}_a}\left(\frac{1}{|\mathbf{r}_a-\mathbf{r}_b|}-\frac{1}{r_a}\right)\\ &= \frac{4\pi}{q^2}\left(\mathrm{e}^{\mathrm{i}\,\mathbf{q}\cdot\mathbf{r}_b}-1\right),\end{aligned} \tag{4.23}$$

where the second equality is obtained using Bethe's integral (C.1).

Concerning the description of the ejected electron-ionized target interaction, here we consider three different options for $U^{m'm}_{\ell'\ell}(r_b)$:

I A Coulomb potential, with charge -1

$$U^{m'm}_{\ell'\ell}(r_b) = -\frac{1}{r_b}\,\delta_{\ell'\ell}\,\delta_{m'm}. \tag{4.24}$$

This potential is used in electron-atom collisions, and for electron-molecule collisions when the ejected electron has high energy.

II The non-central *molecular model potential* (MMP) (2.27) (see Sec. 2.2.3 and App. B for more details)

$$\begin{aligned}U^{m'm}_{\ell'\ell}(r_b) = (-1)^{m'}\sum_{\lambda\mu}\frac{4\pi}{2\lambda+1}\Upsilon^{-m',\mu m}_{\ell'\lambda\ell}\Bigg[-\sum_{n=1}^{M}Z_n\frac{\min(r_b,R_n)^\lambda}{\max(r_b,R_n)^{\lambda+1}}Y^{\mu *}_\lambda\left(\hat{R}_n\right)\\ +\sum_{j=1}^{N_{\mathrm{MO}}}\mathcal{N}_{ij}\sum_{k,l=1}^{n}(-1)^{m_k+\mu}B^*_{jk}B_{jl}\frac{\vartheta^{(\lambda)}_{kl}(r_b)}{r_b}\Upsilon^{-m_k,-\mu,m_l}_{\ell_k\lambda\ell_l}\Bigg].\end{aligned} \tag{4.25}$$

This potential is used to study the effect of the interaction of the ejected electron with all bound electrons and all the nuclei.

III The *angular averaged potential* (AAP) (2.33), that can be obtained from the last definition

$$U^{m'm}_{\ell'\ell}(r_b) = U^{00}_{00}(r_b)\;\delta_{\ell'\ell}\,\delta_{m'm}. \tag{4.26}$$

Similar to the previous case, this potential is used to study the interaction of the ejected electron with the target, where its spatial orientation has been averaged.

For the second potential, the matrix is dense and then the corresponding radial equation is angular-coupled. For the other two, only the diagonal terms are nonzero.

In order to solve the radial equation (4.21), we use the definition of the GSFs to calculate their second derivative, and then the radial equation is projected on $\mathcal{S}_i^{(\ell,E)}(r_b)$. Similar to the PI case, we transform the differential equation (4.21) into a linear system of equations. Using the matrix elements (3.23), the resulting system is

$$\sum_{\ell m}\sum_{j}\left\{\left[(E-E_b)\,O_{ij}^{(\ell,E)}+\mathcal{U}_{ij}^{(\ell,E)}+\beta_j^{(\ell,E)}\mathcal{V}_{ij}^{(\ell,E)}\right]\delta_{\ell'\ell}\delta_{m'm}-\mathcal{P}_{ij}^{(\ell,E)\,m'm}_{\quad\ell'\ell}\left(\hat{\mathfrak{R}}\right)\right\} \times a_j^{(\ell,E)}\left(k_b;\hat{\mathfrak{R}}\right)=\mathbb{k}_i^{(\ell,E)\,m'}_{\quad\ell'}\left(\hat{\mathfrak{R}}\right). \tag{4.27}$$

All matrices are calculated as indicated in Refs. [1, 2], and the linear system of equations is solved using the `LAPACK` [175] subroutine `ZGESV`. But first, the RHS must be calculated, and hereafter we indicate how to express it in the first- and second-Born approximations.

4.4.1. First-Born Approximation

In order to perform calculations in the first-Born approximation, we need to calculate the transition operator $\widehat{T}(\mathbf{r}_a,\mathbf{r}_b)$ at first order (see Eq. (D.11)). We thus need only the interaction potential between the scattered electron and the ionized target, and that with the ejected electron, i.e.

$$\widehat{T}^{(1)}=V(\mathbf{r}_a,\mathbf{r}_b)=\frac{1}{|\mathbf{r}_a-\mathbf{r}_b|}+U(\mathbf{r}_a), \tag{4.28}$$

where $U(\mathbf{r}_a)$ gives the projectile-ion interaction. The Fourier transform of (4.28) yields the one-particle transition operator, $\widehat{\mathcal{T}}(\mathbf{r}_b;\mathbf{q})$. Using Eqs. (4.23), and the expansion (C.8) in partial waves of the exponential function, the analytical form of the RHS function (4.22) can be written in general as

$$\varrho_{\ell'}^{m'}(r_b)=(-1)^{m'}\frac{4\pi}{q^2}\sum_j B_{ij}r_b\mathcal{R}_j(r_b)\left\{\mathcal{Z}(\mathbf{R};\mathbf{q})\delta_{\ell'\ell_j}\delta_{m'm_j} +\sum_{\lambda_q\mu_q}4\pi\mathrm{i}^{\lambda_q}j_{\lambda_q}(qr_b)Y_{\lambda_q}^{\mu\,*}(\hat{q})\Upsilon_{\ell'\lambda_q,\ell_j}^{-m',\mu_q m_j}\right\}. \tag{4.29}$$

As we use only the Coulomb potential to describe the interaction between the ejected electron and the remaining ion

$$\mathcal{Z}(\mathbf{R};\mathbf{q})=-1. \tag{4.30}$$

If one wants to describe such interaction with different model potentials, then $\mathcal{Z}(\mathbf{R};\mathbf{q})$ is replaced by the corresponding Fourier transform, as the indicated in Eq. (C.11).

4.4.2. Second-Born Approximation

Using the closure approximation (see App. E.1), the transition operator (D.11) in the second-Born approximation is [129, 139]

$$\begin{aligned}\widehat{\mathcal{T}}^{(2)}(\mathbf{r}_b;\mathbf{k}_i,\mathbf{k}_a) &= \frac{1}{8\pi^4}\int \frac{\mathrm{d}\mathbf{k}'}{k'^2-\tilde{k}^2}\,\langle \mathbf{k}_a|\,V(\mathbf{r}_a,\mathbf{r}_b)\,|\mathbf{k}'\rangle\,\langle \mathbf{k}'|\,V(\mathbf{r}_a,\mathbf{r}_b)\,|\mathbf{k}_i\rangle \\ &= \frac{1}{8\pi^4}\int \frac{\mathrm{d}\mathbf{k}'}{k'^2-\tilde{k}^2}\,\widehat{\mathcal{T}}(\mathbf{r}_b;\mathbf{k}'-\mathbf{k}_a)\widehat{\mathcal{T}}(\mathbf{r}_b;\mathbf{k}_i-\mathbf{k}'). \end{aligned} \tag{4.31}$$

In this work we use the interaction (4.23), the expansion (C.8) in partial waves of the exponential function, and a similar approach to the one proposed by Marchalant *et al* [123] (see App E). The RHS function (4.22), including also the first-Born term (4.29), is

$$\begin{aligned}\varrho_{\ell'}^{m'}(r_b) = (-1)^{m'}\sum_j B_{ij} r_b \mathcal{R}_j(r_b)\Bigg\{&\left[-\frac{4\pi}{q^2}+\frac{2}{\pi^2}I_{00}\left(\mathrm{i}\,\tilde{k};\mathbf{k}_a,0;\mathbf{k}_i,0\right)\right]\delta_{\ell'\ell_j}\delta_{m'm_j} \\ &+\sum_{\lambda_q\mu_q} 4\pi \mathrm{i}^{\lambda_q}(-1)^{\mu_q}\Bigg[\left(\frac{4\pi}{q^2}+\frac{2}{\pi^2}I_{00}\left(\mathrm{i}\,\tilde{k};\mathbf{k}_a,0;\mathbf{k}_i,0\right)\right) j_{\lambda_q}(qr_b)\,\Upsilon_{\lambda_q}^{\mu_q *}(\hat{q}) \\ &-\frac{2}{\pi^2}\left(\mathcal{J}^{L'\Lambda_q L_j}(r_b\mathbf{k}_a;\mathbf{q})+\mathcal{J}^{L'\Lambda_q L_j}(r_b\mathbf{k}_i;\mathbf{q})\right)\Bigg]\Upsilon_{\ell'\lambda_q,\ell_j}^{-m',\mu_q m_j}\Bigg\}, \end{aligned} \tag{4.32}$$

where I_{00} is called Lewis' integral, defined by Eq. (E.7), and $\mathcal{J}^{L\Lambda_q L_j}$ is a radial function defined by Eq. (E.12) (see Sec. E.2.4 for all the calculation details).

4.4.3. Triple Differential Cross Sections

Similar to its PI counterpart, the transition amplitude (4.3) can be written directly in terms of the expansion coefficients $a_j^{(\ell,E)}\left(k_b;\hat{\mathfrak{R}}\right)$ of the scattering wavefunction (4.19). Indeed, after comparing the asymptotic behavior (4.2) of the scattering wavefunction for the ejected electron, with the asymptotic behavior (4.20) of the GSFs, the TDCS reads

$$\frac{\mathrm{d}^3\sigma}{\mathrm{d}\hat{r}_a\,\mathrm{d}\hat{r}_b\,\mathrm{d}E} = (2\pi)^4\frac{k_a k_b}{k_i}\frac{1}{2\pi}\left|\sum_{\ell m}\mathrm{e}^{\mathrm{i}\left(\delta_\ell-\frac{\pi}{2}\ell\right)}\,Y_\ell^m(\hat{r}_b)\sum_j a_j^{(\ell,E)}\left(k_b;\hat{\mathfrak{R}}\right)\right|^2. \tag{4.33}$$

As a final comment about the strategy followed here to include explicitly the spatial molecular orientation: like for the post-averaged scheme (see Sec. 3.4.2) used for PI, we rotate each initial MO to a given spatial orientation $\hat{\mathfrak{R}}$, before calculating the expansion coefficients $a_j^{(\ell,E)}\left(k_b;\hat{\mathfrak{R}}\right)$. With these, the angular average (4.6) is performed. Since for our calculated PI-ADCSs (see Sec. 3.6), only the post-averaged scheme gave good results, for the present TDCS we use only such a scheme.

4.5. Convergence of GSF Basis Sets and Results for H Atom

To demonstrate the validity of our Sturmian approach, we present in this section its implementation to study $(e, 2e)$ in H atom. To do so, the linear system of equations (4.27) is solved to obtain the expansion coefficients and, with them, the TDCS (4.33). We consider the kinematic conditions specified in the measurements by Lohmann *et al* [163], i.e., the incident electron has an energy $E_i = 250$ eV; the fixed detection energy for the ejected electron is either $E_b = 5$, 10 or 14 eV, and the scattered one is detected at $\theta_a = 3°$, 5° or 8°, in coplanar geometry. We start analyzing the convergence of our methodology, and then we compare our results with analytical and experimental data.

4.5.1. Convergence of GSF Basis Sets

In order to analyze the convergence of the Sturmian approach, we calculate the corresponding TDCSs as a function of the number of GSF functions and the number of partial waves included, for both the scattering wavefunction (4.18) and the interaction operator (4.23). For each partial wave, the GSFs were calculated in a box of length 50 a.u., using as generating potential a Yukawa potential with $\alpha_s = 0.03$, and as auxiliary potential a Coulomb potential with charge $Z = -1$. One issue that is necessary to be aware of when high order partial waves are included, is the length of the used box to calculate the GSFs: it must be large enough in order to guarantee the asymptotic behavior.

First, we include partial waves up to $\ell_{\max} = 8$. In order to check the convergence of the GSF basis set, we calculate the relative error comparing our results at the binary peak with the analytical formula given by Byron *et al* [162]

$$f(\mathbf{q}, \mathbf{k}_b) = -\frac{8\sqrt{2}}{\pi}\frac{e^{\pi/2k_b}}{q^2}\Gamma(1+i\,\eta)\frac{\mathbf{q}\cdot[\mathbf{q}-\mathbf{k}_b\,(1-i\,\eta)]}{\left[q^2-(k_b+i)^2\right]^{1-i\,\eta}\left[(\mathbf{q}-\mathbf{k}_b)^2+1\right]^{2+i\,\eta}}, \tag{4.34}$$

where $\eta = -1/k_b$ is the Sommerfeld parameter. Such relative errors are plotted in Fig. 4.1. We see that if we use more than 25 basis functions, the relative errors are converged to values in the range $0.008\% - 0.2\%$, according to the chosen scattering angle. In comparison with the PI case (see Fig. 3.1) the errors are larger. The partial wave expansion of the Coulomb interaction is known to present slow convergence, in particular for small scattering angles. In order to prove this, we fix now the number of GSFs to 60, and we perform the same calculations but varying the number of included partial waves up to $\ell_{\max} = 12$. Results are shown in Fig. 4.2. For small scattering angles, the error is relatively stable for $\ell \geqslant 6$, and it decreases even more for higher angles, as expected.

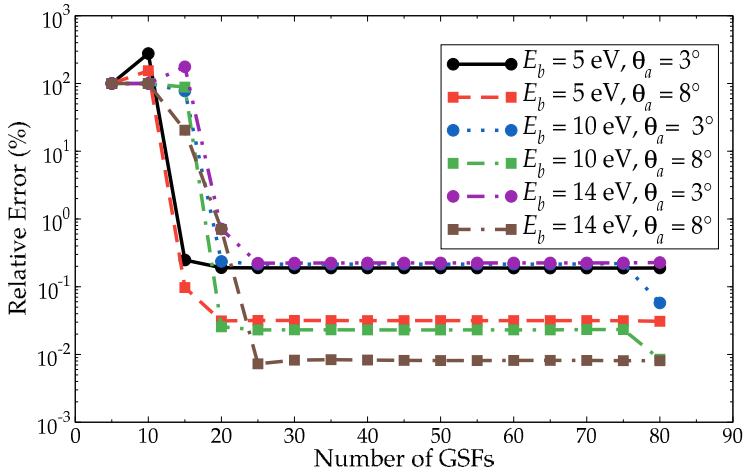

FIGURE 4.1 – Relative errors for the TDCS (4.33) at the binary peak, comparing with the analytical formula (4.34), as a function of the number of used GSFs. The TDCS were calculated for an incident electron with E_i = 250 eV, an ejected electron with E_b = 5, 10 and 14 eV, and the scattered electron detected at θ_a = 3° and 8°.

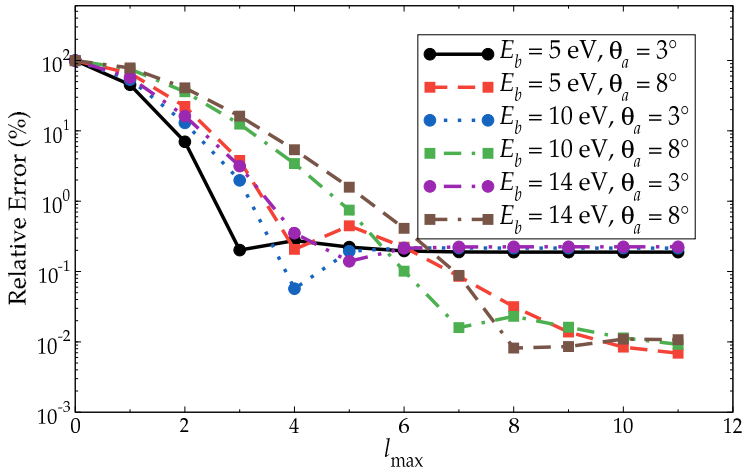

FIGURE 4.2 – Relative errors for the TDCS (4.33) at the binary peak, comparing with the analytical formula (4.34), as a function of the number of partial waves used to expand the operator (4.23). The TDCS were calculated for an incident electron with E_i = 250 eV, an ejected electron with E_b = 5, 10 and 14 eV, and the scattered electron detected at θ_a = 3° and 8°.

From Figs. 4.1 and 4.2 one can conclude that in order to obtain sufficient numerical precision while keeping the method computationally affordable, we can use a moderate number of GSFs, and a relatively small number of partial waves ($\ell \approx$ 6–8).

4.5.2. Results for H Atom

We now report our calculated TDCSs for H atom. Following the conclusions presented above, we limited ourselves to use a maximum of 60 GSFs, and with $\ell_{\max} = 8$ for our scattering wavefunction (4.18) and the corresponding interaction operator (4.23). We compare all our results with the analytical formula (4.34) and with the absolute experimental data by Lohmann *et al* [163].

For the first case ($E_b = 5$ eV), the TDCSs are given in Fig. 4.3. For each scattering angle ($\theta_a = 3°$, 5° or 8°), the orientation of the momentum transfer is $\theta_{\mathbf{q}} = 307.94°$, 296.38° and 289.45°, respectively. We see that our results are in an excellent agreement with the analytical results. Also, the experimental binary peak is quite well reproduced. It is observed that the recoil peak decreases when the scattering angle θ_a increases.

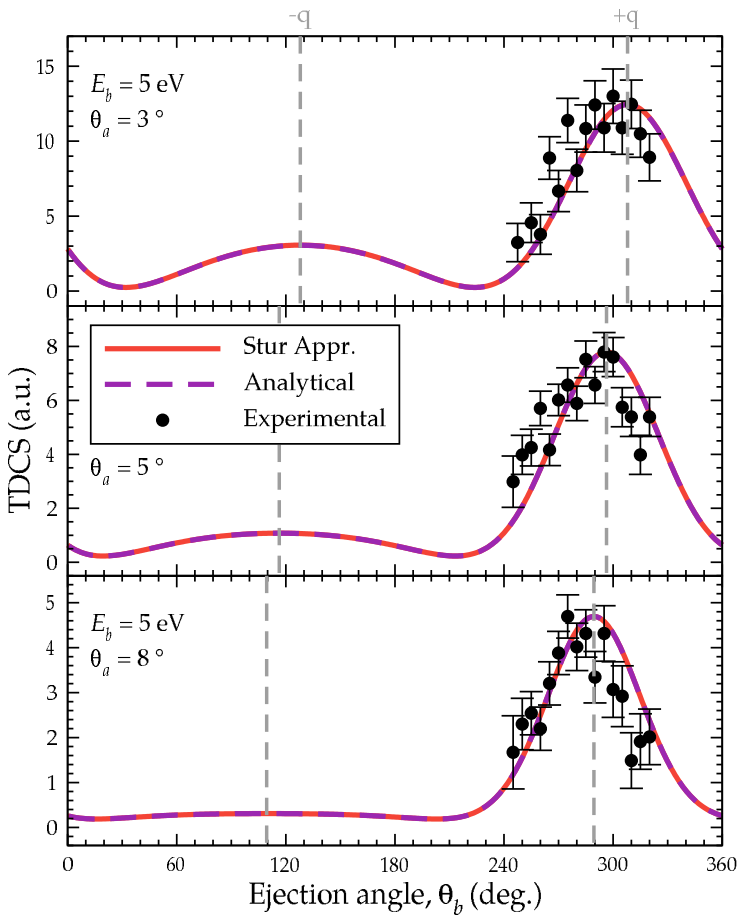

Figure 4.3 – TDCS for H atom, for an incident electron with $E_i = 250$ eV, an electron ejected with $E_b = 5$ eV, and for the three indicated scattering angles θ_a. Our results (red, solid) are compared with those of the analytical formula (4.34) [162] (purple, dash), and with absolute experimental data [163] (black, dots).

Next, in Fig 4.4, we consider ejected electrons with E_b = 10 eV. The orientation of the momentum transfer is $\theta_\mathbf{q}$ = 314.93°, 302.09° and 293.52°. Our results are again in an excellent agreement with the analytical results. At the binary peak the experimental data, however, are shifted.

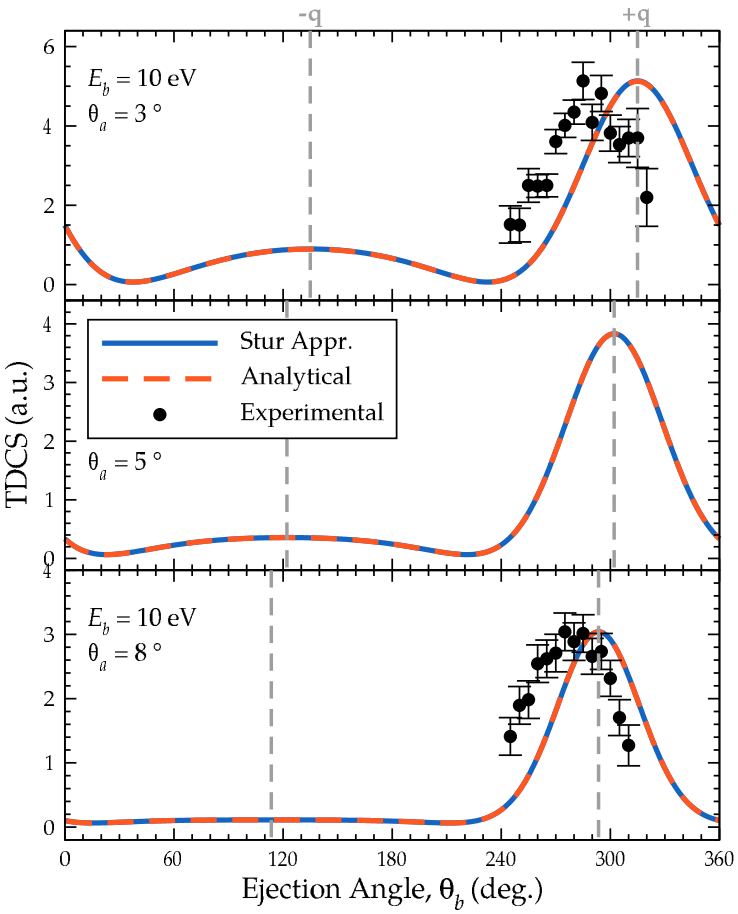

FIGURE 4.4 – Same as Fig. 4.3 for an electron ejected with E_b = 10 eV. Our results (blue, solid) are compared with the analytical result (orange, dash), and with experimental data (black, dots).

The same is observed for ejected electrons with E_b = 14 eV (Fig. 4.5, where $\theta_\mathbf{q}$ = 319.66°, 306.31° and 296.70°). This gives an indication that the first-Born approximation begins to lose its validity for these kinematic conditions [17, 363].

4.6. First Born Approximation: Results for Molecular Systems

We now move to the molecular case, following a procedure similar as for the atomic case, and using the same GSF basis set. A Coulomb potential is used as

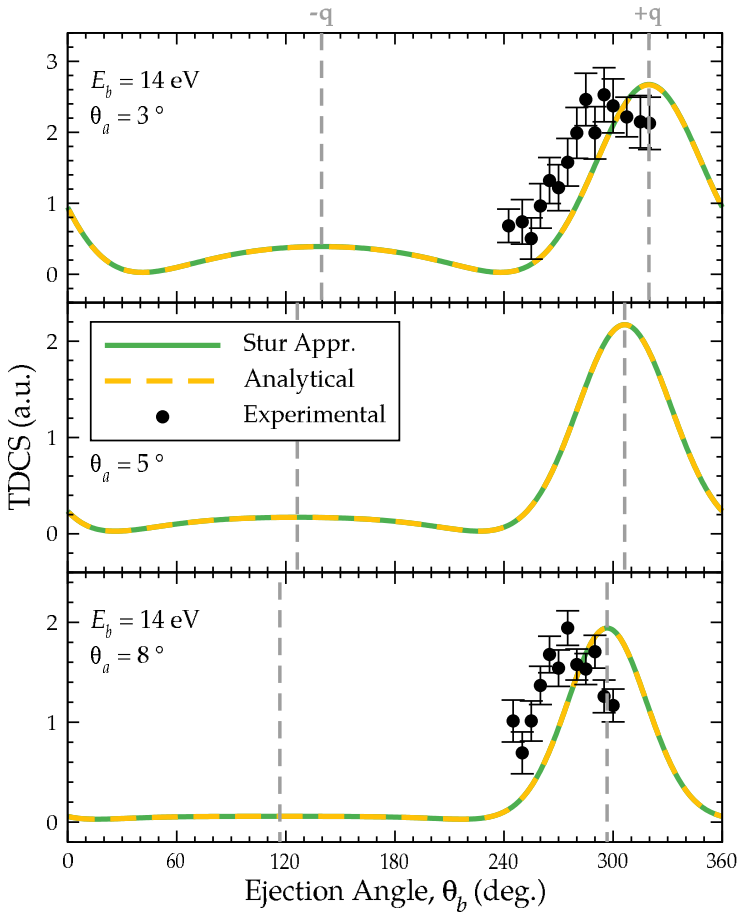

Figure 4.5 – Same as Fig. 4.3 for an electron ejected with E_b = 14 eV. Our results (green, solid) are compared with the analytical result (yellow, dash), and with experimental data (black, dots).

the transition operator, as indicated in Eq. (4.23). To model the ejected electron-molecule interaction, we use one of the three choices: a Coulomb potential (4.24), the AAP (4.25) or the MMP (4.26). For the first two options, calculations are relatively similar to those performed for H atom, while, when using the MMP, we need to solve an angular-coupled system of equations. After calculating all the required matrices, the linear system of equations (4.27) is solved in order to obtain the expansion coefficients, , i.e.,and then the TDCSs. Most of the calculations were performed at the `SIMPA` cluster at the Université de Lorraine. The used nodes are composed, individually, by four dual-core 2.66 GHz processors.

Since all experimental data for the studied molecules are only on a relative scale, we have renormalized each of them, and other theoretical calculations, to our calculated binary peak, obtained using the AAP. This allows for a qualitative comparison. A quantitative analysis is also made for each case by comparing —on

an absolute scale— our TDCSs with those obtained by other theoretical approaches.

4.6.1. CH_4

The TDCSs for ionization from the inner valence orbital $2a_1$ are given in Fig. 4.6, and from the outer valence MO $1t_2$ in Fig. 4.8. We compare our calculations with the CKM results (see App. G.12.2) by Lin *et al* [362] (that uses as initial state wavefunction of the molecule the calculated one using contracted Gaussian functions, in a state-averaged multiconfiguration self-consistent field); we also compare with BBK values (that uses, as we do, the initial state wavefunction calculated by Moccia) and with experimental data, both reported by Lahmam–Bennani *et al* [164]. For both MOs, the kinematic conditions are: the incident electron has an energy of $E_i = 500$ eV; the scattered projectile is detected at $\theta_a = -6°$; the ejected electron is detected with energies $E_b = 12$, 37 or 74 eV. Our calculation times, including all the spatial orientations, for ionization from $2a_1$ were around 8 hours (unparallel); for ionization from $1t_2$, it took about 342 hours for the 12 eV case 180 hours for the other ejection energies. The large difference of computation times is associated with the construction of the MOs themselves: the $2a_1$ orbital is composed basically of s-type STOs, while the three $1t_2$ orbitals involve a combination of STOs with different angular momenta (see Tab. 2.5).

For ionization from $2a_1$ orbital, the direction of the momentum transfer is $\theta_{\mathbf{q}} = 66.84°, 54.72°$ and $40.55°$, respectively. We see that all the binary peaks are essentially along the direction $+\mathbf{q}$. For $E_b = 12$ eV, our results reproduce easily the position and width of the binary peak. The experimental data shows a shoulder that appears at angles slightly larger than $\theta_{\mathbf{q}}$ (around 120°); it is not reproduced neither by BBK, CKM or by our calculations. Concerning the recoil region, the experimental data seem to present three peaks, the major one being shifted from $\theta_{\mathbf{q}}$ by about 25°; these data are only partially reproduced by CKM calculations. Results for our three different potentials are quite similar; only using the MMP potential to model the electron-molecule interaction, gives a small recoil peak, which remains slightly smaller than the experimental observation. For $E_b = 37$ eV, our results also reproduce the experimental binary region, which is now slightly shifted to higher ejection angles. Our calculations follow the behavior of experimental and BBK results. Similar to the previous energy case, BBK and our results are completely flat for the recoil region, but CKM can reproduce the magnitude of the maximum. None of the theoretical calculations produces the extra small structure observable at $\theta_b \approx 270°$. For $E_b = 74$ eV we have a more varied picture. Results for our three model potentials are different with respect to the binary peak widths. The MMP calculations yield practically no recoil peak, and is smaller than the Coulomb calculation; the opposite was

observed for the 12 eV case. The AAP calculation presents a curious minimum at the expected recoil peak position. On the other hand, it shows a rather large binary peak pretty close to the CKM result, both in more or less acceptable agreement with experimental data. Except for CKM, none of the presented calculations can reproduce the recoil peak. Moreover, the binary peak is now more shifted with respect to the **q** direction, indicating that our first-Born approximation is not sufficient to reproduce the experimental data for this case in particular. Both the BBK and CKM manage to better reproduce the peak position, but not so well its width.

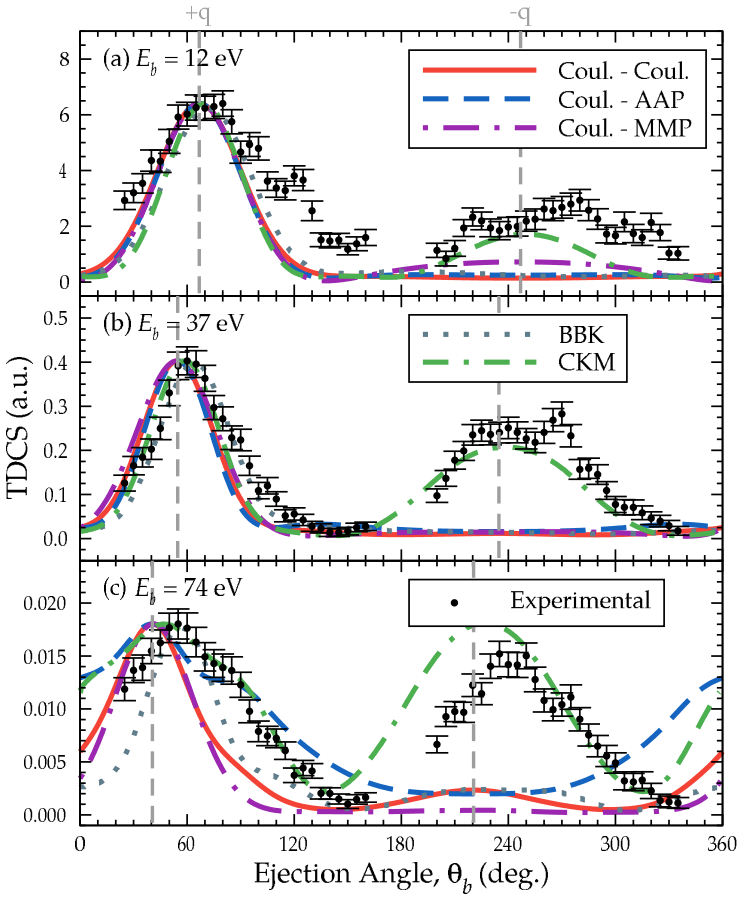

Figure 4.6 – TDCSs for CH_4 $\left(2a_1^{-1}\right)$. The incident electron has an initial energy $E_a = 500$ eV with a scattering angle $\theta_a = -6°$. The ejected electron energies are **(a)** $E_b = 12$ eV, **(b)** $E_b = 37$ eV and **(c)** $E_b = 74$ eV. Our results with the Sturmian approach use, as interaction potential, a Coulomb potential (red, solid), the AAP (blue, dashed), and the MMP (purple, dot-dashed). They are compared with CKM [362] (green, dot-dash-dashed) and BBK calculations (gray, dotted) and experimental data [164] (black, dots), all normalized to the maximum of the AAP binary peak. For each case the direction of the transfer momenta **q** is indicated (gray, dashed vertical lines).

In Fig. 4.7 we compare our TDCSs, obtained using all three interaction potentials and in their absolute scale, with the absolute BBK and CKM results. For all three

studied energies (E_b = 12, 37 and 74 eV), it is clear that MMP calculations have the strongest binary peak, the difference with other results being larger for higher energies. In contrast, CKM values have the lowest peak. Our calculations using the Coulomb potential and the AAP have similar values in such binary region. For BBK results, we find that the local maximum has always values lower to our Coulomb calculations, but higher than those of CKM, except for E_b = 74 eV. The shift with respect to $\theta_\mathbf{q}$ of such BBK peaks is appreciable: it is of about 10° for E_b = 37 eV, and about 20° for E_b = 74 eV. The analysis for the recoil regions is similar, where a complete absence of any recoil peak is notorious, except for our results using the MMP for E_b = 12 eV, and CKM calculations for E_b = 37 and 74 eV.

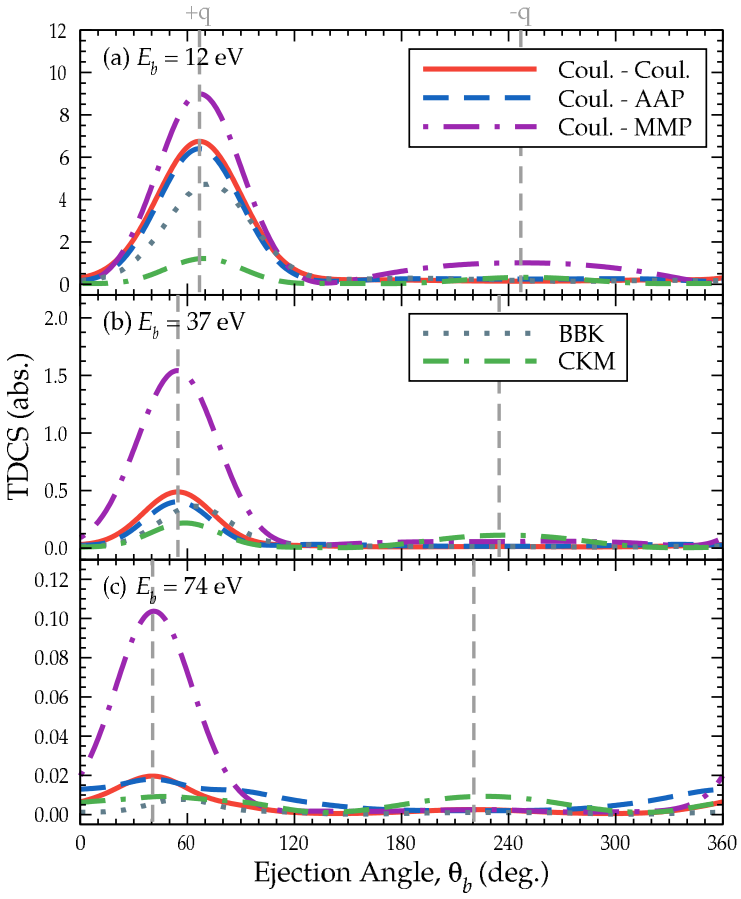

FIGURE 4.7 – Similar to Fig. 4.6, for CH_4 $\left(2a_1^{-1}\right)$. We present our Sturmian approach results, using either the Coulomb potential, the AAP or the MMP as interaction potentials, plus the BBK [164] and CKM [362] calculations, all in their respective absolute scale.

TDCSs for ionization from $1t_2$ orbital are presented in Fig. 4.8, where for the three energies we have, respectively, $\theta_\mathbf{q}$ = 72.86°, 59.97° and 44.40°. Since this MO is triply degenerated (see Tab. 2.5) we calculated separately the cross sections. For E_b = 12

eV we have a relatively varied picture. All our results can reproduce the subtle splitting of the peak in the binary region, that it is attributed to the degeneracy of the MO [164]. For E_b = 37 eV, such splitting in the binary peak is no longer observable. Our results are quite uniform: they reproduce the width of the binary peak, but not the position. The BBK and CKM calculations provide similar results, with the BBK getting the best agreement with experimental data, in particular with respect to the position. Our results predict practically no recoil structure, while the CKM calculation does a slightly better job, although failing in getting the experimental binary-recoil ratio. Finally, for E_b = 74 eV, our three results are consistent with each other, but cannot reproduce the position of the binary peak, with the experimental data being shifted from the $\theta_\mathbf{q}$ direction by about 15°. Similar to the BBK results, ours are flat in the recoil region, while the CKM is doing slightly better.

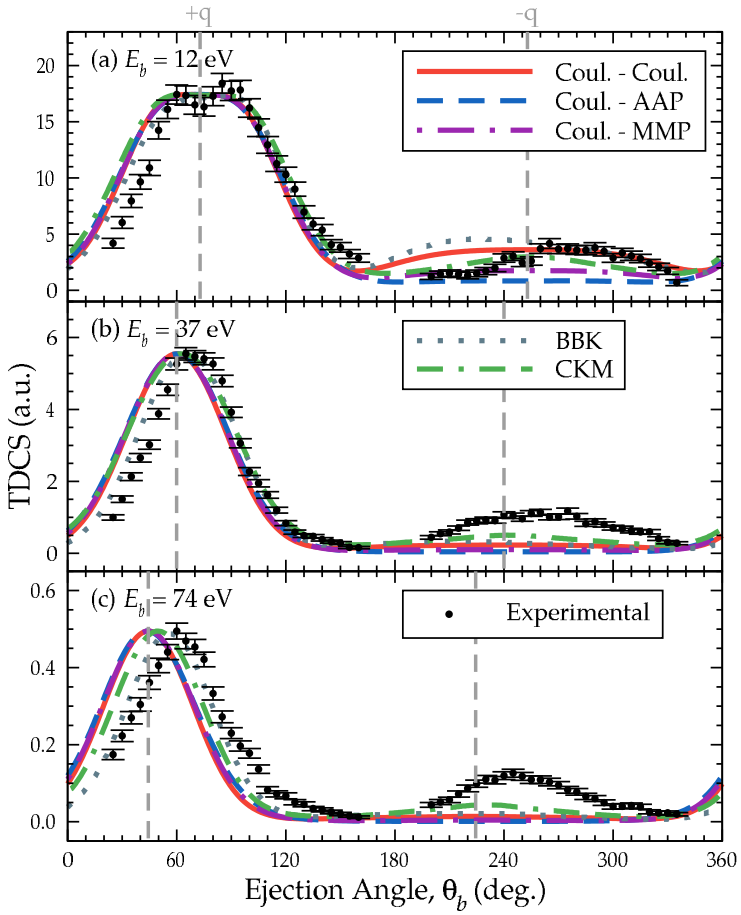

Figure 4.8 – Same as in Fig. 4.6, for CH_4 $\left(1t_2^{-1}\right)$.

Finally, we present in Fig. 4.9 the absolute values of BBK, CKM and our TDCSs. Similar to the results of the $2a_1$, CKM local maxima give the lowest values in the binary region for all studied energies, while our AAP gives the highest value. Contrary to the

$2a_1$ orbital case, the local MMP and AAP maxima are now comparable in magnitude. Also, our Coulomb results give systematically the lowest value for the binary peak, when compared with AAP and MMP values. Furthermore, BBK binary peaks are always lower that our Coulomb results, but higher than those of CKM. BBK results present a shift of the binary peak position with respect to the direction $\theta_{\mathbf{q}}$: about 10° for $E_b = 37$ eV, and 15° for $E_b = 74$ eV. Last, in the recoil region, the maxima obtained by BBK and by our Coulomb potential calculations are very similar in intensity and shape.

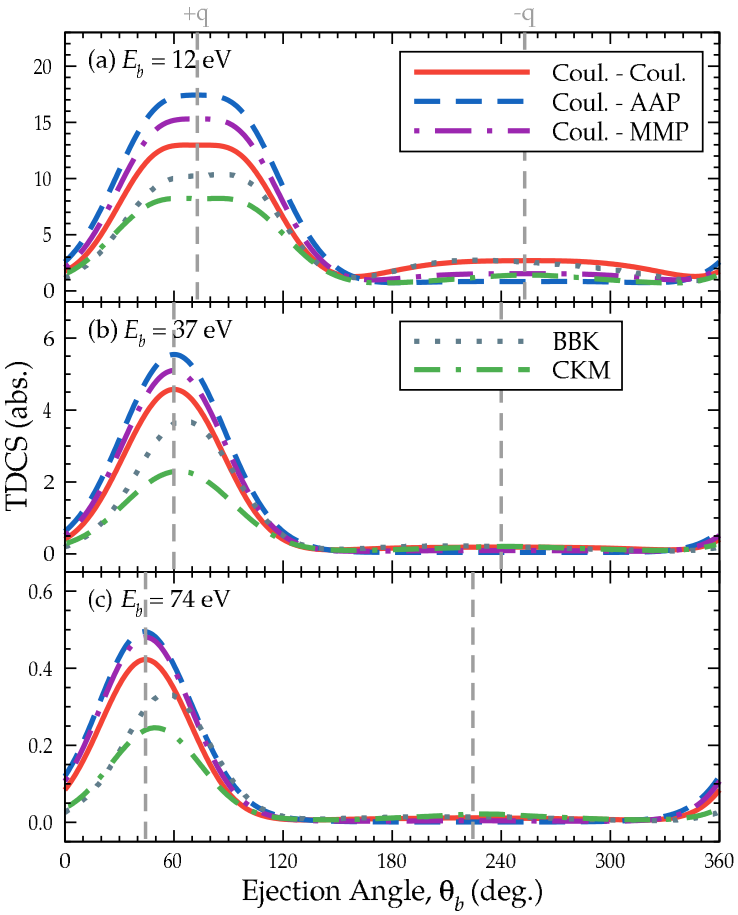

FIGURE 4.9 – Same as in Fig. 4.7, for CH_4 $\left(1t_2^{-1}\right)$.

For all our CH_4 results, we see that we can reproduce the experimental data fairly well in the binary region, in particular for $E_b = 12$ and 37 eV. After performing the angular average over the molecular orientations, all TDCSs acquire a cylindrical symmetry around the direction of the transfer momentum vector $\mathbf{q}$ [140]. Any deviation from this symmetry is understood as a breakdown of the first-Born approximation. One of the most intriguing features of our results is the absence of any recoil peak, no matter how the electron-molecule interaction is modeled. Then, a more detailed

description of the transition operator, via the second-Born approximation is needed, as well of the initial state wavefunction. Regarding the interaction potentials, as we tested different models and the results are similar, in our minds the "missing ingredient" lies more in the transition operator, and probably in the absence of any exchange.

4.6.2. H_2O

Our calculated TDCSs for both valence orbitals $3a_1$ and $1b_1$ are reported in Fig. 4.10. We compare our results with the theoretical calculations using the 1CW model by Champion *et al* [133] (that uses the same initial state wavefunction as us), and the CKM by Lin *et al* [363] (that uses as initial state wavefunction the one calculated with a *self-consistent field* (SCF), using contracted Gaussian functions as basis functions), and with the unnormalized experimental data by Milne–Brownlie *et al* [166]. We normalize the CKM and experimental data to our results, to make them coincide to our AAP maximum at the binary peak (right lobe). The kinematic conditions are: the incident electron has an energy $E_i = 250$ eV, the scattered projectile is observed at $\theta_a = -15°$; the ejected electron in the $3a_1^{-1}$ channel has an energy $E_b = 8$ eV (with $\theta_{\mathbf{q}} = 72.06°$), and in the channel $1b_1^{-1}$ $E_b = 10$ eV (with $\theta_{\mathbf{q}} = 71.89°$). We also calculated the TDCS for single ionization from both valence orbitals, where the ejected electron has an energy $E_b = 10$ eV. Unfortunately, the authors of the experimental data indicate that, for the the two outermost orbitals ($1b_1$ and $3a_1$), "due to the greater scatter in the binding energy data in the recoil region, it was not possible to unambiguously separate the two orbitals in this angular range" [166], and then they only reported, for each MO, the values of the TDCS for the binary region. They also give experimental TDCS values that mixed both ionization channels. Our calculation times for ionization from $1b_1$, including all the individual spatial orientations, were around 318 hours and for ionization from $3a_1$ orbital around 115 hours. The 1CW and our Coulomb potential calculations should be equivalent: both use the same initial state, and the ejected final state is represented by a Coulomb wave (a partial wave expansion for 1CW and in GSFs terms for ours). Any TDCS difference is due to numerical procedures and/or convergence issues.

For ionization from the orbital $1b_1$, in Fig. 4.10(a), all our results reproduce the binary region, in particular the position and width of the double peak; along the direction of the momentum transfer $\theta_{\mathbf{q}}$ one finds a local minimum. At that point, the 1CW and our results have a lower value compared with CKM and experimental data. The height of the maximum of the left lobe ($\theta_b < \theta_{\mathbf{q}}$) is not reproduced by any of the considered theoretical TDCSs, while the right lobe ($\theta_b > \theta_{\mathbf{q}}$) is fully reproduced. For the recoil region, the Coulomb potential and MMP —but not the AAP— calculations

present a strong peak. The intensity of the 1CW peak is comparable with our Coulomb results, while the CKM peak is comparable with our MMP values.

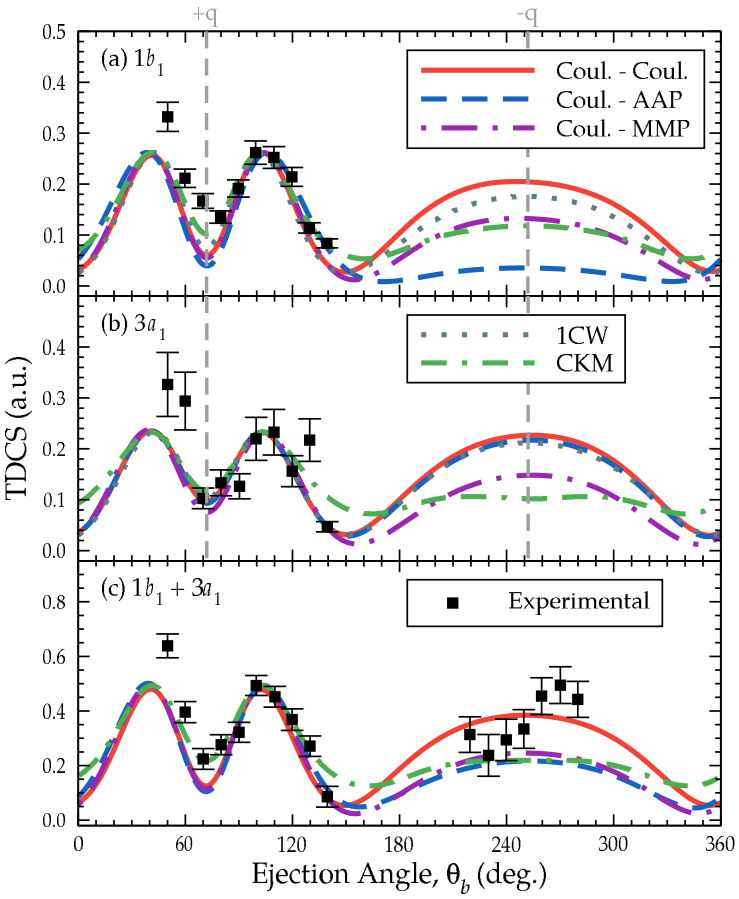

FIGURE 4.10 – TDCS for H_2O. The incident electron has an initial energy $E_a = 250$ eV and a scattering angle $\theta_a = -15°$. **(a)** $H_2O\left(1b_1^{-1}\right)$, ejected electron $E_b = 10$ eV; **(b)** $H_2O\left(3a_1^{-1}\right)$ for $E_b = 8$ eV; **(c)** $H_2O\left((1b_1 + 3a_1)^{-1}\right)$, with $E_b = 10$ eV. Our results use the Coulomb potential (red, solid), the AAP (blue, dashed) or the MMP (purple, dot-dashed) as interaction potentials. They are compared with 1CW [133] (gray, dotted) and CKM [363] (green, dot-dash-dashed) calculations, and with unnormalized experimental data [166] (black, squares), all normalized to the maximum of the AAP binary peak. The orientation of the transfer momentum **q** is indicated (gray, dashed vertical lines).

In Fig. 4.11(a) we present all our calculated TDCSs in their absolute scale, for ionization from the $1b_1$ orbital, and compare them with 1CW and CKM absolute results. In the binary region, except for our Coulomb results and 1CW calculations, that are similar to each other, it is clear that the local maxima of both lobes is different for each calculation, the CKM giving the upper limit, and our Coulomb potential results the lowest one. Except for CKM the local minima located along the direction

$\theta_{\mathbf{q}}$ coincides for all calculations. In the recoil region, results with the Coulomb potential give the upper limit, while the AAP gives the lower limit that, as mentioned above, is particularly low in comparison with Coulomb and MMP calculations. CKM and MMP recoil peaks are similar, and the difference with the BBK peak is small.

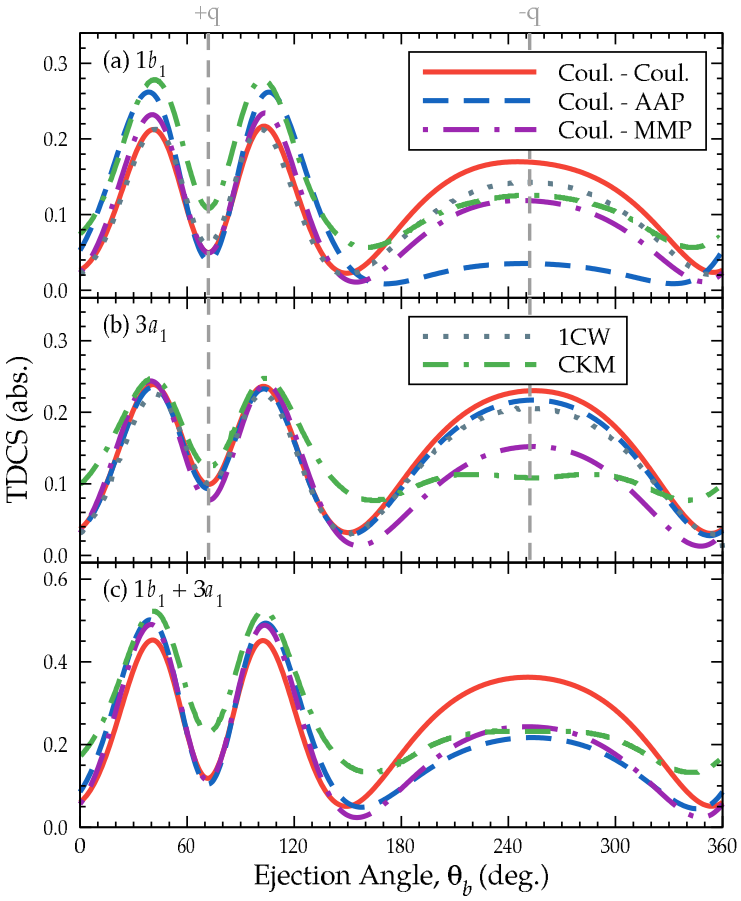

Figure 4.11 – Similar to Fig. 4.10, we present our Sturmian approach results, using either the Coulomb potential, the AAP or the MMP as interaction potentials, plus the 1CW [133] and CKM [363] calculations, all in their respective absolute scale.

For ionization from $3a_1$, presented in Fig. 4.10(b), our three calculations practically coincide with 1CW and CKM results, even at the local minimum at $\theta_b = \theta_{\mathbf{q}}$. We have also an excellent agreement with the experimental data, except for the left lobe, where the corresponding values are greater than any calculation. All our results can reproduce the position and width of the right lobe. For the recoil region, the CKM results present a peculiar behavior, with a local minimum along the direction $-\mathbf{q}$. The magnitude using the MMP is similar, but exhibits a local maximum, similar to the other calculations. The magnitudes of the recoil peak obtained using the Coulomb potential and the AAP are similar to those of 1CW.

The absolute TDCSs for ionization from $3a_1$ are given in Fig. 4.11(b). In the binary

region, all theoretical results are relatively uniform, except for CKM, whose binary peaks are slightly more spread out. Only a few differences appear in the local minima along the direction $\theta_{\mathbf{q}}$, where MMP gives a lower limit, and CKM a upper limit. In the recoil region, our Coulomb and AAP are similar, while MMP gives a lower peak and CKM have a different behavior, as mentioned before. Agreement between Coulomb potential, AAP and 1CW is observed over the whole angular range.

Finally, for the mixed channel, $1b_1+3a_1$, presented in Fig. 4.10(c), we add together the TDCSs for ionization from both $1b_1$ and $3a_1$ orbitals, where both electrons have a final energy $E_b = 10$ eV. We compare our TDCSs with the CKM calculation only. Concerning the binary region, our results, again, can reproduce the experimental data, in particular the position and width of the right lobe. The height of the local maximum of the left lobe (more precisely, the relative left-right magnitudes) is not reproduced by any of the included theoretical TDCSs. Our calculations, using all three interaction potentials, are consistent with each other. Moreover, for this particular configuration, we can compare our results with the experimental data in the recoil region, that has a strong peak. Results obtained using the Coulomb potential are of the same order (the binary-recoil ratio is the same), while such ratio using the AAP or the MMP is higher, and comparable to the CKM one. None of the calculations can reproduce the whole experimental recoil region: neither the position of the maximum at 270° nor the curious experimental point at 220° (which seems strange to us).

In Fig. 4.11(c) we present the absolute TDCSs for the mixed channel. The behavior of all theoretical results is, naturally, derived from the two previous cases. In the binary region, we have similar values for all TDCSs, in particular for our Coulomb potential and AAP calculations, that gives a lower limit in the $\theta_{\mathbf{q}}$ direction; CKM results give there the upper limit. On the other hand, in the recoil region, the Coulomb potential peak gives the upper limit (as in the previous cases), and the AAP the lowest one. The height of AAP, MMP and CKM lobes are comparable.

Results for H_2O are very peculiar, in particular when they are compared with CH_4. The main difference is seen in the recoil region, where all our calculations can reproduced the H_2O observations. As it was suggested in Ref. [164], this is due to the kinematic conditions, that are close the Bethe ridge conditions, where the momentum transfer is fully absorbed by the ejected electron, i.e., $q = k_b$. Under these conditions, the interaction with the ionized target is not strong, and our first-Born approximation is sufficient to describe the process.

4.6.3. NH_3

Our calculated TDCSs for the three valence MOs: $2a_1$, $1e$ and $3a_1$ are shown in Fig. 4.12. Our results are compared with unnormalized experimental data by El Mir *et al* [165] and BBK calculations [165] that use, as we do, the same initial state calculated by Moccia. The incident electron has an energy $E_i = 500$ eV, the scattered electron was detected at $\theta_a = -6°$. Electrons ejected from all the MOs were detected with a unique energy $E_b = 74$ eV; many experimental points were measured, giving clear binary and recoil structures. Our calculation times for ionization from $3a_1$ were around 163 hours, for ionization from $1e$ around 205 hours and for $2a_1$ around 165 hours.

First, for ionization from $3a_1$ orbital, the TDCSs are given in Fig. 4.12(a). The orientation of the momentum transfer is $\theta_{\mathbf{q}} = 45.29°$. We see that all our results are very similar to each other, and can satisfactorily reproduce the experimental data in the binary region, in particular the peak width (the position is shifted, though). On the other hand, BBK results reproduce better the position of the binary peak, but not so well its width. For higher ejection angles, in particular above $\theta_b = 100°$, the experimental binary lobe becomes wider, a behavior not observed for CH_4 and not reproduced by any theoretical calculation. In the recoil region, the experimental data show an important peak; the binary-recoil peak ratio is not reproduced either by BBK or by our calculations. The BBK recoil peak is particularly flat, while ours are slightly larger, but cannot reproduce the position (shifted by 20°) or the apparent structure at around 280°.

In Fig. 4.13(a) we show the absolute TDCSs for ionization from $3a_1$ orbital. In the binary region, all our results are similar, the Coulomb potential calculation being the lowest one. The discrepancy with the BBK binary peak is clear, both in magnitude and position (a shift of about 15°). In the recoil region all results are flat, and differences are no longer appreciable.

For ionization from $1e$, for which $\theta_{\mathbf{q}} = 43.52°$, our TDCSs are given in Fig. 4.12(b). Our three results are similar. In comparison with the experimental data, the binary peak is slightly shifted to smaller ejection angles while BBK results are shifted to higher ejection angles. Our TDCSs can roughly reproduce the width of the experimental binary peak, while the BBK peak is clearly much narrower. Experimental data show again a shoulder for higher ejection angles (above $\theta_b = 90°$) and a clear recoil peak, strongly shifted from $\theta_{\mathbf{q}}$: none of these features can be reproduced by either the BBK or our calculations.

In Fig. 4.13(b) we present absolute TDCSs for ionization from $1e$ orbital. Small differences start to appear in the binary region between our calculations, where the Coulomb potential results give the lowest peak, and the AAP the strongest. The

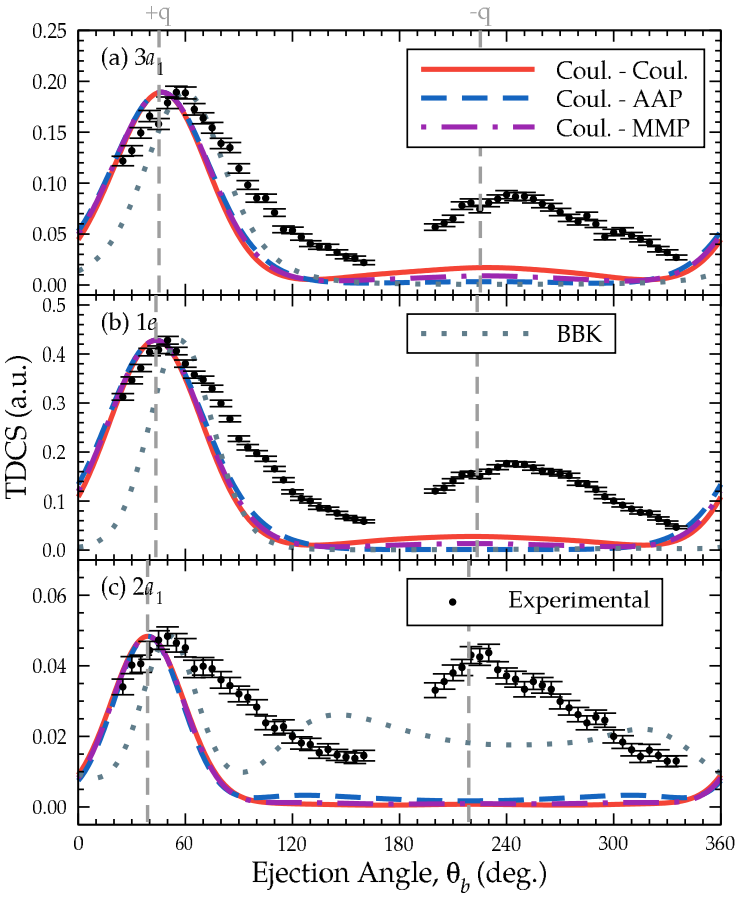

FIGURE 4.12 – TDCS for NH_3. Kinematic parameters: $E_a = 500$ eV, $E_b = 74$ eV, and scattering angle $\theta_a = -6°$, **(a)** $NH_3\left(3a_1^{-1}\right)$, **(b)** $NH_3\left(1e^{-1}\right)$ **(c)** $NH_3\left(2a_1^{-1}\right)$. Our results use the Coulomb potential (red, solid), the AAP (blue, dashed) or the MMP (purple, dot-dashed). They are compared with BBK [165] (gray, dotted) and unnormalized experimental data [165] (black, diamonds), all normalized to the maximum of the AAP binary peak. The orientation of the transfer momentum **q** is indicated (gray, dashed vertical line).

discrepancies with the BBK calculations are also evident: the BBK peak is much narrower, has a higher value and is shifted by about 15°. The recoil region is also completely flat, and similarly to the $3a_1$ case, differences are not appreciable.

Finally, for ionization from $2a_1$ ($\theta_{\mathbf{q}} = 38.82°$), the TDCSs are shown in Fig. 4.12(c). All our results are similar to each other, but they do not reproduce either the peak position or its width. BBK calculations reproduce only the peak position but, again, it is much narrower in comparison with the experimental one. In contrast to results for $3a_1$ or $1e$ orbitals, the measurements present binary and recoil peaks of almost the same intensity; also, the local minimum at $\theta_b \approx 150°$ is particularly high, relative to the binary and recoil peaks. None of the theoretical calculations have these two

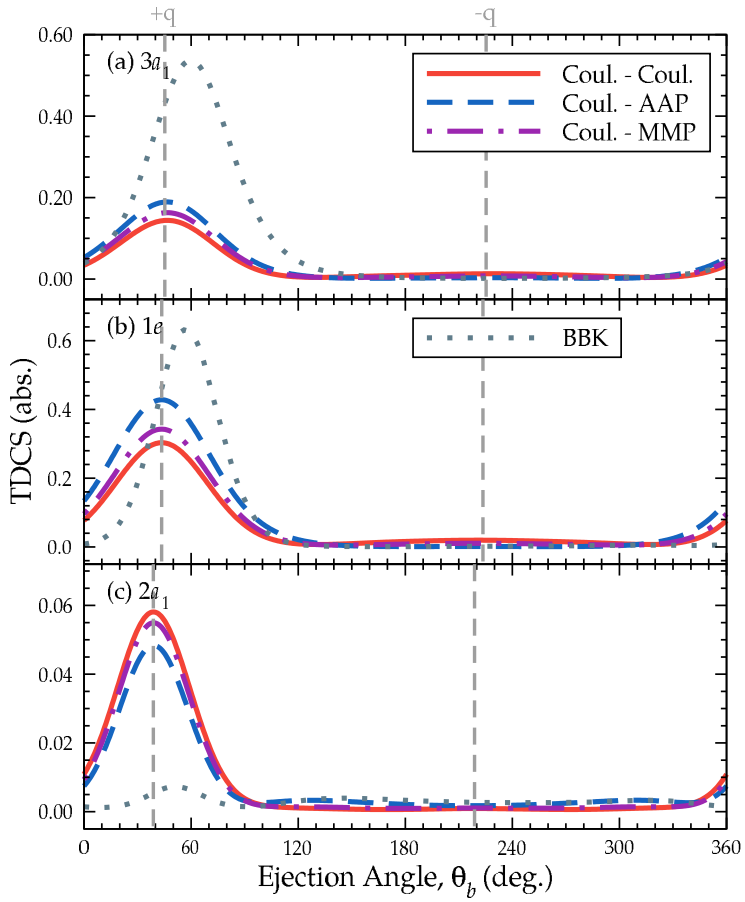

Figure 4.13 – Similar to Fig. 4.12, we present our Sturmian approach results, using either the Coulomb potential, the AAP or the MMP as interaction potentials, plus the 1CW [133] and CKM [363] calculations, all in their respective absolute scale.

features. Moreover, for the recoil region, the BBK calculation shows a very wide, unusual, lobe; it has a peculiar local maximum at $\theta_b \approx 150°$ (exactly where the experimental data presents a minimum) and close to $\theta_{-\mathbf{q}}$ it has a minimum in strong contrast with experimental observations. On the other hand, our results using the Coulomb potential and the MMP are completely flat, while AAP calculations show a behavior similar to the BBK recoil peak, but lower by one order of magnitude.

Comparing the theoretical absolute TDCSs for ionization from $2a_1$, shown in Fig 4.13(c), the observed behavior is slightly different to the other MOs, at least in the binary region. Our Coulomb potential calculations give an upper limit, that is comparable to the MMP results, while the AAP local maximum is slightly lower. Important differences appear when comparing with the BBK results: the latter is about one magnitude order smaller, and with a binary position shift of about 15°.

Results for NH_3 are very puzzling for us. For the PI case (see Sec. 3.6.2), our calculations are very good, in particular using the post-averaged scheme. Here,

we can reproduce only general features of the TDCSs in the binary region, and BBK calculations have similar difficulties. The recoil region is particularly demanding. At the moment of writing this PhD thesis, these issues are still under investigation, in particular with respect to the nature of the strong recoil peak. It is clear that a more sophisticated description of the target, and of the ionization process itself, is needed.

4.7. Conclusions

1. Similar to the PI case (see Chap. 3), the convergence analysis presented in Sec. 4.5.1, indicates that only a relatively small number of GSFs is needed to calculate accurately the scattering wavefunction and, then, the corresponding TDCSs. From Fig. 4.1 it is clear that for H atom we reach converged results very quickly, in particular when more than 30 functions are used. Contrary to the PI case, the description of the transition operator is more complex, and depends additionally on whether or not its own partial wave representation is converged. The dipolar operator in PI is only one of such multipolar terms. Through Fig. 4.2, we also observed that the accuracy of our calculations depends also on the partial wave convergence of the electron-electron interaction, known to be slow. Normally, this does not constitute a problem for our Sturmian approach, since the GSFs can provide the correct asymptotic behavior for each partial wave.

2. Considering our results for H atom, it is clear that we can reproduce within numerical precision the analytical first Born approximation TDCSs, which are in overall good agreement with available absolute experimental data. The first-Born approximation is valid for slow ejected electrons, but less so for increasing ejected energies. Adding a second-Born term could improve the results, getting the theoretical cross sections better reproduce the experimental binary peak position.

3. We explored in this chapter different approaches to model the interaction between the ejected electron and the ionized molecule. The quality of the results for the different considered options depends on the kinematic conditions. It is not possible to generalize our results, but in most cases the calculated TDCS binary peak is similar for all three model potentials (except for some cases with slow ejected electrons, as in CH_4). More differences appear in the description of the recoil region (particularly for slow ejected electrons) which is more sensitive to the electron-parental ion interaction.

4. For CH_4, our three different calculated TDCSs follow a similar behavior, in particular for the binary region: we can reproduce the peak for the lowest energies, i.e., for E_b = 12 and 37 eV, for both $2a_1$ and $1t_2$ orbitals; for E_b = 74 eV we see an important shift in the TDCSs maximum, indicating that it is necessary to go beyond the first-Born approximation. On the other hand, the observed recoil peaks are difficult to reproduce, even within a BBK approach.

5. Our results for H_2O can reproduce quite well the available experimental data, at least in the binary peak. Unfortunately there are no other experimental results to compare with, but the double peak is present. The strength of the first branch is not reproduced by any method, and could be related to measurement issues. The recoil peak is particularly strong for this molecule; as explained by Lahmam–Bennani *et al* [164], this is due to the kinematic conditions (close the Bethe ridge conditions), for which the momentum transfer is fully absorbed by the ejected electron. This means that the interaction of the electrons with the ionized target is not strong, and easily described by any of the proposed interaction potentials.

6. Results for NH_3 are very puzzling. For the studied kinematic conditions, our results with the Sturmian approach can reproduce approximately the experimental maxima in the binary region. However, the width of the measured peaks is rather larger and extends to much larger ejection angles. This was not observed in either CH_4 or H_2O, and no theory shows such a behavior. Also, experimentally, a strong recoil peak is observed (neither the BBK or our calculations can yield the observed binary to recoil ratio). Within our investigations and discussions with the authors of the experimental and BBK results, several explanations have been proposed, including measurement errors and interaction with the vibrational structure of the molecule. At the moment of writing this thesis none of them have been confirmed yet.

7. Analyzing all our results, we see no large differences between using the AAP and the MMP potentials, at least for the considered kinematic conditions and the investigated molecular systems. We therefore deduce that, within our first-Born Sturmian approach, the initial state and the electron-electron interaction (which constitute the ingredients of the driven term) play a dominant role. Therefore a more detailed description of the initial state of each molecule is needed.

As a summary, our first-Born calculation, using GSFs and different molecular model potentials, manage —like other theoretical calculations— to reproduce some,

but not all, of the experimental TDCS features. In most cases, important differences between several theoretical calculations were observed for the binary to recoil ratio. Concerning the absolute scale, large variations were also seen; only absolute experimental data could indicate which model is more adequate, at least for the TDCS magnitude. Better theoretical-experimental agreement can certainly be obtained by improving the initial state description, the model potentials and, mostly, by including second Born effects.

Chapter 5

Conclusions

In this thesis we implemented a Sturmian approach to study single ionization of molecules by photon or electron impact. Within a *single active electron* (SAE), *frozen core* (FC) and *one-center expansion* (OCE) framework, both scattering processes are studied by solving a system of angular-coupled driven equations that result from a first-order perturbation approach. For atomic targets or molecules described by a model central potential, the system is reduced to a single non-homogeneous differential equation. *Generalized Sturmian functions* (GSFs) are used as one particle basis functions to expand the continuum wavefunction representing the electron ejected from the molecular target. Since our GSFs have by construction the correct asymptotic behavior, we can calculate scattering wavefunctions with well defined boundary conditions, without imposing additional restrictions over the basis sets as done in some other theoretical methods. Because of their intrinsic property, GSFs allow for a straightforward extraction of the ionization scattering amplitude. The obtained cross sections for several polyatomic molecules were compared with experimental data and other theoretical calculations, for both *photoionization* (PI) (Chap. 3) and $(e, 2e)$ (Chap. 4) processes. As initial molecular state we used the ground state wavefunctions calculated by Moccia, and considered different model potentials to describe the interaction between the ejected electron and the parental ion. A general picture was

observed: our results —like those of many other theoretical approaches— cannot reproduce all the cross section features observed experimentally. The conclusions given for each process are summarized hereafter.

5.1. Photoionization

For the study of single PI process of molecular targets, we start by validating our Sturmian approach with atoms, in particular with H for which known analytical results allow one to test basis convergence and numerical accuracy. From our investigation it is clear that we only need to use a moderate number of basis elements to obtain a very acceptable degree of accuracy. The convergence of the Sturmian approach is always good regardless of the ejected electron energy, so that there is no virtual energy limit to study the continuum of an atomic or molecular system. This is one of the main differences with other theoretical methods, such as those based on variational principles, for which the validity of the calculations can be heavily limited by the number of basis elements and their ability to represent continuum states of different energies. Our PI cross sections for He and Ne are quite good, in particular for the L gauge, using any of the one-electron model potentials. For Ne we found an important gauge disagreement which is understood as a failure of the target description and the use of the SAE approximation. Clearly, core effects must be treated more carefully.

After validating the method with atoms, we moved to study molecules. Several issues appear, in particular the multicenter nature of the target Hamiltonian and the random orientation of the molecule with respect to the laboratory frame. For the former, in order to simplify our calculations, we use the SAE and the OCE approximations; for the latter we adopt two different approaches: the pre- and post-averaged schemes, employing molecular model potentials. We calculated PI cross sections for ionization from the outer and inner valence orbitals of different molecules (for which the OCE is deemed valid): CH_4, NH_3, H_2O, SiH_4 and H_2S. In either L or V gauges, and from the outer valence orbitals, our calculated cross sections in both pre- and post-averaged schemes are similar, in particular for high energies. On the other hand, closer to the ionization threshold, we observe some differences between the two schemes, and this in both gauges. In general, we see that the V gauge, in the post-averaged scheme, gives the best agreement with experimental data and/or other theoretical results. The description of ionization from inner valence orbitals is generally harder because of the interaction with the other bound electrons is stronger; it is not surprising that our results show a poorer agreement with experimental data, particularly for the L gauge. But again, results for the V gauge are

acceptable, in particular for high photoelectron energies.

We also studied ADCSs for the same molecular targets, and presented the corresponding asymmetry parameters β. For the more "symmetrical" molecules, i.e., for CH_4 and NH_3 we obtained good results in comparison with available experimental data. For other cases, such as H_2O and H_2S, our results are generally not good. We found also that the best way to describe such asymmetry parameters is using the post-averaged scheme, in which the different angular momenta are coupled; indeed, it is the interferences between the scattering wavefunction partial waves that gives origin to the asymmetry in the angular distributions.

Studying molecular ionization is not an easy task, as can be appreciated from all our comparisons, where the agreement between different theoretical approaches is minimal. Since, by construction, the GSFs basis set have the correct asymptotic behavior, improvements should be done in the description of the initial state wavefunctions as well as all other possible many-body interactions. Also more experimental data is required in order to check the validity of different theoretical approaches over the whole energy spectrum, and in particular close to the ionization threshold.

5.2. Electron-Molecule Collisions

For the single ionization by electron collision of molecules, we focused on $(e, 2e)$ processes which provide —through the TDCS— the most detailed ionization information. We worked again within the SAE, FC and OCE framework, and presented the theoretical formulation within the first- and second-Born approximations. For the latter, use is made of the closure approximation, and a numerical strategy is proposed. Similarly to the PI counterpart, we first validated our Sturmian approach with H atom, reproducing very accurately first-Born approximation analytical TDCSs for several kinematical conditions; from the analysis of the relative errors we showed that, again, only a moderate number of basis functions is needed in order to obtain converged results.

We then studied $(e, 2e)$ in molecules, in particular for ionization from the outer and inner valence orbitals of CH_4, H_2O and NH_3. In order to incorporate the random spatial molecular orientation, we adopted a similar strategy to the PI post-averaged scheme, rotating the initial state wavefunctions and performing at the end the corresponding angular average. Analyzing our first-Born approximation results we obtained a widely varied picture, in part because of the different considered orbitals and kinematic conditions. As for PI, it is worth emphasizing once again that not all the experimental data can be reproduced by the theoretical calculations available in the literature. The binary regions are globally well described, but many

discrepancies appear in the recoil region.

For H_2O, our results could reproduce easily experimental data, in particular the recoil region that usually is one of the most challenging to calculate. For CH_4 and NH_3, we reproduced experimental data for the binary region, in particular for slow ejected electrons. We also evidenced some clear first-Born approximation breakdowns, such as the experimental binary peak being shifted away from the momentum transfer direction. Contrary to H_2O, and in particular for NH_3, we found that is not so easy to reproduce the recoil region, even using interaction potentials that describe accurately the projectile-molecule interaction. Several observed TDCS features, including the large peak width for NH_3, cannot be reproduced by our results or by the only other calculation available. Some explanations have been put forward, but at the moment of writing this thesis none of them has been proved yet.

Finally, all the available measurements for molecular electron-impact ionization are given in a relative scale, and then only shape comparisons can be made between theoretical results and experimental data. It is clear that absolute data is needed to perform direct comparisons between the different calculations, particularly to determine which could give, at least, the correct TDCS magnitude of the binary peak.

5.3. Perspectives

After showing the implementation of the Sturmian approach, and after analyzing our results, some aspects need clearly to be improved: the description of the PI cross sections for slow electrons, the gauge agreement of such cross sections and the reproduction of the binary peaks of the $(e, 2e)$ TDCSs. Part of the solution could come from using more accurate initial state wavefunctions, in particular many-body wavefunctions, provided by any of the methods used in quantum chemistry; such tools should also help in investigating ionization of more complex molecular systems, such as DNA basis and small proteins. For $(e, 2e)$, improved results should come from the implementation of the second-Born approximation. Here we proposed a numerical strategy to calculate the corresponding transition amplitudes, but have not yet obtained numerically acceptable results; it is well known that is not easy to achieve a good convergence of such kind of calculations. In addition, in order to speed up the convergence of our Sturmian approach, a more detailed study on the implementation of the Levin's collocation method is desirable, in particular with the kind of numerical grid adopted here to solve the involved single differential equation.

A second stage of calculations, using the Sturmian approach, must go further than the SEA and the SAE approximations. The use of potentials that describe more

accurately the electronic correlation and the use many-body wavefunctions allow one to study a more rich dynamics of the core of the target. Also, it would be interesting to investigate the effects of the inclusion of the vibrational structure of the nuclei (when it is possible). It could account for some of the observed structures in different differential ionization cross sections. Moreover, we do not use symmetry-adapted MOs, in particular for the continuum states. Their use could help us to improve the computing times.

One could envisage adapting the Sturmian approach to study multi-photon ionization. In this thesis we show how to implement it to study only first-order processes (single PI). The extension to second or higher orders is —in principle— relatively direct, using again GSFs for each intermediate or final states. Besides, the solution to the driven equation could allow one to study time-dependent processes, in particular interaction with short-laser pulses and coherent control. In fact, the Sturmian approach is quite well suited to such problems: the correct asymptotic behavior is already built in the basis sets, and it is easy to extract any additional phase shift attributed to any non-Coulombian potential, needed to calculate, for instance, the so-called Eisenbud–Wigner–Smith time-delay [161].

Another natural application is the electron impact double ionization (also called $(e, 3e)$) of molecules, for which one needs two-active electron (three-body) wavefunctions. Similarly to the already studied atomic He case, an angularly coupled double GSF expansion with adequate energies can be used. Another option consists in employing hyperspherical coordinates which facilitate the construction of the double continuum boundary conditions (the hyperspherical front). Application of this Sturmian approach to electron (or proton) double ionization of molecular targets is still unexplored.

Finally, on a separate line of investigation, molecular GSFs for bound states are currently under development within a joint collaboration between the Université de Lorraine, the Universidad Nacional del Sur and the Universidad de Buenos Aires.

Appendix A

Rotation Operator

Here, we show the fundamental properties of the rotation operator [167].

For a given set of Euler angles $\hat{\mathfrak{R}} = (\alpha, \beta, \gamma)$, the rotation operator acting upon an arbitrary eigenfunction of L^2, i.e., a spherical harmonics, noted here as

$$\langle \mathbf{r} | \, \ell m \rangle = Y_\ell^m(\hat{r}), \tag{A.1}$$

is defined by [167]

$$\widehat{D}\left(\hat{\mathfrak{R}}\right) | \, \ell m \rangle = \sum_{m'} | \, \ell m' \rangle \, \langle \ell m' | \, \widehat{D}\left(\hat{\mathfrak{R}}\right) | \ell m \rangle \, , \tag{A.2}$$

where the completeness of the spherical harmonics were used; the matrix element is defined as

$$\begin{aligned} \langle \ell m' | \, \widehat{D}\left(\hat{\mathfrak{R}}\right) | \ell m \rangle =& \mathscr{D}^\ell_{m'm} \\ =& \mathrm{e}^{\mathrm{i}\, m'\alpha} d^{(\ell)}_{m'm}(\beta) \mathrm{e}^{\mathrm{i}\, m\gamma}, \end{aligned} \tag{A.3}$$

and

$$\begin{aligned} d^{(\ell)}_{m'm}(\beta) =& \langle \ell m' | \, \mathrm{e}^{\mathrm{i}\,\beta \hat{J}_y/\hbar} \, | \ell m \rangle \\ =& \left[\frac{(\ell + m')! \, (\ell - m')!}{(\ell + m)! \, (\ell - m)!} \right]^{1/2} \left(\cos \frac{\beta}{2} \right)^{m'+m} \left(\sin \frac{\beta}{2} \right)^{m'-m} P^{(m'-m, m'+m)}_{\ell - m'}(\cos \beta) \end{aligned} \tag{A.4}$$

where $P_n^{(i,j)}(x)$ are the Jacobi polynomials [167].

Appendix B

Integrals for Molecular Potentials

In this Appendix we show the details of the calculation of the angular and radial integrals that appear in the definition of the molecular model potential (2.27).

B.1. Angular Integrals

Besides the orthogonal relation

$$\int \mathrm{d}\hat{r}\, Y_{\ell_1}^{m_1}(\hat{r})^* \, Y_{\ell_2}^{m_2}(\hat{r}) = \delta_{\ell_1\ell_2}\, \delta_{m_1 m_2}, \tag{B.1}$$

one of the integrals we need is that of with three spherical harmonics, given in terms of the Wigner 3-j symbols [167]

$$\begin{aligned} \Upsilon_{\ell_1\ell_2\ell_3}^{m_1 m_2 m_3} &= \int \mathrm{d}\hat{r}\, Y_{\ell_1}^{m_1}(\hat{r})\, Y_{\ell_2}^{m_2}(\hat{r})\, Y_{\ell_3}^{m_3}(\hat{r}) \\ &= \left[\frac{(2\ell_1+1)\,(2\ell_2+1)\,(2\ell_3+1)}{4\pi}\right]^{1/2} \begin{pmatrix} \ell_1 & \ell_2 & \ell_3 \\ 0 & 0 & 0 \end{pmatrix} \begin{pmatrix} \ell_1 & \ell_2 & \ell_3 \\ m_1 & m_2 & m_3 \end{pmatrix}. \end{aligned} \tag{B.2}$$

Another useful expressions are the angular matrix elements for the gradient operator, called simply the gradient formula [167]

$$\langle \ell_1 0 | \nabla_0 \phi_\gamma(r) | \ell_2 0 \rangle = \Delta_{\ell_1 \ell_2} \left(\frac{\partial}{\partial r} + \frac{b_{\ell_1 \ell_2}}{r} \right) \phi_\gamma(r), \tag{B.3a}$$

$$\langle \ell_1 m_1 | \nabla_\mu \phi_\gamma(r) | \ell_2 m_2 \rangle = \Pi^{m_1 \mu m_2}_{\ell_1 1 \ell_2} \langle \ell_1 0 | \nabla_0 | \gamma \ell_2 0 \rangle, \tag{B.3b}$$

where

$$\Pi^{m_1 \mu m_2}_{\ell_1 1 \ell_2} = (-1)^{m_1} \begin{pmatrix} \ell_1 & 1 & \ell_2 \\ -m_1 & \mu & m_2 \end{pmatrix} \begin{pmatrix} \ell_1 & 1 & \ell_2 \\ 0 & 0 & 0 \end{pmatrix}^{-1}, \tag{B.4a}$$

$$\Delta_{\ell_1 \ell_2} = \begin{cases} \dfrac{\ell_2 + 1}{[(2\ell_2 + 1)(2\ell_2 + 3)]^{1/2}} & \text{if } \ell_1 = \ell_2 + 1, \\ \dfrac{\ell_2}{[(2\ell_2 - 1)(2\ell_2 + 1)]^{1/2}} & \text{if } \ell_1 = \ell_2 - 1, \end{cases} \tag{B.4b}$$

$$b_{\ell_1 \ell_2} = \begin{cases} -\ell_2 & \text{if } \ell_1 = \ell_2 + 1, \\ \ell_2 + 1 & \text{if } \ell_1 = \ell_2 - 1. \end{cases} \tag{B.4c}$$

B.2. Radial Integrals

We want to calculate the radial integral

$$\frac{\vartheta^{(\ell)}_{ij}(r)}{r} = \int_0^\infty \mathrm{d}r'\, r'^2\, \mathcal{R}_i(r')\, \frac{r^\ell_<}{r^{\ell+1}_>}\, \mathcal{R}_j(r'), \tag{B.5}$$

where $r_< \equiv \min(r, r')$, $r_> \equiv \max(r, r')$ and the STOs functions are defined as in Eq. (2.22)

$$\mathcal{R}_i(r) = \alpha_i\, r^{n_i - 1}\, \mathrm{e}^{-\zeta_i r}. \tag{B.6}$$

This integral can be separated as

$$\begin{aligned} \frac{\vartheta^{(\ell)}_{ij}(r)}{r} =& \frac{1}{r^{\ell+1}} \int_0^r \mathrm{d}r'\, r'^2\, \mathcal{R}_i(r')\, r'^\ell\, \mathcal{R}_j(r') + r^\ell \int_r^\infty \mathrm{d}r'\, r'^2\, \mathcal{R}_i(r')\, \frac{1}{r'^{\ell+1}}\, \mathcal{R}_j(r') \\ =& \alpha_i \alpha_j \left[\frac{1}{r^{\ell+1}} \int_0^r \mathrm{d}r'\, \mathrm{e}^{-(\zeta_i + \zeta_j) r'} r'^{n_i + n_j + \ell} + r^\ell \int_r^\infty \mathrm{d}r'\, \mathrm{e}^{-(\zeta_i + \zeta_j) r'} r'^{n_i + n_j - \ell - 1} \right] \\ =& \alpha_i \alpha_j \left[\frac{1}{r^{\ell+1}} \int_0^r \mathrm{d}r'\, \mathrm{e}^{-\zeta_{ij} r'} r'^{\delta_{ij\ell}} + r^\ell \int_r^\infty \mathrm{d}r'\, \mathrm{e}^{-\zeta_{ij} r'} r'^{\varepsilon_{ij\ell}} \right] \end{aligned} \tag{B.7}$$

where

$$\zeta_{ij} = \zeta_i + \zeta_j, \tag{B.8a}$$

$$\delta_{ij\ell} = n_i + n_j + \ell, \tag{B.8b}$$

$$\varepsilon_{ij\ell} = n_i + n_j - \ell - 1. \tag{B.8c}$$

If we use the change of variable $x = \zeta_{ij} r$, then the integral (B.7) becomes

$$\frac{\vartheta_{ij}^{(\ell)}(r)}{r} = \alpha_i \alpha_j \left[\frac{1}{r^{\ell+1}} \zeta_{ij}^{-\delta_{ij\ell}-1} \int_0^{\zeta_{ij} r} \mathrm{d}x\, \mathrm{e}^{-x} x^{\delta_{ij\ell}} + r^{\ell} \zeta_{ij}^{-\varepsilon_{ij\ell}-1} \int_{\zeta_{ij} r}^{\infty} \mathrm{d}x\, \mathrm{e}^{-x} x^{\varepsilon_{ij\ell}} \right]. \quad \text{(B.9)}$$

The first integral is given by the incomplete Gamma function (B.13a),

$$\begin{aligned} I_{ij\ell} =& \int_0^{\zeta_{ij} r} \mathrm{d}x\, \mathrm{e}^{-x} x^{\delta_{ij\ell}} \\ =& \gamma\left(\delta_{ij\ell} + 1, \zeta_{ij} r\right), \end{aligned} \quad \text{(B.10)}$$

and the second integral by the complement to the incomplete gamma function (B.13b)

$$\begin{aligned} J_{ij\ell} =& \int_{\zeta_{ij} r}^{\infty} \mathrm{d}x\, \mathrm{e}^{-x} x^{\varepsilon_{ij\ell}} \\ =& \Gamma\left(\varepsilon_{ij\ell} + 1, \zeta_{ij} r\right). \end{aligned} \quad \text{(B.11)}$$

Replacing (B.10) and (B.11) in (B.9), we obtain finally

$$\begin{aligned} \frac{\vartheta_{ij}^{(\ell)}(r)}{r} &= \alpha_i \alpha_j \left[\frac{1}{r^{\ell+1}} \zeta_{ij}^{-\delta_{ij\ell}-1} \gamma\left(\delta_{ij\ell} + 1, \zeta_{ij} r\right) + r^{\ell} \zeta_{ij}^{-\varepsilon_{ij\ell}-1} \Gamma\left(\varepsilon_{ij\ell} + 1, \zeta_{ij} r\right) \right] \\ &= \alpha_i \alpha_j \left[\frac{1}{r^{\ell+1}} \zeta_{ij}^{-(n_i+n_j+\ell+1)} \gamma\left(n_i + n_j + \ell + 1, \left(\zeta_i + \zeta_j\right) r\right) \right. \\ &\quad \left. + r^{\ell} \zeta_{ij}^{-(n_i+n_j-\ell)} \Gamma\left(n_i + n_j - \ell, \left(\zeta_i + \zeta_j\right) r\right) \right]. \end{aligned} \quad \text{(B.12)}$$

Some useful relations used to evaluate the incomplete and the complement gamma functions are summarized hereafter.

B.3. Incomplete Gamma Function

The incomplete gamma function and its complement are defined as [168, 172]

$$\gamma(a, x) = \int_0^x \mathrm{d}t\, \mathrm{e}^{-t}\, t^{a-1}, \ \Re(a) > 0 \quad \text{(B.13a)}$$

$$\Gamma(a, x) = \int_x^{\infty} \mathrm{d}t\, \mathrm{e}^{-t}\, t^{a-1}. \quad \text{(B.13b)}$$

with $\Gamma(a) = \gamma(a, x) + \Gamma(a, x)$.

In order to manipulate the function (B.12), i.e. calculating its values or performing further integration, it is useful to express the incomplete gamma and the complement

gamma functions in a power series expansion (see Sec. 8.352 of [172])

$$\gamma(n+1,x) = n!\left(1 - \mathrm{e}^{-x}\sum_{m=0}^{n}\frac{x^m}{m!}\right), \text{ for } n = 0,1,\cdots \tag{B.14a}$$

$$\Gamma(n+1,x) = n!\,\mathrm{e}^{-x}\sum_{m=0}^{n}\frac{x^m}{m!}, \text{ for } n = 0,1,\cdots \tag{B.14b}$$

$$\Gamma(-n+1,x) = \frac{(-1)^{n+1}}{(n-1)!}\left[\Gamma(0,x) - \mathrm{e}^{-x}\sum_{m=0}^{n-2}\frac{(-1)^m\,m!}{x^{m+1}}\right], \text{ for } n = 2,3,\cdots. \tag{B.14c}$$

Unfortunately, the evaluation of Eqs. (B.14) for several values of the parameter n and the variable x, can become a computational demanding task. For that reason it is useful to have some recursion relations that help us to evaluate these functions for a given x, starting from an given value of n. For the incomplete gamma (B.13a) we have that for the increment of the parameter a by one unity [168]

$$\gamma(a+1,x) = a\gamma(a,x) - \mathrm{e}^{-x}x^a, \tag{B.15}$$

and this can be generalized to $n \in \mathbb{N}$

$$\gamma(a+n,x) = (a)_n\left[\gamma(a,x) - \mathrm{e}^{-x}x^a\sum_{i=0}^{n-1}\frac{x^i}{(a)_{i+1}}\right], \tag{B.16}$$

where the Pochhammer symbol is defined as a rising factorial [168]:

$$(a)_n = a\,(a+1)\cdots(a+n-1)\,. \tag{B.17}$$

Similarly for the complement to the incomplete gamma (B.13b), for $n \in \mathbb{N}$

$$\Gamma(a+n,x) = (a)_n\left[\Gamma(a,x) + \mathrm{e}^{-x}x^a\sum_{i=0}^{n-1}\frac{x^i}{(a)_{i+1}}\right]. \tag{B.18}$$

We can also calculate a recursion for the complement (B.13b) for a decreasing argument. Starting with (B.18), and applying the transformation $a \to a - n$, we obtain

$$\Gamma(a-n,x) = \frac{\Gamma(a,x)}{(a-n)_n} - \mathrm{e}^{-x}x^{a-n}\sum_{i=0}^{n-1}\frac{x^i}{(a-n)_{i+1}}. \tag{B.19}$$

The use of recursion relations (B.16), (B.18) and (B.19) yield values of the incomplete gamma functions which are more accurate than standard numerical routines. We used them to calculate the radial integrals (B.5).

Appendix C

Interaction Operators

In this appendix we calculate the different projectile-target interaction potentials in momentum space, i.e., the Fourier transform of these potentials.

C.1. Coulomb Potential

For the Coulomb potential, the Fourier transform is given by Bethe's integral

$$\int \mathrm{d}\mathbf{r}\, \frac{\mathrm{e}^{\mathrm{i}\,\mathbf{k}\cdot\mathbf{r}}}{|\mathbf{r}-\mathbf{a}|} = \frac{4\pi}{k^2}\, \mathrm{e}^{\mathrm{i}\,\mathbf{k}\cdot\mathbf{a}}, \tag{C.1}$$

and for the subcase $\mathbf{a} = 0$

$$\int \mathrm{d}\mathbf{r}\, \mathrm{e}^{\mathrm{i}\,\mathbf{q}\cdot\mathbf{r}} \frac{1}{r} = \frac{4\pi}{q^2}. \tag{C.2}$$

C.2. Molecular Model Potential

To calculate the Fourier transform of the molecular model potential (2.27), we need to evaluate two integrals. The first one

$$I = \int \mathrm{d}\mathbf{r}_a\, \mathrm{e}^{\mathrm{i}\,\mathbf{q}\cdot\mathbf{r}_a} \left(-\sum_{n=1}^{M} \frac{Z_n}{|\mathbf{r}_a - \mathbf{R}_n|} \right), \tag{C.3}$$

is rather easy and can be calculated using Bethe's integral (C.1)

$$I = -\frac{4\pi}{q^2}\sum_{n=1}^{M} Z_n\, \mathrm{e}^{\mathrm{i}\,\mathbf{q}\cdot\mathbf{R}_n}. \tag{C.4}$$

For the integral involving the second term of the molecular potential (2.27)

$$\Theta(\mathbf{q}) = \sum_j \mathcal{N}_{ij} \int \mathrm{d}\mathbf{r}_a\, \mathrm{e}^{\mathrm{i}\,\mathbf{q}\cdot\mathbf{r}_a} \int \mathrm{d}\mathbf{r}'\, \frac{\left|\phi_j(\mathbf{r}')\right|^2}{|\mathbf{r}_a - \mathbf{r}'|}, \tag{C.5}$$

where, from Eq. (2.24)

$$\phi_j(\mathbf{r}) = \sum_{k=1}^{N_j} B_{jk}\, \mathcal{R}_k(r)\, Y_{\ell_k}^{m_k}(\hat{r}), \tag{C.6}$$

with $\mathcal{R}_k(r)$ the STO defined by Eq. (2.22), and normalization α_k as defined in Eq. (2.23). The inner integral is already given in Eq. (2.31), and reads

$$\int \mathrm{d}\mathbf{r}'\, \frac{\left|\phi_j(\mathbf{r}')\right|^2}{|\mathbf{r}-\mathbf{r}'|} = \sum_{k,l=1}^{n} B_{jk}^* B_{jl} \sum_{\lambda=0}^{\infty}\sum_{\mu=-\lambda}^{\lambda} (-1)^{m_k+\mu}\, \frac{4\pi}{2\lambda+1}\, \Upsilon_{\ell_k\lambda\ell_l}^{-m_k,-\mu,m_l}\, \frac{\vartheta_{kl}^{(\lambda)}(r)}{r}\, Y_\lambda^\mu(\hat{r}), \tag{C.7}$$

where $\Upsilon_{\ell_k\lambda\ell_l}^{-m_k,-\mu,m_l}$ is given by Eq. (B.2) and $\vartheta_{kl}^{(\lambda)}(r)$ is defined by Eq. (B.5) and given explicitly by Eq. (B.12). Now, to calculate the whole integral (C.5), we use the partial wave expansion of the exponential function

$$\mathrm{e}^{\mathrm{i}\,\mathbf{q}\cdot\mathbf{r}} = \sum_{\lambda_q=0}^{\infty}\sum_{\mu_q=-\lambda_q}^{\lambda_q} 4\pi \mathrm{i}^{\lambda_q}\, j_{\lambda_q}(qr)\, Y_{\lambda_q}^{\mu_q *}(\hat{q})\, Y_{\lambda_q}^{\mu_q}(\hat{r}), \tag{C.8}$$

where $j_{\lambda_q}(qr)$ are the spherical Bessel functions. To calculate the resulting integrals, we need to use the power series expansion of the incomplete gamma functions, given in Eqs. (B.14). With the use of this particular definition, we end up with integrals of the form

$$\int_0^\infty \mathrm{d}x\, x^n\, \mathrm{e}^{-\alpha x}\, j_\ell(kx) = \sqrt{\frac{\pi}{2k}} \int_0^\infty \mathrm{d}x\, x^{n-\frac{1}{2}}\, \mathrm{e}^{-\alpha x} J_{\ell+\frac{1}{2}}(kx), \tag{C.9}$$

that are given by formula (6.621) of Ref. [172]

$$\int_0^\infty \mathrm{d}x\, x^{\mu-1}\, \mathrm{e}^{-\alpha x} J_\nu(\beta x) = \left(\alpha^2+\beta^2\right)^{-\frac{1}{2}\mu} \Gamma(\mu+\nu)\, P_{\mu-1}^{-\nu}\left[\alpha\left(\alpha^2+\beta^2\right)^{-1/2}\right], \quad \alpha>0,\ \beta>0,\ \Re\,(\mu+\nu)>0, \tag{C.10}$$

with $\mu = n+1/2$, $\nu = \ell+1/2$ and $P_n^m(x)$ are associated Legendre polynomials.

Putting together the Hankel transform (C.10) with Eqs. (C.7) and (C.8), the resulting radial integrals in (C.5), assuming $n_k + n_l - \lambda - 1 \geqslant 0$ is satisfied, is

$$\Theta(\mathbf{q}) = \sum_j \mathcal{N}_{ij} \sum_{k,l=1}^{N_k,N_l} B^*_{jk} B_{jl} \alpha_k \alpha_l \sum_{\lambda=0}^{\infty} \sum_{\mu=-\lambda}^{\lambda} \frac{(4\pi)^3}{q^2} \frac{\mathrm{i}^\lambda}{2\lambda+1} (-1)^{m_k+\mu} \Upsilon^{-m_k,-\mu,m_l}_{\ell_k \lambda \ell_l} Y^\mu_\lambda(\hat{q}) \left(\frac{\pi}{2q}\right)^{1/2}$$
$$\times \left\{ \frac{\delta_{kl\lambda}!}{\zeta_{kl}^{\delta_{kl\lambda}+1}} \left[\frac{1}{q\,(2\lambda-1)!!} - \sum_{m=0}^{\delta_{kl\lambda}} \frac{(m+1)\,\zeta_{kl}^m}{\left(\zeta_{kl}^2+q^2\right)^{\frac{1}{2}\left(m-\lambda+\frac{3}{2}\right)}} P^{-\lambda-\frac{1}{2}}_{m-\lambda+\frac{1}{2}}\left(\cos\theta^{(q)}_{kl}\right) \right] \right.$$
$$\left. + \frac{\epsilon_{kl\lambda}!}{\zeta_{kl}^{\epsilon_{kl\lambda}+1}} \sum_{m=0}^{\epsilon_{kl\lambda}} \frac{\zeta_{kl}^m\,(2\lambda+m+2)!}{m!\left(\zeta_{kl}^2+q^2\right)^{\frac{1}{2}\left(m+\lambda+\frac{5}{2}\right)}} P^{-\lambda-\frac{1}{2}}_{m+\lambda+\frac{3}{2}}\left(\cos\theta^{(q)}_{kl}\right) \right\}, \tag{C.11}$$

where

$$\delta_{kl\lambda} = n_k + n_l + \lambda, \tag{C.12a}$$
$$\epsilon_{kl\lambda} = n_k + n_l - \lambda - 1, \tag{C.12b}$$
$$\zeta_{kl} = \zeta_k + \zeta_l, \tag{C.12c}$$
$$\cos\theta^{(q)}_{kl} = \frac{\zeta_{kl}}{\left(\zeta_{kl}^2+q^2\right)^{1/2}}. \tag{C.12d}$$

Appendix D

Lippmann–Schwinger Equation, Born Series and Green Operator

In the first part of this appendix we give a brief description of the LSE, in order to introduce the Born series. In the second part we describe the Green's function, in particular the form used in Chap. 4.

D.1. Lippmann–Schwinger Equation and the Born Series

For a system that is described by the Hamiltonian

$$\widehat{\mathcal{H}} = \widehat{\mathcal{H}}_0 + V(\mathbf{r}), \tag{D.1}$$

where $\widehat{\mathcal{H}}_0$ is a simplified Hamiltonian and $V(\mathbf{r})$ is an interaction potential. Any stationary problem described by $\widehat{\mathcal{H}}$ can be studied solving the TISE

$$\left(E - \widehat{\mathcal{H}}_0\right) \Psi(\mathbf{r}) = V(\mathbf{r})\Psi(\mathbf{r}), \tag{D.2}$$

where E is the energy; the solution $\Psi(\mathbf{r})$ contains information of a scattering process. In relation to such differential equation, one defines the Green operator

$$\widehat{G}^0(E) = \left(E - \widehat{\mathcal{H}}_0\right)^{-1}, \tag{D.3}$$

with properties that can be found, for instance, in Ref. [173]. For a general Hamiltonian $\widehat{\mathcal{H}}$, one defines similarly

$$\widehat{G}(E) = \left(E - \widehat{\mathcal{H}}\right)^{-1}, \tag{D.4}$$

and an associated Green's function $G(\mathbf{r}, \mathbf{r}')$ defined via

$$\left[\widehat{G}\Phi\right](\mathbf{r}) = \int \mathrm{d}\mathbf{r}'\, G(\mathbf{r}, \mathbf{r}')\Phi(\mathbf{r}'). \tag{D.5}$$

An alternative to the differential equation (D.2) is the equivalent, integral, *Lippmann–Schwinger equation* (LSE)

$$\Psi(\mathbf{r}) = \Psi_0(\mathbf{r}) + \left[\widehat{G}^0 V \Psi\right](\mathbf{r}), \tag{D.6}$$

where $\Psi_0(\mathbf{r})$ is the solution to the corresponding homogeneous Eq. (D.2), i.e., $\left(E - \widehat{\mathcal{H}}_0\right)\Psi_0(\mathbf{r}) = 0$.

One advantage of using the LSE instead of the TISE when studying scattering processes is that the correct boundary conditions of the problem are automatically incorporated through the use of Green's function (D.5). This is a powerful formulation of the scattering problem, that can provide highly accurate solutions. However, solving the integral equation (D.6) is not easy and usually it is more difficult than dealing with the original problem (D.2). Nevertheless, the LSE can be used to give a formal treatment to different quantities. For example, to study transitions between different quantum levels one defines the transition operator $\widehat{T}$, that couples the final f and initial i states through the transition matrix

$$T_{fi} = \langle f | V | i \rangle, \tag{D.7}$$

that provides the first order scattering information. In analogy to Eq. (D.6), one defines a LSE for the operator $\widehat{T}$

$$\widehat{T}(z) = V + V\widehat{G}(z)\widehat{T}(z), \tag{D.8}$$

where z is a complex variable (in our case the energy). Since in most cases it is not possible to find the analytical solution to the LSE, one can use iterative procedures to find an approximate solution (see, for example, App. G.13.1). We start with the Hamiltonian

$$\widehat{\mathcal{H}} = \widehat{\mathcal{H}}_0 + \lambda V, \tag{D.9}$$

where λ can be considered as a strength parameter of the interaction potential, and $\widehat{T}(z)$ is expanded in a power series in λ

$$\widehat{T}(z) = \sum_{n=0}^{\infty} \lambda^n \widehat{T}^{(n)}(z). \tag{D.10}$$

Substituting this expansion in the LSE (D.8) we find that

$$\widehat{T}^{(0)} = 0, \tag{D.11a}$$
$$\widehat{T}^{(1)} = V, \tag{D.11b}$$
$$\widehat{T}^{(2)} = V\,\widehat{G}^0\,V, \tag{D.11c}$$
$$\widehat{T}^{(3)} = V\,\widehat{G}^0\,V\,\widehat{G}^0\,V, \tag{D.11d}$$
$$\vdots$$
$$\widehat{T}^{(n)} = V\,\widehat{G}^0\,\widehat{T}^{(n-1)}. \tag{D.11e}$$

Thus

$$\widehat{T}(z) = \lambda V + \lambda^2 V\,\widehat{G}^0(z)\,V + \lambda^3 V\,\widehat{G}^0(z)\,V\,\widehat{G}^0(z)\,V + \cdots, \tag{D.12}$$

and, from Eq. (D.7), we obtain the Born series for the T matrix

$$T_{fi} = \lambda\,\langle f|\,V\,|i\rangle + \lambda^2\,\langle f|\,V\,\widehat{G}^0(z)\,V\,|i\rangle + \lambda^3\,\langle f|\,V\,\widehat{G}^0(z)\,V\,\widehat{G}^0(z)\,V\,|i\rangle + \cdots. \tag{D.13}$$

This is the formula used in Chap. 4, in particular the two first terms in λ.

In general, the series (D.13) converges if the strength of the interaction is "small". Details on the convergence of the series are not discussed here, but the reader can be found in Refs. [171, 174].

D.2. Green's Operator

Consider a linear and Hermitian operator $\widehat{L}$, that has a defined set of eigenstates $\{|n\rangle\}_n$ and eigenvalues $\{\lambda_n\}_n$

$$\widehat{L}\,|n\rangle = \lambda_n\,|n\rangle\,. \tag{D.14}$$

Such a spectrum can be discrete and/or continuum, and the eigenstates form a complete set

$$\sum\!\!\!\!\!\!\int_n |n\rangle\langle n| = \widehat{1}, \tag{D.15}$$

where the sum is over the discrete states and the integral over the continuum states.

For such an operator $\widehat{L}$, the associated Green function $G(z)$ is defined as the solution to the equation

$$\left(z - \widehat{L}\right) G(z) = 1, \tag{D.16}$$

where z is a complex variable. Inverting this equation, we obtain then

$$G(z) = \left(z - \widehat{L}\right)^{-1}. \tag{D.17}$$

Now, for a general function $F\left(\widehat{L}\right)$ one always has [170]

$$F\left(\widehat{L}\right)|n\rangle = F(\lambda_n)\,|n\rangle\,, \tag{D.18}$$

so that, using the completeness relation (D.15), we have

$$\begin{aligned} G(z) &= \frac{1}{z-\widehat{L}} \sum\!\!\!\!\!\!\int_n |n\rangle\langle n| \\ &= \sum\!\!\!\!\!\!\int_n \frac{|n\rangle\langle n|}{z-\lambda_n} \\ &= \sum_n \frac{|n\rangle\langle n|}{z-\lambda_n} + \int \mathrm{d}n\, \frac{|n\rangle\langle n|}{z-\lambda_n}. \end{aligned} \tag{D.19}$$

Clearly $G(z)$ is an analytic function of z, except at the eigenvalues of $\widehat{L}$. Since $\widehat{L}$ is an Hermitian operator, λ_n are real, and then $G(z)$ has simple poles on the real axis (for the discrete spectrum, usually for $z_0 < 0$) and a branch cut (for the continuum spectrum, for $0 < z_0 < \infty$). In order to avoid this problem, one defines

$$G^{\pm}(z) = \lim_{\eta\to 0^+} G(z \pm \mathrm{i}\,\eta), \tag{D.20}$$

where the sign "+" indicates that for any z the value of $G(z)$ is approached from above ($z = z_0 + i\eta$) and for the sign "−" that the same point is approached from below ($z = z_0 - i\eta$). The value of both limits is, usually, different and

$$\begin{aligned} G^+(z) - G^-(z) &= \lim_{\eta\to 0^+} \sum\!\!\!\!\!\!\int_n \left[\frac{|n\rangle\langle n|}{z_0-\lambda_n+\mathrm{i}\,\eta} - \frac{|n\rangle\langle n|}{z_0-\lambda_n-\mathrm{i}\,\eta}\right] \\ &= -2\pi\mathrm{i} \sum\!\!\!\!\!\!\int_n \delta(z_0-\lambda_n)\,|n\rangle\langle n|\,. \end{aligned} \tag{D.21}$$

Finally, $G(z)$ can be used to solve the non-homogeneous equation

$$\left(z-\widehat{L}\right)\Psi(\mathbf{r}) = \Phi(\mathbf{r}), \tag{D.22}$$

if the solutions to the homogeneous equation

$$\left(z-\widehat{L}\right)\Psi_0(\mathbf{r}) = 0, \tag{D.23}$$

are known. Indeed, for a given function $\Phi(\mathbf{r})$, where $\Psi(\mathbf{r})$ has the same boundary conditions as $G(z)$, one has

$$\Psi(\mathbf{r}) = \Psi_0(\mathbf{r}) + G(z)\Phi(\mathbf{r}), \tag{D.24}$$

which coincides with the LSE of Eq. (D.6).

Appendix E

Second-Born Integrals

In this appendix we introduce the closure approximation, and we then present the details of the calculation of all the resulting three-dimensional integrals that appear in the second-Born approximation.

E.1. Closure Approximation

In contrast to the the first-order transition amplitude (4.8), which can be calculated numerically in a routinely way, the second-order amplitude (4.14) is in practice quite difficult (if not impossible) to calculate, since it requires using all the (infinite) spectra (4.12) of the target Hamiltonian. In order to simplify this "quixotic" (unfeasible) task, we are aware of only the following approximations: the pseudo-state expansion [141, 142] and the closure approximation (see, for example, Refs. [139, 143, 144]). In this work we use the latter which is based on the closure relation

$$\sum_m^{\text{fs}} |m\rangle\langle m| = \mathbb{1}. \tag{E.1}$$

To use the closure approximation, one must fix the energy of the intermediate states, i.e., $k_m^2/2 = \tilde{k}^2/2 = \tilde{E}$, where $\tilde{k}^2/2$ is known as the closure energy. Hereafter we shall

denote the plane wave as

$$\langle \mathbf{r} | \mathbf{k} \rangle = e^{i\,\mathbf{k}\cdot\mathbf{r}}. \tag{E.2}$$

Then, Eq. (4.14), can be rewritten as

$$f_{B2} = \frac{1}{8\pi^4} \int \frac{d\mathbf{k}'}{k'^2 - \tilde{k}^2} \left\langle \mathbf{k}_a, \Phi^{(1)} \right| V(\mathbf{r}_a, \mathbf{r}_b) \left| \mathbf{k}' \right\rangle \left\langle \mathbf{k}' \right| V(\mathbf{r}_a, \mathbf{r}_b) \left| \mathbf{k}_i, \Phi^{(0)} \right\rangle. \tag{E.3}$$

Using Bethe's integral (C.1), one defines the Fourier transform of the potential as

$$\begin{aligned} \langle \mathbf{k}_1 | V(\mathbf{r}_a, \mathbf{r}_b) | \mathbf{k}_2 \rangle &= \int d\mathbf{r}_a e^{-i\,\mathbf{k}_1\cdot\mathbf{r}_a} \left(\frac{1}{|\mathbf{r}_a - \mathbf{r}_b|} + U(\mathbf{r}_a, \mathbf{r}_b) \right) e^{i\,\mathbf{k}_2\cdot\mathbf{r}_a} \\ &= \frac{4\pi}{q_{21}^2} \left[e^{i\,\mathbf{q}_{21}\cdot\mathbf{r}_b} + \mathcal{Z}(\mathbf{q}_{21}, \mathbf{r}_b) \right], \end{aligned} \tag{E.4}$$

where $\mathbf{q}_{21} = \mathbf{k}_2 - \mathbf{k}_1$, and $4\pi\mathcal{Z}(\mathbf{q}_{21}, \mathbf{r}_b)/q_{21}^2$ is the Fourier transform of the potential $U(\mathbf{r}_a, \mathbf{r}_b)$. Then, defining $\mathbf{q}_a = \mathbf{k}' - \mathbf{k}_a$ and $\mathbf{q}_i = \mathbf{k}_i - \mathbf{k}'$, the transition amplitude (E.3) is transformed into

$$\begin{aligned} f_{B2} &= \frac{1}{8\pi^4} \int \frac{d\mathbf{k}'}{k'^2 - \tilde{k}^2} \left\langle \Phi^{(1)} \right| \frac{4\pi}{q_a^2} \frac{4\pi}{q_i^2} \left[e^{i\,\mathbf{q}_a\cdot\mathbf{r}_b} + \mathcal{Z}(\mathbf{q}_a, \mathbf{r}_b) \right] \left[e^{i\,\mathbf{q}_i\cdot\mathbf{r}_b} + \mathcal{Z}(\mathbf{q}_i, \mathbf{r}_b) \right] \left| \Phi^{(0)} \right\rangle \\ &= \frac{2}{\pi^2} \left\langle \Phi^{(1)} \right| \int \frac{d\mathbf{k}'}{\left(k'^2 - \tilde{k}^2\right) q_a^2 q_i^2} \left[e^{i\,\mathbf{q}\cdot\mathbf{r}_b} + \mathcal{Z}(\mathbf{q}_a, \mathbf{r}_b)\mathcal{Z}(\mathbf{q}_i, \mathbf{r}_b) \right. \\ &\quad \left. + \mathcal{Z}(\mathbf{q}_i, \mathbf{r}_b) e^{i\,\mathbf{q}_a\cdot\mathbf{r}_b} + \mathcal{Z}(\mathbf{q}_a, \mathbf{r}_b) e^{i\,\mathbf{q}_i\cdot\mathbf{r}_b} \right] \left| \Phi^{(0)} \right\rangle. \end{aligned} \tag{E.5}$$

An issue that is crucial in this kind of approximation is the value of the closure energy. In order to choose an adequate value, many different criteria have been proposed: $\tilde{E}$ may be chosen as to satisfy the optical theorem, or so that it gives the correct polarizability of the target (see Ref. [139] for more details). For the study of inelastic collisions (as ionization) it is more convenient to choose $\tilde{E}$ to coincide with the ionization limit [129, 130, 139], i.e.,

$$\tilde{E} - E_0 = I_0, \tag{E.6}$$

where I_0 is the ionization potential of the initial state.

E.2. Second-Born Integrals

Before calculating all the integrals needed in (E.5), we will consider here only the case where the interaction between the projectile and the target is given by a Coulomb potential with charge −1, and then $\mathcal{Z}(\mathbf{q}_a, \mathbf{r}_b) = \mathcal{Z}(\mathbf{q}_i, \mathbf{r}_b) = -1$.

E.2.1. Lewis' Integral

In Eq. (E.5) the first and second integrals can be calculated analytically using Lewis' integral [145], given by

$$I_{00}(\lambda;\mathbf{k}_1,\mu_1;\mathbf{k}_2,\mu_2) = \int \mathrm{d}\mathbf{k}\, \frac{1}{(k^2+\lambda^2)\left(|\mathbf{k}-\mathbf{k}_1|^2+\mu_1^2\right)\left(|\mathbf{k}-\mathbf{k}_2|^2+\mu_2^2\right)}$$
$$= \pi^2\left(\beta^2-\alpha\gamma\right)^{-1/2}\ln\left[\frac{\beta+\left(\beta^2-\alpha\gamma\right)^{1/2}}{\beta-\left(\beta^2-\alpha\gamma\right)^{1/2}}\right], \tag{E.7}$$

where

$$\alpha\gamma = \left[(\mathbf{k}_1-\mathbf{k}_2)^2+(\mu_1+\mu_2)^2\right]\left[k_1^2+(\mu_1+\lambda)^2\right]\left[k_2^2+(\mu_2+\lambda)^2\right], \tag{E.8a}$$
$$\beta = \lambda\left[(\mathbf{k}_1-\mathbf{k}_2)^2+(\mu_1+\mu_2)^2\right]+\mu_2\left(\lambda^2+k_1^2+\mu_1^2\right)+\mu_1\left(\lambda^2+k_2^2+\mu_2^2\right). \tag{E.8b}$$

Explicitly the first integral reads

$$I = \left\langle\Phi^{(1)}\right|\int\frac{\mathrm{d}\mathbf{k}'}{\left(k'^2-\tilde{k}^2\right)q_a^2q_i^2}\left|\Phi^{(0)}\right\rangle$$
$$= \sum_{\ell m}\left\langle\varphi_\ell\ell m\right| I_{00}\left(\mathrm{i}\tilde{k};\mathbf{k}_a,0;\mathbf{k}_b,0\right)\sum_j B_{ij}\left|j\ell_j m_j\right\rangle$$
$$= \sum_{\ell m}\sum_j B_{ij}\left\langle\varphi_\ell\right| I_{00}\left(\mathrm{i}\tilde{k};\mathbf{k}_a,0;\mathbf{k}_b,0\right)|j\rangle\ \delta_{\ell\ell_j}\delta_{mm_j}. \tag{E.9}$$

E.2.2. 3-D Integrals

To perform the third and fourth integrals in Eq. (E.5) different strategies have been proposed. Those integrals are far from easy to calculate because of the singularity related to the presence of the closure energy. Here we follow the approach proposed by Marchalant *et al* [123], where the angular integrals are performed in terms of partial transfer momenta. Also we propose to exploit the fact that in our molecular target description the initial wavefunction is expressed analytically and, consequently, part of the angular integrals can be performed analytically.

The last two integrals in Eq. (E.5) contain an exponential $\mathrm{e}^{\mathrm{i}\,\boldsymbol{\nu}\cdot\mathbf{r}_b}$, where $\boldsymbol{\nu}$ is either the intermediate transfer momentum $\boldsymbol{\nu}=\mathbf{q}_a=\mathbf{k}'-\mathbf{k}_a$ or $\boldsymbol{\nu}=\mathbf{q}_i=\mathbf{k}_i-\mathbf{k}'$; both can be treated in a similar way. It is convenient to introduce an auxiliary momentum $\mathbf{k}_{\mathrm{aux}}$, defined as

$$\mathbf{k}_{\mathrm{aux}} = -\mathbf{k}_a = \boldsymbol{\nu}-\mathbf{k}',\ \text{if}\ \boldsymbol{\nu}=\mathbf{q}_a \tag{E.10a}$$
$$\mathbf{k}_{\mathrm{aux}} = \mathbf{k}_i = \mathbf{k}'+\boldsymbol{\nu},\ \text{if}\ \boldsymbol{\nu}=\mathbf{q}_i. \tag{E.10b}$$

We shall also use the compact notation $L=\{\ell,m\}$, $L_j=\left\{\ell_j,m_j\right\}$ and $\Lambda_q=\left\{\lambda_q,\mu_q\right\}$.

Using the representation of the MOs in STOs given in Eq. (2.24), the expansion of the scattering wavefunction in partial waves (4.18), the partial wave expansion of the plane wave Eq. (C.8), the two last integrals in Eq. (E.5) can be written as

$$
\begin{aligned}
I_{\mathbf{r}_b}(\mathbf{k}_{\text{aux}}, \mathbf{q}) &= \left\langle \Phi^{(1)} \right| \int \mathrm{d}\mathbf{k}' \, \frac{\mathrm{e}^{\mathrm{i}\,\boldsymbol{\nu}\cdot\mathbf{r}_b}}{\left(k'^2 - \tilde{k}^2\right) q_i^2 q_a^2} \left| \Phi^{(0)} \right\rangle \\
&= \sum_{\ell m} \left\langle \varphi_\ell \ell m \right| \int \mathrm{d}\mathbf{k}' \sum_{\lambda_q=0}^{\infty} \sum_{\mu_q=-\lambda_q}^{\lambda_q} 4\pi \mathrm{i}^{\lambda_q} \\
&\quad \times \frac{j_{\lambda_q}(\nu r_b) Y_{\lambda_q}^{\mu_q *}(\hat{\nu}) Y_{\lambda_q}^{\mu_q}(\hat{r}_b)}{\left(k'^2 - \tilde{k}^2\right) q_i^2 q_a^2} \sum_j B_{ij} \left| j \ell_j m_j \right\rangle \\
&= \sum_{\ell m} \sum_j B_{ij} \sum_{\lambda_q=0}^{\infty} \sum_{\mu_q=-\lambda_q}^{\lambda_q} 4\pi \mathrm{i}^{\lambda_q} \left\langle \varphi_\ell \right| \int_0^\infty \mathrm{d}k' \, k'^2 j_{\lambda_q}(\nu r_b) \\
&\quad \times \int \mathrm{d}\hat{k}' \, \frac{Y_{\lambda_q}^{\mu_q *}(\hat{\nu})}{\left(k'^2 - \tilde{k}^2\right) q_i^2 q_a^2} \left\langle \ell m \right| Y_{\lambda_q}^{\mu_q}(\hat{r}_b) \left| \ell_j m_j \right\rangle |j\rangle \\
&= \sum_{\ell m} \sum_j B_{ij} \sum_{\lambda_q=0}^{\infty} \sum_{\mu_q=-\lambda_q}^{\lambda_q} (-1)^{m+\mu_q} 4\pi \mathrm{i}^{\lambda_q} \Upsilon_{\ell\lambda_q\ell_j}^{-m,\mu_q m_j} \left\langle \varphi_\ell \right| \mathcal{J}_{L\Lambda_q L_j}(r_b \mathbf{k}_{\text{aux}}; \mathbf{q}) \left| j \right\rangle ,
\end{aligned}
\tag{E.11}
$$

where $\Upsilon_{\ell\lambda_q\ell_j}^{-m,\mu_q m_j}$ is given in Eq. (B.2) and

$$
\mathcal{J}_{L\Lambda_q L_j}(r_b \mathbf{k}_{\text{aux}}; \mathbf{q}) = \int_0^\infty \mathrm{d}k' k'^2 j_{\lambda_q}(\nu r_b) \int \mathrm{d}\hat{k}' \, \frac{Y_{\lambda_q}^{-\mu_q}(\hat{\nu})}{\left(k'^2 - \tilde{k}^2\right) q_i^2 q_a^2}. \tag{E.12}
$$

As the spherical Bessel functions and the spherical harmonics in Eq. (E.12) depend explicitly on $\boldsymbol{\nu}$, to perform the integral over all $\mathbf{k}'$ it is convenient to make a change of variable, as proposed in Ref. [123]. Since $\boldsymbol{\nu} = \mathbf{k}_{\text{aux}} \pm \mathbf{k}'$, the integral over $\mathbf{k}'$ can be transformed as

$$
\int_0^\infty k'^2 \mathrm{d}k' \int \mathrm{d}\hat{k}' \, f(\mathbf{k}') \to \int_{k_{\text{aux}}}^\infty \nu^2 \mathrm{d}\nu \int \mathrm{d}\hat{\nu} \, f(\mathbf{k}_{\text{aux}}, \boldsymbol{\nu}). \tag{E.13}
$$

In order to obtain an integral over a finite domain, a second transformation of variables can be made. With $\nu \to k_{\text{aux}}/x$ we get

$$
\int_{k_{\text{aux}}}^\infty f(\nu) \nu^2 \mathrm{d}\nu \to \int_0^1 f\left(\frac{k_{\text{aux}}}{x}\right) \frac{k_{\text{aux}}^3}{x^4} \, \mathrm{d}x, \tag{E.14}
$$

so that

$$
\mathcal{J}_{L\Lambda_q L_j}(r_b \mathbf{k}_{\text{aux}}; \mathbf{q}) = \int_0^1 \frac{k_{\text{aux}}}{x^2} \mathrm{d}x \, j_{\lambda_q}\left(\frac{k_{\text{aux}}}{x} r_b\right) I_{\hat{\nu}}\left(\Lambda_q; x; \mathbf{k}_{\text{aux}}, \mathbf{q}\right), \tag{E.15}
$$

where the angular integral is

$$I_{\hat{v}}\left(\Lambda_q; x; \mathbf{k}_{\text{aux}}, \mathbf{q}\right) = \int \mathrm{d}\hat{v}\, \frac{Y_{\lambda_q}^{-\mu_q}(\hat{v})}{\left(k'^2 - \tilde{k}^2\right)|\mathbf{q} - \boldsymbol{\nu}|^2}. \tag{E.16}$$

Explicitly, the latter becomes

$$I_{\hat{v}}\left(\Lambda_q; x; \mathbf{k}_{\text{aux}}, \mathbf{q}\right) = \left(\frac{x}{k_{\text{aux}}}\right)^4 \int \mathrm{d}\hat{v}\, Y_{\lambda_q}^{-\mu_q}(\hat{v}) \frac{\left[\frac{q^2}{k_{\text{aux}}^2}x^2 - 2\frac{q}{k_{\text{aux}}}x\cos\theta_{\boldsymbol{\nu}\mathbf{q}} + 1\right]^{-1}}{\left[x^2\left(1 - \frac{\tilde{k}^2}{k_{\text{aux}}^2}\right) \pm 2x\cos\theta_{\boldsymbol{\nu}\mathbf{k}_{\text{aux}}} + 1\right]}, \tag{E.17}$$

where $\cos\theta_{\mathbf{k}_1\mathbf{k}_2} = \cos\theta_1\cos\theta_2 + \sin\theta_1\sin\theta_2\cos(\phi_1 - \phi_2)$, and the "+" ("−") sign corresponds to $\mathbf{k}_{\text{aux}} = -\mathbf{k}_a$ ($\mathbf{k}_{\text{aux}} = \mathbf{k}_i$).

E.2.3. Polar Integral

We first define

$$a_0^2 = 1 - \left(\tilde{k}k_{\text{aux}}^{-1}\right)^2, \tag{E.18a}$$
$$a_1 = \cos\theta_{\boldsymbol{\nu}}\cos\theta_{\mathbf{k}_{\text{aux}}}, \tag{E.18b}$$
$$a_2 = \sin\theta_{\boldsymbol{\nu}}\sin\theta_{\mathbf{k}_{\text{aux}}}, \tag{E.18c}$$
$$b_0 = qk_{\text{aux}}^{-1}, \tag{E.18d}$$
$$b_1 = \cos\theta_{\boldsymbol{\nu}}\cos\theta_{\mathbf{q}}, \tag{E.18e}$$
$$b_2 = \sin\theta_{\boldsymbol{\nu}}\sin\theta_{\mathbf{q}}, \tag{E.18f}$$

and

$$p_1^{(\pm)} = a_0^2x^2 \pm 2a_1x + 1, \tag{E.19a}$$
$$p_2 = b_0^2x^2 - 2b_0b_1x + 1, \tag{E.19b}$$
$$r_1 = 2a_2x, \tag{E.19c}$$
$$r_2 = -2b_0b_2x. \tag{E.19d}$$

In coplanar geometry ($\phi_{\mathbf{q}} = 0$), the angular integral (E.17) can be written as

$$I_{\hat{v}}\left(\Lambda_q; x; \mathbf{k}_{\text{aux}}, \mathbf{q}\right) = \left(\frac{x}{k_{\text{aux}}}\right)^4 \int_0^\pi \sin\theta_{\boldsymbol{\nu}}\,\mathrm{d}\theta_{\boldsymbol{\nu}}\, Y_{\lambda_q}^{-\mu_q}(\theta_{\boldsymbol{\nu}}, 0)\, I_{\phi_{\boldsymbol{\nu}}}\left(\mu_q; x, \theta_{\boldsymbol{\nu}}; \mathbf{k}_{\text{aux}}, \mathbf{q}\right) \tag{E.20}$$

where

$$\begin{aligned} I_{\phi_{\boldsymbol{\nu}}}\left(\mu_q; x, \theta_{\boldsymbol{\nu}}; \mathbf{k}_{\text{aux}}, \mathbf{q}\right) &= \int_0^{2\pi} \mathrm{d}\phi_{\boldsymbol{\nu}}\, \mathrm{e}^{-\mathrm{i}\,\mu_q\phi_{\boldsymbol{\nu}}} \frac{\left[b_0^2x^2 - 2b_0x\left(b_1 + b_2\cos\phi_{\boldsymbol{\nu}}\right) + 1\right]^{-1}}{\left[a_0^2x^2 \pm 2x\left(a_1 + a_2\cos\phi_{\boldsymbol{\nu}}\right) + 1\right]} \\ &= \int_0^{2\pi} \mathrm{d}\phi_{\boldsymbol{\nu}} \frac{\mathrm{e}^{-\mathrm{i}\,\mu_q\phi_{\boldsymbol{\nu}}}}{\left(p_1^{(\pm)} \pm r_1\cos\phi_{\boldsymbol{\nu}}\right)\left(p_2 + r_2\cos\phi_{\boldsymbol{\nu}}\right)}. \end{aligned} \tag{E.21}$$

The integrand of the latter can be split in two

$$I_{\phi_\nu}\left(\mu_q; x, \theta_\nu; \mathbf{k}_{\text{aux}}, \mathbf{q}\right) = \frac{1}{p_2 r_1 \mp p_1^{(\pm)} r_2} \int_0^{2\pi} \mathrm{d}\phi_\nu \, \mathrm{e}^{-\mathrm{i}\,\mu_q \phi_\nu} \times \left(\frac{r_1}{p_1^{(\pm)} \pm r_1 \cos\phi_\nu} \mp \frac{r_2}{p_2 + r_2 \cos\phi_\nu} \right). \tag{E.22}$$

The imaginary part vanishes because of symmetry. For the real part, the integration needs to be performed only on the $[0, \pi]$ interval, and we make use of Eq. (3.613) of Ref. [172]

$$I_\phi = \int_0^\pi \mathrm{d}\phi \, \frac{\cos(n\phi)}{1 + a\cos\phi} = \frac{\pi}{\sqrt{1-a^2}} \left(\frac{\sqrt{1-a^2} - 1}{a} \right)^n, \; a^2 < 1, n \geqslant 0. \tag{E.23}$$

For the third term in (E.5), the integral (E.21) is given by

$$I_{\phi_\nu}\left(\mu_q; x, \theta_\nu; -\mathbf{k}_a, \mathbf{q}\right) = \frac{2\pi}{p_2 r_1 - p_1^+ r_2} \left[\frac{r_1 \operatorname{sign}\left(p_1^+\right)^{1-|\mu_q|}}{\sqrt{p_1^{+2} - r_1^2}} \left(\frac{\sqrt{p_1^{+2} - r_1^2} - \left|p_1^+\right|}{r_1} \right)^{|\mu_q|} - \frac{r_2 \operatorname{sign}(p_2)^{1-|\mu_q|}}{\sqrt{p_2^2 - r_2^2}} \left(\frac{\sqrt{p_2^2 - r_2^2} - |p_2|}{r_2} \right)^{|\mu_q|} \right]. \tag{E.24}$$

For the fourth term in (E.5), since $\theta_{\mathbf{k}_i} = 0$, we have $a_2 = r_1 = 0$, and integral (E.21) becomes

$$I_{\phi_\nu}\left(\mu_q; x, \theta_\nu; \mathbf{k}_i, \mathbf{q}\right) = \frac{2\pi \operatorname{sign}(p_2)^{1-|\mu_q|}}{p_1^- \sqrt{p_2^2 - r_2^2}} \left(\frac{\sqrt{p_2^2 - r_2^2} - |p_2|}{r_2} \right)^{|\mu_q|}. \tag{E.25}$$

Unfortunately, for the case $a^2 \geqslant 1$, integral (E.22) has a pole for $\phi = \phi_\mathrm{c} = \cos^{-1}(-1/a)$. It must be calculated using the Cauchy principal value $\mathfrak{P}$

$$I_\phi = \mathfrak{P} \int_0^\pi \mathrm{d}\phi \, \frac{\cos(n\phi)}{1 + a\cos\phi} + \mathrm{i}\,\pi \int_0^\pi \mathrm{d}\phi \, \cos(n\phi)\, \delta(\phi - \phi_\mathrm{c}). \tag{E.26}$$

In this work, such a principal value is calculated numerically using Levin's collocation method [178–180] (see App. F, in particular Sec. F.5).

Finally, for some specific values of x, the results (E.24) and (E.25) have poles at $\theta_\nu = \theta_\mathrm{c}$. In such cases, the integrals (E.20) over θ_ν are also evaluated using the

Cauchy principal value

$$I_{\hat{\nu}}\left(\Lambda_q; x; \mathbf{k}_{\text{aux}}, \mathbf{q}\right) = \mathfrak{P} I_{\hat{\nu}}\left(\Lambda_q; x; \mathbf{k}_{\text{aux}}, \mathbf{q}\right) + \mathrm{i}\,\pi \left(\frac{x}{k_{\text{aux}}}\right)^4 \int_0^\pi \sin\theta_{\boldsymbol{\nu}}\, \mathrm{d}\theta_{\boldsymbol{\nu}}\, Y_{\lambda_q}^{-\mu_q}(\theta_{\boldsymbol{\nu}}, 0) \times I_{\phi_{\boldsymbol{\nu}}}\left(\mu_q; x, \theta_{\boldsymbol{\nu}}; \mathbf{k}_{\text{aux}}, \mathbf{q}\right) \delta(\theta_{\boldsymbol{\nu}} - \theta_{\text{c}}). \tag{E.27}$$

E.2.4. Total Integral

Collecting the previous results, the total integral over $\boldsymbol{\nu} = \mathbf{q}_a$ is given by (indicating only the angular integral over $\mathbf{r}_b$)

$$I_{\hat{r}_b}(r_b, \mathbf{k}_a, \mathbf{q}) = \left\langle \ell m \right| \int \mathrm{d}\mathbf{q}_a \, \frac{\mathrm{e}^{\mathrm{i}\,\mathbf{q}_a \cdot \mathbf{r}_b}}{\left(|\mathbf{q}_a + \mathbf{k}_a|^2 - \tilde{k}^2\right) q_a^2 \, |\mathbf{q} - \mathbf{q}_a|^2} \left| \ell_j m_j \right\rangle = (-1)^m \sum_{\lambda_q=0}^{\infty} \sum_{\mu_q=-\lambda_q}^{\lambda_q} (-1)^{\mu_q}\, 4\pi \mathrm{i}^{\lambda_q} \Upsilon^{-m, \mu_q m_j}_{\ell \lambda_q \ell_j} \mathcal{J}^{L \Lambda_q L_j}(r_b \mathbf{k}_a; \mathbf{q}). \tag{E.28}$$

where

$$\mathcal{J}^{L\Lambda_q L_j}(r_b \mathbf{k}_a; \mathbf{q}) = \frac{1}{k_a^3} \int_0^1 \mathrm{d}x\, x^2 j_{\lambda_q}\left(\frac{k_a r_b}{x}\right) \int_0^\pi \sin\theta_{\mathbf{q}_a} \mathrm{d}\theta_{\mathbf{q}_a}\, Y_{\lambda_q}^{-\mu_q}\left(\theta_{\mathbf{q}_a}, 0\right) \times I_{\phi_{\mathbf{q}_a}}\left(\mu_q; x, \theta_{\mathbf{q}_a}; -\mathbf{k}_a, \mathbf{q}\right). \tag{E.29}$$

Similarly, using (E.25), the integral over $\boldsymbol{\nu} = \mathbf{q}_i$ reads

$$I_{\hat{r}_b}(r_b, \mathbf{k}_i, \mathbf{q}) = \left\langle \ell m \right| \int \mathrm{d}\mathbf{q}_i \, \frac{\mathrm{e}^{\mathrm{i}\,\mathbf{q}_i \cdot \mathbf{r}_b}}{\left(|\mathbf{k}_i - \mathbf{q}_i|^2 - \tilde{k}^2\right) |\mathbf{q} - \mathbf{q}_i|^2 \, q_i^2} \left| \ell_j m_j \right\rangle = (-1)^m \sum_{\lambda_q=0}^{\infty} \sum_{\mu_q=-\lambda_q}^{\lambda_q} (-1)^{\mu_q}\, 4\pi \mathrm{i}^{\lambda_q} \Upsilon^{-m, \mu_q m_j}_{\ell \lambda_q \ell_j} \mathcal{J}^{L \Lambda_q L_j}(r_b \mathbf{k}_i; \mathbf{q}) \tag{E.30}$$

where

$$\mathcal{J}^{L\Lambda_q L_j}(r_b \mathbf{k}_i; \mathbf{q}) = \frac{1}{k_i^3} \int_0^1 \mathrm{d}x\, x^2 j_{\lambda_q}\left(\frac{k_i r}{x}\right) \int_0^\pi \sin\theta_{\mathbf{q}_i} \mathrm{d}\theta_{\mathbf{q}_i}\, Y_{\lambda_q}^{-\mu_q}\left(\theta_{\mathbf{q}_i}, 0\right) \times I_{\phi_{\mathbf{q}_i}}\left(\mu_q; x, \theta_{\mathbf{q}_i}; \mathbf{k}_i, \mathbf{q}\right). \tag{E.31}$$

The integrals over x, to obtain $\mathcal{J}^{L\Lambda_q L_j}(r_b \mathbf{k}_{\text{aux}}, \mathbf{q})$ in Eqs. (E.28) and (E.30), are performed using Levin's collocation method [178, 180], as explained in App. F.

Collecting these results, we have finally that the transition amplitude (E.5) is expressed as

$$
\begin{aligned}
f_{\mathrm{B2}} = \frac{2}{\pi^2} \sum_{L,j} B_{ij} \langle \varphi_\ell | \left\langle \ell m \right| I_{00}\left(\mathrm{i}\,\tilde{k}; \mathbf{k}_a, 0; \mathbf{k}_i, 0\right) \left(\mathrm{e}^{\mathrm{i}\,\mathbf{q}\cdot\mathbf{r}_b} + 1\right) \left| \ell_j m_j \right\rangle \\
+ \sum_{\Lambda_q} (-1)^{m+\mu_q}\, 4\pi \mathrm{i}^{\lambda_q} \Upsilon^{-m,\mu_q m_j}_{\ell \lambda_q \ell_j} \left[-\mathcal{J}_{L\Lambda_q L_j}(r_b \mathbf{k}_a; \mathbf{q}) - \mathcal{J}_{L\Lambda_q L_j}(r_b \mathbf{k}_i; \mathbf{q}) \right] |j\rangle \\
= \frac{2}{\pi^2} \sum_{\ell m} \sum_{j} B_{ij} \langle \varphi_\ell | \, I_{00}\left(\mathrm{i}\,\tilde{k}; \mathbf{k}_a, 0; \mathbf{k}_i, 0\right) \delta_{\ell,\ell_j} \delta_{m,m_j} + (-1)^m \sum_{\lambda_q=0}^{\infty} \sum_{\mu_q=-\lambda_q}^{\lambda_q} (-1)^{\mu_q} \\
\times 4\pi \mathrm{i}^{\lambda_q} \Upsilon^{-m,\mu_q m_j}_{\ell \lambda_q \ell_j} \left[I_{00}(0; \mathbf{k}_a, 0; \mathbf{k}_i, 0)\; j_{\lambda_q}(q r_b) Y^{\mu_q *}_{\lambda_q}(\hat{q}) \right. \\
\left. - \mathcal{J}_{L\Lambda_q L_j}(r_b \mathbf{k}_a; \mathbf{q}) - \mathcal{J}_{L\Lambda_q L_j}(r_b \mathbf{k}_i; \mathbf{q}) \right] |j\rangle \,.
\end{aligned}
\tag{E.32}
$$

Appendix F

Levin's Collocation Method

In this appendix we describe Levin's collocation method, used to approximate integrals that have a highly oscillating kernel, as those appearing in second-Born integrals, for $(e, 2e)$ calculations in Chap. 4 and in App. E.

F.1. Collocation Method

We start with the integral

$$I = \int_a^b \mathrm{d}x\, f(x) S(rx), \tag{F.1}$$

where $f(x)$ is a smooth function, $S(rx)$ is an oscillatory function, r is a large parameter, and a and b are real and finite. In general, it is not easy to calculate accurately such integrals using traditional numerical methods, such as Simpson's rule or quadrature techniques (as Gauss–Legendre), since a huge number of integration points is required. Different techniques have been proposed in order to approximate these integrals, such as Filon [181], Chung, Evans and Webster method [182], steepest descent methods [183, 184], stationary phase method [185], Fourier oscillators [186] or Longman methods [187, 188] (see also Refs. [180, 189] for a more comprehensive list

and explanation for the mentioned methods). Their efficiency can vary considerably according to the function S.

In Chap. 4 (and also in App. E) we adopt Levin's collocation method [178, 179], developed at the beginning of the 1980 decade. It was used initially to calculate Fourier transforms, and later extended to calculate more general integrals that involve integrands with rapid and irregular oscillations. The method transforms the problem into an ordinary differential equation, with no boundary conditions, and which is solved by a collocation technique [190]. We start with a generalization in notation of the integral (F.1)

$$I = \int_a^b \mathrm{d}x\, \mathbf{f}^{\mathsf{T}}(x) \cdot \mathbf{W}(x), \tag{F.2}$$

where $\mathbf{f}(x) = (f_1(x), \ldots, f_m(x))^{\mathsf{T}}$ is a m-vector of non-rapidly oscillatory functions and $\mathbf{W} = (\mathcal{W}_1(x), \ldots, \mathcal{W}_m(x))^{\mathsf{T}}$ is a m-vector of linearly independent rapidly oscillatory functions, that satisfy a system of ordinary differential equations

$$\frac{\mathrm{d}}{\mathrm{d}x}\mathbf{W}(x) = \mathbb{A}(x)\mathbf{W}(x), \tag{F.3}$$

where $\mathbb{A}(x)$ is a $m \times m$ matrix of non-rapidly oscillatory functions. Defining the vector $\mathbf{g}(x) = (g_1(x), \ldots, g_m(x))^{\mathsf{T}}$ such that

$$\frac{\mathrm{d}}{\mathrm{d}x}\left[\mathbf{g}^{\mathsf{T}}(x) \cdot \mathbf{W}(x)\right] \approx \mathbf{f}^{\mathsf{T}}(x) \cdot \mathbf{W}(x), \tag{F.4}$$

the integral (F.2) is approximated by

$$I \approx \int_a^b \mathrm{d}x\, \frac{\mathrm{d}}{\mathrm{d}x}\left[\mathbf{g}^{\mathsf{T}}(x) \cdot \mathbf{W}(x)\right] = \mathbf{g}^{\mathsf{T}}(b) \cdot \mathbf{W}(b) - \mathbf{g}^{\mathsf{T}}(a) \cdot \mathbf{W}(a). \tag{F.5}$$

Now, using (F.3), expression (F.4) can be rewritten as

$$\begin{aligned}
\mathbf{f}^{\mathsf{T}}(x) \cdot \mathbf{W}(x) \approx \frac{\mathrm{d}}{\mathrm{d}x}\left[\mathbf{g}^{\mathsf{T}}(x) \cdot \mathbf{W}(x)\right] &= \left[\frac{\mathrm{d}}{\mathrm{d}x}\mathbf{g}(x)\right]^{\mathsf{T}} \cdot \mathbf{W}(x) + \mathbf{g}^{\mathsf{T}}(x) \cdot \frac{\mathrm{d}}{\mathrm{d}x}\mathbf{W}(x) \\
&= \left[\frac{\mathrm{d}}{\mathrm{d}x}\mathbf{g}(x)\right]^{\mathsf{T}} \cdot \mathbf{W}(x) + \mathbf{g}^{\mathsf{T}}(x) \cdot \left[\mathbb{A}(x)\mathbf{W}(x)\right] \\
&= \left[\frac{\mathrm{d}}{\mathrm{d}x}\mathbf{g}(x) + \mathbb{A}^{\mathsf{T}}(x)\mathbf{g}(x)\right]^{\mathsf{T}} \cdot \mathbf{W}(x),
\end{aligned} \tag{F.6}$$

from which one can conclude that $\mathbf{g}$ is the approximation to a solution of the system of ordinary differential equations

$$\widehat{L}\,\mathbf{g} \equiv \frac{\mathrm{d}}{\mathrm{d}x}\mathbf{g} + \mathbb{A}^{\mathsf{T}}\mathbf{g} = \mathbf{f}. \tag{F.7}$$

The problem is transformed into solving this system of differential equations. To do so, we can use linearly independent basis functions $\left\{u_k^{(i)}\right\}_{k=1}^{n}$, with $i = 1, \ldots, m$ on $[a, b]$. A n-point collocation approximation [190] to the solution of (F.7) is defined as

$$\mathbf{g}^{(n)}(x) = \left(g_m^{(n)}(x), \ldots, g_1^{(n)}(x)\right)^{\mathsf{T}}$$

where for each element we have

$$g_i^{(n)}(x) = \sum_{k=1}^{n} c_k^{(i)} u_k^{(i)}(x), \; i = 1, \ldots, m. \tag{F.8}$$

The coefficients $\left\{c_k^{(i)}\right\}_{i=1,k=1}^{m,n}$ are determined by the collocation conditions

$$\widehat{L}\, g^{(n)}\left(x_j\right) = f\left(x_j\right), \; j = 1, \ldots, n, \tag{F.9}$$

where $\left\{x_j\right\}_{j=1}^{n}$ are regularly distributed in $[a, b]$, with the restriction $x_1 = a$ and $x_n = b$. Some different choices for such collocation points are given in Sec. F.2. The corresponding n-point approximation to the integral (F.1) is given by

$$I_n \equiv \left(\mathbf{g}^{(n)}(b)\right)^{\mathsf{T}} \cdot \mathbf{W}(b) - \left(\mathbf{g}^{(n)}(a)\right)^{\mathsf{T}} \cdot \mathbf{W}(a). \tag{F.10}$$

F.2. "Integration" Basis Functions

In order to find a solution to Eq. (F.9), we must choose a set of functions that should be suitable to approximate the functions $\mathbf{f}(x)$, together with the set of collocation points $\left\{x_j\right\}_{j=1}^{n}$. In principle, by analyzing the differential equation (F.7) one should be able to find such a set of basis functions $\{u_k\}_{k=1}^{n}$ suitable for the collocation approximation, keeping the order n as low as possible, in order to avoid numerical difficulties with large linear systems; generally, it is desirable to subdivide the integration domain, in particular if it is large, to improve the accuracy [178]. In our numerical investigations we made two choices:

1. A set of n equidistant collocation points, together with the monomial basis

$$u_k^{(i)}(x) = x^k, \; x = 1, \ldots, n; \tag{F.11}$$

2. A set of $n - 2$ Gauss–Legendre quadrature points in the interval $[a, b]$, plus both boundary points (for a total of n points), together with n B-splines functions [191] of order k (which are polynomials of order $k - 1$) defined by

$$u_j^{(i)}(x) = B_j^{(k)}(x) = \frac{x - t_j}{t_{j+k-1} - t_j} B_j^{(k-1)}(x) + \frac{t_{j+k} - x}{t_{j+k} - t_{j+1}} B_{j+1}^{(k-1)}(x), \tag{F.12}$$

where $t_j < t_{j+1}$ is a set of knot-points and the B-spline of order $k = 1$ is defined as $B_j^1(x) = 1$ for $t_j \leqslant x \leqslant t_{j+1}$ (see Ref. [191] for more details).

The convergence of different integrals using both type of basis functions, is analyzed in Secs. F.3 and F.4 for spherical Bessel functions, and in Sec. F.5 for exponential functions.

F.3. Spherical Bessel Functions I

In order to adapt Levin's collocation method to our purposes, we start with the recursion relations for the first derivatives of the spherical Bessel functions

$$\frac{\mathrm{d}}{\mathrm{d}x} j_\ell(x) = -j_{\ell+1}(x) + \frac{\ell}{x} j_\ell(x), \tag{F.13a}$$

$$\frac{\mathrm{d}}{\mathrm{d}x} j_\ell(x) = j_{\ell-1}(x) - \frac{\ell+1}{x} j_\ell(x). \tag{F.13b}$$

As the derivative for an individual $j_\ell(x)$ depends on two different functions, the order of the vectors in Sec. F.1 is $m = 2$, and Eq. (F.3) can be written as

$$\frac{\mathrm{d}}{\mathrm{d}x} \begin{pmatrix} j_\ell(x) \\ j_{\ell+1}(x) \end{pmatrix} = \begin{pmatrix} \frac{\ell}{x} & -1 \\ 1 & -\frac{\ell+2}{x} \end{pmatrix} \begin{pmatrix} j_\ell(x) \\ j_{\ell+1}(x) \end{pmatrix}. \tag{F.14}$$

The matrix $\mathbb{A}$ for a kernel $\mathbf{W}(x) = (j_\ell(rx), j_{\ell+1}(rx))^\mathsf{T}$, is given by

$$\mathbb{A} = \begin{pmatrix} \frac{\ell}{x} & -r \\ r & -\frac{\ell+2}{x} \end{pmatrix}, \tag{F.15}$$

and the corresponding collocation equation to solve, using Eqs. (F.8) and (F.9) is

$$\begin{pmatrix} \frac{\mathrm{d}}{\mathrm{d}x} u_k^{(1)} + \frac{\ell}{x} u_k^{(1)} & r u_k^{(2)} \\ -r u_k^{(1)} & \frac{\mathrm{d}}{\mathrm{d}x} u_k^{(2)} - \frac{\ell+2}{x} u_k^{(2)} \end{pmatrix} \begin{pmatrix} c_k^{(1)} \\ c_k^{(2)} \end{pmatrix} = \begin{pmatrix} f \\ 0 \end{pmatrix}. \tag{F.16}$$

We have considered two different test integrals with spherical Bessel functions as kernels,

$$I_1 = \int_1^3 \mathrm{d}x\, \mathrm{e}^{-25|x-3|} j_\ell(rx), \tag{F.17}$$

$$I_2 = \int_2^3 \mathrm{d}x\, \frac{1}{x^2 - 1} j_\ell(rx). \tag{F.18}$$

We applied Levin's collocation method using as basis functions, the monomial functions (F.11) or B-splines (F.12) of order $k = 20$. We compare our results with those obtained with standard routines for numerical integration of `Mathematica`®, hereafter called reference values. The relative errors with respect to the latter are given, for I_1 and I_2, in Tabs. F.1 and F.2, respectively, with $\ell = 0$ and 1.

The errors using B-splines are quite good, between 10^{-1}% and 10^{-9}% for most cases, using between 50 and 150 functions, particularly for $r \ll 1$, where the errors

for the other used basis functions are greater. The relative errors obtained using the monomial basis (F.11) are similar or even smaller than those obtained with B-splines, including more than 100 functions for $r \ll 1$, but for larger values of the r parameter such a number decreases, and with less than 50 functions we obtain relative errors of about 10^{-8}%. In most cases, the relative errors are significantly smaller than those obtained using the Simpson integral rule with the same number of points, indicating the rapid convergence of the method.

Table F.1 – Relative errors for the integral (F.17), calculated using Levin's collocation method, as a function of the number of basis elements used, either with the monomial basis (F.11) or with B-splines (F.12) of order $k = 20$. We also show the errors obtained using the Simpson integral rule with the same number of integration points. We take as reference values the integrals calculated using `Mathematica`®.

r	Basis	$n = 25$	$n = 50$	$n = 100$	$n = 150$
			$\ell = 0$		
0.10	Monomial	$1.645\,76 \times 10^{12}$	$2.856\,30 \times 10^{8}$	8.696 29	3.648 97
	Bsplines	$2.901\,14 \times 10^{4}$	$1.809\,56 \times 10^{-3}$	$1.124\,03 \times 10^{-1}$	8.295 34
	Simpson	6.754 85	2.167 33	$1.984\,36 \times 10^{-1}$	$4.465\,98 \times 10^{-2}$
1.00		$3.505\,77 \times 10^{-2}$	$2.008\,13 \times 10^{-3}$	$1.681\,59 \times 10^{-8}$	$1.681\,59 \times 10^{-8}$
		$8.121\,68 \times 10^{-5}$	$1.681\,59 \times 10^{-8}$	$2.519\,01 \times 10^{-4}$	$8.074\,97 \times 10^{-1}$
		1.783 10	$6.056\,77 \times 10^{-1}$	$3.892\,48 \times 10^{-2}$	$7.442\,61 \times 10^{-3}$
10.00		$5.961\,87 \times 10^{-2}$	$3.148\,90 \times 10^{-4}$	$2.010\,31 \times 10^{-8}$	$2.010\,31 \times 10^{-8}$
		$2.010\,31 \times 10^{-8}$	$2.010\,31 \times 10^{-8}$	$3.481\,34 \times 10^{-7}$	$3.555\,55 \times 10^{2}$
		4.961 35	1.589 36	$1.100\,19 \times 10^{-1}$	$2.172\,95 \times 10^{-2}$
			$\ell = 1$		
0.10		$1.956\,65 \times 10^{10}$	$1.457\,72 \times 10^{7}$	1.001 49	5.117 68
		$2.306\,82 \times 10^{6}$	$5.562\,73 \times 10^{-1}$	2.047 82	4.153 69
		8.004 98	3.165 14	1.091 76	$9.289\,83 \times 10^{-1}$
1.00		$3.208\,45 \times 10^{-2}$	$8.217\,37 \times 10^{-4}$	$2.594\,22 \times 10^{-8}$	$2.594\,22 \times 10^{-8}$
		$7.346\,19 \times 10^{-7}$	$2.594\,22 \times 10^{-8}$	$5.971\,55 \times 10^{-5}$	$8.152\,47 \times 10^{-1}$
		6.306 60	2.026 37	$1.838\,46 \times 10^{-1}$	$4.123\,98 \times 10^{-2}$
10.00		$4.126\,83 \times 10^{-2}$	$1.133\,44 \times 10^{-5}$	$1.495\,65 \times 10^{-8}$	$1.495\,65 \times 10^{-8}$
		$1.495\,65 \times 10^{-8}$	$1.495\,65 \times 10^{-8}$	$1.924\,35 \times 10^{-5}$	2.317 54
		$3.971\,51 \times 10^{1}$	$1.216\,05 \times 10^{1}$	1.208 12	$2.776\,00 \times 10^{-1}$

F.4. Spherical Bessel Functions II

To test the convergence of Levin's collocation method in a case that appear in App. E (see, for instance, Eqs. (E.28) and (E.30)), we now consider a spherical Bessel of the form $j_\ell(r/x)$. The matrix $\mathbb{A}$ is then written as

$$\mathbb{A} = \begin{pmatrix} -\frac{\ell}{x} & \frac{r}{x^2} \\ -\frac{r}{x^2} & \frac{\ell+2}{x} \end{pmatrix}, \tag{F.19}$$

Table F.2 – Same as Tab. (F.1), for the integral (F.18).

r	Basis	$n = 25$	$n = 50$	$n = 100$	$n = 150$
			$\ell = 0$		
0.10	Monomial	$3.122\,78 \times 10^{6}$	$4.633\,31 \times 10^{3}$	$1.202\,96 \times 10^{4}$	$1.191\,80 \times 10^{3}$
	Bsplines	$1.449\,18 \times 10^{-3}$	$4.477\,10 \times 10^{-4}$	$3.098\,38 \times 10^{-2}$	$9.481\,16 \times 10^{-2}$
	Simpson	$2.311\,84 \times 10^{-5}$	$6.508\,93 \times 10^{-7}$	$5.308\,77 \times 10^{-8}$	$3.270\,62 \times 10^{-9}$
1.00		$8.168\,78 \times 10^{-10}$	$5.429\,48 \times 10^{-8}$	$8.168\,78 \times 10^{-10}$	$1.864\,28 \times 10^{-8}$
		$8.168\,78 \times 10^{-10}$	$8.168\,78 \times 10^{-10}$	$2.387\,86 \times 10^{-6}$	$4.952\,16 \times 10^{-3}$
		$6.969\,87 \times 10^{-5}$	$1.942\,21 \times 10^{-6}$	$1.239\,65 \times 10^{-7}$	$1.700\,91 \times 10^{-8}$
10.00		$3.394\,61 \times 10^{-7}$	$5.253\,75 \times 10^{-7}$	$6.487\,80 \times 10^{-8}$	$1.260\,60 \times 10^{-7}$
		$2.511\,73 \times 10^{-9}$	$2.511\,73 \times 10^{-9}$	$4.068\,50 \times 10^{-7}$	$1.090\,72 \times 10^{2}$
		$8.360\,77 \times 10^{-3}$	$1.422\,15 \times 10^{-3}$	$1.042\,88 \times 10^{-4}$	$2.149\,98 \times 10^{-5}$
			$\ell = 1$		
0.10		$5.560\,91 \times 10^{3}$	$2.468\,24 \times 10^{2}$	$6.266\,24 \times 10^{2}$	$1.112\,20 \times 10^{3}$
		$9.505\,83 \times 10^{1}$	$9.506\,23 \times 10^{1}$	$9.507\,70 \times 10^{1}$	$9.506\,74 \times 10^{1}$
		$6.121\,07 \times 10^{-1}$	$6.120\,97 \times 10^{-1}$	$6.120\,97 \times 10^{-1}$	$6.120\,97 \times 10^{-1}$
1.00		$2.501\,83 \times 10^{-7}$	$2.411\,76 \times 10^{-8}$	$3.212\,09 \times 10^{-10}$	$3.212\,09 \times 10^{-10}$
		$4.023\,39 \times 10^{1}$	$4.023\,39 \times 10^{1}$	$4.023\,39 \times 10^{1}$	$4.021\,50 \times 10^{1}$
		$1.688\,32 \times 10^{-5}$	$4.280\,14 \times 10^{-7}$	$2.347\,52 \times 10^{-8}$	$3.212\,09 \times 10^{-10}$
10.00		$1.280\,69 \times 10^{-7}$	$1.709\,55 \times 10^{-8}$	$1.709\,55 \times 10^{-8}$	$1.709\,55 \times 10^{-8}$
		$1.360\,14 \times 10^{2}$	$1.360\,14 \times 10^{2}$	$1.360\,14 \times 10^{2}$	$1.362\,53 \times 10^{2}$
		$1.897\,44 \times 10^{-2}$	$2.707\,25 \times 10^{-3}$	$1.575\,10 \times 10^{-4}$	$3.033\,43 \times 10^{-5}$

and the corresponding collocation equation to solve, using Eqs. (F.8) and (F.9), is

$$\begin{pmatrix} \frac{\mathrm{d}}{\mathrm{d}x}u_k^{(1)} - \frac{\ell}{x}u_k^{(1)} & -\frac{r}{x^2}u_k^{(2)} \\ \frac{r}{x^2}u_k^{(1)} & \frac{\mathrm{d}}{\mathrm{d}x}u_k^{(2)} + \frac{\ell+2}{x}u_k^{(2)} \end{pmatrix} \begin{pmatrix} c_k^{(1)} \\ c_k^{(2)} \end{pmatrix} = \begin{pmatrix} f \\ 0 \end{pmatrix}. \tag{F.20}$$

The test integrals are similar to the previous case, i.e.,

$$I_1 = \int_1^3 \mathrm{d}x\, \mathrm{e}^{-25|x-3|} j_\ell\left(\frac{r}{x}\right), \tag{F.21}$$

$$I_2 = \int_2^3 \mathrm{d}x\, \frac{1}{x^2-1} j_\ell\left(\frac{r}{x}\right), \tag{F.22}$$

and the relative errors are given in Tabs. F.3 and F.4, again for $\ell = 0$ and 1.

This time we see that the convergence of results using Levin's collocation method is slower, but our conclusions remain the same: we obtain comparable results using the monomial (F.11) and the B-splines (F.12) bases, the later having the best performance for $r \ll 1$, if enough basis functions are used.

Table F.3 – Same as Tab. F.1, for the integral (F.21).

r	Basis	$n = 25$	$n = 50$	$n = 100$	$n = 150$
			$\ell = 0$		
0.10	Monomial	$1.315\,29 \times 10^{4}$	$1.248\,37 \times 10^{1}$	$5.340\,27 \times 10^{-7}$	$6.505\,35 \times 10^{-5}$
	Bsplines	$4.613\,56 \times 10^{1}$	$1.591\,38 \times 10^{-6}$	$1.519\,13 \times 10^{-3}$	$3.345\,28 \times 10^{4}$
	Simpson	6.763 81	2.170 14	$1.987\,26 \times 10^{-1}$	$4.472\,77 \times 10^{-2}$
1.00		$8.210\,25 \times 10^{6}$	$2.394\,52 \times 10^{1}$	$8.943\,81 \times 10^{-5}$	$1.473\,43 \times 10^{-4}$
		$3.733\,23 \times 10^{5}$	$8.338\,55 \times 10^{-3}$	$7.479\,77 \times 10^{-1}$	$5.328\,70 \times 10^{-1}$
		6.774 68	2.173 56	$1.990\,73 \times 10^{-1}$	$4.480\,85 \times 10^{-2}$
10.00		$2.300\,08 \times 10^{-2}$	$1.101\,27 \times 10^{-4}$	$1.201\,21 \times 10^{-9}$	$1.201\,21 \times 10^{-9}$
		$6.343\,35 \times 10^{-6}$	$1.201\,21 \times 10^{-9}$	$2.750\,39 \times 10^{-5}$	$4.458\,32 \times 10^{-1}$
		2.854 12	$9.415\,00 \times 10^{-1}$	$7.229\,62 \times 10^{-2}$	$1.515\,25 \times 10^{-2}$
			$\ell = 1$		
0.10		$1.156\,87 \times 10^{9}$	$6.386\,96 \times 10^{6}$	$2.484\,45 \times 10^{-1}$	$5.372\,39 \times 10^{-1}$
		$1.958\,65 \times 10^{5}$	$2.433\,43 \times 10^{-2}$	$2.250\,66 \times 10^{-2}$	$1.266\,13 \times 10^{5}$
		6.486 03	2.090 73	$2.008\,81 \times 10^{-1}$	$5.399\,06 \times 10^{-2}$
1.00		$5.224\,46 \times 10^{8}$	$3.502\,26 \times 10^{6}$	1.401 30	1.290 13
		$1.574\,84 \times 10^{7}$	$5.401\,15 \times 10^{-2}$	$2.573\,67 \times 10^{-1}$	$7.161\,98 \times 10^{2}$
		7.662 68	3.212 36	1.309 90	1.156 89
10.00		$2.673\,62 \times 10^{-2}$	$4.473\,44 \times 10^{-5}$	$2.958\,09 \times 10^{-8}$	$2.958\,09 \times 10^{-8}$
		$1.937\,04 \times 10^{-6}$	$2.958\,09 \times 10^{-8}$	$3.728\,45 \times 10^{-4}$	$1.521\,60 \times 10^{-2}$
		7.584 49	2.427 83	$2.248\,95 \times 10^{-1}$	$5.082\,09 \times 10^{-2}$

F.5. Exponential Functions

Finally, to show the real power of Levin's collocation method, in view of our purposes (see App. E and Eq. (E.26) in particular), we consider integrals of the form

$$I = \int_0^b \mathrm{d}x \, \frac{\mathrm{e}^{-\mathrm{i}\,\ell x}}{1 + a\cos x}, \quad |a| \geqslant 1, \tag{F.23}$$

where, comparing with Eq. (F.1), $f(x) = 1/(1 + a\cos x)$ and $S(x) = \mathrm{e}^{-\mathrm{i}\,\ell x}$. Such integrals appear when calculating some of the polar integrals (E.22), with a possible singularity in $x_s = \arccos(-1/a)$ in the integration domain. Integral (F.23) can be evaluated using the Cauchy principal value, but numerically remains the challenge of calculating it close enough to such singularity. To deal with this problem, we can first divide the integral into two parts:

$$I = \int_0^{x_1} \mathrm{d}x \, \frac{\mathrm{e}^{-\mathrm{i}\,\ell x}}{1 + a\cos x} + \int_{x_1}^{x_s - \delta} \mathrm{d}x \, \frac{\mathrm{e}^{-\mathrm{i}\,\ell x}}{1 + a\cos x}, \tag{F.24}$$

where x_1 is a value far enough from the singularity and δ is a small value.

Both integrals in Eq. (F.24) can be evaluated with the collocation method, but basically all efforts must be concentrated in the second one. We proceed with the

Table F.4 – Same as Tab. F.1, for the integral (F.22).

r	Basis	$n = 25$	$n = 50$	$n = 100$	$n = 150$
			$\ell = 0$		
0.10	Monomial	$6.198\,89 \times 10^{-3}$	$9.590\,04 \times 10^{-4}$	$6.697\,32 \times 10^{-4}$	$5.469\,64 \times 10^{-2}$
	Bsplines	$1.844\,23 \times 10^{-6}$	$4.133\,48 \times 10^{-7}$	$1.169\,07 \times 10^{-4}$	$1.787\,33 \times 10^{3}$
	Simpson	$2.291\,27 \times 10^{-5}$	$6.600\,51 \times 10^{-7}$	$1.862\,21 \times 10^{-8}$	$1.862\,21 \times 10^{-8}$
1.00		1.705 17	1.541 41	4.116 04	7.358 01
		$1.779\,64 \times 10^{-2}$	$1.946\,08 \times 10^{-3}$	$1.795\,78 \times 10^{-1}$	$3.854\,39 \times 10^{-2}$
		$2.070\,43 \times 10^{-5}$	$5.800\,87 \times 10^{-7}$	$2.108\,05 \times 10^{-8}$	$2.108\,05 \times 10^{-8}$
10.00		$3.934\,51 \times 10^{-8}$	$1.559\,00 \times 10^{-8}$	$1.187\,76 \times 10^{-8}$	$1.187\,76 \times 10^{-8}$
		$1.187\,76 \times 10^{-8}$	$1.187\,76 \times 10^{-8}$	$5.560\,31 \times 10^{-6}$	$9.676\,60 \times 10^{-3}$
		$9.430\,78 \times 10^{-5}$	$6.027\,26 \times 10^{-6}$	$3.689\,55 \times 10^{-7}$	$6.681\,26 \times 10^{-8}$
			$\ell = 1$		
0.10		$1.141\,20 \times 10^{3}$	$1.747\,84 \times 10^{3}$	$1.014\,94 \times 10^{3}$	$1.946\,64 \times 10^{3}$
		$9.915\,07 \times 10^{1}$	$9.915\,07 \times 10^{1}$	$9.915\,07 \times 10^{1}$	$1.436\,33 \times 10^{2}$
		$1.830\,40 \times 10^{-2}$	$1.825\,59 \times 10^{-2}$	$1.825\,43 \times 10^{-2}$	$1.825\,42 \times 10^{-2}$
1.00		$6.661\,55 \times 10^{2}$	$1.075\,59 \times 10^{3}$	$7.332\,19 \times 10^{2}$	$6.607\,29 \times 10^{2}$
		$9.144\,85 \times 10^{1}$	$9.144\,66 \times 10^{1}$	$9.146\,69 \times 10^{1}$	$9.420\,15 \times 10^{1}$
		$9.699\,31 \times 10^{-2}$	$9.478\,70 \times 10^{-2}$	$9.371\,63 \times 10^{-2}$	$9.015\,02 \times 10^{-2}$
10.00		$6.048\,22 \times 10^{-8}$	$7.042\,46 \times 10^{-8}$	$7.904\,12 \times 10^{-7}$	$2.013\,31 \times 10^{-7}$
		$2.233\,98 \times 10^{2}$	$2.233\,98 \times 10^{2}$	$2.233\,98 \times 10^{2}$	$2.761\,62 \times 10^{2}$
		$6.329\,84 \times 10^{-5}$	$1.021\,57 \times 10^{-5}$	$5.940\,51 \times 10^{-7}$	$1.358\,78 \times 10^{-7}$

derivative of the kernel, which is very simple in this case

$$\frac{\mathrm{d}}{\mathrm{d}x}\mathrm{e}^{-\mathrm{i}\,\ell x} = -\mathrm{i}\,\ell \mathrm{e}^{-\mathrm{i}\,\ell x}, \tag{F.25}$$

and as we need only one function to evaluate the integral, the order of the vectors in Eq. (F.2) is $m = 1$. The corresponding collocation equation to solve, using Eqs. (F.8) and (F.9), is then

$$\left(\frac{\mathrm{d}}{\mathrm{d}x}u_k - \mathrm{i}\,\ell u_k\right) c_k = f, \tag{F.26}$$

where f is the integrand.

To test numerically this integral, we set the parameters in Eq. (F.24) as: $a = 1.000025$, (and then $x_s = 3.13473582$), $x_1 = x_s - 0.1$ and $\delta = 10^{-4}$. In order to solve Eq. (F.26), we use B-splines of order $k = 30$ and $k = 50$ to calculate, respectively, the first and second integrals in Eq. (F.24). In Tabs. F.5 and F.6 we show the corresponding relative errors as a function of the number of basis elements. Such errors were obtained comparing our results with those given by `Mathematica®`, taken as reference values. We compare also with results obtained with the Simpson method. For the first integral, it is clear that using a relatively small number of functions we obtain very good results, with relative errors of the order of 10^{-6}%, while using the

Simpson integral rule, with the same number of points, the errors vary from 1% to 10^{-1}%. For the second integral, we have results with similar relative errors as long as we use more functions. However, this number remains relatively small, even in a domain close to a singularity. On the other hand, the results with the Simpson method are always far from the reference values.

Table F.5 – Relative errors of the first integral in Eq. (F.24), for $a = 1.000025$, $x_1 = x_s - 0.1$ and $\delta = 10^{-4}$, using Levin's collocation method with B-splines (F.12) of order $k = 30$, and with the indicated number n of functions. We also show the errors obtained when using the Simpson integral rule, with the same number of points. We take as reference values the integrals calculated using `Mathematica`®.

m	Basis	$n = 50$	$n = 60$	$n = 70$	$n = 80$
0	Bsplines	$9.039\,17 \times 10^{-6}$	$8.503\,57 \times 10^{-6}$	$8.503\,57 \times 10^{-6}$	$8.503\,57 \times 10^{-6}$
	Simpson	2.022 22	1.224 56	$7.874\,83 \times 10^{-1}$	$5.304\,98 \times 10^{-1}$
1		$1.001\,57 \times 10^{-5}$	$1.007\,96 \times 10^{-5}$	$1.007\,96 \times 10^{-5}$	$1.007\,96 \times 10^{-5}$
		2.414 65	1.462 20	$9.403\,04 \times 10^{-1}$	$6.334\,48 \times 10^{-1}$
2		$11.167\,15 \times 10^{-5}$	$1.206\,17 \times 10^{-5}$	$1.206\,17 \times 10^{-5}$	$1.206\,17 \times 10^{-5}$
		2.946 13	1.784 04	1.147 27	$7.728\,73 \times 10^{-1}$
10		$3.175\,81 \times 10^{-5}$	$3.184\,20 \times 10^{-5}$	$3.184\,20 \times 10^{-5}$	$3.184\,20 \times 10^{-5}$
		$2.339\,08 \times 10^{1}$	$2.012\,83 \times 10^{1}$	$1.767\,15 \times 10^{1}$	$1.575\,29 \times 10^{1}$

Table F.6 – Same as Tab. F.5, for the second integral in Eq. (F.24), and using B-splines of order $k = 50$.

m	Basis	$n = 90$	$n = 100$	$n = 110$	$n = 120$
0	Bsplines	$1.626\,62 \times 10^{-3}$	$3.988\,35 \times 10^{-4}$	$5.135\,96 \times 10^{-2}$	$6.500\,89 \times 10^{-5}$
	Simpson	$5.717\,18 \times 10^{1}$	$4.927\,42 \times 10^{1}$	$4.296\,57 \times 10^{1}$	$3.783\,04 \times 10^{1}$
1		$1.627\,39 \times 10^{-3}$	$4.021\,87 \times 10^{-4}$	$5.228\,89 \times 10^{-5}$	$4.580\,87 \times 10^{-5}$
		$5.718\,02 \times 10^{1}$	$4.928\,14 \times 10^{1}$	$4.297\,20 \times 10^{1}$	$3.783\,60 \times 10^{1}$
2		$1.708\,54 \times 10^{-3}$	$4.032\,93 \times 10^{-4}$	$5.265\,75 \times 10^{-5}$	$4.590\,11 \times 10^{-5}$
		$5.720\,53 \times 10^{1}$	$4.930\,31 \times 10^{1}$	$4.299\,09 \times 10^{1}$	$3.785\,26 \times 10^{1}$
10		$1.656\,48 \times 10^{-3}$	$4.050\,58 \times 10^{-4}$	$4.416\,83 \times 10^{-5}$	$5.514\,19 \times 10^{-5}$
		$5.799\,50 \times 10^{1}$	$4.998\,37 \times 10^{1}$	$4.358\,44 \times 10^{1}$	$3.837\,51 \times 10^{1}$

Appendix G

Survey on Theoretical Methods

We provide here a brief presentation of different methods (and their acronyms) that have been used to study ionization on molecules. Whenever it applies, we cite the calculations we refer to in Chaps. 3 and 4. A more detailed survey has been given in Ref. [14].

G.1. CI

One of the "classical" methods used to study electronic structure in atoms and molecules is *configuration-interaction* (CI); a description of its use for the study of PI of molecules can be found in Ref. [193].

G.2. Hartree–Fock Methods

G.2.1. Self-Consistent Field

Hartree–Fock (HF) and *self-consistent field* (SCF) are also "classical" methods to study electronic structure in atomic and molecular physics (a comprehensive review can be found in Refs. [207, 208]).

G.2.2. Multiconfiguration Time-Dependent Hartree–Fock

The *multiconfiguration time-dependent Hartree-Fock* (MCTDHF) approach is a method that uses a linear combination of determinants of time-dependent orbitals, and is flexible enough to describe the response of a molecule to short and intense laser pulses. The formalism can be found in Refs. [209–211].

G.3. Density Functional Theory

The *density functional theory* (DFT) is widely used in quantum chemistry [224, 225]. It allows to determine easily the electronic structure of a given system (an atom, a molecule, a crystal, etc), regardless of its extension or the number of particles that constitute it. DFT uses the one-electron electronic density $n(\mathbf{r})$, and is based on two theorems, called the Hohenberg–Kohn theorems [226]. In different implementations of the DFT to study PI of molecules, $n(\mathbf{r})$ is calculated using a conventional *linear combination of atomic orbitals* (LCAO).

G.3.1. Kohn–Sham DFT

In the *Kohn–Sham DFT* (KS DFT) [227] (one of the widest used versions of DFT) the Hamiltonian of the molecular system is determined by the density of the occupied orbitals in the ground state, and in terms of the Hartree potential, the electron-nuclei interaction, and the so-called exchange-correlation potential which contains all the "unknowns" of the system.

In Chap. 3 we cite the work of Stener [223] *et al* for PI of H_2S.

G.3.2. Time-Dependent DFT

The *time-dependent DFT* (TD-DFT) [228] constitutes another line of development of the DFT methods. In the first order time-dependent perturbative scheme, the linear response of the electronic density $n(\mathbf{r})$ to an external weak time-dependent electromagnetic field can be described by a SCF potential, given by Zangwill and Soven [229].

In Chap. 3 we use as reference the results of Stener *et al* for PI of CH_4, NH_3, H_2O [230], and of Fronzoni *et al* for PI of SiH_4 [222].

G.4. Complex Methods

G.4.1. Complex Scaling

The *complex scaling* (CS) method [249, 250] has been used extensively to study ionization and, mainly, resonance phenomena in atoms and molecules. The idea behind this method is to scale the coordinates of all particles in the Hamiltonian by a complex-valued scale factor: $r \rightarrow r\, e^{i\,\theta}$. One variant of the CS is the so-called *exterior complex scaling* (ECS) [251–253], whereby the coordinates scale only outside a fixed radius R_0.

The ECS is especially well suited to study ionization processes in molecules, since the definition of the exterior scaling avoids complicated scaling expressions in the nuclear attraction terms of the Hamiltonian [252] when R_0 is large enough to enclose all the molecular nuclei.

G.4.2. Complex Basis Functions

In the *complex basis function* (CBF) technique [254–256] (the CS method can be considered a particular case of the CBF) the continuum scattering information is extracted from a finite-matrix representation of the electronic Hamiltonian in a set of complex square-integrable basis functions.

G.5. Linear Algebraic Method

The *linear algebraic method* (LAM), developed by Collins and Schneider [264, 265], initially developed to study electron collisions, was also adapted to study PI in molecules [266]. The LAM presents the advantage of including explicitly an effective optical potential in order to introduce correlation effects into the scattering solution [266].

The LAM is used to calculate directly the ejected electron unbound wavefunction that satisfies the TISE, dividing the configuration space into two different regions (see Ref. [266]). A set of differential equations in the SEA is obtained and finally converted into a set of linear-algebraic equations. More details on the effective optical potential are given in the Refs. [264, 266, 267].

G.6. Multi-Scattering

The *multiple-scattering method* (MSM) has been developed in different physics fields, as in nuclear physics [268], solid state physics [269], and also in atomic and molecular physics (see, for example, Refs. [270] and [271], and references therein).

The idea behind the MSM is to represent the molecular field, that in general is highly non-central in the molecular core region, by a set of three potentials defined in different non-overlapping spheres (called muffin-tin partitioning). One can construct the photoelectron continuum wavefunction taking into account the continuity conditions between all three regions, and imposing the incoming boundary conditions (3.3) in the external region.

G.7. Plane-Wave-Based Methods

G.7.1. Plane-Wave and Orthogonalized Plane-Wave Approximations

The simplest description of an ionized electron is the *plane-wave approximation* (PWA), but it is not expected to give accurate results near threshold [285]. The final state of the molecule describes one electron that has been excited from a given initial MO to a continuum normalized plane-wave orbital. This plane-wave is not necessarily orthogonal to any of the occupied MOs; if orthonormality is imposed, we have the orthogonalized PWA.

G.7.2. Ground Inversion Potential Method

The so-called *ground state inversion potential method* (GIPM) has been developed by Hilton *et al* [286, 287] with the aim of obtaining a chemical theory of PI intensities [288]. This method uses the standard one-electron PWA, the orthogonalized PWA or the energy shifted PWA [286] in order to calculate the electronic continuum final wavefunction. The cross section is obtained from an atomic summation theory together with a plane wave analysis of diffraction effects from photoelectron amplitudes from different atoms that interfere with each other [288, 289]. The main difference of GIPM with a standard PWA is that the potential felt by an electron when leaving an atomic center in a molecule is calculated directly by inversion of the ground state HF orbital [287, 288]. The GIPM theory can include three important effects: the change in the nature of the atomic orbitals upon formation of the molecule, diffraction effects [288] and exchange in an exact way.

In Chap. 3 we use the results of Kilcoyne *et al* for PI of CH_4, H2O and NH_3 [284].

G.8. Quantum Defect Theory

The *quantum defect theory* (QDT) is a method developed to study properties of an electron in the field of a positive ion (atomic or molecular). Based in the work of Rydberg on the analysis of alkali spectra, the general features of this method are reviewed in Refs. [300–303]. The idea behind QDT is to find for a potential $V(r)$

(with a Coulomb asymptotic behavior) eigenvalues in terms of *effective quantum numbers* ν_n [300] that, in general, are not integers. The quantum defects $\mu_n = n - \nu_n$ (where n is the principal quantum number associated to the Coulomb potential) provide a measure of the difference between the potential $V(r)$ and the Coulomb potential. With these, it is possible to calculate analytical functions for both bound and continuum states [300]. There are some generalizations of standard QDT as the multichannel QDT [301, 302] or the molecular QDT [304].

G.9. R-Matrix Method

Originally introduced in nuclear physics by Wigner [312], the *R-matrix method* (RMM) has been adapted to atomic and molecular physics by Burke and coworkers (see Ref. [313] and references therein). Applications of this method, in particular for electron collisions, have been reviewed elsewhere [314–316]. The idea behind the RMM is to enclose the scattering particles and the target within a sphere of radius a, and to characterize the system using the eigenenergies and the eigenstates computed within the sphere; then by matching them to the known asymptotic solutions, one can extract all the scattering parameters. The R-matrix is defined as the matrix that connects the two regions in which the space is divided into. With the expansion coefficients in such eigenstates for the initial and final wavefunctions, it is possible to calculate the required transition dipole moments, and thus the PI cross section.

G.10. Random Phase Approximation

The *random-phase approximation* (RPA) is a method that has been applied with success to study PI in atoms and molecules [326, 327]. In the standard RPA procedure, the ground state and the one-electron wavefunctions for the excited and continuum states of the molecule are calculated at HF level. With these, all required matrix elements and in particular the Coulomb and dipole matrix elements, can be determined directly. Then, RPA dipole matrix elements are calculated solving the corresponding equation, and the results are used to obtain PI cross sections or the required observables [328–331].

In Chap. 3 we use the results of Cacelli *et al* [325] to study PI of H_2S.

G.11. Stieltjes–Tchebycheff Technique

The *Stieltjes–Tchebycheff technique* (STT), developed by Langhoff and coworkers (see, for example, Refs. [346, 347] and references therein), is based on theorems from

the theory of moments [348]; its flexibility allows the use of different type of basis sets [347, 349, 350].

The strength of the interaction of unpolarized radiation with a target gas is described using the Kramers–Heisenberg expression of the polarizability (frequency-dependent) of the constituent molecules, and is written as a Stieltjes integral over the appropriate oscillator strength distribution [346, 350]. Alternatively, it is expressed in terms of the cumulative oscillator-strength distribution which can be approximated by an histogram (Stieltjes procedure). Even if such an histogram cannot represent adequately the continuum of the molecule, it can give good approximations to the related power moments, and it rigorously bounds the correct distribution through Tchebycheff inequalities [348]. Technical details about the direct computational implementation of the STT are provided in Ref. [347].

In Chap. 3, we use the result of Cacelli *et al* for PI of CH_4 [344], and for H_2O and NH_3 [345].

G.12. The Kohn Variational Method

Among different approximate methods used to determine the energy spectra and the corresponding wavefunctions, we have the standard Ritz variational method [170], but also the *Kohn variational method* (KVM) [364]. The idea behind the latter is to find a variational expression that allows one to calculate the wavefunction with a correct asymptotic behavior, using two arbitrary $f_\ell(r)$ and $g_\ell(r)$ functions, that behave asymptotically as the regular $F_\ell(kr)$ and, irregular $G_\ell(kr)$ Coulomb functions, respectively. A trial wavefunction, with a trial parameter, can be constructed using both f_ℓ and g_ℓ functions, and a linear combination of L^2 functions in order to describe any additional dynamics of the problem. Two options are distinguished for such a trial wavefunction: (1) if f_ℓ and g_ℓ are the regular and irregular Coulomb functions, the variational parameter is related with a short range potential phase shift; (2) if $g_\ell = h_\ell^{(-)}$ is an outgoing wavefunction called "regularized" irregular Coulomb function (defined as $h_\ell^{(-)}(r) = \mathrm{i}\, k^{-1/2}\,[F_\ell(kr) - \mathrm{i}\, c(r)\, G_\ell(kr)]$, where $c(r)$ is a cutoff function), the variational parameter is the T-matrix. In this case we have the complex Kohn method [365, 366].

Two different implementations of the KVM in the study of PI of molecules are separately hereafter described.

G.12.1. Logarithmic Derivative Kohn Method

The *logarithmic derivative Kohn method* (LDKM) [367, 368], and its variant, the finite-volume variational method [369], were originally proposed to generate a transla-

tional basis for reactive scattering, using Lobatto shape functions [368, 370, 371]. In this method, all the required radial integrals are performed explicitly over a finite volume V, usually a sphere. The main difference between the LDKM and the standard KVM is that different coefficients are added to the functions f_ℓ and g_ℓ [371, 372].

G.12.2. Complex Kohn method

The *complex Kohn method* (CKM), developed by McCurdy, Rescigno and coworkers to study excitation and ionization of molecules by electron collisions [366, 373, 374], has been adapted to study PI in molecules by Lynch and Schneider [375]. Different elections of the arbitrary cutoff function $c(r)$ or the irregular function $g_\ell(r)$ have been tested [375, 376].

In Chap. 4 we use the reported TDCSs by Lin *et al* in Ref. [362] for CH_4 and in Ref. [363] for H_2O.

G.13. The Schwinger Variational Method

While many variational methods are based on the TISE (a differential equation), several others, as the *Schwinger variational method* (SVM) [382] are based on the equivalent integral equation, the *Lippmann–Schwinger equation* (LSE) (see App. D.1 and Refs. [383, 384]); with the latter correct *boundary conditions* (BCs) can be incorporated though the Green function. The SVM can provide highly accurate solutions without requiring expansions in very large basis sets [174, 385]. The idea behind this method is to obtain a stationary variational condition over the T-matrix. In general, one can obtain better converged results using the SVM compared to the KVM results.

The implementation of the SVM has been developed along two methods, named the Schwinger multichannel method [386] and the ISM. The latter, and a variant using continued fractions, are now briefly described.

G.13.1. Iterative Schwinger

The *iterative-Schwinger method* (ISM) is an iterative approach to the solution of collisions problems using the SVM [174] to solve the LSE. The first ISM implementation [385, 387, 388] was the study of scattering of low-energy electrons by atoms and molecules. In the case of molecules, the fixed-nuclei approximation was used together with the assumption that the interaction between the ionized electron and the molecular ion is described by the static-exchange potential [388, 389]. The description of the ISM implementation to study PI is given with details in Refs. [390] and [391].

In Chap. 3 we use the reported calculations of Machado *et al* [381] to study PI of SiH_4.

G.13.2. Continued Fractions

The *method of continued fractions* (MCF), originally proposed by Horáček and Sasakawa [392, 393] for the study of elastic scattering of fast electrons by atoms, has been adapted by Lee *et al* to study scattering of slow electrons by atoms [394] and by linear molecules [395], and extended further to study ionization by electron collisions in polyatomic molecules [396, 397]. The extension of the MCF to the PI study of molecules is explained with details in Ref. [398]. The idea is to represent the scattering matrix as a continued fraction. The continuum wavefunction is obtained from the solution of the LSE using the static-exchange potential, with the long-range Coulomb potential of the ionic core removed. The MCF does not require basis functions and it is characterized by rapid convergence.

G.14. Crank–Nicolson

The *Crank–Nicolson* (CN) method [410] was originally developed to solve numerically differential equations of heat-conduction type, employing a combination of backward/forward finite-difference of all involved variables. The CN scheme is numerically stable and can be used to propagate an initial wavefunction with an imaginary time evolution operator, in which, by the Wick rotation, the time t is replaced by $-\mathrm{i}\,\tau$. In such a way, any initial arbitrary state can converge directly to a particular desired state (bound or continuum), just by adjusting the time-step of the propagator.

Appendix H

List of Photoionization Calculations for Different Molecules

We provide here, molecule by molecule, a rather complete list of references of all theoretical PI studies.

Homonuclear diatomic

1. H_2^+ [254, 255, 257–259, 369, 371, 411–414]
2. H_2 [192, 194–197, 211–213, 231, 257, 260–263, 266, 272, 290–293, 305, 306, 317–320, 331–334, 351, 375, 377, 399, 413]
3. HD [306, 307]
4. D_2 [192, 306, 318]
5. Li_2 [214]
6. C_2 [206]
7. N_2 [198, 215, 232–234, 256, 266, 272–275, 288, 290–292, 294–297, 308, 321, 326, 329, 330, 335–338, 350, 352, 372, 375, 390]
8. O_2 [199]
9. F_2 [353]
10. Cl_2 [235]

Heteronuclear diatomic

11. HeH^{2+} [411]
12. HeH^+ [200, 322]

13. LiH [339]
14. CH [354]
15. OH [400]
16. HF [216, 221, 223, 288, 294, 309, 340, 344]
17. CN^- [326]
18. CO [215, 217, 230, 234, 236, 237, 272, 273, 275, 286, 289, 291, 294–296, 298, 326, 355, 372, 378]
19. NO [266, 310, 321]
20. HCl [201, 223, 356]

Polyatomic

21. BH_3 [223]
22. H_2O [12, 14, 16, 221, 223, 284, 286, 291, 293–297, 309, 326, 340, 345, 357–359, 401, 402]
23. NH_2^- [293]
24. NH_3 [14, 16, 221, 223, 284, 295, 309, 326, 340, 345, 379, 398]
25. ND_3 [311]
26. LiCN [202]
27. AlH_3 [223]
28. H_2S [16, 223, 291, 295, 325, 360, 402]
29. PH_3 [223, 233, 295]
30. SiH_4 [16, 222, 223, 276, 381]
31. CO_2 [203, 218, 266, 275, 298, 323, 326, 352, 391, 403]
32. N_2O [309]
33. NO_2 [219, 298, 324, 326, 352]
34. NO_2^- [326]
35. O_3 [204]
36. C_2N_2 [294, 352]
37. CaHN [294]
38. C_2O_2 [235]
39. COS [275]
40. NF_3 [277]
41. CS_2 [238, 275]
42. CF_4 [239, 240, 278, 404]
43. PF_3 [277, 279]
44. CF_3Cl [280]
45. SiF_4 [276]
46. SF_6 [352, 380, 405]
47. CCl_4 [404]
48. $SiCl_4$ [276, 281]
49. $TiCl_4$ [352]

Organic molecules

50. CH_3 [402]
51. CH_4 [12, 14–16, 220, 221, 223, 278, 284, 286, 290–292, 295, 296, 326, 340, 344, 404, 406]
52. H_2CO [293, 309, 402]
53. H_4CO [293]
54. CH_3I [282]
55. C_2H_2 [231, 232, 241, 242, 293, 296, 326, 337, 341, 407, 408]

56. C_2H_4 [242, 283, 286, 290, 291, 293, 299, 326]
57. C_2H_6 [326]
58. $C_2(CN)_2$ [294]
59. C_3H_4 [293]
60. C_3H_6O (methyl-oxirane) [243]
61. C_3H_8 [326]
62. $(CH_3)_2S$ [295]
63. C_4H_6 (butadiene) [205]
64. C_4H_6 (butyne) [293]
65. C_4H_8 (butene) [293]
66. C_4H_4O (furan) [294]
67. C_4H_5N (pyrrole) [294]
68. $C_4H_4N_2$ (pyrimidine) [244]
69. $C_4H_4N_2$ (pyrazine) [244]
70. $C_4H_4N_2O_2$ (uracil) [245]
71. C_6H_6 (benzene) [246, 247, 299, 361, 372]
72. C_6F_6 [295]
73. $C_4F_4N_2$ [294]
74. $Cr(CO)_6$ [235, 352]
75. $C_{10}H_8$ (naphthalene) [247]
76. $C_{14}H_{10}$ (anthracene) [247]
77. $C_{16}H_{10}$ (pyrene) [247]

Fullerenes

78. C_{20} [342]
79. C_{60}^+ [343]
80. C_{60} [248, 342, 409]

Bibliography

Generalized Sturmian Functions

[1] Gasaneo G, Ancarani L U, Mitnik D M, Randazzo J M, Frapiccini A L and Colavecchia F D 2013 *Adv. Quantum Chem.* **67** 153

[2] Mitnik D M, Colavecchia F D, Gasaneo G and Randazzo J M 2011 *Comp. Phys. Comm.* **182** 1145

[3] Frapiccini A L, Randazzo J M, Gasaneo G and Colavecchia F D 2010 *Phys. Rev. A* **82** 042503

[4] Randazzo J M, Ancarani L U, Gasaneo G, Frapiccini A L and Colavecchia F D 2010 *Phys. Rev. A* **81** 042520

[5] Randazzo J M, Mitnik D, Gasaneo G, Ancarani L U and Colavecchia F D 2015 *Eur. Phys. J. D* **69** 189

[6] Ambrosio M J, Colavecchia F D, Gasaneo G, Mitnik D M and Ancarani L U 2015 *J. Phys. B: At. Mol. Opt. Phys.* **48** 055204

[7] Ambrosio M J, Mitnik D M, Ancarani L U, Gasaneo G and Gaggioli E L 2015 *Phys. Rev. A* **92** 042704

[8] Ambrosio M J, Punta J A D, Rodriguez K V, Gasaneo G and Ancarani L U 2012 *J. Phys. A: Math. Theor.* **45** 015201

[9] Gasaneo G and Ancarani L U 2012 *J. Phys. A: Math. Theor.* **45** 045304

[10] Randazzo J M, Buezas F, Frapiccini A L, Colavecchia F D and Gasaneo G 2011 *Phys. Rev. A* **84** 052715

[11] Frapiccini A L, Gonzalez V Y, Randazzo J M, Colavecchia F D and Gasaneo G 2007 *Int. J. Quantum Chem.* **107** 832–844

— Results This Work —

[12] Granados-Castro C M, Ancarani L U, Gasaneo G and Mitnik D M 2015 *J. Phys.: Conf. Ser.* **601** 012009

[13] Granados-Castro C M, Ancarani L U, Gasaneo G and Mitnik D M 2015 Perturbative-generalized sturmian method for the study of photoionization in atoms (Submitted for publication)

[14] Granados-Castro C M, Ancarani L U, Gasaneo G and Mitnik D M 2016 *Adv. Quantum Chem.* **73** 3

[15] Granados-Castro C M, Ancarani L U, Gasaneo G and Mitnik D M 2014 *Few-Body Syst.* **55** 1029

[16] Granados-Castro C M, Ancarani L U, Gasaneo G and Mitnik D M 2015 Photoionization from valence orbitals of methane, ammonia, water, silane and hydrogen sulfide. a sturmian approach study (In preparation)

[17] Granados-Castro C M, Ancarani L U, Gasaneo G and Mitnik D M 2015 Sturmian approach to molecular ionization by electron impact: Methane, water and ammonia (In preparation)

— Sturmian Functions —

[18] Bromley M W J and Mitroy J 2007 *Int. J. Quantum Chem.* **107** 1150
[19] Randazzo J M, Frapiccini A L, Colavecchia F D and Gasaneo G 2009 *Int. J. Quantum Chem.* **109** 125
[20] Eiglsperger J, Piraux B and Madroñero J 2009 *Phys. Rev. A* **80** 022511
Eiglsperger J, Piraux B and Madroñero J 2010 *Phys. Rev. A* **81** 042527
Eiglsperger J, Piraux B and Madroñero J 2010 *Phys. Rev. A* **81** 042528
[21] Eiglsperger J, Schönwetter M, Piraux B and Madroñero J 2012 *At. Data Nucl. Data Tables* **98** 120
[22] Calderini D, Cavalli S, Coletti C, Grossi G and Aquilanti V 2012 *J. Chem. Sci.* **124** 187
[23] Avery J S and Avery J E 2012 *Mol. Phys.* **110** 1593
[24] Duchon C, Dumont-Lepage M C and Gazeau J P 1982 *J. Chem. Phys.* **76** 445
Duchon C, Dumont-Lepage M C and Gazeau J P 1982 *J. Phys. A: Math. Gen.* **15** 1227
[25] Aquilanti V and Caligiana A 2004 *J. Mol. Struct. THEOCHEM* **709** 15
[26] Avery J and Avery J 2009 *J. Phys. Chem. A* **113** 14565
[27] Papp Z and Plessas W 1996 *Phys. Rev. C* **54** 50
Papp Z, Darai J, Hu C Y, Hlousek Z T, Kónya B and Yakovlev S L 2002 *Phys. Rev. A* **65** 032725
[28] Maquet A 1977 *Phys. Rev. A* **15** 1088
[29] Huens E, Piraux B, Bugacov A and Gajda M 1997 *Phys. Rev. A* **55** 2132
[30] Foumouo E, Kamta G L, Edah G and Piraux B 2006 *Phys. Rev. A* **74** 063409
[31] Taïeb R, Véniard V, Maquet A, Vucic S and Potvliege R M 1991 *J. Phys. B: At. Mol. Opt. Phys.* **24** 3229
[32] Knyr V A, Nasyrov V V, Popov Y V and Ya Stotland L 1996 *J. Exp. Theor. Phys.* **82** 190
[33] Ngoko Djiokap J M, Foumouo E, Kwato Njock M G, Urbain X and Piraux B 2010 *Phys. Rev. A* **81** 042712
[34] Silenou Mengoue M, Kwato Njock M G, Piraux B, Popov Y V and Zaytsev S A 2011 *Phys. Rev. A* **83** 052708
[35] Winter T G 2013 *Phys. Rev. A* **87** 032704
[36] Shull H and Loöwdin P O 1959 *J. Chem. Phys.* **30** 617
[37] Goscinski O 2002 *Adv. Quantum Chem.* **41** 51 preliminary research unpublished. Included as an appendix.
[38] Aquilanti V, Cavalli S, Coletti C and Grossi G 1996 *Chem. Phys.* **209** 405
[39] Aquilanti V, Cavalli S and De Fazio D 1998 *J. Chem. Phys.* **109** 3792
[40] Avery J and Shim R 2001 *Int. J. Quantum Chem.* **83** 1
[41] Avery J and Avery J 2003 *J. Math. Chem.* **33** 145
[42] Rawitscher G 1982 *Phys. Rev. C* **25** 2196
Adams D 1979 *The Hitchhiker's Guide to the Galaxy* (UK: Pan Books)
[43] Rawitscher G 2012 *Phys. Rev. E* **85** 026701
[44] Ovchinnikov S Y and Macek J H 1997 *Phys. Rev. A* **55** 3605

[45] Macek J H, Yu Ovchinnikov S and Gasaneo G 2006 *Phys. Rev. A* **73** 032704
[46] Rotenberg M 1962 *Ann. Phys. (N. Y).* **19** 262
[47] Rotenberg M 1970 *Adv. At. Mol. Phys.* **6** 233

— Model Potentials —

[48] McDowell M R C and Coleman J P 1970 *Introduction to the theory of ion-atom collisions* (North-Holland Pub. Co.)
[49] Rogers F J 1981 *Phys. Rev. A* **23** 1008
Rogers F J, Wilson B G and Iglesias C A 1988 *Phys. Rev. A* **38** 5007
[50] Mendez M P A, Mitnik D M and Miraglia J E 2015 Orbital-Specific Exchange Potentials for Noble Gases with Depurated Inversion of Hartree–Fock wave-functions (*Preprint* 1509.02161)
[51] Fernández-Menchero L and Otranto S 2010 *Phys. Rev. A* **82** 022712
[52] Fernández-Menchero L and Otranto S 2014 *J. Phys. B: At. Mol. Opt. Phys.* **47** 035205

Generalities on PI

— Experimental and Theoretical Techniques —

[53] Fano U and Cooper J 1968 *Rev. Mod. Phys.* **40** 441
[54] Schmidt V 1992 *Rep. Prog. Phys.* **55** 1483
[55] Martín F 2007 *J. Phys. Conf. Ser.* **88** 012001
[56] Samson J A 1976 *Phys. Rep.* **28** 303
[57] Huang K N, Johnson W and Cheng K 1981 *At. Data Nucl. Data Tables* **26** 33
[58] Samson J A 1966 *Adv. At. Mol. Phys.* **2** 177
[59] Samson J A R and Yin L 1989 *J. Opt. Soc. Am. B* **6** 2326
[60] Vilesov F I, L K B and Terenin A N 1961 *Sov. Phys. Doklady* **6** 490
[61] Turner D W and Jobory M I A 1962 *J. Chem. Phys.* **37** 3007
[62] Carlson T A and Krause M O 1965 *Phys. Rev.* **137** A1655
[63] Hayaishi T, Murakami E, Yagishita A, Koike F, Morioka Y and Hansen J E 1988 *J. Phys. B: At. Mol. Opt. Phys.* **21** 3203
[64] Tegeler E, Wiech G and Faessler A 1980 *J. Phys. B At. Mol. Phys.* **13** 4771
[65] Werner U and Jitschin W 1988 *Phys. Rev. A* **38** 4009
[66] Sanz-Vicario J, Bachau H and Martín F 2006 *Phys. Rev. A* **73** 033410
[67] Pérez-Torres J F, Morales F, Sanz-Vicario J L and Martín F 2009 *Phys. Rev. A* **80** 011402
[68] Fernández J and Martín F 2009 *New J. Phys.* **11** 043020
[69] Lambropoulos P, Maragakis P and Zhang J 1998 *Phys. Rep.* **305** 203
[70] Chandra N 1987 *J. Phys. B: At. Mol. Phys.* **20** 3405
[71] Senftleben A, Pflüger T, Ren X, Al-Hagan O, Najjari B, Madison D, Dorn a and Ullrich J 2010 *J. Phys. B: At. Mol. Opt. Phys.* **43** 081002
[72] Senftleben A, Al-Hagan O, Pflüger T, Ren X, Madison D, Dorn A and Ullrich J 2010 *J. Chem. Phys.* **133** 044302
[73] Jones D B, Yamazaki M, Watanabe N and Takahashi M 2013 *Phys. Rev. A* **87** 022714
[74] Ali E, Ren X, Dorn A, Ning C and Madison D 2015 *J. Phys. B: At. Mol. Opt. Phys.* **48** 115201

— Applications —

[75] Liedahl D A and Paerels F 1996 *Astrophys. J.* **468** L33
[76] Bautista M A, Romano P and Pradhan A K 1998 *Astrophys. J. Suppl. Ser.* **118** 259
[77] Dopita M A and Meatheringham S J 1991 *Astrophys. J.* **367** 115
[78] García-Segura G, Langer N, Rożyczka M and Franco J 1999 *Astrophys. J.* **517** 767
[79] Monteiro H, Schwarz H E, Gruenwald R and Heathcote S 2004 *Astrophys. J.* **609** 194
[80] Mallard G, Miller J H and Smyth K C 1982 *J. Chem. Phys.* **76** 3483
[81] Robb D B and Blades M W 2008 *Anal. Chim. Acta* **627** 34
[82] Levine J S and Javan A 1973 *Appl. Phys. Lett.* **22** 55
[83] Killian T C, Kulin S, Bergeson S D, Orozco L A, Orzel C and Rolston S L 1999 *Phys. Rev. Lett.* **83** 4776
[84] Amusia M Y and Baltenkov A S 2006 *Phys. Rev. A* **73** 062723
[85] Hubbell J H 1999 *Phys. Med. Biol.* **44** R1
[86] Stepanek J, Blattmann H, Laissue J A, Lyubimova N, Di Michiel M and Slatkin D N 2000 *Med. Phys.* **27** 1664
[87] Horsley J A, Stöhr J, Hitchcock A P, Newbury D C, Johnson A L and Sette F 1985 *J. Chem. Phys.* **83** 6099
[88] Piancastelli M N, Lindle D W, Ferrett T A and Shirley D A 1987 *J. Chem. Phys.* **86** 2765
[89] Sheehy J A, Gil T J, Winstead C L, Farren R E and Langhoff P W 1989 *J. Chem. Phys.* **91** 1796
[90] Cassuto A, Mane M and Jupille J 1991 *Surf. Sci. Lett.* **249** 8
[91] Tonner B P, Kao C M, Plummer E W, Caves T C, Messmer R P and Salaneck W R 1983 *Phys. Rev. Lett.* **51** 1378
[92] Stöhr J, Outka D A, Baberschke K, Arvanitis D and Horsley J A 1987 *Phys. Rev. B* **36** 2976
[93] Solomon J L, Madix R J and Stöhr J 1988 *J. Chem. Phys.* **89** 5316
[94] Liu A C, Stöhr J, Friend C M and Madix R J 1990 *Surf. Sci.* **235** 107

Experimental and Reference Data of PI

— Atoms —

[95] Kandula D Z, Gohle C, Pinkert T J, Ubachs W and Eikema K S E 2010 *Phys. Rev. Lett.* **105** 063001
[96] Kaufman V and Minnhagen L 1972 *J. Opt. Soc. Am.* **62** 92
Saloman E B and Sansonetti C J 2004 *J. Phys. Chem. Ref. Data* **33** 1113
[97] Harriman J 1956 *Phys. Rev.* **101** 594
[98] Shafer N and Bersohn R 1990 *Phys. Rev. A* **42** 1313
Shafer N and Bersohn R 1991 *Phys. Rev. A* **44** 7855
[99] Granados-Castro C M 2012 *Time-dependent Feshbach method for the dynamical study of photoionization and autoionization in two-electron atomic systems* Master's thesis Universidad de Antioquia
[100] Granados-Castro C M and Sanz-Vicario J L 2013 *J. Phys. B: At. Mol. Opt. Phys.* **46** 055601
[101] Samson J A R, He Z X, Yin L and Haddad G N 1994 *J. Phys. B: At. Mol. Opt.*

Phys. **27** 887–898
[102] Farnoux F C and Lamoureux M 1976 *J. Phys. B: At. Mol. Phys.* **9** 897
[103] Samson J and Stolte W 2002 *J. Electron Spectrosc. Relat. Phenom.* **123** 265

— Molecules —

[104] Moccia R 1964 *J. Chem. Phys.* **40** 2164
[105] Moccia R 1964 *J. Chem. Phys.* **40** 2176
[106] Moccia R 1964 *J. Chem. Phys.* **40** 2186
[107] Backx C and van der Wiel M J V 1975 *J. Phys. B: At. Mol. Phys.* **8** 3020
[108] Marr G V and Holmes R M 1980 *J. Phys. B: At. Mol. Phys.* **13** 939
[109] Brion C, Hamnett A, Wight G and van der Wiel M 1977 *J. Electron Spectros. Relat. Phenomena* **12** 323
[110] Banna M S, Kossmann H and Schmidt V 1987 *Chem. Phys.* **114** 157
[111] Banna M S, McQuaide B H, Malutzki R and Schmidt V 1986 *J. Chem. Phys.* **84** 4739
[112] Cooper G, Ibuki T and Brion C 1990 *Chem. Phys.* **140** 133
[113] Brion C, Iida Y and Thomson J 1986 *Chem. Phys.* **101** 449
[114] Adam M Y, Morin P, Cauletti C and Piancastelli M N 1985 *J. Electron Spectros. Relat. Phenomena* **36** 377

Generalities on (e, 2e)

— Experimental and Theoretical Techniques —

[115] Gao J, Madison D H and Peacher J L 2005 *Phys. Rev. A* **72** 020701
Gao J, Peacher J L and Madison D H 2005 *J. Chem. Phys.* **123** 204302
Gao J, Madison D H and Peacher J L 2005 *J. Chem. Phys.* **123** 204314
[116] Märk T D and Dunn G H (eds) 1985 *Electron Impact Ionization* 1st ed (Wien: Springer-Verlag)
[117] Ehrhardt H, Jung K, Knoth G and Schlemmer P 1986 *Z. Phys. D: At., Mol. Clusters* **1** 3
[118] Lahmam-Bennani A 1991 *J. Phys. B: At. Mol. Opt. Phys.* **24** 2401
[119] Lane N 1980 *Rev. Mod. Phys.* **52** 29
[120] Tennyson J 2010 *Phys. Rep.* **491** 29
[121] Woollings M J and McDowell M R C 1972 *J. Phys. B: At. Mol. Phys.* **5** 1320
[122] Tweed R J 1973 *J. Phys. B: At. Mol. Phys.* **6** 398
[123] Marchalant P J, Whelan C T and Walters H R J 1998 *J. Phys. B: At. Mol. Opt. Phys.* **31** 1141
[124] Reid R H G, Bartschat K and Raeker A 1998 *J. Phys. B: At. Mol. Opt. Phys.* **31** 563
Reid R H G, Bartschat K and Raeker A 2000 *J. Phys. B: At. Mol. Opt. Phys.* **33** 5261
[125] Kheifets A S 2004 *Phys. Rev. A* **69** 032712
[126] Dal Cappello C, Hmouda B, Naja A and Gasaneo G 2013 *J. Phys. B: At. Mol. Opt. Phys.* **46** 145203
[127] Ajana I, Makhoute A, Khalil D and Dubois A 2014 *J. Phys. B: At. Mol. Opt. Phys.* **47** 175001
[128] Houamer S, Mansouri A, Cappello C D, Lahmam-Bennani A, Elazzouzi S, Moulay M and Charpentier I 2003 *J. Phys. B: At. Mol. Opt. Phys.* **36** 3009

[129] Dal Cappello C, Haddadou A, Menas F and Roy A C 2010 *J. Phys. B: At. Mol. Opt. Phys.* **44** 015204
[130] Dal Cappello C, Rezkallah Z, Houamer S, Charpentier I, Hervieux P a, Ruiz-Lopez M F, Dey R and Roy a C 2011 *Phys. Rev. A* **84** 032711
[131] Sahlaoui M and Bouamoud M 2012 *J. Phys. B: At. Mol. Opt. Phys.* **45** 085201
[132] McCarthy I E and Weigold E 1991 *Rep. Prog. Phys.* **54** 789
[133] Champion C, Cappello C D, Houamer S and Mansouri A 2006 *Phys. Rev. A* **73** 012717
[134] Madison D H and Al-Hagan O 2010 *J. At. Mol. Opt. Phys.* **2010** 1
[135] Tóth I and Nagy L 2010 *J. Phys. B: At. Mol. Opt. Phys.* **43** 135204
[136] Brauner M, Briggs J S and Klar H 1989 *J. Phys. B: At. Mol. Opt. Phys.* **22** 2265
[137] Naja A, Staicu-Casagrande E M, Lahmam-Bennani A, Nekkab M, Mezdari F, Joulakian B, Chuluunbaatar O and Madison D H 2007 *J. Phys. B: At. Mol. Opt. Phys.* **40** 3775
[138] Catoire F, Staicu-Casagrande E M, Lahmam-Bennani A, Duguet A, Naja A, Ren X G, Lohmann B and Avaldi L 2007 *Rev. Sci. Instrum.* **78** 013108
[139] Walters H 1984 *Phys. Rep.* **116** 1
[140] Golecki P and Klar H 2001 *J. Phys. B: At. Mol. Opt. Phys.* **34** L779
[141] Zon B A 1974 *J. Phys. B: At. Mol. Phys.* **7** L483
[142] Bransden B H and Dewangan D P 1979 *J. Phys. B: At. Mol. Phys.* **12** 1377
[143] Massey H S W and Mohr C B O 1934 *Proc. R. Soc. A* **146** 880
[144] Joachain C J, Winters K H, Cartiaux L and Mendez-Moreno R M 1977 *J. Phys. B: At. Mol. Phys.* **10** 1277
[145] Lewis R R 1956 *Phys. Rev.* **102** 537

— Applications —

[146] Demaria A J 1973 *Proc. IEEE* **61** 731
[147] Dalgarno A 1968 *Adv. At. Mol. Phys.* **4** 381
[148] Takayanagi K and Itikawa Y 1970 *Space Sci. Rev.* **11** 380
[149] Dalgarno A and McCray R A 1972 *Annu. Rev. Astron. Astrophys.* **10** 375
[150] Thaddeus P 1972 *Astrophys. J.* **173** 317
[151] Dickinson A S, Phillips T G, Goldsmith P F, Percival I C and Richards D 1977 *Astron. Astrophys.* **54** 645
[152] Röllig M, Abel N P, Bell T, Bensch F, Black J, Ferland G J, Jonkheid B, Kamp I, Kaufman M J, Bourlot J L, Petit F L, Meijerink R, Morata O, Ossenkopf V, Roueff E, Shaw G, Spaans M, Sternberg A, Stutzki J, Thi W F, van Dishoeck E F, van Hoof P a M, Viti S and Wolfire M G 2007 *Astron. Astrophys.* **206** 187
[153] Fuente A, García-Burillo S, Usero A, Gerin M, Neri R, Faure A, Bourlot J L, González-García M, Rizzo J R, Alonso-Albi T and Tennyson J 2008 *Astron. Astrophys.* **492** 10
[154] Geppert W and Larsson M 2008 *Mol. Phys.* **106** 2199
[155] Becker K H and Tarnovsky V 1995 *Plasma Sources Sci. Technol.* **4** 307
[156] Janev R K (ed) 1995 *Atomic and molecular Processes in Fusion Edge Plasmas* (NY: Springer)
[157] Huestis D L, Bougher S W, Fox J L, Galand M, Johnson R E, Moses J I and Pickering J C 2008 *Space Sci. Rev.* **139** 63
[158] Ajello J 2001 *Icarus* **152** 151

[159] Luque A, Ebert U and Hundsdorfer W 2008 *Phys. Rev. Lett.* **101** 075005
[160] Boudaïffa B, Cloutier P, Hunting D, Huels M A and Sanche L 2000 *Science* **287** 1658
[161] Wigner E P 1955 *Phys. Rev.* **98** 145
Pazourek R, Nagele S and Burgdörfer J 2015 *J. Phys. B: At. Mol. Opt. Phys.* **48** 061002

Experimental and Reference Data of $(e, 2e)$

— Atoms —

[162] Byron F W, Joachain C J and Piraux B 1980 *J. Phys. B: At. Mol. Phys.* **13** L673
[163] Lohmann B, McCarthy I, Stelbovics A and Weigold E 1984 *Phys. Rev. A* **30** 758

— Molecules —

[164] Lahmam-Bennani A, Naja A, Staicu Casagrande E M, Okumus N, Dal Cappello C, Charpentier I and Houamer S 2009 *J. Phys. B: At. Mol. Opt. Phys.* **42** 165201
[165] El Mir R, Staicu Casagrande E M, Naja A, Dal Cappello C, Houamer S and El Omar F 2015 *J. Phys. B: At. , Mol. Opt. Phys.* **48** 175202
[166] Milne-Brownlie D S, Cavanagh S J, Lohmann B, Champion C, Hervieux P A and Hanssen J 2004 *Phys. Rev. A* **69** 032701

General Books

[167] Edmonds A R 1957 *Angular Momentum in Quantum Mechanics* (Princeton: Princeton University Press)
[168] Lebedev N N 1965 *Special Functions and Their Applications* 1st ed (Englewood Cliffs, NJ: Prentice-Hall)
[169] Bethe H A and Salpeter E E 1957 *Quantum Mechanics of One- and Two-Electron Atoms* (Berlin: Springer-Verlag)
[170] Messiah A 1972 *Quantum Mechanics* (Amsterdam: North-Holland)
[171] Newton R G 1982 *Scattering Theory of Wave and Particles* 2nd ed (New York: Springer)
[172] Gradshteyn I S and Ryzhik I M 2007 *Table of Integrals, Series and Products* seventh ed (Academic Press)
[173] Economou E N 2006 *Green's Functions in Quantum Physics* 3rd ed (Berlin Heidelberg: Springer)
[174] Taylor J R 1972 *Scattering Theory: The Quantum Theory of Nonrelativistic Collisions* (NY: Wiley)

Numerical Methods and Related

[175] Anderson E, Bai Z, Bischof C, Blackford S, Demmel J, Dongarra J, Du Croz J, Greenbaum A, Hammarling S, McKenney A and Sorensen D 1999 *LAPACK Users' Guide* 3rd ed (Philadelphia, PA: Society for Industrial and Applied Mathematics)
[176] Luk F T and Qiao S 2000 *Linear Algebra Appl.* **316** 171
[177] Golub G H and van Loan C F 1996 *Matrix Computations* 3rd ed (Baltimore, USA: The Johns Hopkins University Press)
[178] Levin D 1982 *Math. Comput.* **38** 531

[179] Levin D 1996 *J. Comput. Appl. Math.* **67** 95
[180] Olver S 2008 *Numerical Approximation of Highly Oscillatory Integrals* Ph.D. thesis University of Cambridge
[181] Filon L N G 1928 *Proc. Roy. Soc. Edinburgh* **49** 38
[182] Evans G and Webster J 1997 *Appl. Numer. Math.* **23** 205
[183] Bleistein N and Handelsman R 1986 *Asymptotic expansions of integrals* (NY: Dover)
[184] Wong R 1989 *Asymptotic Approximations of Integrals* (NY: Academic Press)
[185] Muller K E 2001 *Numer. Math.* **90** 179
[186] Evans G and Webster J 1999 *J. Comput. Appl. Math.* **112** 55
[187] Longman I M and Miller J C P 1956 *Math. Proc. Cambridge Philos. Soc.* **52** 764
[188] Longman I M 1960 *Math. Comput.* **14** 53
[189] Huybrechs D and Olver S 2009 Highly oscillatory quadrature *Highly Oscil. Probl.* (Cambridge University Press) chap 2, p 25
[190] de Boor C and Swartz B 1973 *SIAM J. Numer. Anal.* **10** 582
[191] Bachau H, Cormier E, Decleva P, Hansen J E and Martín F 2001 *Rep. Prog. Phys.* **64** 1815

Survey on Methods and PI of Molecules

— CI —

[192] Sansone G, Kelkensberg F, Pérez-Torres J F, Morales F, Kling M F, Siu W, Ghafur O, Johnsson P, Swoboda M, Benedetti E, Ferrari F, Lépine F, Sanz-Vicario J L, Zherebtsov S, Znakovskaya I, L'huillier A, Ivanov M Y, Nisoli M, Martín F and Vrakking M J J 2010 *Nature* **465** 763
[193] Langhoff P W 1983 Aspects of electronic configuration interaction in molecular photoionization *Electron-Atom and Electron-Molecule Collisions* ed Hinze J (New York: Springer)
[194] Sanz-Vicario J, Palacios A, Cardona J, Bachau H and Martín F 2007 *J. Electron Spectros. Relat. Phenomena* **161** 182
[195] Apalategui A and Saenz A 2002 *J. Phys. B: At. Mol. Opt. Phys.* **35** 1909
[196] Fojón O A, Fernández J, Palacios A, Rivarola R D and Martín F 2004 *J. Phys. B: At. Mol. Opt. Phys.* **37** 3035
[197] Dowek D, Pérez-Torres J F, Picard Y J, Billaud P, Elkharrat C, Houver J C, Sanz-Vicario J L and Martín F 2010 *Phys. Rev. Lett.* **104** 233003
[198] Stratmann R E, Bandarage G and Lucchese R R 1995 *Phys. Rev. A* **51** 3756
[199] Stratmann R E and Lucchese R R 1995 *J. Chem. Phys.* **102** 8493
[200] Vanne Y V and Saenz A 2004 *J. Phys. B: At. Mol. Opt. Phys.* **37** 4101
[201] van Dishoeck E F, van Hemert M C and Dalgarno A 1982 *J. Chem. Phys.* **77** 3693
[202] Klinkusch S, Saalfrank P and Klamroth T 2009 *J. Chem. Phys.* **131** 114304
[203] Daasch W R, Davidson E R and Hazi A U 1982 *J. Chem. Phys.* **76** 6031
[204] Decleva P, De Alti G and Lisini A 1988 *J. Chem. Phys.* **89** 367
[205] Sonk J A and Schlegel H B 2011 *J. Phys. Chem. A* **115** 11832

— HF, SCF and MCTDHF —

[206] Padial N T, Collins L A and Schneider B I 1985 *Astrophys. J.* **298** 369
[207] Fischer C F 2006 21. atomic structure: Multiconfiguration hartree–fock theories

Springer Handbook of Atomic, Molecular and Optical Physics ed Drake G W F (New York: Springer)
[208] Fischer C F, Brage T and Jönsson P 1997 *Computational Atomic Structure. An MCHF Approach* (London: Institute of Physics Publishing)
[209] Nest M, Klamroth T and Saalfrank P 2005 *J. Chem. Phys.* **122** 124102
[210] Alon O E, Streltsov A I and Cederbaum L S 2009 *Phys. Rev. A* **79** 022503
[211] Kato T and Kono H 2008 *J. Chem. Phys.* **128** 184102
[212] Kelly H P 1973 *Chem. Phys. Lett.* **20** 547
[213] Haxton D J, Lawler K V and McCurdy C W 2011 *Phys. Rev. A* **83** 063416
[214] Larkins F P and Richards J A 1986 *Aust. J. Phys.* **39** 809
[215] Schirmer J, Cederbaum L, Domcke W and von Niessen W 1977 *Chem. Phys.* **26** 149
[216] Haxton D J, Lawler K V and McCurdy C W 2012 *Phys. Rev. A* **86** 013406
[217] Semenov S K, Cherepkov N A, Jahnke T and Dörner R 2004 *J. Phys. B: At. Mol. Opt. Phys.* **37** 1331
[218] Saito N, Fanis A D, Kubozuka K, Machida M, Takahashi M, Yoshida H, Suzuki I H, Cassimi A, Czasch A, Schmidt L, Dörner R, Wang K, Zimmermann B, McKoy V, Koyano I and Ueda K 2003 *J. Phys. B: At. Mol. Opt. Phys.* **36** L25
[219] Saito N, Toffoli D, Lucchese R R, Nagoshi M, De Fanis A, Tamenori Y, Oura M, Yamaoka H, Kitajima M, Tanaka H, Hergenhahn U and Ueda K 2004 *Phys. Rev. A* **70** 062724
[220] Dalgarno A 1952 *Proc. Phys. Soc. Sect. A* **65** 663

— DFT, KS-DFT and TD-DFT —

[221] Stener M, Fronzoni G, Toffoli D and Decleva P 2002 *Chem. Phys.* **282** 337
[222] Fronzoni G, Stener M and Decleva P 2003 *J. Chem. Phys.* **118** 10051
[223] Stener M and Decleva P 1998 *J. Electron Spectros. Relat. Phenomena* **94** 195
[224] Stener M, Toffoli D, Fronzoni G and Decleva P 2007 *Theor. Chem. Acc.* **117** 943
[225] Jones R O 2015 *Rev. Mod. Phys.* **87** 897
[226] Hohenberg P and Kohn W 1964 *Phys. Rev.* **136** B864
[227] Kohn W and Sham L J 1965 *Phys. Rev.* **140** A1133
[228] Runge E and Gross E K U 1984 *Phys. Rev. Lett.* **52** 997
[229] Zangwill A and Soven P 1980 *Phys. Rev. A* **21** 1561
[230] Stener M, Decleva P, Cacelli I, Moccia R and Montuoro R 2001 *Chem. Phys.* **272** 15
[231] Russakoff A and Varga K 2015 *Phys. Rev. A* **92** 053413
[232] Levine Z H and Soven P 1984 *Phys. Rev. A* **29** 625
[233] Stener M and Decleva P 2000 *J. Chem. Phys.* **112** 10871
[234] Plésiat E, Decleva P and Martín F 2012 *J. Phys. B: At. Mol. Opt. Phys.* **45** 194008
[235] Toffoli D, Stener M, Fronzoni G and Decleva P 2002 *Chem. Phys.* **276** 25
[236] Stener M 2002 *Chem. Phys. Lett.* **356** 153
[237] Kukk E, Ayuso D, Thomas T D, Decleva P, Patanen M, Argenti L, Plésiat E, Palacios A, Kooser K, Travnikova O, Mondal S, Kimura M, Sakai K, Miron C, Martín F and Ueda K 2013 *Phys. Rev. A* **88** 033412
[238] Stener M, Fronzoni G and Decleva P 2005 *J. Chem. Phys.* **122** 234301
[239] Toffoli D, Stener M, Fronzoni G and Decleva P 2006 *J. Chem. Phys.* **124** 214313
[240] Patanen M, Kooser K, Argenti L, Ayuso D, Kimura M, Mondal S, Plésiat E,

Palacios A, Sakai K, Travnikova O, Decleva P, Kukk E, Miron C, Ueda K and Martín F 2014 *J. Phys. B: At. Mol. Opt. Phys.* **47** 124032
[241] Fronzoni G, Stener M and Decleva P 2004 *Chem. Phys.* **298** 141
[242] Russakoff A, Bubin S, Xie X, Erattupuzha S and Kitzler M 2015 *Phys. Rev. A* **91** 023422
[243] Stranges S, Turchini S, Alagia M, Alberti G, Contini G, Decleva P, Fronzoni G, Stener M, Zema N and Prosperi T 2005 *J. Chem. Phys.* **122** 244303
[244] Holland D M P, Potts A W, Karlsson L, Stener M and Decleva P 2011 *Chem. Phys.* **390** 25
[245] Toffoli D, Decleva P, Gianturco F A and Lucchese R R 2007 *J. Chem. Phys.* **127** 234317
[246] Venuti M, Stener M and Decleva P 1998 *Chem. Phys.* **234** 95
[247] Woon D E and Park J 2004 *Astrophys. J.* **607** 342
[248] Madjet M E, Chakraborty H S, Rost J M and Manson S T 2008 *J. Phys. B: At. Mol. Opt. Phys.* **41** 105101

— Complex Methods —

[249] Reinhardt W P 1982 *Ann. Rev. Phys. Chem.* **33** 223
[250] Moiseyev N 1998 *Phys. Rep.* **302** 212
[251] Nicolaides C A and Beck D R 1978 *Phys. Lett. A* **65** 11
[252] Simon B 1979 *Phys. Lett. A* **71** 211
[253] McCurdy C W and Martín F 2004 *J. Phys. B: At. Mol. Opt. Phys.* **37** 917
[254] McCurdy C W and Rescigno T N 1980 *Phys. Rev. A* **21** 1499
[255] Rescigno T N and McCurdy C W 1985 *Phys. Rev. A* **31** 624
[256] Yu C h, Pitzer R M and McCurdy C W 1985 *Phys. Rev. A* **32** 2134
[257] Morita M and Yabushita S 2008 *J. Comput. Chem.* **29** 2471
[258] Tao L, McCurdy C W and Rescigno T N 2009 *Phys. Rev. A* **79** 012719
[259] Tao L, McCurdy C W and Rescigno T N 2009 *Phys. Rev. A* **80** 013402
[260] Vanroose W, Martín F, Rescigno T N and McCurdy C W 2004 *Phys. Rev. A* **70**
[261] Vanroose W, Horner D A, Martín F, Rescigno T N and McCurdy C W 2006 *Phys. Rev. A* **74** 052702
[262] Rescigno T N, Vanroose W, Horner D A, Martín F and McCurdy C W 2007 *J. Electron Spectros. Relat. Phenomena* **161** 85
[263] Tao L, McCurdy C W and Rescigno T N 2010 *Phys. Rev. A* **82** 023423

— Linear Algebraic Method —

[264] Collins L A and Schneider B I 1981 *Phys. Rev. A* **24** 2387
Schneider B I and Collins L A 1981 *Phys. Rev. A* **24** 1264
[265] Collins L A and Schneider B I 1995 2. the linear algebraic method for electron-molecule collisions *Computational Methods for Electron-Molecule Collisions* ed Huo M W and Gianturco F A (New York: Springer)
[266] Collins L and Schneider B 1984 *Phys. Rev. A* **29** 1695
[267] Schneider B I and Collins L A 1983 *Phys. Rev. A* **27** 2847

— Multiple-Scattering —

[268] Agassi D and Gal A 1973 *Ann. Phys. (NY)* **75** 56
[269] Korringa J 1947 *Physica* **13** 392
Kohn W and Rostoker N 1954 *Phys. Rev.* **94** 1111
Morse P M 1956 *Proc. Nat. Acad. Sci. U. S.* **42** 276

[270] Dill D and Dehmer J L 1974 *J. Chem. Phys.* **61** 692
[271] Johnson K H 1973 Scattered-wave theory of the chemical bond *Advances in Quantum Chemistry* vol 7 ed Lödwin P O (NY: Academic)
[272] Davenport J W 1977 *Int. J. Quantum Chem.* **12** 89
[273] Davenport J 1976 *Phys. Rev. Lett.* **36** 945
[274] Dehmer J L and Dill D 1976 *J. Chem. Phys.* **65** 5327–5334
[275] Grimm F A, Carlson T A, Dress W B, Agron P, Thomson J O and Davenport J W 1980 *J. Chem. Phys.* **72** 3041
[276] Ishikawa H, Fujima K, Adachi H, Miyauchi E and Fujii T 1991 *J. Chem. Phys.* **94** 6740
[277] Jürgensen A and Cavell R G 2003 *J. Electron Spectros. Relat. Phenomena* **128** 245
[278] Rosi M, Sgamellotti A, Tarantelli F, Andreev V A, Gofman M and Nefedov V 1986 *J. Electron Spectros. Relat. Phenomena* **41** 439
[279] Powis I 1993 *Chem. Phys. Lett.* **215** 269
[280] Powis I 1997 *J. Chem. Phys.* **106** 5013
[281] Tse J S, Liu Z F, Bozek J D and Bancroft G M 1989 *Phys. Rev. A* **39** 1791
[282] Powis I 1995 *Chem. Phys.* **201** 189
[283] Grimm F A 1983 *Chem. Phys.* **81** 315

— Plane-Wave-Based Methods —

[284] Kilcoyne D A L, Nordholm S and Hush N S 1986 *Chem. Phys.* **107** 213
[285] Ellison F O 1974 *J. Chem. Phys.* **61** 507
[286] Hilton P R, Nordholm S and Hush N S 1976 *Chem. Phys.* **15** 345
[287] Hilton P R, Nordholm S and Hush N S 1977 *J. Chem. Phys.* **67** 5213
[288] Kilcoyne D A L, McCarthy C, Nordholm S, Hush N S and Hilton P R 1985 *J. Electron Spectros. Relat. Phenomena* **36** 153–185
[289] Hilton P R, Nordholm S and Hush N S 1980 *J. Electron Spectros. Relat. Phenomena* **18** 101
[290] Rabalais J W, Debies T P, Berkosky J L, Huang J J and Ellison F O 1974 *J. Chem. Phys.* **61** 516
[291] Dewar M J S, Komornicki A, Thiel W and Schweig A 1975 *Chem. Phys. Lett.* **31** 286
[292] Huang J T J and Ellison F O 1975 *Chem. Phys. Lett.* **32** 196
[293] Gozem S, Gunina A O, Ichino T, Osborn D L, Stanton J F and Krylov A I 2015 *J. Phys. Chem. Lett.* **6** 4532
[294] Beerlage M J M and Feil D 1977 *J. Electron Spectros. Relat. Phenomena* **12** 161
[295] Schweig A and Thiel W 1974 *J. Electron Spectros. Relat. Phenomena* **3** 27
[296] Deleuze M, Pickup B T and Delhalle J 1994 *Mol. Phys.* **83** 655
[297] Hilton P R, Hordholm S and Hush N S 1979 *Chem. Phys. Lett.* **64** 515
[298] Kilcoyne D A L, Nordholm S and Hush N S 1986 *Chem. Phys.* **107** 225
[299] Kilcoyne D A L, Nordholm S and Hush N S 1986 *Chem. Phys.* **107** 255

— Quantum Defect Theory —

[300] Seaton M J 1966 *Proc. Phys. Soc.* **88** 801
[301] Seaton M J 1983 *Rep. Prog. Phys.* **46** 167
[302] Moores D L and Saraph H E 1983 Applications of quantum defect theory *Atoms in Astrophysics* ed Burke P G, Eissner W B, Hummer D G and Percival I C (NY: Plenum Press) chap 6, p 173

[303] Jungen C (ed) 1996 *Molecular Applications of Quantum Defect Theory* (NY: Taylor & Francis)
[304] Guérout R, Jungen M and Jungen C 2004 *J. Phys. B: At. Mol. Opt. Phys.* **37** 3043
[305] Raşeev G and Le Rouzo H 1983 *Phys. Rev. A* **27** 268
[306] Chupka W A, Dehmer P M and Jivery W T 1975 *J. Chem. Phys.* **63** 3929
[307] Du N Y and Greene C H 1986 *J. Chem. Phys.* **85** 5430
[308] Tuckwell H C 1970 *J. Phys. B: At. Mol. Phys.* **3** 293
[309] Vega M V, Lavín C and Velasco A M 2012 *J. Chem. Phys.* **136** 214308
[310] Giusti-Suzor A and Jungen C 1984 *J. Chem. Phys.* **80** 986
[311] Duggan L, Raunhardt M, Schäfer M, Hollenstein U, Softley T and Merkt F 2010 *Mol. Phys.* **108** 1069

— R-Matrix —

[312] Wigner E P 1946 *Phys. Rev.* **70** 606
Wigner E P 1948 *Phys. Rev.* **73** 1002
[313] Burke P G and Berrington K A (eds) 1993 *Atomic and Molecular Processes, an R-Matrix Approach* (Bristol: Institute of Physics Publishing)
[314] Bartschat K 1998 *Comput. Phys. Commun.* **114** 168
[315] Schneider B I 1995 8. an *r*-matrix approach to electron-molecule collisions *Computational Methods for Electron-Molecule Collisions* ed Huo M W and Gianturco F A (New York: Springer)
[316] Noble C J 1995 14. *r*-matrix for intermediate energy scattering and photoionization *Computational Methods for Electron-Molecule Collisions* ed Huo M W and Gianturco F A (New York: Springer)
[317] Tennyson J, Noble C and Burke P 1986 *Int. J. Quantum Chem.* **XXIX** 1033
[318] Tennyson J 1987 *J. Phys. B: At. Mol. Phys.* **20** L375
[319] Burke P G, Colgan J, Glass D H and Higgins K 2000 *J. Phys. B: At. Mol. Opt. Phys.* **33** 143
[320] Colgan J, Glass D H, Higgins K and Burke P G 2001 *J. Phys. B: At. Mol. Opt. Phys.* **34** 2089
[321] Tashiro M 2010 *J. Chem. Phys.* **132** 134306
[322] Saenz A 2003 *Phys. Rev. A* **67** 033409
[323] Harvey A G, Brambila D S, Morales F and Smirnova O 2014 *J. Phys. B: At. Mol. Opt. Phys.* **47** 215005
[324] Brambila D S, Harvey A G, Mašín Z, Gorfinkiel J D and Smirnova O 2015 *J. Phys. B: At. Mol. Opt. Phys.* **48** 245101

— Random Phase Approximation —

[325] Cacelli I, Carravetta V and Moccia R 1994 *Chem. Phys.* **184** 213
[326] Amusia M Y and Cherepkov N A 1975 *Case Stud. At. Phys.* **5** 47
[327] Amusia M Y 1996 Theory of photoionization: Vuv and soft x-ray frequency region *VUV and Soft X–Ray Photoionization* ed Becker U and Shirley D A (NY: Plenum)
[328] Rowe D 1968 *Rev. Mod. Phys.* **40** 153
[329] Yabushita S, McCurdy C and Rescigno T 1987 *Phys. Rev. A* **36** 3146
[330] Semenov S, Cherepkov N, Fecher G and Schönhense G 2000 *Phys. Rev. A* **61** 032704
[331] Semenov S K and Cherepkov N A 2003 *J. Phys. B: At. Mol. Opt. Phys.* **36** 1409

[332] Martin P H S, Rescigno T N, McKoy V and Henneker W H 1974 *Chem. Phys. Lett.* **29** 496
[333] Schirmer J and Mertins F 1996 *J. Phys. B: At. Mol. Opt. Phys.* **29** 3559
[334] Semenov S K and Cherepkov N A 1998 *Chem. Phys. Lett.* **291** 375
[335] Lucchese R and Zurales R 1991 *Phys. Rev. A* **44** 291
[336] Semenov S and Cherepkov N 2002 *Phys. Rev. A* **66** 022708
[337] Montuoro R and Moccia R 2003 *Chem. Phys.* **293** 281
[338] Cherepkov N, Semenov S, Hikosaka Y, Ito K, Motoki S and Yagishita A 2000 *Phys. Rev. Lett.* **84** 250
[339] Carmona-Novillo E, Moccia R and Spizzo P 1996 *Chem. Phys.* **210** 435
[340] Cacelli I, Carravetta V, Moccia R and Rizzo A 1988 *J. Phys. Chem.* **92** 979
[341] Yasuike T and Yabushita S 2000 *Chem. Phys. Lett.* **316** 257
[342] Ivanov V K, Kashenock G Y, Polozkov R G and Solov'yov A V 2001 *J. Phys. B: At. Mol. Opt. Phys.* **34** L669
[343] Polozkov R G, Ivanov V K and Solov'yov A V 2005 *J. Phys. B: At. Mol. Opt. Phys.* **38** 4341

— Stieltjes–Tchebycheff Method —

[344] Cacelli I, Carravetta V and Moccia R 1985 *J. Phys. B: At. Mol. Phys.* **18** 1375
[345] Cacelli I, Moccia R and Carravetta V 1984 *Chem. Phys.* **90** 313
[346] Langhoff P W 1973 *Chem. Phys. Lett.* **22** 60
[347] Langhoff P W 1979 Stieltjes-tchebycheff moment-tehory approach to molecular photoionization studies *Electron-Molecule and Photon-Molecule Collisions* ed Rescigno T, McKoy V and Schneider B (NY: Plenum)
[348] Shohat J A and Tamarkin J D 1943 *The Problem of Moments* (*Mathematical Surveys* vol 1) (Providence: American Mathematical Society)
[349] Corcoran C T and Langhoff P W 1977 *J. Math. Phys.* **18** 651
[350] Rescigno T N, Bender C F, McKoy B V and Langhoff P W 1978 *J. Chem. Phys.* **68** 970
[351] ONeil S V and Reinhardt W P 1978 *J. Chem. Phys.* **69** 2126
[352] Stener M, Decleva P and Lisini A 1995 *J. Electron Spectrosc. Relat. Phenom.* **74** 29
[353] Orel A E, Rescigno T N, Mckoy B V and Langhoff P W 1980 *J. Chem. Phys.* **72** 1265
[354] Barsuhn J and Nesbet R K 1978 *J. Chem. Phys.* **68** 2783
[355] Görling A and Rösch N 1990 *J. Chem. Phys.* **93** 5563
[356] Cacelli I, Carravetta V and Moccia R 1986 *Mol. Phys.* **59** 385
[357] Delaney J J, Saunders V R and Hillier I H 1981 *J. Phys. B: At. Mol. Phys.* **14** 819
[358] Diercksen G H F, Kraemer W P, Rescigno T N, Bender C F, Mckoy B V, Langhoff S R and Langhoff P W 1982 *J. Chem. Phys.* **76** 1043
[359] Williams G R J and Langhoff P W 1979 *Chem. Phys. Lett.* **60** 201
[360] Cacelli I, Carravetta V and Moccia R 1988 *Chem. Phys.* **120** 51
[361] Gokhberg K, Vysotskiy V, Cederbaum L S, Storchi L, Tarantelli F and Averbukh V 2009 *J. Chem. Phys.* **130** 064104

— Kohn Variational Method —

[362] Lin C y, McCurdy C W and Rescigno T N 2014 *Phys. Rev. A* **89** 052718
[363] Lin C Y, McCurdy C W and Rescigno T N 2014 *Phys. Rev. A* **89** 012703

[364] Kohn W 1948 *Phys. Rev.* **74** 1763
[365] Rescigno T N, McCurdy C W, Orel A E and Lengsfield III B H 1995 1. the complex kohn variational method *Computational Methods for Electron-Molecule Collisions* ed Huo M W and Gianturco F A (New York: Springer)
[366] McCurdy C W and Rescigno T N 1989 *Phys. Rev. A* **39** 4487
[367] Manolopoulos D and Wyatt R 1988 *Chem. Phys. Lett.* **152** 23
[368] Manolopoulos D E, Wyatt R E and Clary D C 1990 *J. Chem. Soc. Faraday Trans.* **86** 1641
[369] Le Rouzo H and Raşeev G 1984 *Phys. Rev. A* **29** 1214
[370] Manolopoulos D E 1993 Lobatto shape functions *Numerical Grid Methods and Their Application to Schrödinger's Equation* ed Cerjan C (Netherlands: Springer)
[371] Rösch N and Wilhelmy I 1992 *Chem. Phys. Lett.* **189** 499
[372] Wilhelmy I, Ackermann L, Görling A and Roösch N 1994 *J. Chem. Phys.* **100** 2808
[373] Orel A E and Rescigno T N 1990 *Phys. Rev. A* **41** 1695
[374] Rescigno T, Lengsfield B and McCurdy C 1990 *Phys. Rev. A* **41** 2462
[375] Lynch D L and Schneider B I 1992 *Phys. Rev. A* **45** 4494
[376] Nesbet R K 1981 *Phys. Rev. A* **24** 2975
[377] Raşeev G 1985 *J. Phys. B: At. Mol. Phys.* **18** 423
[378] Rescigno T N, Lengsfield B H and Orel A E 1993 *J. Chem. Phys.* **99** 5097
[379] Orel A E and Rescigno T N 1997 *Chem. Phys. Lett.* **269** 222
[380] Jose J, Lucchese R R and Rescigno T N 2014 *J. Chem. Phys.* **140** 204305

— Schwinger Variational Method —

[381] Machado L E, Lee M T and Brescansin L M 1999 *J. Chem. Phys.* **110** 7228
[382] Schwinger J 1947 *Phys. Rev.* **72** 738 see p. 742
[383] Lippmann B A and Schwinger J 1950 *Phys. Rev.* **79** 469
[384] Huo W M 1995 15. the schwinger variational method *Computational Methods for Electron-Molecule Collisions* ed Huo M W and Gianturco F A (New York: Springer)
[385] Lucchese R R and McKoy V 1979 *J. Phys. B: At. Mol. Phys.* **12** L421
[386] Takatsuka K and McKoy V 1981 *Phys. Rev. A* **24** 2473
Takatsuka K and McKoy V 1984 *Phys. Rev. A* **30** 1734
[387] Watson D K and McKoy V 1979 *Phys. Rev. A* **20** 1474
[388] Lucchese R R, Watson D K and McKoy V 1980 *Phys. Rev. A* **22** 421
[389] Lucchese R and McKoy V 1981 *Phys. Rev. A* **24** 770
[390] Lucchese R, Raşeev G and McKoy V 1982 *Phys. Rev. A* **25** 2572
[391] Lucchese R and McKoy V 1982 *Phys. Rev. A* **26** 1406
[392] Horáček J and Sasakawa T 1983 *Phys. Rev. A* **28** 2151
[393] Horáček J and Sasakawa T 1984 *Phys. Rev. A* **30** 2274
[394] Lee M T, Iga I, Fujimoto M M and Lara O 1995 *J. Phys. B: At. Mol. Opt. Phys.* **28** L299
[395] Lee M T, Iga I, Fujimoto M M and Lara O 1995 *J. Phys. B: At. Mol. Opt. Phys.* **28** 3325
[396] Ribeiro E M S, Machado L E, Lee M T and Brescansin L M 2001 *Comput. Phys. Commun.* **136** 117
[397] Machado A, Fujimoto M, Taveira A, Brescansin L and Lee M T 2001 *Phys. Rev.*

A **63** 032707
[398] Nascimento E M, Ribeiro E M S, Brescansin L M, Lee M T and Machado L E 2003 *J. Phys. B: At. Mol. Opt. Phys.* **36** 3621
[399] Machado A M and Masili M 2004 *J. Chem. Phys.* **120** 7505
[400] Stephens J A and McKoy V 1988 *J. Chem. Phys.* **88** 1737
[401] Machado L E, Brescansin L M, Lima M A P, Braunstein M and McKoy V 1990 *J. Chem. Phys.* **92** 2362
[402] Wiedmann R T, White M G, Wang K and McKoy V 1994 *J. Chem. Phys.* **100** 4738
[403] Lucchese R and McKoy V 1983 *Phys. Rev. A* **28** 1382
[404] Natalense A, Brescansin L and Lucchese R 2003 *Phys. Rev. A* **68** 032701
[405] Natalense A P P and Lucchese R R 1999 *J. Chem. Phys.* **111** 5344
[406] Braunstein M, McKoy V, Machado L E, Brescansin L M and Lima M A P 1988 *J. Chem. Phys.* **89** 2998
[407] Lynch D, Lee M T, Lucchese R R and McKoy V 1984 *J. Chem. Phys.* **80** 1907
[408] Wells M and Lucchese R R 1999 *J. Chem. Phys.* **110** 6365
[409] Gianturco F and Lucchese R 2001 *Phys. Rev. A* **64** 032706

— Crank–Nicolson Method —

[410] Crank J and Nicolson P 1947 *Proc. Cambridge Philos. Soc.* **43** 50
[411] Bian X B 2014 *Phys. Rev. A* **90** 033403
[412] Picón A, Bahabad A, Kapteyn H C, Murnane M M and Becker A 2011 *Phys. Rev. A* **83** 013414
[413] Yuan K J, Lu H and Bandrauk A 2011 *Phys. Rev. A* **83** 043418
[414] Silva R E F, Catoire F, Rivière P, Bachau H and Martín F 2013 *Phys. Rev. Lett.* **110** 113001